

---

# Investigating Purinergic Signalling in Chondrocytes

---

A thesis submitted to the School of Biological Sciences  
at the University of East Anglia for the degree of Doctor  
of Philosophy

Daniel Saffer

2024

© This copy of the thesis has been supplied on condition that anyone who consults it is understood to recognise that its copyright rests with the author and that use of any information derived there from must be in accordance with current UK Copyright Law. In addition, any quotation or extract must include full attribution.

# Abstract

Chondrocytes are the sole cell type in cartilage and are highly specialised to produce the cartilaginous extracellular matrix that gives rise to unique biochemical properties facilitating joint movement. This includes reducing friction on the articular surface, distributing load across the joint and in embryogenesis, forming the scaffold for bone synthesis. One of the most common disease states of the synovial joint is osteoarthritis (OA), of which the common pathophysiological finding is degraded and thinned cartilage. This deformation reduces its ability to maintain a functioning joint and leads to the pain and reduced mobility associated with OA. Purinergic signalling is the interaction between extracellular nucleotides and a host of nineteen receptors, dubbed purinergic receptors, which include seven ion channels (P2X1-7) and twelve GPCRs (G-protein coupled receptors) (A1, A2A, A2B, A3, P2Y1, P2Y2, P2Y4, P2Y6, P2Y11-14). Previous research has showed that purinergic signalling can influence key phenotypic changes in chondrocytes and bone cells, and that chondrocytes release nucleotides in response to certain stimuli.

The aim of the project was to establish a role for purinergic receptors in chondrocyte function, in health and disease. Analysis of existing datasets revealed that *P2Y6* is upregulated in OA, which was confirmed experimentally. Primary human chondrocytes (PHC) had a UDP-elicited calcium response whilst two commonly used chondrocyte cell lines did not. Moreover, MRS2578, a specific P2Y6 antagonist, inhibited the chondrocyte's ability to upregulate catabolic genes in response to interleukin 1- $\beta$ , at both the mRNA and protein level. In addition, MRS2578 inhibited chondrogenesis in a murine cell line, ATDC5, at low concentrations by many outcomes. Furthermore, global RNAseq detected that UDP- $\beta$ S, a stable P2Y6 agonist, reduced inflammatory cytokine expression by PHC, an ef-

fect that may be mediated by STAT6. As such, whilst there are many aspects of P2Y6 signalling in chondrocytes that remain unclear, a role for this receptor has been established in various aspects of chondrocyte physiology and may be pertinent in the effort to find better treatments for OA.

## **Access Condition and Agreement**

Each deposit in UEA Digital Repository is protected by copyright and other intellectual property rights, and duplication or sale of all or part of any of the Data Collections is not permitted, except that material may be duplicated by you for your research use or for educational purposes in electronic or print form. You must obtain permission from the copyright holder, usually the author, for any other use. Exceptions only apply where a deposit may be explicitly provided under a stated licence, such as a Creative Commons licence or Open Government licence.

Electronic or print copies may not be offered, whether for sale or otherwise to anyone, unless explicitly stated under a Creative Commons or Open Government license. Unauthorised reproduction, editing or reformatting for resale purposes is explicitly prohibited (except where approved by the copyright holder themselves) and UEA reserves the right to take immediate 'take down' action on behalf of the copyright and/or rights holder if this Access condition of the UEA Digital Repository is breached. Any material in this database has been supplied on the understanding that it is copyright material and that no quotation from the material may be published without proper acknowledgement.

# Contents

<b>1</b>	<b>Introduction</b>	<b>16</b>
1.1	The Synovial Joint . . . . .	16
1.1.1	Articular Cartilage . . . . .	18
1.2	Developmental Chondrogenesis and Endochondral Ossification . .	21
1.2.1	Epiphyseal Plate . . . . .	22
1.2.2	Bone . . . . .	24
1.2.3	Diseases of the Synovial Joint . . . . .	25
1.3	Osteoarthritis . . . . .	26
1.3.1	Pathophysiology . . . . .	27
1.3.2	Signalling Factors . . . . .	28
1.4	Purinergic Signalling . . . . .	34
1.4.1	Adenosine Receptors . . . . .	36
1.4.2	P2X Receptors . . . . .	36
1.4.3	P2Y Receptors . . . . .	37
1.4.4	GPCR Intracellular Signalling . . . . .	37
1.5	Purinergic Signalling in the Joint . . . . .	38
1.5.1	Purinergic Signalling in Bone . . . . .	38
1.5.2	ATP as a Modulator of Chondrocyte Phenotype . . . . .	39
1.5.3	Adenosine Receptors . . . . .	41
1.5.4	P2X Receptors . . . . .	42
1.5.5	P2Y Receptors . . . . .	43
1.5.6	Hypothesis and Aims . . . . .	44
<b>2</b>	<b>Methods</b>	<b>46</b>
2.1	Cell Culture . . . . .	46

2.1.1	SW1353	46
2.1.2	C28/I2	46
2.1.3	1321N1	47
2.1.4	ATDC5	47
2.1.5	Human BM-MSC	47
2.1.6	Primary Human Chondrocytes	48
2.2	Compounds & Reagents	48
2.3	RNA Extraction and Reverse Transcription	49
2.3.1	RNA Extraction	49
2.3.2	Reverse Transcription	49
2.4	(q)PCR	50
2.5	SDS PAGE	52
2.5.1	Biotinylation Assay	54
2.6	Fura-2 AM Calcium Mobilisation Assay	54
2.6.1	DNA Constructs & Transformation	55
2.7	Enzyme-linked Immunosorbance Assay (ELISA)	56
2.8	Lactate Dehydrogenase Release Assay (LDH)	56
2.9	Alcian Blue Staining	57
2.10	Sirius Red Staining	57
2.11	Luciferase Reporter Assay	57
2.11.1	Optimisation of Transfection	57
2.12	RNA Interference (RNAi)	58
2.13	Transcriptome Sequencing	59
2.14	CRISPR-Cas9 knockout of P2Y6	59
2.14.1	Plasmid Delivery	60
2.14.2	Ribonucleoprotein Delivery	61
2.14.3	Lentiviral Delivery	63
2.14.4	Assessment of Indel Formation	63
2.14.5	Clonal Dilution	64
2.15	Protein Arrays	64
2.16	Statistical Analyses	66

<b>3</b>	<b>Investigating Expression and Function of P2Y6 in PHC</b>	<b>67</b>
3.1	Introduction . . . . .	67
3.2	Results . . . . .	68
3.2.1	Chondrocyte cell lines and PHC express multiple puriner- gic receptors . . . . .	68
3.2.2	SkeletalVis reveals P2Y6 to be upregulated in OA . . . . .	71
3.2.3	Expression of functional P2Y6 in cell lines . . . . .	74
3.2.4	Expression of functional P2Y6 in PHC . . . . .	79
3.2.5	The Function of P2Y6 in PHC . . . . .	83
3.2.6	UDP- $\beta$ S nor MRS2578 has any effect on collagen deposition in PHC . . . . .	83
3.2.7	MRS2578 abrogates IL-1 $\beta$ induced MMP expression in PHC	85
3.3	Discussion . . . . .	100
3.3.1	Two commonly used chondrocyte cell lines have pheno- typic differences to PHC. . . . .	100
3.3.2	P2Y6 is over-expressed in OA . . . . .	101
3.3.3	Functionality of P2Y6 in PHC . . . . .	102
3.3.4	MRS2578 inhibits the inflammatory response to IL-1 $\beta$ in PHC	104
<b>4</b>	<b>Investigating Role of P2Y6 in Chondrogenesis</b>	<b>107</b>
4.1	Introduction . . . . .	107
4.2	Results . . . . .	108
4.2.1	Human BM-MSC failed to undergo chondrogenesis . . . . .	109
4.2.2	ATDC5 cells follow a process analogous to chondrogenesis .	110
4.2.3	MRS2578 inhibits ATDC5 chondrogenesis at low concentra- tions . . . . .	111
4.2.4	Knockout of P2Y6 in ATDC5 cell line . . . . .	114
4.2.5	Ribonucleoprotein (RNP) Delivery . . . . .	115
4.2.6	All-in-one Plasmid Delivery . . . . .	119
4.2.7	Lentiviral Delivery of Cas9 and transient transfection of gRNA.	121
4.3	Discussion . . . . .	127
4.3.1	Establishment of Chondrogenesis Model . . . . .	127
4.3.2	MRS2578 inhibits ATDC5 Chondrogenesis . . . . .	128

4.3.3	Failure of CRISPR-Cas9 Knockout of P2Y6 in ATDC5 cells . . . . .	129
<b>5</b>	<b>Transcriptomics</b>	<b>134</b>
5.1	Introduction . . . . .	134
5.2	Results . . . . .	135
5.2.1	MRS2578 induces differential expression of over 6,000 genes whilst UDP- $\beta$ S causes differential expression of less than 300 genes in non-stimulated cells. . . . .	135
5.2.2	UDP- $\beta$ S causes reduced expression of multiple pro-inflammatory mediators. . . . .	139
5.2.3	Some of the DEG caused by UDP- $\beta$ S also change at the protein level. . . . .	153
5.2.4	UDP- $\beta$ S may mediate these effects via inhibition of STAT6. . . . .	156
5.2.5	UDP- $\beta$ S and MRS2578 cause differential gene expression often in the same direction of change. . . . .	162
5.2.6	MRS2578 may inhibit the IL-1 induced expression of MMPs through likely more than one mechanism. . . . .	165
5.3	Discussion . . . . .	172
5.3.1	Analysis Methods for RNAseq Data. . . . .	172
5.3.2	UDP- $\beta$ S vs UDP and receptor desensitisation . . . . .	174
5.3.3	Action of UDP- $\beta$ S . . . . .	175
5.3.4	Action of MRS2578 . . . . .	179
5.3.5	Next Steps . . . . .	183
<b>6</b>	<b>Discussion</b>	<b>184</b>
6.1	Methods Development . . . . .	184
6.2	What functional effect does P2Y6 have on chondrocyte phenotype? . . . . .	186
6.3	Is MRS2578 a reliable tool? . . . . .	189
6.4	Future Directions . . . . .	191
<b>7</b>	<b>Bibliography</b>	<b>227</b>
<b>8</b>	<b>Appendix</b>	<b>228</b>
8.1	Primer Sequences . . . . .	228

8.2 Proteomic Arrays . . . . .	232
--------------------------------	-----

# List of Figures

1.1	Structure of the Synovial Joint . . . . .	17
1.2	Articular Cartilage Structure . . . . .	18
1.3	Cartilage ECM Components . . . . .	21
1.4	Bone Development Diagram . . . . .	23
1.5	Structure of the Growth Plate . . . . .	24
1.6	Wnt Signalling . . . . .	29
1.7	Interleukin Signalling . . . . .	34
1.8	Nucleotide Structure . . . . .	35
2.1	ATDC5 Transfection Optimisation . . . . .	58
2.2	Cas9 Graphic . . . . .	59
2.3	PX459 Plasmid Map . . . . .	61
2.4	Proteomic Array Membrane Analysis . . . . .	66
3.1	mRNA Expression of Purinergic Receptors . . . . .	70
3.2	Analysis of Existing Datasets for Purinergic Expression . . . . .	72
3.3	Detecting <i>P2RY6</i> mRNA in OA and NOF . . . . .	73
3.4	Alomone P2Y6 Western . . . . .	74
3.5	Abcam P2Y6 Western . . . . .	75
3.6	UDP elicited calcium responses in C28/I2 and SW1353 . . . . .	76
3.7	Thapsigargin and exogenous P2Y6 calcium responses . . . . .	77
3.8	SW1353 Biotin Western . . . . .	78
3.9	FURA-2 Optimisation in PHC . . . . .	80
3.10	PHC nucleotide elicited calcium responses. . . . .	81
3.11	MRS2578 Pharmacology and Toxicity . . . . .	82
3.12	<i>P2RY6</i> mRNA Expression changes in response to IL-1 $\beta$ . . . . .	83

3.13	Effect of P2Y6 on collagen deposition in PHC . . . . .	85
3.14	Effect of MRS2578 on IL-1 $\beta$ induced MMP expression . . . . .	87
3.15	ELISA and Luciferase assay showing effect of MRS2578 on PHC . . . . .	88
3.16	MRS2578 effect on MMPs - UDP Reversal, MMP13 . . . . .	90
3.17	MRS2578 effect on MMPs - UDP Reversal, MMP1 . . . . .	91
3.18	MRS2578 effect on MMPs - UDP Reversal, MMP3 . . . . .	92
3.19	MRS2578 effect on MMPs - Changing concentration of IL-1 $\beta$ . . . . .	94
3.20	MRS2578 Cytotoxicity . . . . .	95
3.21	Effect of RNAi KD of P2Y6 on MRS2578 effects . . . . .	96
3.22	siRNA KD P2Y6 . . . . .	97
3.23	Effect of MRS2578 on IL-1 $\beta$ or TNF $\alpha$ induced MMP expression in SW1353 . . . . .	98
3.24	Effect of MRS2578 on IL-1 induced MMP expression in parental and P2Y6+ 1321N1 cells . . . . .	99
4.1	Human BM-MSC Chondrogenesis . . . . .	109
4.2	ATDC5 Chondrogenesis . . . . .	110
4.3	ATDC5 Chondrogenesis - qRT-PCR . . . . .	112
4.4	ATDC5 Chondrogenesis - Alcian Blue/LDH . . . . .	113
4.5	T7E1 Assay from HPRT RNP transfection . . . . .	118
4.6	T7E1 from RNP transfection with TransIT-X2 . . . . .	118
4.7	T7E1 Assay from electroporation of plasmid . . . . .	120
4.8	PCR for Cas9 . . . . .	123
4.9	T7E1 assay from lentiviral Cas9 delivery . . . . .	123
4.10	Sequence analysis of AC group clones . . . . .	124
4.11	AC.5.2 mRNA Expression of P2Y6 . . . . .	125
4.12	CRISPR Clones Western . . . . .	126
5.1	Venn Diagram of Differential Expression . . . . .	136
5.2	Non-stimulated DEG Volcano Plot . . . . .	137
5.3	IL-1 $\beta$ Stimulated DEG Volcano Plot . . . . .	138
5.4	Non-stimulated Heatmap . . . . .	141
5.5	GO Term Enrichment Analysis for VC vs UDP- $\beta$ S . . . . .	142

5.6	Reactome Enrichment Analysis for VC vs UDP- $\beta$ S . . . . .	143
5.7	KEGG Pathway Analysis for VC vs UDP- $\beta$ S . . . . .	144
5.8	KEGG Pathway Analysis for VC vs UDP- $\beta$ S . . . . .	145
5.9	KEGG Pathway Analysis for VC vs UDP- $\beta$ S . . . . .	146
5.10	Enrichr TF Analysis . . . . .	147
5.11	qRT-PCR Validation of RNAseq . . . . .	148
5.12	ATDC5 RNAseq Validation . . . . .	149
5.13	GO Term Enrichment Analysis for IL-1 vs IL-1 + UDP- $\beta$ S . . . . .	150
5.14	Cytokine Proteomic Array 24 Hrs post stimulation . . . . .	154
5.15	Cytokine Proteomic Array 48 Hrs post stimulation . . . . .	155
5.16	Proteomic Array - NF $\kappa$ B . . . . .	157
5.17	Proteomic Array - MAPK . . . . .	158
5.18	Proteomic Array - AKT . . . . .	159
5.19	Proteomic Array - JAK/STAT . . . . .	160
5.20	Proteomic Array - TGF . . . . .	161
5.21	Non-stimulated Reciprocal Heatmap . . . . .	163
5.22	IL-1 $\beta$ Stimulated Heatmap . . . . .	164
5.23	Reactome Enrichment Analysis for IL-1 vs IL-1 + MRS2578 . . . . .	166
5.24	Gene Ontology Enrichment Analysis for VC vs MRS2578 . . . . .	169
5.25	KEGG Pathway Analysis for IL-1 vs IL-1 + MRS2578 - MAPK . . . . .	170
5.26	KEGG Pathway Analysis for IL-1 vs IL-1 + MRS2578 (JAK/STAT) . . . . .	171
5.27	Structure of UDP and UDP- $\beta$ S. . . . .	174
5.28	Action of P2Y6 on NF $\kappa$ B Signalling . . . . .	180
6.1	Structure of MRS2578 . . . . .	189
8.1	Array Maps. Taken from Raybiotech.com. . . . .	232
8.2	Phosphorylated Protein Pathway Arrays . . . . .	234
8.3	Cytokine Arrays . . . . .	235

# List of Tables

1.1	Adenosine Receptors . . . . .	36
1.2	P2X Receptors . . . . .	37
1.3	P2Y Receptors . . . . .	37
1.4	Summary of Purinergic Receptors' action on Bone . . . . .	40
2.1	1X Reverse Transcriptase Reaction . . . . .	50
2.2	1X PCR Reaction . . . . .	51
2.3	1X qPCR Reaction . . . . .	51
2.4	PCR cycling conditions . . . . .	51
2.5	qPCR cycling conditions . . . . .	51
2.6	10% (v/v) Acrylamide Gel 1X . . . . .	53
2.7	Antibodies . . . . .	53
2.8	sgRNA-targeting sequences . . . . .	61
2.9	gRNA-targeting sequences . . . . .	62
2.10	RNP Formation . . . . .	62
3.1	$C_T$ values for Purinergic Receptor Profiling . . . . .	71
3.2	Publications Collated from SkeletalVis . . . . .	72
3.3	Nucleotide Elicited Calcium Responses in PHC . . . . .	79
4.1	RNP gRNA Doench scores . . . . .	116
4.2	RNP Lipofection Optimisation . . . . .	117
4.3	Plasmid gRNA Doench Scores . . . . .	119
4.4	Deconvolution algorithm output from CRISPR plasmid transfection.	120
4.5	Deconvolution Algorithm Output for Lentiviral Cas9 Delivery of CRISPR components . . . . .	122

5.1	VC vs UDP Top 50 DEG by p value . . . . .	151
5.2	IL-1 vs IL-1 + UDP- $\beta$ S Top 50 DEG by p value . . . . .	152
5.3	VC vs MRS2578 Top 50 DEG by p value . . . . .	167
5.4	IL-1 vs IL-1 + MRS2578 Top 50 DEG by p value . . . . .	168
8.1	Mouse qPCR Primers SYBR. Primers 1-6 Taken from [311]. . . . .	228
8.2	ATDC5 CRISPR sequencing primers . . . . .	229
8.3	Human SYBR qPCR Primers. Taken from [312]. . . . .	230
8.4	Human qPCR Primers . . . . .	231

# List of Abbreviations

ECM	Extracellular Matrix
OA	Osteoarthritis
STZ	Superficial tangential zone
TRPV4	Transient receptor potential cation channel V 4
BRU	Bone remodelling unit
MMP	Matrix metalloproteinase
MSK	Musculoskeletal
FGF	Fibroblast growth factor
ADAMTS	A disintegrin and metalloproteinase with thrombospondin motifs
BMP	Bone morphogenetic protein
SOX	SRY-box transcription factor
VEGF	Vascular endothelial growth factor
TGF	Transforming growth factor
IGF	Insulin growth factor
DAMP	Damage associate molecular pattern
GPCR	G-protein coupled receptor
Fzd	Frizzled
Dvl	Dishevelled
NFAT	Nuclear factor of activated T cells
NLK	Nemo like kinase
MSC	Mesenchymal stem cell
HOA	Hip OA primary chondrocyte
KOA	Knee OA primary chondrocyte
NICD	Notch intracellular domain

COX2	Cyclo-oxygenase 2
PGE2	Prostaglandin E2
NOS	Nitric oxide synthase
HIF	Hypoxia inducible factor
bHLH	Basic helix-loop-helix transcription factor
MAPK	Mitogen activated kinase
PI3K	Phosphoinositide-3 kinase
JAK	Janus kinase
STAT	Signal transducer and activator of transcription
JNK	c-Jun NH2-terminal kinase
DMM	Destabilisation of the medial meniscus
RUNX	Runt-related transcription factor
WT	Wild-type
IL	Interleukin
ATP	Adenosine triphosphate
UDP	Uridine triphosphate
DNA	Deoxyribonucleic acid
RNA	Ribonucleic acid
DMARD	Disease modifying anti-rheumatic drug
ROS	Reactive oxygen species
ANK	Ankyrin
CPPD	Calcium pyrophosphate disease
MIA	Monosodium iodoacetate
FCS	Fetal calf serum
DMEM	Dulbecco's modified eagle medium
DMSO	Dimethyl sulfoxide
PHC	Primary human chondrocyte
IHH	Indian hedgehog signalling
NO	Nitric oxide
DEG	Differentially expressed gene

# Chapter 1

## Introduction

### 1.1 The Synovial Joint

The synovial joint is a complex skeletal structure which facilitates movement, examples being the hip, knee, neck and elbow, and are found where the two adjoining bones end. For example, the femur and tibia meet at the knee, a type of hinge joint, that allows for the regulated movement of one bone relative to the other. There are multiple tissues that form a synovial joint, each with a specialised function to allow for controlled locomotion.

Bone is a calcified rigid tissue that provides structural support and houses the marrow, which is where some types of blood and immune cells differentiate or mature. It also functions to provide the framework for soft tissue and protect organs. The structures that tether bones to each other are ligaments, which prevent uncontrolled movements and serve to stabilise the joint. Ligaments in the knee joint include the anterior/posterior cruciate ligaments and the medial/lateral collateral ligaments. Tendons are the fibrous structures that tether a bone to muscle, and can function differently depending on the location. For example, tendons in the fingers serve to help position the bones, whereas in the calves, can act more like springs to store energy. The outer membrane of the joint is the capsule, which is an avascular fibrous tissue that surrounds the synovial joint. The inner membrane of the joint is the synovium, which is vascularised (unlike cartilage) and encapsulates the inner structures. It also houses the synovial fluid. Synovial fluid is a viscous filtrate from the blood, and enables diffusion of nutrients and

waste products into/out of the joint. The synovial fluid contains proteoglycans such as lubricin and hyaluronic acid, which are produced by the fibroblast-like synoviocytes found in the synovium, and serves to lubricate the joint as well as provide some shock absorption due to its viscosity. Some joints (including the knee) have a crescent shaped pad of fibrocartilage called a meniscus, that sits between the articulated ends of bones and provides resistance to mechanical force. Articular cartilage is a separate layer of hyaline cartilage that lines the articular surface of the bones at the joint [1]. Hyaline cartilage differs from fibrocartilage in that it contains predominantly collagen II, whereas fibrocartilage will contain predominantly collagen I.

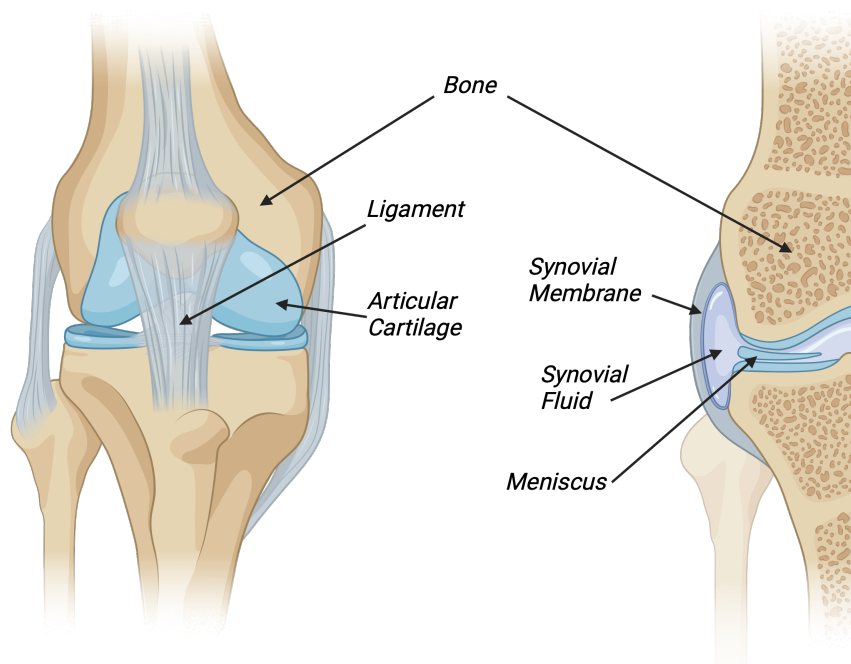


**Figure 1.1: Structure of the Synovial Joint.** The synovial joint is a complex skeletal structure made of many highly specialised tissues. The joint capsule has an outermost layer of non-vascularised fibrocartilage and an inner layer of vascularised synovium. Within the joint, synovial fluid facilitates oxygen and nutrient exchange and provides lubrication whilst articular cartilage, made by chondrocytes, lines the articular surface and reduces friction. Created with biorender.com.

### 1.1.1 Articular Cartilage

Articular cartilage is the viscoelastic tissue that lines the articular surface of bones. It is an avascular, aneural and alymphatic tissue, relying on passive diffusion from the synovial fluid for homeostasis. It serves a significant function in the joint, which is to reduce friction during movement and facilitate the transfer of mechanical load to the subchondral bone. The extracellular matrix (ECM) of articular cartilage gives rise to the unique biochemical properties of the tissue that allow it to perform as it does. Articular cartilage has distinct layers, which differ in their ECM composition and cellular morphology as well as cellular density and distribution (Fig. 1.2).

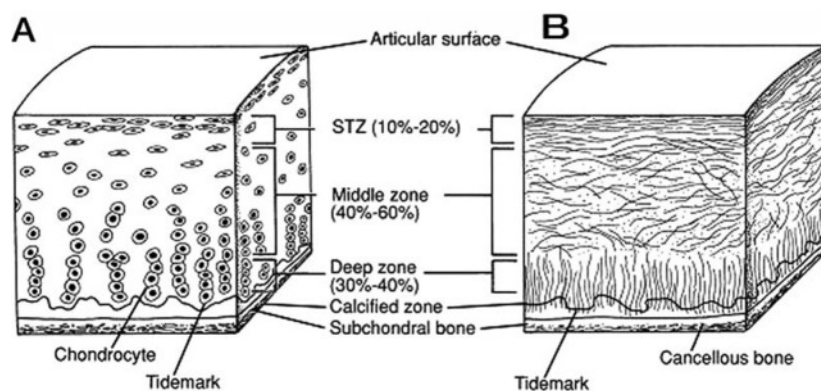


**Figure 1.2: Structure of Articular Cartilage.** There are many layers in articular cartilage that differ in their cellular morphology and arrangement of matrix components. Closest to the subchondral bone, the deep zone contains columnar chondrocytes that are round, with collagen arranged perpendicular to the bone. Moving up towards the articular surface, the middle zone and superficial tangential zone (STZ) have a sparser population of flatter chondrocytes with collagen fibrils arranged parallel to the subchondral bone. Taken from [2]

The first layer of articular cartilage from the subchondral bone is the calcified zone, where the ECM is partially calcified. This section anchors the cartilage to the bone through the arrangement of the collagen fibrils perpendicular to the articular surface and has a sparse population of hypertrophic chondrocytes. The deep zone also contains the same orientation of perpendicular collagen fibrils but has a higher density of columnar, round chondrocytes that are not hypertrophic. The deep zone provides the highest resistance to compressive forces due to its higher concentration of proteoglycans. The middle zone provides the transition

from the deep zone to the superficial zone, in that it has a slightly more sparse population of spherical chondrocytes and the collagen is arranged obliquely. The superficial (tangential) zone (STZ) is the uppermost layer and is the most responsive to shear/mechanical stress in that it is more pliable and able to deform due to its lower proteoglycan content and higher water and collagen content. Its collagen fibres align parallel to the articular surface and it has a more flat, sparser population of chondrocytes that reside in lacunae [3, 4].

## **Chondrocytes**

Chondrocytes are the sole cell type in cartilage, and are responsible for the production and turnover of the extracellular matrix. They differentiate from bone marrow mesenchymal stem cells and express proteins that form both the pericellular and extracellular matrix, as well as catabolic enzymes such as matrix metalloproteinases and ADAMTS. A chondrocyte surrounded by its pericellular matrix is referred to as a chondron, and reside in spaces within the matrix called lacunae in the zones of articular cartilage closer to the articular surface.

Chondrocytes are sparsely populated compared to other tissues, especially in the uppermost STZ layer. This has implications for cellular communication and how they respond to their environment. It is thought that chondrocytes rely mainly on autocrine signalling or paracrine signalling via simple diffusion, however do express gap junction proteins, so have the ability to form gap junctions, at least in monolayer culture [5]. ECM-cell interactions play an important role in chondrocyte behaviour [6]. Integrins are membrane receptors whose ligands are components of the extracellular matrix, and can regulate proliferation, apoptosis and matrix remodelling. There are 24 heterodimeric integrin receptors, recognising proteins like collagen, fibronectin and laminin [7]. As well as integrins, ECM components can also signal to other receptors as damage associated molecular patterns (DAMPs). These can be intracellular components released from apoptotic or necrotic cells or extracellular components like proteoglycan or fibronectin fragments. These signal to pattern recognition receptors (PRR), such as toll-like receptors (TLR), NOD-like receptors (NOD) or receptor for advanced glycosylation end products (RAGEs) and can initiate inflammatory cascades in this way

[8]. Another facet of chondrocyte homeostasis is the effect of loading. Chondrocytes are subjected to constant mechanical force, being the first tissue to receive the pressure of the adjacent bone. This mechanical load has shown to be critical for chondrocyte homeostasis [9, 10] and is why moderate joint loading is thought to be protective in the joint. Multiple mechanosensitive ion channels, such as Piezo1/2 and TRPV4 have been shown to transduce the physical force to cellular signalling in chondrocytes [11, 12]. Chondrocytes also have primary cilia that are formed by microtubules and have been shown to be important for signalling cascades, such as hedgehog signalling. Loss of primary cilia on chondrocytes has also proven to be detrimental [13].

### **Extracellular Matrix**

The extracellular matrix of articular cartilage is what gives rise to its high surface tension and viscoelasticity, allowing it to be able to perform its function in the joint. Its biochemical composition is a precise balance of most abundantly water (70-80%), collagens and proteoglycans. The predominantly type II collagen network provides tensile strength, whilst the proteoglycans (i.e. aggrecan) provide osmotic potential and resulting elasticity and compressive resistance [3]. Proteoglycans arrange in a macromolecular structure. Each aggrecan monomer has glycosaminoglycan side chains (namely chondroitin and keratan sulfate) that are covalently linked and provide the osmotic pressure due to their negative charge. Aggrecan monomers polymerise along a hyaluronan backbone, utilising link protein. These aggrecan-hyaluronan structures are arranged between collagen fibrils, giving rise to a regular repeating structure [14]. The supramolecular structure of cartilage alters at different distances from chondrocytes and with depth from the articular surface. Whilst collagen II comprises over 90% of the collagen content of the cartilage ECM, others are present including collagens I, IV, V VI and XI as well as other glycoproteins such as perlecan, versican and decorin. The pericellular matrix (that surrounding a chondrocyte) has more type VI collagen and perlecan, which are thought to be important in relaying signals to individual chondrocytes through ECM interactions [15]. As well as providing the structural integrity, proteoglycans have also been shown to sequester important signalling

factors in the ECM, such as decorin being able to retain transforming growth factor beta (TGF- $\beta$ ) in the matrix [16].

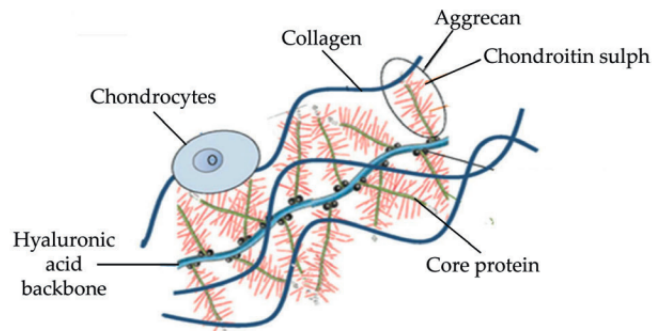


**Figure 1.3: Cartilage Extracellular Matrix Composition.** The ECM of cartilage provides the unique biochemical properties that give rise to its function. Aggrecan polymers align along a hyaluronan backbone, which is arranged between collagen fibrils, producing a supramolecular structure that has high osmotic potential and compressive resistance [17].

## 1.2 Developmental Chondrogenesis and Endochondral Ossification

Chondrogenesis is the development of chondrocytes and the cartilage tissue from their mesenchymal progenitors. Mesenchymal stem cells are pluripotent and can differentiate into osteoblasts, chondrocytes, adipocytes or myogenic/cardiac cell types [18]. There are two types of bone development - endochondral and intramembranous. In intramembranous ossification, connective tissues are replaced by bone, however most bones in the skeleton are developed by endochondral ossification. Examples of bones formed by intramembranous ossification include the flat bones of the skull, clavicle and maxilla, whereas long bones like the humerus and ulna are formed by endochondral ossification. In the latter process, during embryonic development, chondrocytes form the cartilaginous scaffold which is eventually replaced by bone and becomes the developing skeleton.

The process begins with the condensation of mesenchymal stem cells in either the neural crest or mesoderm. This condensation is dependent on a number of prerequisite factors, such as bone morphogenetic proteins (BMPs), which signal via SMAD4, and expression of cell-cell communication proteins such as N-

cadherin and versican [19]. Within this mesenchyme, the interior cells begin the differentiation process into chondrocytes, and the peripheral cells form the perichondrium, demarcating the developing tissue. The initial differentiation of the stem cells is again controlled by a number of factors, but most importantly cannot occur without SRY-box transcription factor 9 (SOX9) expression, along with SOX5 and SOX6 [20]. Targets of SOX9 as a transcription factor include ECM components such as collagen II and aggrecan, increasing their expression during this stage of development. This catalyses deposition of matrix by the chondrogenic cells as well as proliferation, driving longitudinal growth. Fibroblast growth factor (FGF) signalling is also essential for the condensation and differentiation steps [21], with impaired cartilage nodule formation in FGFR3-null cultures of MSCs [22].

As the cells proliferate, those in the center become terminally hypertrophic. This results in hypertrophy in the classical sense, of increase cell size and volume as well as exit from the cell cycle, nuclear condensation and eventual apoptosis. Accompanied by this is a change in their expression profile from collagen II to X, expression of matrix degrading factors, such as matrix metalloproteinase 13 and 9 (MMP13/9) [23] and alkaline phosphatase to aid in calcification. Vascular endothelial growth factor (VEGF) and receptor activator of nuclear factor kappa-B ligand (RANKL) are also expressed by chondrocytes, causing neovascularisation and infiltration by bone precursor cells [24], which differentiate and mineralise the matrix. RANKL is required for osteoclastogenesis. This process continues, creating a long bone, with a bony diaphysis flanked by epiphyses (containing the secondary ossification center) and metaphyses. There is some evidence that the idea of terminal differentiation and apoptosis of hypertrophic chondrocytes is incorrect, and that they can undergo a further differentiation or 'transdifferentiation' into osteoblasts at the ossification center [25].

### **1.2.1 Epiphyseal Plate**

After birth, the bones continue to grow until the end of puberty. The epiphyseal plate (growth plate) is the center with which bones grow, whereby cartilage becomes replaced with bone, facilitating skeletal growth, in a similar way to

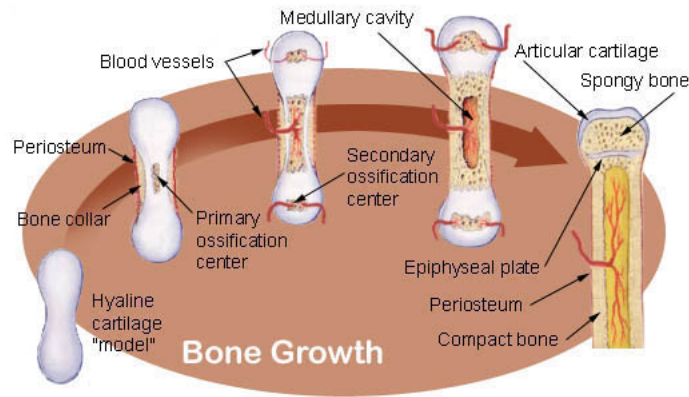


**Figure 1.4: Bone Development.** Development of the skeleton begins with mesenchyme condensation, followed by the creation of a primary ossification center, caused by a phenotypic shift of the cells in the center. Longitudinal growth is achieved by proliferation of chondrocytes in the proliferative zone, followed by hypertrophy, vascular invasion and calcification by bone cells [26].

skeletogenesis during embryonic development. In humans, the epiphyseal plate becomes fused at the end of puberty, halting bone growth. It is thought that the stem-like cells in the reserve zone have a limited proliferative potential, and when exhausted, the bone cannot grow any further [27].

There are three zones of the growth plate, where the stages of endochondral ossification occur. In the reserve zone, the singular stem-like chondrocytes are round and maintain a cartilaginous matrix. In the proliferative zone, chondrocytes flatten, proliferate, and continue to deposit a collagen II rich matrix. These chondrocytes eventually become mature and switch phenotype to a terminally hypertrophic one, forming the hypertrophic zone. In this zone, the cells change their expression profile from collagen II to X amongst other changes discussed in 1.2. Angiogenesis, bone cell infiltration and calcification also occurs, leading to bone formation and chondrocyte apoptosis [28].

This process is controlled by a number of signalling factors. Initially, one of the main factors controlling chondrocyte proliferation in the proliferative zone are BMPs, which signal via the indian hedgehog pathway (Ihh) [29]. BMPs are also thought to be important in the initiation of hypertrophy in chondrocytes, specifically BMP-2 and BMP-4 [30]. Transforming growth factor beta (TGF- $\beta$ ) is also crucial to bone growth and development, as mutations can cause phenotypes such as chondrodysplasias [31]. As chondrocytes become hypertrophic, cells be-

gin to reduce expression of SOX9 and increase expression of RUNX2, the transcription factor responsible for many bone-related genes (such as VEGF, MMP13 and collagen X) [32]. Hormonal factors such as insulin-like growth factor 1 (IGF-1) also have an impact on skeletal growth during puberty, with direct effects on cells. For example, it has been shown to directly stimulate chondrocyte proliferation [33].

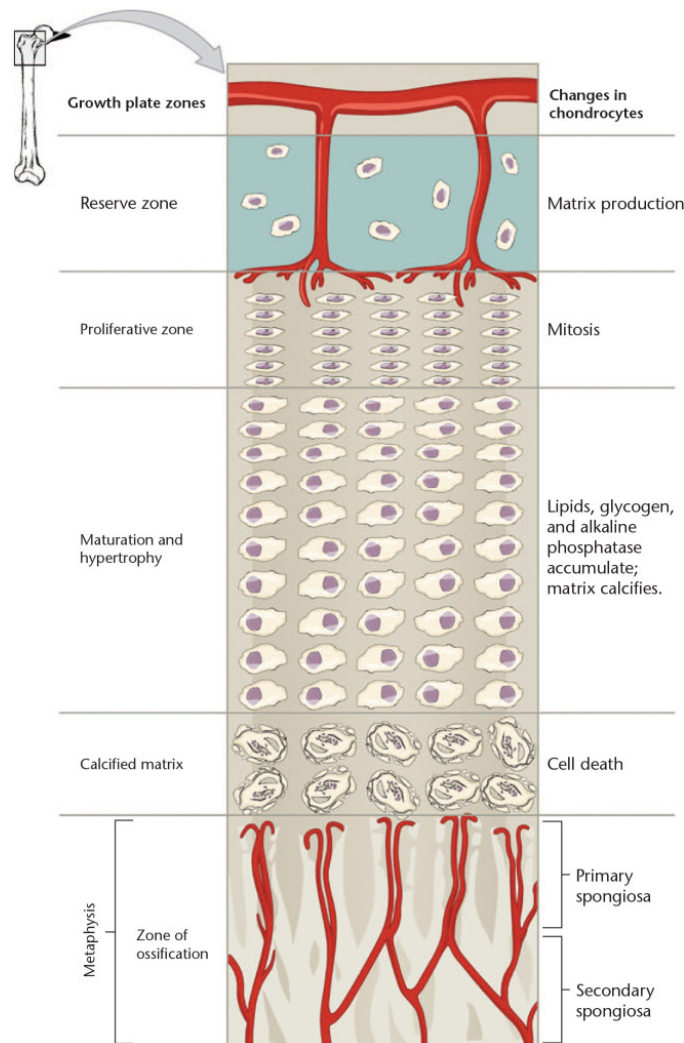


**Figure 1.5: Structure of the Growth Plate.** The growth plate is the center with which long bones grow, by replacing cartilage with bone. During this process, chondrocytes proliferate, mature and become hypertrophic. The change of phenotype from proliferative to hypertrophic allows for vascular infiltration and calcification of the matrix by bone cells, forming an ossification center [34].

## 1.2.2 Bone

Bone is a mineralised tissue that provides structural support to the other organs of the body. There are three cell types found in bone - osteocytes, osteoclasts and os-

teoblasts. In a similar way to cartilage, albeit more rapidly, bone cells are continuously remodelling the calcified structure in response to environmental stimuli to maintain homeostasis, at a rate of 2-3% turnover per year [35]. Osteocytes form an interconnected network within the osseous tissue and are the cells thought to orchestrate the remodelling process. They also sense changes in mechanical loading and react to loading stimuli. Osteoclasts carry out bone resorption and osteoblasts deposit new bone [36].

The homeostatic remodelling process can be initiated by a number of stimuli, including hormonal (PTH/oestrogen) or mechanical, which can lead to osteocyte apoptosis or increased RANKL expression, which recruits the basic multicellular unit (BMU) and stimulates osteoclastogenesis. The BMU is a collection of osteoblasts and osteoclast precursors, which differentiate. The mature multinucleated osteoclasts initiate resorption of the defective bone, via lysosomal enzymes, creating a lacunae. The osteoblast will then fill this space with osteoid (a mixture of collagen I and other proteins). The osteoid becomes mineralised via the action of matrix vesicles, which take up calcium and inorganic phosphate and form hydroxyapatite crystals. Mature osteoblasts also produce alkaline phosphatase, which increases the local concentration of phosphate, aiding mineralisation. Osteoblasts then either undergo apoptosis, differentiate into osteocytes embedded within the mineralised matrix or become a cell that lines the surface of the bone [37, 38].

### **1.2.3 Diseases of the Synovial Joint**

Owing to the integral nature of the synovial joint, diseases of the tissue are often debilitating and challenging to cure. Most prevalent is osteoarthritis, which will be discussed in 1.3. In England, 17% of the population have a disease of the musculoskeletal system, of which the cost to the NHS is estimated to be £5bn annually [39]. Rheumatoid arthritis (RA) is an autoimmune condition and has a systemic inflammatory component, whereby immune cells cause synovitis and chronic inflammation. This leads to thickening of the joint capsule, pain, reduced movement and swelling. RA is more common in the small joints of the hands and feet, whereas OA is found more in the load-bearing joints eg hips and can often

be asymmetrical, although either can be found in any synovial joint [40]. Gout is another inflammatory condition caused by chronic hyperuricemia, which leads to the deposition of uric acid crystals in, most commonly, the toe joint. The uric acid crystals then initiate inflammation and damage to the joint, leading to pain and reduced mobility. Some MSK conditions are congenital, such as achondroplasia, which is caused by mutations to the FGFR3 gene and causes dwarfism due to defective chondrogenesis, or osteogenesis imperfecta, which leads to brittle bones as a result of a mutation to the collagen I genes amongst others.

### **1.3 Osteoarthritis**

Osteoarthritis (OA) is a locally inflammatory condition that is highly prevalent in society. In the UK, 10 million adults have been diagnosed with OA, with 350,000 new diagnoses every year [41] and is expected to rise in the coming decades as the ageing population grows. In the US, the lifetime risk of being diagnosed with OA is estimated to be between 14% and 45% [42]. It is a condition characterised by pain, reduced mobility, stiffness, swelling and local, but not systemic inflammation. Risk factors for the disease include age, heredity, obesity, injury, occupational use and underlying physiological abnormalities [43]. OA is most common in those aged 45 and over, and is more common and severe in women [44]. Moreover, OA patients often have other co-morbidities, as those diagnosed with OA are three times more likely to have ischaemic cardiac disease or heart failure [45]. The disease has also been shown to negatively impact other outcomes such as mental health, work participation, sleep and mortality [46]. The treatment axis for OA includes pain management, intra-articular injection of corticosteroids to relieve inflammation and eventual surgical replacement of the joint, which results in a long period of convalescence. There are currently no disease-modifying drugs to treat or slow the progression of OA, and as such has a large socio-economic burden, with an absenteeism cost in the US of \$10.3 billion. It is also the third most rapidly increasing condition by prevalence, associated with disability, posterior to diabetes and dementia [46, 47].

### 1.3.1 Pathophysiology

OA is a disease of the whole joint. It is characterised by a degradation and thinning of the articular cartilage, which is caused by an imbalance in the anabolic and catabolic activity of chondrocytes, with higher expression of matrix degrading enzymes [48]. This is also known as joint space narrowing, whereby the two subchondral bones become closer together. What initiates this imbalance is not entirely clear, however it is thought to be the function of a host of mechanical, biochemical and genetic factors. Cartilage is also thought to have a poor ability to repair itself owing to the low proliferative potential of mature chondrocytes and their sparse distribution within the tissue [49], in addition to it being avascular. These two hallmarks also decrease with age and injury [50, 51]. As well as thinning of the articular cartilage, there is focal erosion and fibrillation at the articular surface, hindering its function as a viscoelastic tissue to lubricate joint articulation. There are also changes to the subchondral bone, namely osteophyte formation and sclerosis (thickening and hardening of bone). Osteophytes are fibrocartilage bony outgrowths at the junction between cartilage and bone. It is thought that the TGF- $\beta$  family of signalling molecules may be responsible for initiating their development, although it is not clear whether they contribute to the pathological nature of OA [52]. It has been well documented that asymptomatic bone lesions present prior to any articular cartilage pathophysiological changes or pain associated with OA [53]. It is also thought that there is paracrine signalling between different cell types in the joint that may contribute to the pathology of OA. Co-culture systems have shown that osteoblasts can significantly alter chondrocyte phenotype, for example, the soluble 14-3-3 $\epsilon$  protein secreted by osteoblasts can increase expression of catabolic enzymes by chondrocytes [54]. There is potentially a metabolic component to OA as well. Chondrocytes are adapted to survive in the relatively hypoxic, low-nutrient environment and during cartilage damage, the oxygen tension is imbalanced and can lead to reactive oxygen species (ROS) accumulation and dysregulation of the glycolytic metabolic pathway [55]. Synovial inflammation is also a hallmark of OA, which is thought to contribute to the pathogenesis of the disease. One such mechanism by which this arises is through the release of damage associated molecular patterns (DAMPs) as

a result of injury/joint damage that signal to pattern recognition receptors (PRRs) expressed by chondrocytes, synovial macrophages or fibroblast-like synoviocytes to initiate inflammatory cascades [56].

There are similarities between the events that occur in OA and the latter stages of endochondral ossification. Chondrocytes in healthy tissue resist a terminal differentiation, however chondrocytes in diseased tissues proliferate and become hypertrophic. There is also a characteristic increase in expression of hypertrophy markers, such as MMP-13, collagen X and VEGF. This is accompanied by vascularisation and focal calcification, which also occur during endochondral ossification [57]. Some of the signalling pathways that regulate skeletal development have also shown to be important to the progression of OA, some of which are discussed below.

### 1.3.2 Signalling Factors

Chondrocytes are subject to a number of molecular signalling pathways whose dysregulation contributes to the progression of OA.

#### Wnt

In the canonical wingless (Wnt) pathway, Wnt is the ligand for a group of GPCRs called Frizzled (Fzd). In the absence of Wnt/Fzd signalling,  $\beta$ -catenin is continuously degraded by GSK3 $\beta$ , a multiprotein complex, in the cytoplasm. Where there is Wnt/Fzd signalling, activation of Dishevelled (Dvl) results in deactivation of GSK3 $\beta$ , and subsequent accumulation of  $\beta$ -catenin. It then translocates to the nucleus and initiates transcription of a number of target genes. In chondrocytes, this pathway has shown to be important to homeostasis. Wnt can also exert effects in the non-canonical,  $\beta$ -catenin - independent pathway. This can involve activation of protein kinase C and calcium signalling, leading to transcriptional regulation via NFAT. The non-canonical pathway can also regulate the canonical pathway, via expression of NLK, which can inhibit  $\beta$ -catenin [58].

Genomic studies have revealed that functional polymorphisms in the gene encoding frizzled-related protein 3, an antagonist of Wnt signalling, are associated with an increased risk of OA in females [59]. Furthermore, in a mouse model of

OA, exogenous activation of  $\beta$ -catenin results in an OA-like phenotype [60]. Wnt signalling has been shown to be able to induce expression of matrix degrading enzymes, a hallmark of OA tissue [61], and has a role in cell-fate determination in mesenchymal stem cells (MSC) [18]. To this end, Lorecivivint, an inhibitor of the Wnt pathway, has entered phase III clinical trials as a disease modifying OA drug [62].

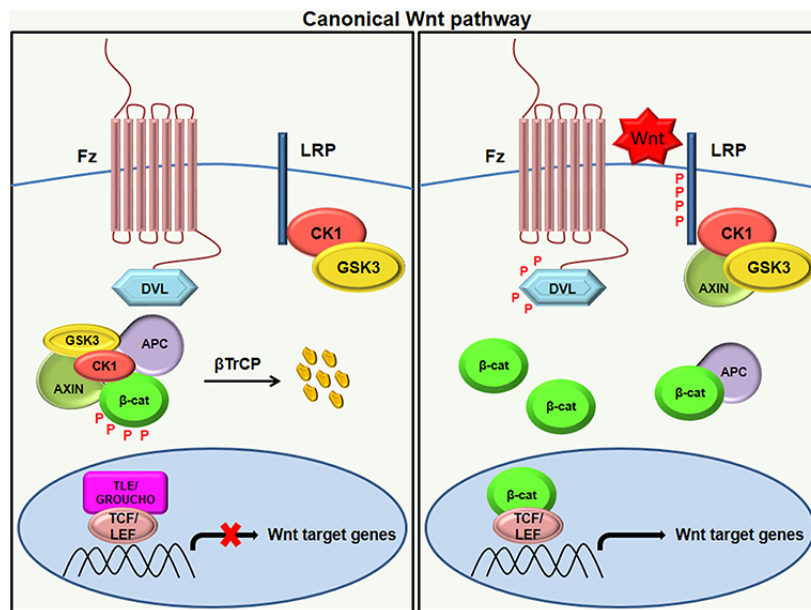


**Figure 1.6: Wnt Signalling.** Wingless (Wnt) signalling is thought to contribute to OA pathology. In the canonical pathway, Wnt activates GPCR Fzd, which causes phosphorylation and deactivation of GSK3. This allows  $\beta$ -catenin to translocate to the nucleus and activation transcription of target genes [63].

## Notch

Notch signalling is a type of juxtacrine signalling, whereby (in the canonical pathway) membrane bound proteins (Delta-like 1,3,4 or Jagged 1,2) act as ligands for notch receptors (Notch1-4) on an adjacent cell. Upon this interaction taking place, the transmembrane receptor is cleaved and the notch intracellular domain (NICD) is released into the cytoplasm [64]. In the nucleus, the NICD acts as a transcriptional activator in unison with RBPj $\kappa$  (recombination signal binding protein for Ig kappa j), enhancing the transcription of target genes.

In chondrocytes, notch signalling has been shown to influence both endochondral ossification and the pathophysiology of OA [65]. Human chondrocytes express notch receptors and ligands, which was found to be highest in chondrocytes

closer to the articular surface [66]. In a surgical mouse model of OA, there was higher expression of Jagged 1 by OA chondrocytes compared to sham. Moreover, mice that lacked the RBPj $\kappa$  protein showed a resistance to developing OA, suggesting notch signalling contributes to the OA phenotype [67]. In development, conditional knockout of RBPj $\kappa$  in mice, whilst lethal, caused embryonic dwarfism through impairment of the terminal differentiation steps of endochondral ossification, namely vascularisation and matrix degradation (with decreases in expression of MMP13 and VEGF, but not collagen X) [67], suggesting it is responsible for orchestrating the latter stages of endochondral ossification. Its role of inducing hypertrophy and inducing catabolic gene expression is consistent in both the OA and development context, indicating that it has significant function.

## **NF $\kappa$ B**

Nuclear factor kappa B (NF $\kappa$ B) is a pathway involving many transcription factors that are often activated in stressed and inflammatory environments. It is an umbrella term for RelA/p65, RelB, c-Rel, p50 and p52, which share a common feature of an N-terminal Rel homology domain, which is responsible for their dimerisation properties. This can be with inhibitors, such as inhibitor kappa B proteins (I $\kappa$ Bs), or promoter/enhancer complexes. Upon recognition of various stimuli, I $\kappa$ B becomes phosphorylated by IKK (I $\kappa$ B Kinase) and is thus targeted for degradation by the ubiquitin system. This allows NF $\kappa$ B dimers to translocate to the nucleus and initiate transcription of an array of genes.

In chondrocytes, this inflammatory pathway is central to OA pathophysiology. Many catabolic genes, such as matrix metalloproteinases (MMP) and a disintegrin and metalloproteinase with thrombospondin motifs protease (ADAMTS') contain NF $\kappa$ B response elements in their promoters [68, 69]. In this way, NF $\kappa$ B activation enhances catabolic activity in chondrocytes, as well as upregulating other inflammatory mediators such as COX2, PGE2 and iNOS [70]. Accordingly, chondrocyte-specific overexpression of IKK- $\beta$  (causing lack of tonic control of NF $\kappa$ B by I $\kappa$ B) resulted in more rapid onset of OA-like phenotypic changes [71]. The activation of NF $\kappa$ B itself can be initiated by interleukins, adipokines, cytokines and activators of toll-like receptors, as well as physical stimuli like UV

exposure [72]. Chondrocyte viability is also influenced by NF $\kappa$ B signalling. Activation correlates with apoptotic signals and reduced chondrocyte viability [73], and its knockdown is protective against injury-induced chondrocyte apoptosis in mice [74]. NF $\kappa$ B has also been studied in the context of chondrogenesis and development. Genetic ablation of NF $\kappa$ B in mice leads to abnormal limb development and delayed bone growth [75]. *In vitro*, it has also been shown that NF $\kappa$ B signalling promoted growth plate chondrocyte function and longitudinal bone growth. This effect has also shown to be mediated by growth hormone (GH) and insulin-like growth factor 1 (IGF-1) [76].

### **Hypoxia inducible factors**

Hypoxia inducible factors (HIF) are a group of proteins that are involved in the response to hypoxic environments, but have also been shown to regulate aspects of the pathophysiology of osteoarthritis. Owing to the relatively hypoxic environment found in cartilage due to the lack of vascularisation, it is thought that HIF proteins play an important role in homeostasis [77, 78]. HIFs are heterodimers of one of three HIF- $\alpha$  subunits and HIF- $\beta$  subunits, which are classified as basic helix-loop-helix transcription factors (bHLH). HIF proteins are negatively regulated by the ubiquitin ligase system via the hydroxylation of proline residues by HIF-prolyl hydroxylases. This process requires oxygen, and so in hypoxic conditions, the prolyl hydroxylase activity is lessened and HIF proteins are allowed to dimerise and become functional. Genes under HIF protein control often have hypoxia response elements in their promoters.

Importantly, HIF-1 $\alpha$  has been shown to regulate SOX9 and is therefore important to skeletogenesis and development, as SOX9 transcriptionally regulates a number of key chondrocyte genes, such as collagen II [79]. As such it follows that hypoxia has been shown to promote chondrogenic differentiation of mesenchymal stem cells [80]. Moreover, HIF-1 $\alpha$  is a direct regulator of the aggrecan gene [81]. The expression of HIF-1 $\alpha$  is higher in mouse and human OA cartilage, compared to normal [82], and inflammatory/catabolic stimuli increase its expression in chondrocytes via PI3K and p38 MAPK [83]. Interestingly, both OA and normal chondrocytes kept in hypoxic conditions express higher levels of matrix

genes (collagen II, aggrecan) and lower levels of hypertrophic marker collagen X and MMPs, suggesting hypoxia is protective [84]. Additionally, HIF-1 $\alpha$  protects against IL-1 $\beta$  induced apoptosis [85]. HIF-2 $\alpha$  is also significant to skeletogenesis and aspects that are analogous to OA, in that it is a significant regulator of collagen X, which is a marker of hypertrophy, as well as MMP13 and VEGF [86]. Its exogenous expression also initiated cartilage destruction in rabbit and mice [87], however the study of hypoxia in mouse cartilage may not be fully representative of human as it is very thin, and thus does not have a sufficient oxygen barrier [88]. As such, the HIF proteins clearly regulate a number of important homeostatic genes but their involvement in development and OA is somewhat hazy.

### **Cytokines and Chemokines**

Osteoarthritis is traditionally not considered to be a systemically inflammatory disease, although elements of local inflammation are present, such as synovitis as well as chondrocyte phenotype alterations induced by chemokines and cytokines [89]. Cytokines are a broad group of molecules that regulate inflammatory responses, such as interleukins. Chemokines are a subset of the cytokine family whose function is to elicit the chemotaxis of immune cells. Cytokines often exert their effects through GPCRs on the target cell (or the secreting cell, if autocrine), and can mediate a wide range of effects. Chondrocytes express both chemokines and their receptors [90], the former of which has been shown to interact with glycosaminoglycan chains in the ECM [91].

One hypothesis as to the initiation of OA is that tissue damage leads to production of damage associated molecular patterns (DAMPs), such as fibronectin or hyaluronan fragments, which activate toll-like receptors (TLR) and/or nod-like receptors (NLR) on chondrocytes or other cells in the joint microenvironment. Downstream signalling from these receptors can then initiate inflammatory signalling cascades which cause upregulation of catabolic factors and begin the pathologic cycle of inflammation [92]. For example, fibronectin fragments have been shown to cause chondrocyte apoptosis and inhibit chondrocyte differentiation via NOD2 [93]. OA has also been likened to a chronic wound in the sense of inflammation that leads to tissue damage without resolution [94].

The GPCR signalling that arises from chemokine-receptor interactions often activates some of the classical inflammatory signalling pathways, such as NF $\kappa$ B, PI3K/AKT, and JNK/AP-1.

Interleukin-1 $\beta$  has long been an interest for the OA research field and is often used in *in vitro* research as it has the ability to upregulate ECM catabolic genes, such as *MMP13* and *ADAMTS5*. It also is found in higher levels in the synovial fluid of OA joints, in addition to TNF- $\alpha$  [95]. However, its utility as a model of OA in research, its relevance in OA pathophysiology and its utility as a potential target for OA therapy has been questioned [96]. Knockout of IL-1 $\beta$  as well as ICE (a metabolic enzyme essential for conversion of pro-IL1 to active IL-1) in mice did not reduce disease severity when they were subjected to DMM (destabilisation of the medial meniscus) surgery, a murine model of OA [97]. Moreover, human studies have shown that blockade of this pathway does not lead to reduced disease severity nor any significant improvement in the course of the disease [98–101]. Nevertheless, some polymorphisms in the IL-1 gene are increased in OA compared to non-OA [102] and it is useful for *in vitro* research as an activator of catabolic gene expression, even if this might not be disease relevant.

The role of other more classical chemokines have also been studied within the context of OA pathophysiology. Sherwood et al. [103] show a chondroprotective/homeostatic role for CXCR2 in chondrocytes. Its ligand, CXCL6, is maintained within the cartilage ECM by association with HSPG (heparan sulfate proteoglycans) and positively affects homeostasis by stimulating *SOX9* expression and thus maintaining the chondrocyte phenotype. Moreover, in CXCR2 deficient mice, those subjected to the DMM model had more severe OA [104]. Conversely, a *CCL2* knockout mouse had reduced expression of a number of inflammatory genes six hours post DMM surgery compared to WT. Whilst these mice only had a moderately reduced histological OA score compared to WT, they did have significantly delayed onset of pain [105]. Human chondrocytes from OA patients displayed higher levels of hypertrophic markers (*collagen X*, *RUNX2*, *IHH*) when stimulated with exogenous *CCL2* and also upregulated both *CCL2* and *CCR2* in response to IL-17A. These effects were reversed with suppression of *CCR2* [106]. *CCL2* also activated ERK/MAPK pathways via *CCR2* to upregulate MMPs in

both healthy and diseased human chondrocytes, indicating *CCL2* catalyses progression of OA [107]. Conversely, IL3 has been shown to be protective, in reducing the upregulation of catabolic genes stimulated by IL-1 and reducing cartilage destruction in mouse models of OA [108]. Inhibition of another aspect of the innate immune system, the NLRP3 inflammasome, has been shown to reduce cartilage degeneration and inflammation in DMM mice [109]. As such, whilst OA is not necessarily thought of as having an inflammatory aetiology, components of the innate immune system are involved in its progression/course of disease in both *in vitro* and *in vivo* studies.

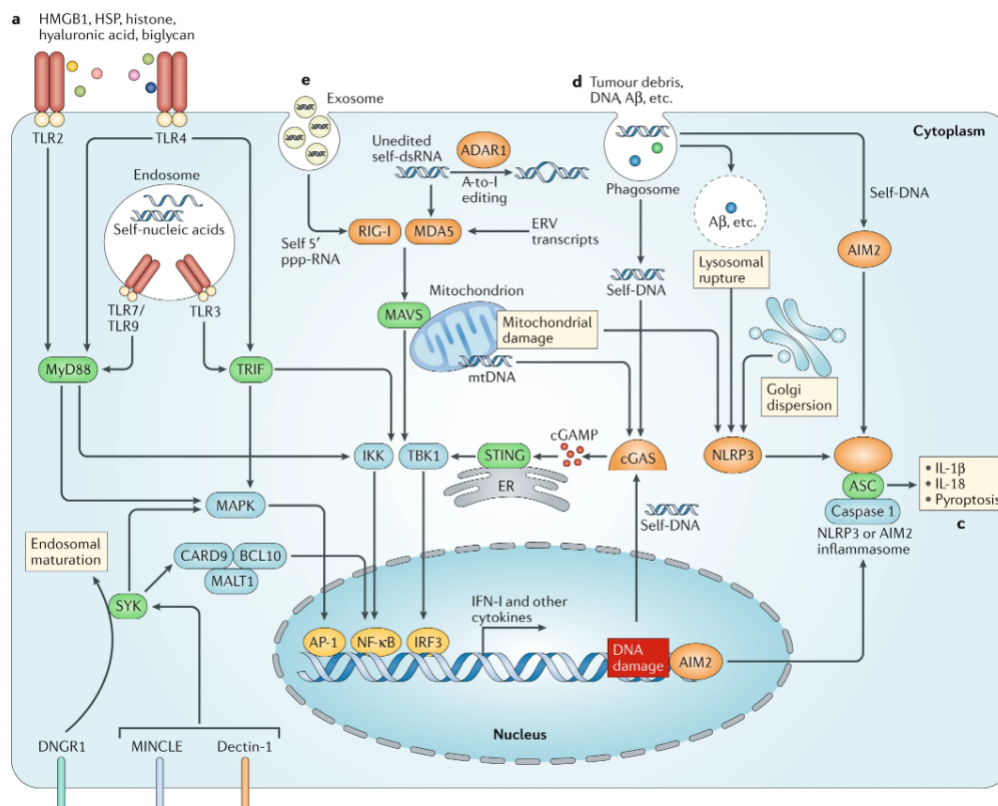


**Figure 1.7: DAMP Signalling Pathway.** Damage associate molecular patterns (DAMP), such as extracellular matrix components can signal to toll-like receptors (TLR) to initiate inflammatory cascades via  $\text{NF}\kappa\text{B}$ , AP-1 and IRF3. This signalling is thought to propagate inflammation in chondrocytes and may contribute to the pathophysiology of OA. Taken from [110].

## 1.4 Purinergic Signalling

The central dogma of purinergic signalling is the idea that nucleotides can act extracellularly as discrete signalling molecules. It was first introduced by Geoffrey

Burnstock in 1972 [111] as a novel transmitter in non-adrenergic, non-cholinergic nerves supplying the guinea pig taenia coli. It was, however, met with incredulity in the field owing to the reputation of ATP as the universal intracellular energy store [112]. Nevertheless, the first purinergic receptor (P2Y1) was cloned in 1993 [113], followed by identification of a further 18 receptors, which today, have been shown to have widespread expression and function [114]. There are a number of sources of extracellular ATP. It is a large molecule with a net negative charge, so cannot pass the plasma membrane by simple diffusion. Its release is thought to be mediated by vesicular exocytosis or release via connexin/pannexin channels in homeostatic conditions, the release of which can be increased in response to hypoxia, mechanical stress or apoptosis. Its release from cells can also occur as a result of cell membrane instability and disruption by traumatic forces [115]. Pharmacological manipulation of purinergic signalling has been translated into human benefit, as clopidogrel and ticagrelor (clinically used P2Y12 antagonists) inhibit platelet aggregation and are thus used as anti-thrombotic drugs.

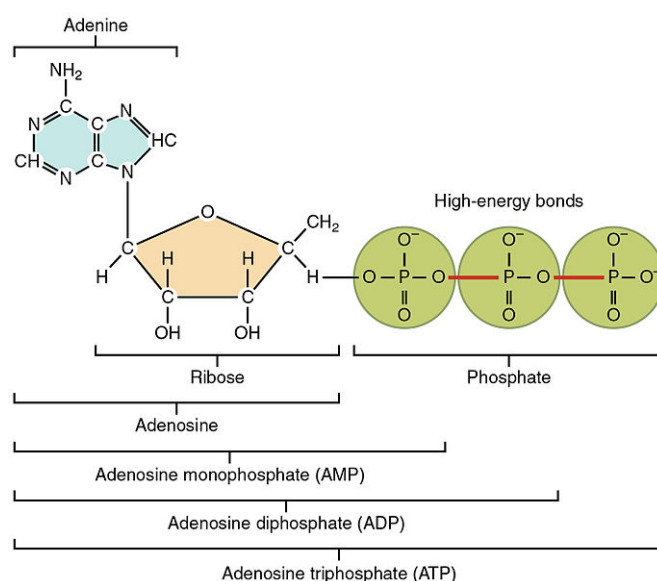


**Figure 1.8: Nucleotide Structure.** Nucleotides are biological molecules composed of a nitrogenous base, a ribose sugar and phosphate groups. They form the basis of DNA, RNA and are essential in cellular metabolism - as well as being agonists for a group of receptors called purinergic receptors [116].

Nucleotides are important molecules for cellular metabolism, as well as the structure of biological molecules like DNA and RNA. The basic structure begins with adenine, a purine nitrogenous base, which when bonded to a ribose sugar

molecule via a glycosidic bond, becomes adenosine. Uracil and uridine (uracil bonded to a ribose sugar) nucleotides also have action at some purinergic receptors. The ribose sugar can be phosphorylated to form adenosine tri/di/monophosphate. These are high energy bonds, which makes the molecule useful in energy metabolism.

### 1.4.1 Adenosine Receptors

There are four GPCR adenosine receptors (namely A1, A2A, A2B, A3) and have the characteristic seven transmembrane domains of a GPCR. They are responsive to adenosine, a nucleoside produced from the complete dephosphorylation of ATP. Adenosine can be synthesised rapidly extracellularly due to membrane bound ectonucleotidases and as such has ubiquitous distribution within human physiology. Adenosine itself is metabolised by adenosine deaminase to inosine. Research into adenosine signalling has unveiled a role for it in many disease processes and there is currently an A2A receptor antagonist licensed for Parkinson's disease in Japan and the US [117]. Interestingly, there is also epidemiological evidence for protective effects of caffeine intake (a broad adenosine receptor antagonist) on the risk of getting cardiovascular disease and cancer, yet confers a higher risk of fracture in women [118].

**Table 1.1: Adenosine Receptors.** Adenosine Receptors are a group of four GPCRs that are activated by adenosine and couple to  $G_i$ ,  $G_q$  or  $G_s$ , each receptor being activated by differing concentrations of adenosine [119].

Receptor	A1	A2A	A2B	A3
G Protein	$G_{i/o}$	$G_s$	$G_s/G_q/11$	$G_i/G_q/11$
Adenosine EC <sub>50</sub> (nM)	1-10	30	1000	100

### 1.4.2 P2X Receptors

P2X receptors are ionotropic ligand gated ion channels whose ligand is ATP, of which there are seven named chronologically (P2X1-7). They are trimeric i.e. formed from three subunits which can be the same (homomeric) or different (heteromeric). The binding site of ATP lies between subunits, and when bound, it causes a conformational change in the protein, allowing for the passage of cations across the plasma membrane. This process can have varying downstream effects

based on cell type. Research into this signalling system has uncovered a role for P2X receptors in the cardiovascular system [120], cancer progression [121] and inflammation [122]. Clinically, gefapixant, a P2X3 antagonist, has been recently approved in Japan for chronic cough [123].

**Table 1.2: P2X Receptors.** P2X receptors are ionotropic receptors gated by ATP. They are formed from three subunits, which can be the same or different, forming a heterogeneous receptor group. [124].

Homomeric Receptor	P2X1	P2X2	P2X3	P2X4	P2X5	P2X6	P2X7
ATP EC <sub>50</sub> (μM)	0.56-0.7	2-8	0.5-1	1-10	0.4-10	12	100

### 1.4.3 P2Y Receptors

P2Y receptors are GPCRs that are responsive to a wider range of nucleotides (including uridine nucleotides), of which there are eight (P2Y1,2,4,6,11-14). Whilst the origin of adenosine nucleotides arises from the metabolism of ATP as the universal energy molecule, UTP and its metabolites (including UDP-glucose) are thought to arise from acting as donors in glycosylation reactions. UDP and UDP-sugars are synthesised in the cytosol and translocate to the lumen of the golgi apparatus and endoplasmic reticulum (ER), where both molecules can be released by vesicle exocytosis. UDP can also be generated from the extracellular metabolism of UTP, however UDP-glucose cannot be metabolised by NTPDases [125]. As well as the previously mentioned anti-thrombotics targeting P2Y12 that are already used therapeutically, P2Y1 inhibition is being investigated for utility in treating Alzheimer's disease [126].

**Table 1.3: P2Y Receptors.** P2Y receptors are a group of eight GPCRs which couple to  $G_q$ ,  $G_s$  or  $G_i$ , which are activated by adenosine and uridine nucleotides. [127].

Receptor	P2Y1	P2Y2	P2Y4	P2Y6	P2Y11	P2Y12	P2Y13	P2Y14
G Protein	$G_q$	$G_q$	$G_q$	$G_q$	$G_q/G_s$	$G_i$	$G_i$	$G_i$
Agonist	ADP	UTP	UTP	UDP	ATP	ADP	ADP	UDP-glucose
EC <sub>50</sub> (μM)	10	0.06	0.63	0.63	1.9	0.06	0.01	0.39

### 1.4.4 GPCR Intracellular Signalling

G protein coupled receptors (GPCRs) are a ubiquitous class of seven-transmembrane domain proteins that are paramount to cellular signalling. They initiate signalling

cascades from extracellular stimuli that allow the cell to respond to its environment. The seven transmembrane domains are associated with an intracellular G protein, which facilitates the downstream signalling. A G protein is a complex of three subunits namely alpha, beta and gamma, of which there are four major G protein families;  $G_s$ ,  $G_{q/11}$ ,  $G_{i/o}$  and  $G_{12/13}$ .

In its resting state, the  $G\alpha$  subunit of the G protein is bound to the nucleotide GDP and the two other subunits,  $G\beta$  and  $G\gamma$ . Upon ligand binding, there is a conformational change in the transmembrane domains, leading to dissociation of the inactive g protein heterotrimer. Initially,  $G\alpha$  dissociates from GDP, leading to separation of the  $G\alpha$  and  $G\beta,G\gamma$  homodimer. The  $G\alpha$  subunit then binds GTP owing to the high intracellular concentrations. Dependent on from which family the G protein is, it will go on to elicit different downstream signalling effectors. For example,  $G_{q/11}$  enhances phospholipase C activity to cleave phosphatidylinositol 4,5-bisphosphate (PIP2) into inositol 1,4,5-trisphosphate (IP3) and diacylglycerol (DAG). IP3 can then activate IP3 receptors on the endo/sarcoplasmic reticulum and cause calcium release. The increase in intracellular calcium concentrations can then affect other cellular behaviours, often mediated by calmodulin/calmodulin kinase II (CaMKII).  $G_s$  differs in that it often enhances adenylate cyclase activity, whereas  $G_{i/o}$  inhibits it, and can influence cell behaviour via this pathway.  $G_{12/13}$  activates RhoGEF. Signalling is terminated when GTP is hydrolysed and the inactive heterotrimer of G protein subunits is reformed. Alternatively, receptors can be phosphorylated by GPCR kinases (GRKs) and internalised by arrestin-mediated endocytosis.

## 1.5 Purinergic Signalling in the Joint

### 1.5.1 Purinergic Signalling in Bone

The effects of purinergic signalling in bone have been better characterised than that of cartilage. The P2Y2 receptor (whose primary ligand is UTP) has been shown to have definite physiological effects in bone, but there is not a general consensus on whether it is protective or deleterious. One knockout model shows P2Y2 to be a negative modulator of bone formation, as osteoblasts from P2Y2

null mice displayed increased bone formation, which is supported by *in vitro* data showing an inhibitory role for P2Y2 in this process [128, 129]. However, a separate P2Y2 null mouse had decreased bone volume, thickness and stiffness, suggesting a protective role for P2Y2 [130]. This is also supported by epidemiological evidence, as a gain of function P2Y2 SNP resulted in increased bone mineral density [131]. Moreover, P2Y2-null mice were not rescued from muscle paralysis induced bone loss, suggesting it is not protective in this process [132].

P2X7 has also shown to play a role in the homeostasis of bone cells, through expression by osteocytes and osteoblasts, but also by immune cells in the microenvironment [133]. It has been shown to be involved in the anabolic response to mechanical loading in bone, as P2X7-null mice do not increase bone volume to the same extent as wild type mice [134], an effect which may be mediated by  $\beta$ 3-integrins [135]. There has also been a link drawn between P2X7 and Wnt signalling in bone cells as BzATP enhanced the Wnt3a elicited nuclear localisation of  $\beta$ -catenin, an effect that was inhibited by P2X7 antagonists. Moreover, responses to Wnt3a were diminished in calvarial cells lacking P2X7 [136]. Contrastingly, another group found that BzATP diminished Wnt signalling and inhibited markers of osteogenesis [137]. Polymorphisms in the P2X7 gene have been associated with increased risk of stress fractures [138]. The action of other receptors has been summarised in Table 1.4.

### **1.5.2 ATP as a Modulator of Chondrocyte Phenotype**

Evidence for the role of purinergic signalling in cartilage dates back to as early as 1991, where ATP and ADP were found to increase prostaglandin E2 (PGE2) production in human articular chondrocytes alongside mRNA expression for some adenosine receptors and *P2RY2* [157, 158]. PGE2 was an emerging mediator of inflammation at the time, and has since been shown to induce collagen degradation and enhance IL-1 signalling [159]. In bovine chondrocytes, conflicting studies found ATP to inhibit proteoglycan release as explants [160], whereas it stimulated proteoglycan and collagen accumulation in pellet cultures [161]. Mechanical loading, a significant factor in the joint, was found to cause ATP release by cells in both bovine and porcine chondrocytes, an effect that may be mediated

**Table 1.4: Action of Purinergic Receptors on Bone.**

Receptor	Action	Reference
A1	A1R null mice have increased bone volume.	[139]
A2A	Inhibits osteoclast differentiation. A2A null mice had decreased bone volume.	[140]
A2B	A2B null mice have reduced bone mineral density and bone formation.	[141]
P2X1	Negatively regulates bone mineralisation.	[142]
P2X4	KO mice have improved bone structure and strength, dependent on age and gender.	[143]
	Dose dependent reduction in bone formation with two antagonists, 5-BDBD and PSB-12062.	[144]
P2X5	Mediates ATP-induced inflammasome activation and inflammatory resorptive activity in osteoclasts. No P2X5 null phenotype.	[145]
	Involved in osteoclast maturation in association with MEP50.	[146]
P2X7	Negatively regulates bone mineralisation.	[142]
	P2X7 null mouse had increased bone loss in osteoporosis model.	[147]
P2Y1	Ultrasound-induced osteoblast proliferation mediated by P2Y1.	[148]
	Mediates ADP-induced bone resorption by osteoclasts.	[149]
P2Y2	P2Y2 knockout does not prevent bone loss in dystrophic model.	[132]
	Mediates ERK1/2 phosphorylation in response to fluid flow and enhances osteogenesis.	[130]
P2Y6	Stimulates osteoclastogenesis and resorptive activity.	[150]
	Activates NFkB and mediates osteoclast survival.	[151]
	Involved in bone cell mechanotransduction.	[152]
P2Y12	Osteoclasts from P2Y12 null mice had diminished resorptive activity	[153]
	P2Y12 antagonist inhibits mineralised bone nodule formation and osteoclast resorptive activity.	[154]
	Clopidogrel (P2Y12 antagonist) use associated with fracture risk.	[155]
P2Y14	Causes osteoblast proliferation and knockout had longer tibias.	[156]

by primary cilia [162–164]. Fluid flow shear stress increased ATP secretion as well and promoted lubricin production [165]. Chondrocytes were also found to possess the enzymes responsible for metabolism of extracellular ATP in 1995 [166]. In 1997, chick chondrocytes were shown to possess a nucleotide-dependent intracellular calcium elevation from the endoplasmic reticulum in their mature state, which was one of the first of many to show this response to ATP in chondrocytes [167–169]. Addition of inflammatory mediators like interleukin-1 $\beta$  enhanced this response, eluding to its involvement in inflammation [170]. Interleukin-1 $\beta$  has also been shown to reduce ATP release from murine chondrocytes [171].

### 1.5.3 Adenosine Receptors

There has been a long standing link between activity of adenosine at its receptors and inflammation, in chondrocytes in addition to other cell types. Methotrexate, a commonly used disease modifying anti-rheumatic drug (DMARD), is thought to mediate its effects in part due to its ability to increase adenosine release at sites of inflammation [172]. Interestingly, prenatal caffeine (a broad adenosine receptor antagonist) administration caused offspring to have reduced cartilage integrity in mice, suggesting a protective role for adenosine [173]. However the action of adenosine may have different effects at each receptor, which may facilitate a dose-dependent effect as the receptors have different affinities for adenosine i.e. the A<sub>2B</sub> receptor has the lowest affinity and is therefore only activated in high concentrations [119].

There is relatively scant data regarding the A<sub>1</sub> and A<sub>3</sub> receptors in chondrocytes. All four receptors are expressed by bovine chondrocytes [174]. There are reports that neither A<sub>1</sub> nor A<sub>3</sub> are expressed by human articular chondrocytes [158], however A<sub>1</sub> mRNA was detected and possibly implicated in facilitating calcium transients in response to adenosine in human chondroprogenitor cells [175]. An A<sub>3</sub> receptor knockout mouse developed progressive articular cartilage loss, hypertrophy and matrix degradation, suggesting the A<sub>3</sub> receptor is protective [176]. This effect may be mediated by inhibition of the NLRP3 inflammasome and caspase-1/GSDMD signalling [177].

Comparatively, there is much more data and more of a consensus in the field pertaining to the impact of the other adenosine receptors. Intraarticular injection of adenosine in both rat and mouse models of OA was found to be protective [178]. More specifically, A<sub>2A</sub> null mice develop spontaneous OA within 16 weeks, a phenotype that is also seen with ablation of ecto-5′nucleotidase gene, the enzyme that catalyses adenosine metabolism from ATP [171]. Moreover, the A<sub>2A</sub> null chondrocyte transcriptome mimics that of OA chondrocytes [179], an effect that is potentially mediated by effects on mitochondrial metabolism. A<sub>2A</sub> null mice have mitochondrial swelling, dysfunction and ROS accumulation, a phenotype that is common to OA pathophysiology [180]. This effect is thought to be mediated by the FoxO group of transcription factors [181], and has also been

shown to reduce markers of senescence, including p53 variants and p21 and p16 [182]. A2A agonism is being tested currently as a therapeutic in canine models of OA [183]. The protective effect of adenosine was reversed by antagonism of the A2A receptor, but not the A2B receptor [171], suggesting their signalling is heterogeneous. The role of A2B has been investigated in the context of chondrogenesis. A2B agonism, in combination with shockwaves, inhibited the chondrogenic differentiation of human mesenchymal stem cells [184], and was separately found to push cells towards an osteogenic differentiation fate [185].

#### **1.5.4 P2X Receptors**

Expression of *P2RX2*, *P2RX4* and *P2RX7* has been documented in all layers human articular cartilage [186]. *P2RX1* and *P2RX3* mRNA was identified in bovine chondrocytes and found to be functional in terms of NO and PGE2 release [174]. Connexin 43 was also found to be expressed by articular chondrocyte primary cilia [186], which is significant, as ATP release, potentially by connexin hemichannels in response to loading, and subsequent purinergic signalling has been suggested to be involved in the mechanism by which chondrocytes can detect mechanical load. Porcine chondrocytes have been shown to release ATP in response to loading in pellet culture [162]. Early evidence used bovine chondrocytes in mechanically loaded agarose constructs. When loaded, there was suppressed nitric oxide (NO) release, an effect that was reversed by gadolinium and suramin, broad spectrum inhibitors of stretch-activated calcium ion channels and purinergic signalling, respectively [187]. A study from the same year found intracellular calcium release caused by cyclic compression in the same agarose model, that was blocked by similar inhibitors of purinergic signalling [188]. CITED2 may also be involved in this mechanotransductive pathway, along with HIF-1 $\alpha$ . Uniaxial strain on chondrocytes caused downregulation of some MMPs, which was accompanied by upregulation of CITED2. This effect was blocked by some inhibitors of purinergic signalling, including EGTA and suramin [189], and may be mediated by primary cilia [164]. ATP release from porcine chondrocytes was stimulated by ANK and increased by ivermectin, a P2X4 positive allosteric modulator, but inhibited by Brilliant Blue G, a more broad-spectrum inhibitor (includ-

ing P2X4) [190]. Extracellular ATP is relevant to the pathology of CPPD (calcium pyrophosphate disease) as ATP is broken down to inorganic pyrophosphate and complexes with calcium to form crystals [191]. The idea that ATP may be involved in chondrocyte mechanotransduction is being utilised in the effort to engineer cartilage tissue for therapeutic purposes. Exogenous ATP is thought to mimic the stimulatory and protective effect of mechanical loading on engineered tissue and has led to progress in this effort [192, 193].

There is also literature surrounding a role for *P2RX4* in chondrogenesis. In ATDC5 cells, *P2X4* mRNA was expressed along with *P2RX3*, *P2RX5* and *P2RX7*. It mediated calcium oscillations that are a prerequisite for cellular condensation via cAMP PKA signalling. Moreover, blockade of P2X4 with 5-BDBD blocked the chondrogenic differentiation of the cells [194]. In a separate model system, chick high density chondrocyte cultures, P2X4 caused intracellular calcium transients on the third day of culturing, and exogenous ATP addition upregulated SOX9 and matrix production [195].

The P2X7 receptor, also reported to be reproducibly expressed by chondrocytes, is often associated with inflammation [196]. In rabbit articular chondrocytes, P2X7 mediates ATP-induced cytotoxicity and increased PGE2 release [197]. P2X7 antagonism reduced cartilage damage in a rat MIA (monosodium iodoacetate) model of OA, suggesting its signalling has a catabolic effect on cartilage [198], potentially via activation of NF $\kappa$ B [199].

### 1.5.5 P2Y Receptors

*P2RY2* has shown to be expressed by human articular chondrocytes [158], as well as other subtypes in mouse cell lines (ATDC5) [200] and rat chondrocytes [201]. Early evidence also showed the P2Y2 receptor to increase the IL-1 induced release of PGE2 in human chondrocytes [158]. A similar effect of P2Y2-mediated PGE2 release was also seen in rabbit chondrocytes, accompanied by phosphorylation of p38 MAPK and ERK proteins [202]. In a different context, in differentiated ATDC5 cells, oscillatory flow caused increased *COX-2* and *aggrecan* expression. P2Y2 was upregulated with oscillatory flow, and its overexpression caused increased ERK phosphorylation [203]. ERK phosphorylation was also

seen in rat chondrocytes, upon stimulation by ATP, UDP and ADP (and their non-hydrolysable phosphorothiorate analogues), an effect that was dependent on protein kinase C and phospholipase D as well as integrin interactions with certain ECM structures like fibronectin [201].

In the ATDC5 chondrogenesis model, *P2RY1* and *P2RY13* were more highly expressed in differentiated cells than undifferentiated, and it was found that UDP and ADP caused migration of differentiated ATDC5 cells and upregulation of collagen II [200], indicating these nucleotides are protective. P2Y12 may also be protective. Clopidogrel, a clinical P2Y12 antagonist used for anti-thrombotic activity, increased circulating levels of cytokines and histological markers of inflammation in a rat model of arthritis. This may not be relevant to OA as systemic inflammation is more commonly found in rheumatoid arthritis, but indicates that P2Y12 is involved in inflammation in the joint [204]. Conversely, an inhibitor of P2Y11, NF157, reduced the TNF- $\alpha$ -induced expression of MMPs and ADAMTSs and subsequent action of these enzymes to degrade the ECM in SW1353 cells. The expression of *P2RY11* in OA chondrocytes is also higher than normal chondrocytes [205], suggesting P2Y11 may contribute to pathology. In rat bone marrow mesenchymal stem cells (BM-MSC), the effect of P2Y6 in conjunction with titanium dioxide nanotubes has been studied in the pursuit of improving osseointegration of titanium implants. Titanium nanotubes stimulate osteogenesis in these cells, which both upregulated P2Y6 expression, and the osteogenic effect was enhanced by P2Y6 activation/reduced by its inhibition. This effect was mediated by PKC- $\alpha$  and ERK1/2 [206]. UDP was also found to cause NF $\kappa$ B nuclear translocation in rabbit osteoclasts, as determined by immunofluorescent methods [151], which is a regulator of chondrogenesis and endochondral ossification [207]. In a separate system, the differentiating chick mesenchyme, ATP was demonstrated to be released, and P2Y1 inhibited cartilage formation in micromass cultures via overexpression, suggesting it negatively regulates this process [208].

## 1.5.6 Hypothesis and Aims

Whilst there is relatively little known about the role of purinergic signalling in chondrocytes, there is evidence that extracellular nucleotides can affect signalling.

This is evident from the publications that detail expression of purinergic receptors by chondrocytes, as well as larger studies involving animal models of disease. There is a large significance to understanding better how chondrocytes signal because of the large disease burden that Osteoarthritis presents. As a disease, it is poorly understood and as a result, has sub-optimal treatment options. Consequently, pursuing previously untapped facets of basic chondrocyte biology is important in the endeavour to improve treatment outcomes. The overarching hypothesis is that purinergic signalling has an influence on overall chondrocyte phenotype, potentially with relevance to disease states. The aims and objectives of the thesis are;

- To undertake methods development in the field of chondrocyte research pertaining to which models are appropriate to use.
- To determine if there are any differentially expressed purinergic receptors across disease states
- To determine if any such receptors may influence disease processes and overall chondrocyte homeostasis

# Chapter 2

## Methods

### 2.1 Cell Culture

SW1353, C28/I2 and ATDC5 cells were grown to approximately 80% confluency and passaged in a 1 to 4 ratio every 2-3 days. Primary chondrocytes were used at passage 1 or 2. Cells were cryopreserved in foetal calf serum (FCS) containing 10% (v/v) DMSO and frozen in a Nalgene Mr. Frosty at -80°C to facilitate slow cooling, with subsequent long-term storage in liquid nitrogen.

#### 2.1.1 SW1353

SW1353 cells (ATCC) are a human chondrosarcoma cell line. They were cultured in Dulbecco's modified eagle medium (DMEM) low glucose GlutaMAX (Gibco) with 10% (v/v) heat-inactivated FCS (Gibco) and 1% (v/v) penicillin/streptomycin (10,000U/mL) (Gibco).

#### 2.1.2 C28/I2

C28/I2 cells are a human SV40 immortalised costal chondrocyte cell line and were donated from the lab of Mary Goldring (Hospital for Special Surgery, New York). They were maintained in the same conditions as SW1353 except for the use of 10% non-heat inactivated FCS.

### **2.1.3 1321N1**

1321N1 are a human astrocytoma cell line that do not have any nucleotide-elicited calcium responses. P2Y6 expressing 1321N1 were made previously by lentiviral integration by past members of the Fountain lab, University of East Anglia. They were maintained in the same conditions as SW1353.

### **2.1.4 ATDC5**

ATDC5 cells are a murine embryonic teratocarcinoma cell line and were kindly supplied by Dr. Katarzyna Pirog (Newcastle University). They were maintained in 1:1 DMEM/Hams F12 Nutrient Mix (Gibco), supplemented with 5% (v/v) heat inactivated FCS and 1% (v/v) 10,000 U/mL Pen/Strep (Gibco).

#### **Induction of ATDC5 Chondrogenic Differentiation**

ATDC5 cells were plated in 24 well plates at a density of  $5 \times 10^4$  cells/well, and grown to confluency in normal growth medium. To induce differentiation, media was changed to differentiation media (normal growth media supplemented with Insulin, Transferrin and Selenium (ITS) 1X (Invitrogen) and 50 $\mu$ g/mL L-ascorbic acid 2-phosphate (Sigma)) and cultured for 21 days, with media changes thrice weekly, being careful not to dislodge the cell layer.

### **2.1.5 Human BM-MSC**

Human BM-MSC (bone-marrow derived mesenchymal stem cells) were kindly provided by Dr. Matt Barter (Newcastle University) and isolated as previously described [209]. They were maintained in the same conditions as SW1353 with the addition of 5ng/mL FGF-2 (Invitrogen) for maintenance of phenotype.

#### **Induction of BM-MSC Chondrogenic Differentiation**

Cells were pelleted by centrifugation and resuspended in chondrogenic medium (DMEM GlutaMax high glucose supplemented with 10ng/mL TGF- $\beta$ 3, 100nM dexamethasone, 1X ITS premix (Invitrogen), 50 $\mu$ g/mL L-ascorbate 2-phosphate and 40 $\mu$ g/mL L-proline) to 1 million cells/mL. 100 $\mu$ L of cell suspension was then

pipetted into a round bottom 96 well plate and centrifuged in the plate for 5 minutes at 500xg. The cell pellets were then maintained in this media for 14 days, with media changes every 3 days, being careful not to aspirate the pellet.

### **2.1.6 Primary Human Chondrocytes**

Human cartilage was collected under University of East Anglia and Norwich Research Park Biorepository ethical approval from patients undergoing arthroplasty surgery. Cells were maintained in the same conditions as SW1353 cells, grown to confluency and used in experiments at passage 1 or 2.

#### **PHC Isolation**

Femoral heads or knee joints were obtained in sterile phosphate buffered saline (PBS) following surgical procedures. In a ducted biosafety hood, cartilage pieces were dissected off the subchondral bone and placed in PBS. The cartilage pieces were incubated overnight at 37°C, shaking at 180rpm in 5ml/g cartilage digestion medium (DMEM GlutaMAX low glucose supplemented with 0.4% (w/v) HEPES, 0.1% (w/v) collagenase type 1A (Sigma), 1% (v/v) 10,000 U/mL pen/strep). Following the digestion period, cells were passed over a 70µM cell strainer (BD Falcon) and the eluent was centrifuged at 180xg for 5 minutes. The cell pellet was washed in standard culture media (described above) and centrifuged again. The cells were then plated at a density of  $4 \times 10^4$  cells/cm<sup>2</sup> of culture vessel and allowed to adhere over a 9-day period and were either used in experiments or cryopreserved.

## **2.2 Compounds & Reagents**

UDP, ADP, MRS2578, MRS2693 and thapsigargin were purchased from Tocris Bioscience. UDP-βS was purchased from Jena Bioscience. Recombinant human IL-1β, TNF-α and TGF-β3 were purchased from R&D Biosystems. ATP and FURA-2 AM were purchased from Abcam. All else was purchased from Sigma Aldrich or Thermo Fisher.

## **2.3 RNA Extraction and Reverse Transcription**

### **2.3.1 RNA Extraction**

Media was removed from cultured cells and 500 $\mu$ L of TRIzol (Invitrogen) was added to each well of a six-well plate to lyse cells and transferred to a 1.5mL Eppendorf. Following a 10-minute incubation at room temperature with TRIzol, 250 $\mu$ L of chloroform was added and the Eppendorf was inverted 10 times. After another 10 minute incubation at 4°C, the sample was centrifuged at 12,000xg for 15 minutes at 4 °C. The upper, aqueous layer was carefully pipetted into a new Eppendorf, avoiding transferring any interface of the aqueous and organic layers. For small inputs, 10 $\mu$ g of RNase-free glycogen (Invitrogen) was added to the aqueous phase to aid in nucleic acid recovery by forming a more visible pellet. 400 $\mu$ L of 2-propanol was added and inverted to mix thoroughly, in order to precipitate the RNA. Another 10 minute incubation at 4°C allowed for complete precipitation, followed by centrifugation at 12,000xg for 10 minutes at 4°C. Subsequently, the supernatant was removed carefully, avoiding disrupting the pellet. 500 $\mu$ L of cold 75% (v/v) ethanol was added to the pellet, and vortexed briefly, followed by another centrifugation step at 7,500xg for 5 minutes at 4°C. The ethanol supernatant was removed and the pellet was allowed to air dry for 10 minutes. The pellet was then resuspended in 20 $\mu$ L RNase-free water and incubated at 50°C for 5 minutes followed by storage at -80°C. If TRIzol was not used, RNeasy kit (Qiagen) was used according to manufacturers' instructions.

### **2.3.2 Reverse Transcription**

MMLV (moloney murine leukaemia virus) reverse transcriptase (Invitrogen) was used to synthesise cDNA from RNA. Extracted RNA was quantified using Nanodrop spectrophotometer (Invitrogen) and equalised across experimental samples in 8 $\mu$ L of RNase-free water. 2 $\mu$ L of 200ng/ $\mu$ L random hexamers (Invitrogen) were added and incubated at 65°C for 5 minutes. Reactions were then set up as in Table 2.1.

Following addition of 11 $\mu$ L of MMLV reaction mix, samples were incubated

**Table 2.1:** 1X Reverse Transcriptase Reaction

MMLV	1 $\mu$ L (200 U)
5X RT buffer	4 $\mu$ L
DTT 0.1M	2 $\mu$ L
dNTPs (2.5mM each)	2 $\mu$ L
Water	2 $\mu$ L

at 25°C for 10 minutes, 37°C for 50 minutes followed by 70°C for 10 minutes to inactivate the enzyme.

## 2.4 (q)PCR

### Primer Design

Primers were either taken from publications as indicated or designed using NCBI primer blast to be specific to the sequence, be intron spanning, have a GC content not exceeding 60% and have no or low predicted secondary structures. Primers were ordered lyophilised from Merck, reconstituted to 100 $\mu$ M and stored at -20°C. They were used at a final concentration of 200nM. Annealing temperatures for primers pairs were tested in optimisation stages  $\pm$  5°C around the specified melting temperature.

### PCR

cDNA was amplified using 2X PCR Master Mix (Promega) or Cloneamp HiFi PCR Premix (Takara) and visualised using agarose gel electrophoresis. PCR products were run on a 1% (w/v) agarose gel in 1X TAE (10X: 400mM Tris, 200mM glacial acetic acid and 10mM EDTA pH 8.0) and run for 1 hour at 100V. Subsequently, the gel was bathed in 5% (v/v) ethidium bromide in 1X TAE buffer (v/v) for 15 minutes and imaged using a UVP ultraviolet imager.

For quantitative PCR, reactions are set up as follows for 20 $\mu$ L reactions in a 96 well plate. 384 well plates were prepared at 0.5X. The polymerase used was PCR Biosystems 2X probe mix Lo ROX. Primers and probes were purchased from Merck and supplied lyophilised. Once reconstituted to 100 $\mu$ M, they were further diluted to 10 $\mu$ M as a working stock. Probe-based assays utilised an oligo tagged

with a 5' FAM and 3' TAMRA, also supplied lyophilised from Merck, and were reconstituted to a working stock of 5 $\mu$ M. Some assays were designed using the Roche Universal Probe library assay design center, and Roche universal probes were used also at 5 $\mu$ M working stock. Some primers were used with SYBR green 100X (Invitrogen), in which case the probe was replaced with 0.2 $\mu$ L of 100X SG and made up to volume with water. Where SYBR green was used in place of a probe, a melt curve analysis was run post amplification, and PCR products were run on an agarose gel to confirm specificity of the primers.

**Table 2.2:** 1X PCR Reaction

2X Taq Master Mix	12.5 $\mu$ L
10 $\mu$ M F/R Primers	0.5 $\mu$ L each
cDNA	50ng
Water	To 25 $\mu$ L

**Table 2.3:** 1X qPCR Reaction

2X Probe Mix	10 $\mu$ L each
10 $\mu$ M F/R Primers	0.5 $\mu$ L
cDNA (2ng/ $\mu$ L)	2.5 $\mu$ L housekeeper, 5 $\mu$ L GOI
Probe (5 $\mu$ M)	0.5 $\mu$ L
Water	5 $\mu$ L housekeeper, 2.5 $\mu$ L GOI

Cycling conditions were as follows.

**Table 2.4:** PCR cycling conditions

1X Denaturation 95 $^{\circ}$ C 2 mins
40X: Denaturation 95 $^{\circ}$ C 30s Annealing T <sub>m</sub> $^{\circ}$ C (variable) Extension 72 $^{\circ}$ C 60s.
1X Final Extension 72 $^{\circ}$ C 5 mins

**Table 2.5:** qPCR cycling conditions

1X Initial hold 50 $^{\circ}$ C 2 mins
1X Denaturation 95 $^{\circ}$ C 2 mins
40X: Denaturation 95 $^{\circ}$ C 10s Annealing 60 $^{\circ}$ C 30s

qPCR C<sub>T</sub> values were analysed using the Comparative C<sub>T</sub> method [210, 211]. C<sub>T</sub> values from gene of interest (GOI) were subtracted from housekeeper values.

Biological and technical replicates of housekeeper genes were within 1.5  $C_T$  of each other as a quality check of technical variation, as theoretically there should be no biological variation in housekeeper gene expression.  $2^{-C_T}$  was then carried out to reverse the direction of change i.e. so that a lower  $C_T$  value results in a higher value. If there was high inter-replicate variability, fold change was calculated from an experimental control.

## 2.5 SDS PAGE

SDS PAGE (sodium dodecylsulfate polyacrylamide gel electrophoresis) was used to detect proteins in cell lysates. Cultured cells were scraped into 1mL of cold PBS pH 8.0 and centrifuged at 300xg for 3 minutes. The cell pellet was then re-suspended in 100 $\mu$ L of RIPA buffer (Thermo Fisher) supplemented with 1X Halt protease inhibitor cocktail (Fisher) and incubated on a vertical rotary mixer for 30 minutes at 4°C, followed by centrifugation at 14,000xg for 15 minutes to collect cell debris. The supernatant was collected and the protein measured and equalised using the Bradford assay (Bio-Rad). Bovine serum albumin (BSA) was used to construct a standard curve (2mg/mL to 50 $\mu$ g/mL) by mixing 200 $\mu$ L of 1X Bradford reagent with 2 $\mu$ L of protein lysate or BSA standard. The reaction was mixed by pipetting and the absorbance read at 595nm. Protein concentrations were extrapolated from the BSA standard curve. Once equalised to the same concentration, DTT was added to a concentration of 50mM as well as 5X loading buffer (Bio-Rad), and the samples were boiled at 96°C for 5 minutes prior to loading.

10% (w/v) polyacrylamide gels were cast according to the following recipe using the Bio-Rad mini-PROTEAN system (Table 2.6), using 10X resolving buffer (1.5M Tris base, 0.4% (w/v) SDS, pH 8.8) and 10X stacking buffer (500mM Tris base, 0.4% SDS, pH 6.8). Initially, the resolving layer was cast first, and covered in a layer of isopropanol. When set, the isopropanol was poured off and the stacking layer was cast and allowed to set with the combs in place.

**Table 2.6:** 10% (v/v) Acrylamide Gel 1X

Lower Resolving Layer	Upper Stacking Layer
3mL 30% (w/v) acrylamide 2.5mL 10X resolving buffer 4.5mL water 50µL 10% (w/v) APS 7µL TEMED	0.65mL 30% (w/v) acrylamide 1.25mL 10X stacking buffer 3mL water 25µL 10% (w/v) APS 5µL TEMED

Once loaded into the polyacrylamide gel along with the Bio-Rad precision plus dual colour standards, running buffer (25mM Tris base, 190mM glycine, 0.1% (w/v) SDS, pH 8.3) was added to the inner chamber. Voltage was applied at 90V until the samples had passed the stacking layer, and then increased to 140V until the samples had reached the bottom of the gel.

Transfer of the protein to a polyvinylidene difluoride (PVDF) membrane was achieved by sandwiching the gel on top of the membrane flanked by filter paper soaked in transfer buffer (25mM Tris base, 190mM glycine, 20% (v/v) MeOH, pH 8.3). Transfer buffer was added to the rest of the chamber and voltage was applied at 90V for 90 minutes. Following transfer, the membrane was blocked in 2.5% (w/v) non-fat milk in TBST (20mM Tris base, 150mM NaCl, 0.1% (v/v) Tween-20, pH 7.6) for 1 hour at room temperature with gentle agitation. The membrane was then incubated in primary antibody diluted in milk overnight at 4°C, followed by 3x 5 minute TBST washes with gentle agitation. Subsequently, the membrane was incubated with HRP-conjugated secondary antibody for 1 hour at room temperature, followed by a further 3x 5 minute TBST washes. Chemiluminescence was then detected using the Pierce ECL chemiluminescent detection kit (Invitrogen) and a Bio-Rad chemidoc imager.

**Table 2.7:** Antibodies

Target	Antibody	Dilution
P2Y6	Abcam ab92504	1:10,000
P2Y6	Alomone APR-011	1:550
P2Y6	Invitrogen PA5-106912	1:1250
$\alpha$ -tubulin	CST 2144	1:1000
GAPDH	CST 14C10	1:1000
$\beta$ -actin HRP	Invitrogen 15739	1:1000
Na/K ATPase	Antibodies.com A94985	1:1000
Goat anti-rabbit HRP	Invitrogen 31460	1:1000

### **2.5.1 Biotinylation Assay**

To assess whether proteins were on the cell surface, intact cells (and therefore proteins only found on the cell membrane) were treated with biotin and the biotinylated proteins were extracted using streptavidin beads. Briefly, cells were washed in cold PBS pH 8 and treated with 0.5mg/mL EZlink Sulfo-NHS Biotin (Thermo Fisher) at 4°C for 1 hour. The reaction was then quenched with ice-cold PBS-TG (1x PBS, 25mM Tris, 192mM glycine) by washing the cells twice. Protein was then extracted as normal (as in 2.5).

25µL of Pierce streptavidin agarose resin (Thermo Fisher) was aspirated using a wide-mouth pipette tip and placed into an Eppendorf. The resin was washed by adding 200µL of RIPA buffer, inverting a few times and centrifuging at 5000xg for 30s. The beads collect at the bottom, and the supernatant is removed carefully using gel loading tips. This 'purge' was repeated before 80µg of biotinylated protein lysate was added to the resin. The volume was made to 500µL with RIPA buffer (with protease inhibitor) and the resin/lysate was incubated overnight at 4°C on a rotary mixer. The next day, the resin was purged three times with cold RIPA buffer, and the remaining proteins were eluted in 5X loading buffer containing 50mM DTT by boiling at 96°C for 10 minutes. Protein was re-quantified and loaded as normal onto a polyacrylamide gel.

### **2.6 Fura-2 AM Calcium Mobilisation Assay**

Cells to be assayed were seeded in a 96 well plate at a density between 10,000 and 20,000 cells/well, dependent on cell type, and allowed to adhere overnight. The following day, cells were washed once in salt buffered saline (SBS) (130mM NaCl, 5mM KCl, 1.2mM MgCl<sub>2</sub>, 1.5mM CaCl<sub>2</sub>, 8mM D-Glucose, 10mM HEPES, pH 7.4, mOsm 310), followed by a 30 minute incubation at 37°C with 2µM FURA-2 AM (Abcam) in loading buffer (0.1% (w/v) Pluronic F-27 in SBS). After this, the cells were washed twice with SBS and loaded into the Flexstation III, along with sterile tips and a drug plate. The Flexstation dilutes a specified amount of drug (50µL) into the media that the cells are bathed in (200µL). Drug concentrations in the drug plate were 5X the final concentration to account for this final dilution step.

MRS2578 and ionomycin were dissolved in dimethyl sulfoxide (DMSO) to a stock of 10mM and diluted in SBS to a final DMSO concentration of 0.5% (v/v) in the well. A vehicle control of 0.5% (v/v) DMSO was included on each plate and subtracted from readings. Nucleotides were dissolved in water to a stock of 10mM, and aliquoted and stored at -20°C, to be diluted in SBS prior to use. Post addition of drug to cells, the plate was read at dual excitation of 340/380nm and emission of 510nm for a period of 240 seconds. The data is presented as an F ratio, which is a ratio of the fluorescence at ex340/ex380, as FURA-2 AM is ratiometric, meaning that as intracellular calcium concentrations rise, there is increased fluorescence at ex340/em510 and decreased fluorescence at ex380/em510. Pre-stimulation fluorescence is reported as a raw F ratio, whereas stimulation data is presented as a change from a zero baseline. Initially, background from negative control wells were subtracted from experimental readings. The raw peak f ratio value for each experimental condition was normalised to a maximal agonist response (including vehicle control) and presented as a percentage. The data was then analysed using the Hill equation ( $y = start + (end - start) \frac{x^n}{k^n + x^n}$ ) in OriginLab 2021, where  $k$  = michaelis constant and  $n$  = cooperative sites (Hill coefficient).

## 2.6.1 DNA Constructs & Transformation

In some experiments, cells were transfected with exogenous DNA prior to being used in the calcium mobilisation assay. To overexpress P2Y6, a pcDNA3.1+ construct containing the P2Y6 ORF (open reading frame) and a DYKDDDDK C-terminus flag-tag sequence was purchased from Genscript, as well as an empty vector. The plasmids were transformed using DH5 $\alpha$  competent cells. Briefly, cells were thawed on ice and 400ng of plasmid DNA was added, mixed well and incubated on ice for a further 30 minutes. To facilitate uptake, the cells were heat shocked at 42°C for 30 seconds, followed by addition of 500 $\mu$ L of SOC medium. The cells were then allowed to proliferate by shaking at 180rpm for 1 hour at 37°C. Subsequently, the cells were pelleted by centrifugation at 6000xg for 2 minutes, resuspended in 100 $\mu$ L of SOC medium and spread on ampicillin containing (100 $\mu$ g/mL) LB agar plates. The plates were incubated upside down overnight at 37°C. The next day, single colonies were picked and placed in 5mL of ampicillin

containing (100µg/mL) LB broth, and incubated at 37°C with shaking at 180rpm overnight again. Plasmid DNA was then purified from these cultures using the Qiagen plasmid DNA miniprep kit. Glycerol stocks of these cultures were made by mixing equal parts of glycerol and culture, and stored at -80°C. Cells were transfected with constructs in a T25 flask using Lipofectamine 3000, using 4µg of plasmid DNA and 10µL of Lipofectamine 3000, according to manufacturers protocol. The next day, cells were seeded into a 96 well plate and assayed the day after.

## **2.7 Enzyme-linked Immunosorbance Assay (ELISA)**

MMP-3 Duo-Set ELISA (RnD Biosystems) was used to assay MMP-3 concentrations in cell culture supernates. Briefly, cell culture supernates from various experimental conditions were collected and stored at -80°C. Maxisorp 96-well plates (Fisher) were coated with the working concentration of capture antibody overnight, followed by 3X washes in wash buffer (0.05% (v/v) Tween in PBS). Samples were added, followed by biotin-conjugated detection antibody, streptavidin-HRP and TMB substrate with wash steps between each addition. The substrate colour was allowed to develop for 20 minutes, and the absorbance was read at 450nm with background subtraction at 570nm using a Perkin Elmer Envision plate reader.

## **2.8 Lactate Dehydrogenase Release Assay (LDH)**

LDH release was used as a measure of the cytotoxicity of compounds to different cell types. Briefly, cells were cultured in 96 well plates and incubated for various time periods with experimental compounds. 45 minutes prior to harvest, 10X lysis solution was added in triplicate to the cells to create an experimental maximal LDH release. After this time period, 50µL of culture media was mixed with 50µL of Cytotox 96 non-radioactive assay (Promega) in a new 96 well plate and incubated for 30 minutes at room temperature, followed by the addition of 50µL of stop solution. Bubbles were popped with a needle and absorbance was read at 492nm. Data was analysed using Graphpad Prism.

## 2.9 Alcian Blue Staining

Cells were fixed in 4% (w/v) paraformaldehyde (PFA) in PBS for 15 minutes at room temperature, followed by 2X PBS washes. 1% (w/v) Alcian Blue (Sigma) in 0.1M HCl was added to the fixed cell layer overnight with gentle agitation. The following day, the Alcian blue was removed and the cells were washed 2X with 0.1M HCl and pictures were taken under a light microscope. The dye was then eluted in 200 $\mu$ L of 6M Guanidine HCl (Invitrogen) with gentle agitation for 1 hour at room temperature, and the absorbance was read at 650nm using the Flexstation III (Molecular Devices).

## 2.10 Sirius Red Staining

Cells were cultured in regular growth media supplemented with 50 $\mu$ g/mL 2-phospho-L-ascorbic acid (Invitrogen) and any experimental compounds for a period of 48 hours. Cells were then fixed in Bouin's fluid (Fisher) for 1 hour at room temperature, followed by 3X PBS washes. Picro-Sirius Red solution (Abcam) was added to the cells for 1 hour at room temperature with gentle agitation. Following removal of the dye, the cell layer was allowed to dry overnight. Cells were then washed 4X with 0.01M HCl and the dye was eluted in 0.1M 200  $\mu$ L NaOH. The absorbance of the eluted dye was then read at 550nm. Adapted from [212].

## 2.11 Luciferase Reporter Assay

### 2.11.1 Optimisation of Transfection

Optimisation of transfection of ATDC5 cells was carried out using Turbofect (Invitrogen) and Fugene HD (Promega) at different ratios of transfection reagent : plasmid DNA. The plasmid used to optimise transfection was E8491 pGL4.32[luc2P/NF- $\kappa$ B-RE] (Promega), which is an NF $\kappa$ B response element-driven luciferase plasmid. The plasmid was transformed (as in 2.6.1) using DH5 $\alpha$  cells and purified using the Qiagen miniprep kit. ATDC5 cells were seeded at 7,500 cells/well in a black clear-bottom 96 well plate and the next day transfected with 100ng

of plasmid DNA and varying transfection conditions in antibiotic-free complete media. After 48 hours, the cells were stimulated with 5ng/mL interleukin-1 $\beta$  for four hours and firefly luciferase expression was measured using the Dual Glo luciferase assay (Promega) and a Perkin Elmer Envision luminometer. For future experiments, the same procedure was carried out, using a 6:1 ratio of Turbofect:plasmid.

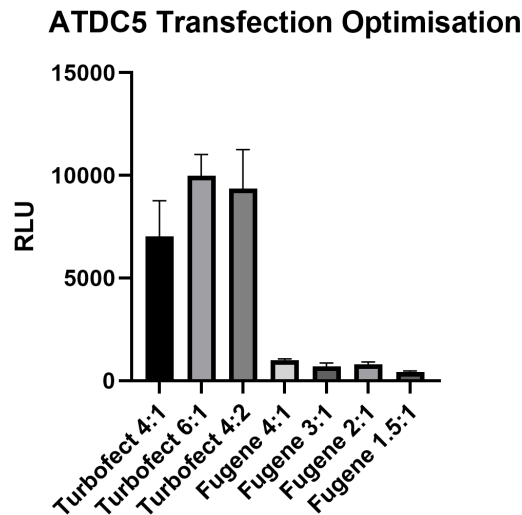


**Figure 2.1: ATDC5 Transfection Optimisation.** ATDC5 cells were transfected with either Turbofect (Thermo Fisher) or Fugene HD (Promega) using different ratios of transfection reagent to NF- $\kappa$ B luciferase plasmid ( $\mu$ L reagent:100X ng DNA). After 48 hours, IL-1 $\beta$  (5ng/mL) was added for four hours and luciferase activity was quantified using Dual-Glo luciferase kit (Promega).

## 2.12 RNA Interference (RNAi)

Small interfering RNAs (siRNA) were used for RNA interference in primary chondrocytes. Two Flexitube siRNAs (Qiagen) targeting P2Y6 and AllStar non-targeting siRNA (Qiagen) were purchased and resuspended in diethyl pyrocarbonate (DEPC) treated water to a concentration of 20nmol. Primary chondrocytes were seeded in 24 well plates at a density of 40,000 cells/well and left to adhere overnight. The media was then changed to antibiotic-free complete media and both siRNAs were co-transfected using Lipofectamine 3000 (Invitrogen) to a final concentration of 50nM (25nM each) following manufacturer's protocol. After 48 hours, experimental conditions were added and downstream processing occurred.

## 2.13 Transcriptome Sequencing

Cells were cultured as previously described and total RNA was extracted using Qiagen RNeasy kit using on-column DNase digestion (Qiagen RNase-free DNase kit) to remove any genomic DNA present. RNA purity and integrity was quantified using Nanodrop spectrophotometer and Agilent 4200 TapeStation. 260/280nm ratio values above 1.8 and a RIN (RNA integrity number) of above 7 was considered suitable for sending. A minimum of 200ng of RNA was sent to Novogene (Cambridge, UK) for poly(A) selection, library preparation and adapter ligation, Illumina sequencing and bioinformatic analysis. Analysis was conducted using the DESeq2 method of differential gene expression by Novogene [213].

## 2.14 CRISPR-Cas9 knockout of P2Y6

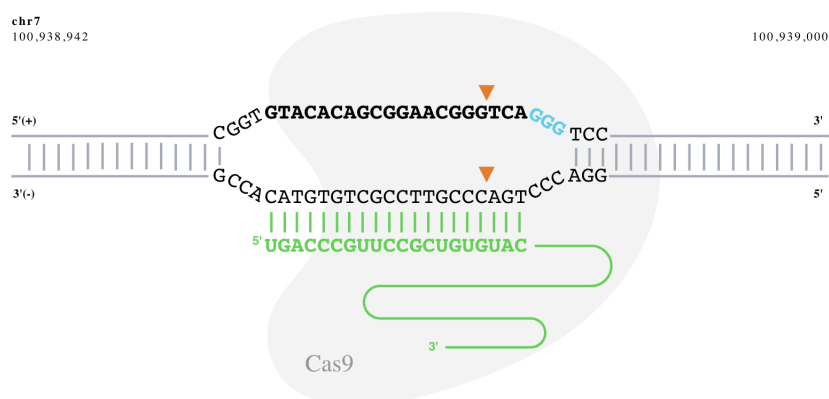


**Figure 2.2: Cas9 Activity.** Short oligonucleotide guide RNAs, composed of the crRNA and tracrRNA and displayed in green, direct the Cas9 enzyme to a specific locus of the genome. When complexed, Cas9 cleaves the DNA at a site just upstream of a PAM sequence, creating a double strand break. The repair process (non-homologous end joining) facilitates ligation of the break, but often produces indels and can result in a non-functional gene (synthego.com).

## **2.14.1 Plasmid Delivery**

### **gRNA Design**

Genscript algorithms were used to design two sgRNA sequences targeting P2Y6 in the mouse genome for knockout of P2Y6 in the ATDC5 cell line. They were screened for both on- and off- target activity and the two top performing sequences were selected. The target sites were in exons thought to be crucial for protein functionality. These sequences were cloned separately into the PX459 plasmid backbone [214] by Genscript and delivered lyophilised.

### **Transformation**

The plasmids were transformed using recombination deficient Stbl3 competent cells (Invitrogen) due to the presence of long terminal repeats (LTR) in the PX459 plasmid. Transformation was performed as in 2.6.1. Plasmid DNA was isolated using Qiagen Maxiprep kit to achieve a high concentration minimum of 1µg/µL.

### **Puromycin Toxicity**

To determine the lowest concentration of puromycin that maintains its cytotoxic effects, cells were seeded in 96 well plates and treated with varying concentrations of puromycin. After 2 days of treatment, cells were washed 2X with PBS to remove detached cells and the cell layer was fixed for 15 minutes at room temperature with 4% PFA. The cell layer was stained for DNA content with Crystal violet (0.5% (w/v) in 20% (v/v) methanol) (Invitrogen) for 1 hour at room temperature with gentle agitation. The cell layer was subsequently washed with PBS 2X, allowed to dry overnight and the bound dye was eluted in 50µL 100% methanol. The absorbance was read at 540nm.

### **Transfection**

Plasmids were transfected into ATDC5 cells using Turbofect (Fisher Scientific) in antibiotic-free media using previously optimised conditions. The PX459 plasmids were also electroporated into the cells using Ingenio Electroporation Solution (Mirus Bio). Briefly, 1 million cells were pelleted and resuspended in 250

$\mu\text{L}$  of electroporation solution and transferred to a 4mm cuvette with 5  $\mu\text{g}$  of high concentration plasmid (1  $\mu\text{g}/\mu\text{L}$ ). The cells were then electroporated using a square-wave form pulse of 280V for 15 ms using the Bio-Rad XCell Electroporation System. Following electroporation, the cells were transferred to a T25 flask containing pre-warmed media. After 24 hours, the cells were selected with puromycin as above for a further 48 hours prior to assaying for genomic indel formation as in 2.14.4.

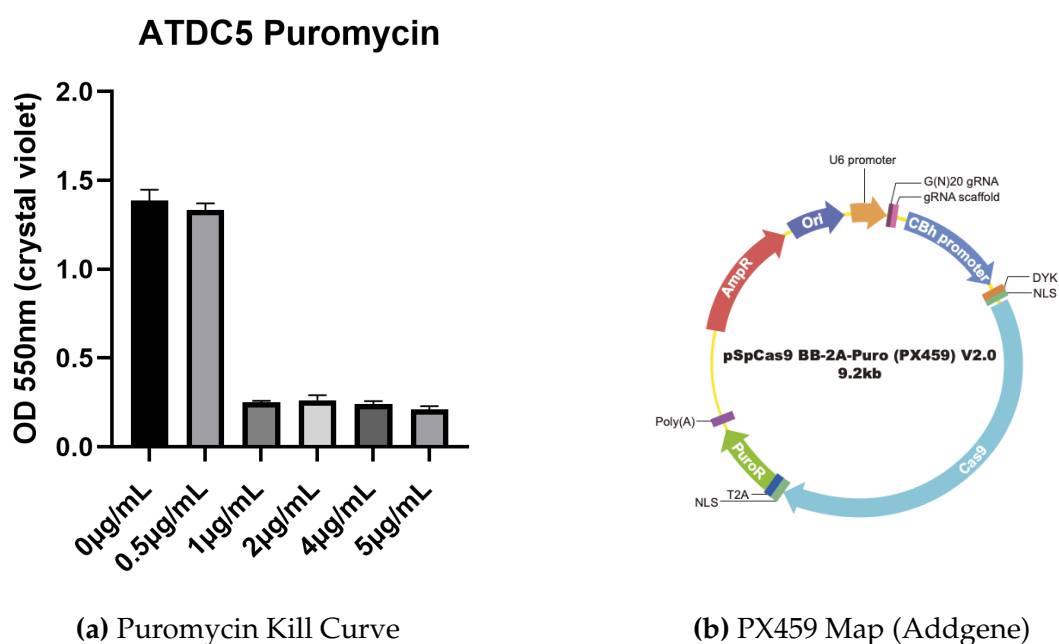


**Figure 2.3: Puromycin Kill Curve & PX459 Plasmid Map** ATDC5 cells were treated with varying concentrations of puromycin for 48 hours, before the cell layer was fixed and stained with crystal violet, as an estimation of remaining cells that had survived the puromycin challenge.

**Table 2.8: sgRNA-targeting sequences**

	Targeting Sequence	PAM
sgRNA 1	CAGCACCACCGAGTATACCG	GTG
sgRNA 2	CGGCAGGCGAGGTCTCCGAA	CTT

## 2.14.2 Ribonucleoprotein Delivery

### gRNA Design

3 pre-designed synthetic crRNA (crispr RNA) were purchased from Integrated DNA Technologies (IDT). IDT also supplied the tracrRNA (trans-activating crispr

RNA) and recombinant Cas9 enzyme. The guide RNAs were selected for highest on target specificity and lowest predicted off-target effects. Positive control HPRT guide RNA was also supplied by IDT.

**Table 2.9:** gRNA-targeting sequences

	Targeting Sequence	PAM
AA	GCGTCTACCGTGAGGATTTC	AGG
AB	TGACCCGTTCCGCTGTGTAC	GGG
AC	TATGGTATGGCCCTCACGGT	GGG

### RNP Formation and Transfection

Synthetic crRNAs and tracrRNA were resuspended in supplied nuclease-free duplex buffer to a concentration of 100 $\mu$ M. In sterile, nuclease-free conditions, gRNA complexes were formed by diluting each individual crRNA with tracrRNA separately to a final concentration of 1 $\mu$ M in duplex buffer. The RNA was heated to 95°C for 5 minutes, and allowed to cool to room temperature. The Cas9, supplied at 52 $\mu$ M was diluted to 1 $\mu$ M in Opti-MEM (Invitrogen), again in sterile, nuclease-free conditions. Lipofectamine CrisprMAX (Invitrogen) and TransIT-X2 (Mirus Bio) were used to transfect. To form the RNP complex, the following was combined and allowed to incubate at RT for 5 minutes.

**Table 2.10:** RNP Formation

1 $\mu$ M gRNA	8 $\mu$ L each (x3)
1 $\mu$ M Cas9	28.8 $\mu$ L
Cas9 PLUS reagent	12.5 $\mu$ L
Opti-MEM	59.7 $\mu$ L

In a separate tube, 7.5 $\mu$ L of Lipofectamine CrisprMAX reagent was added to 125 $\mu$ L of Opti-MEM, and vortexed. The diluted lipofection reagent was then added to the RNP complex and allowed to incubate for 15 minutes at room temperature. In this time, ATDC5 cells were trypsinised and diluted to a concentration of 400,000 cells/mL in antibiotic-free complete media. After the incubation period, 250 $\mu$ L of RNP-transfection mix was added to a 6 well plate and 500 $\mu$ L of cell suspension was added. Forward transfection was also tested, using the same concentration of gRNA and Cas9, but plating cells 24 hours before adding the

transfection complex. The media was changed after 24 hours and incubated for a further 24 hours before proceeding. This protocol was also scaled down to 24 well plates for subsequent experiments, maintaining the concentration of gRNA/Cas9. Where TransIT-X2 (Mirus Bio) was used, manufacturer guidelines were followed.

### **2.14.3 Lentiviral Delivery**

#### **Generation of a stable ATDC5-Cas9 line**

Cells were plated in 6 well plates at a density of 20,000 cells/well to achieve approximately 50% confluency the next day. After an overnight incubation, the cells were transduced with pLV[Exp]-CBh/hCas9/Hygro lentiviral particles (Vector Builder) and 5 $\mu$ g/mL of polybrene (Vector Builder) at an MOI (multiplicity of infection) of 100. The cells were incubated overnight, and the media was replaced the next day. After a further 24 hours to allow for sufficient expression of antibiotic resistance genes, 200 $\mu$ g/mL of hygromycin B (Invitrogen) was added to the media. After 10 days, the resistant cells were expanded in normal growth media. PCR was used to detect the insertion of the Cas9 gene in the genomic DNA. All lentiviral waste was treated with 10% (v/v) Chemgene for 24 hours.

#### **Transfection of Guide RNAs**

Synthetic guide RNAs that were used in the RNP delivery method were transfected into the ATDC5-Cas9 cells alone using Turbofect at a final concentration of 30nM.

### **2.14.4 Assessment of Indel Formation**

Genomic DNA was extracted from a mixed population of cells using Monarch genomic DNA extraction kit (New England Biolabs) or LGC QuickExtract DNA solution. A region of DNA spanning the gRNA cut sites (primer sequences in 8.1) was amplified using CloneAmp HiFi PCR 2X premix (Takara) and purified using the Macherey Nagel PCR purification kit.

### **T7E1 Cleavage Assay**

17 $\mu$ L of the purified amplicon ( $\sim$ 400ng) was mixed with 2 $\mu$ L of 10X NEBuffer 2 and heated to 95°C for 10 minutes, followed by cooling to 85°C at a ramp rate of -2°C/s and a subsequent cooling step to 25°C at a ramp rate of -0.3°C/s to create heterodimers. 10U of T7E1 (New England Biolabs) was then added to the reaction and incubated at 37°C for 15 minutes, followed by the addition of 1 $\mu$ L of 0.25M EDTA to quench the reaction. DNA products were then analysed by agarose gel electrophoresis. Multiple products indicates heterodimers were formed by indel formation and cleaved by the nuclease.

### **Sanger Sequencing**

Amplicons were also sent for sanger sequencing by Source Bioscience and entered into deconvolution algorithms to estimate the percentage of cells in the mixed pool that had genomic indels. Four algorithms were used; SeqScreener (Thermo Fisher), TIDE (Tracking of Insertion and Deletion Events) [215], DECODR (Deconvolution of Complex DNA Repair) [216] and ICE (Inference of CRISPR Edits, Synthego) [217].

### **2.14.5 Clonal Dilution**

To obtain a knockout cell line that originates from a single cell, the mixed population of cells that were verified to have indels were serially diluted. 4000 cells were put into the top left corner of a 96 well plate and diluted 1 in 2 down the first column and then every row across the plate to achieve single cell suspensions at the lower right hand corner of the plate. The plate was incubated for around two weeks until colonies were seen in individual wells. These were trypsinised and expanded into larger plates/flasks and assayed for P2Y6 knockout by sanger sequencing, PCR and western blot.

## **2.15 Protein Arrays**

Protein arrays were purchased from RayBiotech. They were supplied as 8 sample kits, detecting phosphorylation of proteins from common signalling pathways

(AAH-PPP-1-8) and cytokines (AAH-CYT-5-8). For the phosphorylation array, cells were cultured in twelve-well plates at a density of 50,000 cells/well and following an overnight incubation, cultured in serum free media. Following another overnight incubation to serum starve the cells, they were stimulated with UDP- $\beta$ S and harvested using the lysis buffer provided supplemented with phosphatase and protease inhibitors. Protein was quantified using the Bradford assay (as in 2.5) and equalised to 150 $\mu$ g/mL in supplied blocking buffer. Membranes spotted with antibodies were blocked for 30 mins at room temperature, followed by incubation with the sample for 4 hours at room temperature. After five washes (three with wash buffer I and two with wash buffer II, 5 minutes each on a rotary rocker), the membranes were incubated with supplied detection antibody overnight at 4°C on a rotary rocker. The next day, another wash sequence was performed and the membranes were incubated with supplied rabbit IgG-HRP for two hours at room temperature, followed by another wash sequence and detection using chemiluminescent detection kit (also supplied).

For the cytokine array, cells were plated and serum starved as above. Prior to stimulation, media was changed to fresh serum-free media, and cells were stimulated with UDP- $\beta$ S for 48 hours, collecting cell culture supernatants at 24 and 48 hours post stimulation and stored at -80°C. The procedure for detection was similar to the phosphorylation protein array, except for the use of biotinylated detection antibodies and streptavidin-bound IgG-HRP for chemiluminescent detection.

## **Data Analysis**

Following chemiluminescent detection, data was analysed in ImageJ. Initially the image was inverted and the mean pixel density of each spot was measured. Background values from the negative control spots of each corresponding membrane were subtracted from the test spots. From this, technical duplicates were averaged. Fold change was calculated by taking into account the variability between each membrane, as each time point was assayed on a different membrane. There was a positive control spot on each membrane, which accounts for inter-membrane variability and allows for comparison. The time point 0/control mem-

brane ( $T_0$ ) was used to determine fold change of each subsequent time point ( $T_x$ ) from. The formula  $FC = (x^2 * r^1 / r^2) / x^1$  was used.  $x^1$  is the  $T_0$  test spot,  $x^2$  is the experimental ( $T_x$ ) test spot,  $r^1$  is the  $T_0$  positive control spot,  $r^2$  is the positive control spot on the  $T_x$  membranes.

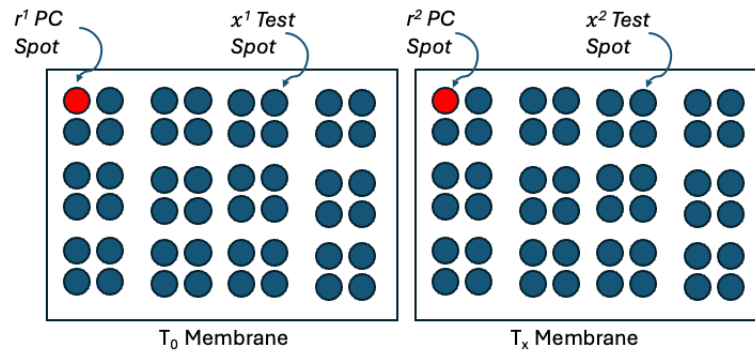


**Figure 2.4: Proteomic Membrane Analysis.** For analysis of the solid phase proteomic arrays, positive control spots on both the time point 0 ( $T_0$ ) and later time point membranes ( $T_x$ ) were used to account for inter-membrane variability using the formula described in section 2.15.

## 2.16 Statistical Analyses

Graphpad Prism 9.0 was used for statistical analyses. Data was tested for normal distribution with a Shapiro-Wilk test. For normally distributed data, an ANOVA with Tukey's post-hoc test of multiple comparisons was used to test for significance between more than two groups. For two groups, a t-test was carried out. For non-normally distributed data, a Kruskal-Wallis ANOVA followed by post-hoc tests was carried out. To test if a fold change is significantly different from a hypothetical fold change of 1 (i.e. where there was no change), a one sample t test was used where there was Gaussian distribution. A p value  $<0.05$  was taken as significant. N represents biological replicates, n represents technical replicates.

# Chapter 3

## Investigating Expression and Function of P2Y6 in PHC

### 3.1 Introduction

Whilst there has been some exploration of the purinergic expression profile of chondrocytes in the literature, this has often been in non-human cells [161], and the full expression profile of both human cell lines and primary human chondrocytes has not been fully elucidated. Moreover, whilst the purinergic system has been very well characterised functionally in other physiological modalities, e.g. the cardiovascular system where there are clinically used antagonists, the role of purinergic signalling in chondrocytes and whether this pathway may be exploited for treatment of disease remains to be as fully explored. In disease states such as OA, chondrocytes' dysregulated signalling contributes to the degradation of the tissue and their inability to repair, thus propagating the disease. Understanding better which signalling pathways contribute to this dysfunctional state may illuminate new strategies to prevent cartilage degradation and maintain the chondrocyte phenotype as well as structural integrity of the ECM tissue. The use of transgenic mice has revealed skeletal phenotypes that indicate an important role for purinergic signalling. For example, A3 and A2A knockout mice both develop signs of OA, such as cartilage loss and pain [171, 176]. Moreover chondrocytes have been shown to release nucleotides in response to hypoxia and mechanical stress [218] and P2X4 has been shown to mediate calcium currents that

are a prerequisite for chondrogenic condensation, which itself is a prerequisite to the first stages of chondrogenesis [194]. It is clear from the existing literature that there is involvement of nucleotides in the regulation of cells found in the musculoskeletal system. As such, the hypothesis of this chapter was that one or more purinergic receptors may be differentially expressed across disease phenotypes and may play a role in homeostasis of cartilage tissue and pathogenesis.

The aims of this chapter are to:

- To investigate functional expression of purinergic receptors by human chondrocyte models, both primary and immortalised cell lines.
- To analyse existing datasets to see if expression changes in disease states.
- To understand how any identified receptors may influence expression of key chondrocyte genes that are disease relevant.

## 3.2 Results

### 3.2.1 Chondrocyte cell lines and PHC express multiple purinergic receptors

Initially, RT-PCR and gel electrophoresis was carried out to investigate purinergic mRNA expression by chondrocytes, however owing to the lack of reproducibility, specificity and quantitation, a qRT-PCR approach was chosen. Figure 3.1 compares the expression of all nineteen purinergic receptors across three cell types - C28/I2 immortalised costal chondrocyte line, SW1353 chondrosarcoma line and KOA (knee osteoarthritis) PHC (primary human chondrocytes). The  $C_T$  values are shown in Table 3.1 with 18S housekeeper  $C_T$  values subtracted from them. *P2RY13* mRNA is not expressed by any of the cells, and *P2RX3* was only expressed by KOA PHC. The cell lines are consistent with primary cells in the lack of *P2RY13* expression, however, the cell lines lack *P2RX3* expression, whereas PHC do express mRNA for this receptor.

Expression levels of each receptor was compared within each cell type. For KOA cells, the most highly expressed receptor was *A1R*, whereas for C28/I2 and

SW1353, it was *ADORA2B* and *P2RX4*, respectively. However, *P2RX4* was also highly expressed by C28/I2 and KOA, being ranked as second mostly highly expressed by those two cell lines. Other receptors that are ranked in the top five for all three cell lines include *ADORA2B* and *P2RY6*. *P2RX5* is third most highly expressed by C28/I2, whereas expression levels are much lower in the other two cell types. Of note, SEM values are much higher in the KOA means than the two cell lines, which is consistent with donor heterogeneity.  $C_T$  values over 35 were assumed to be non-specific amplification as a high amount of cDNA was used (12.5ng).

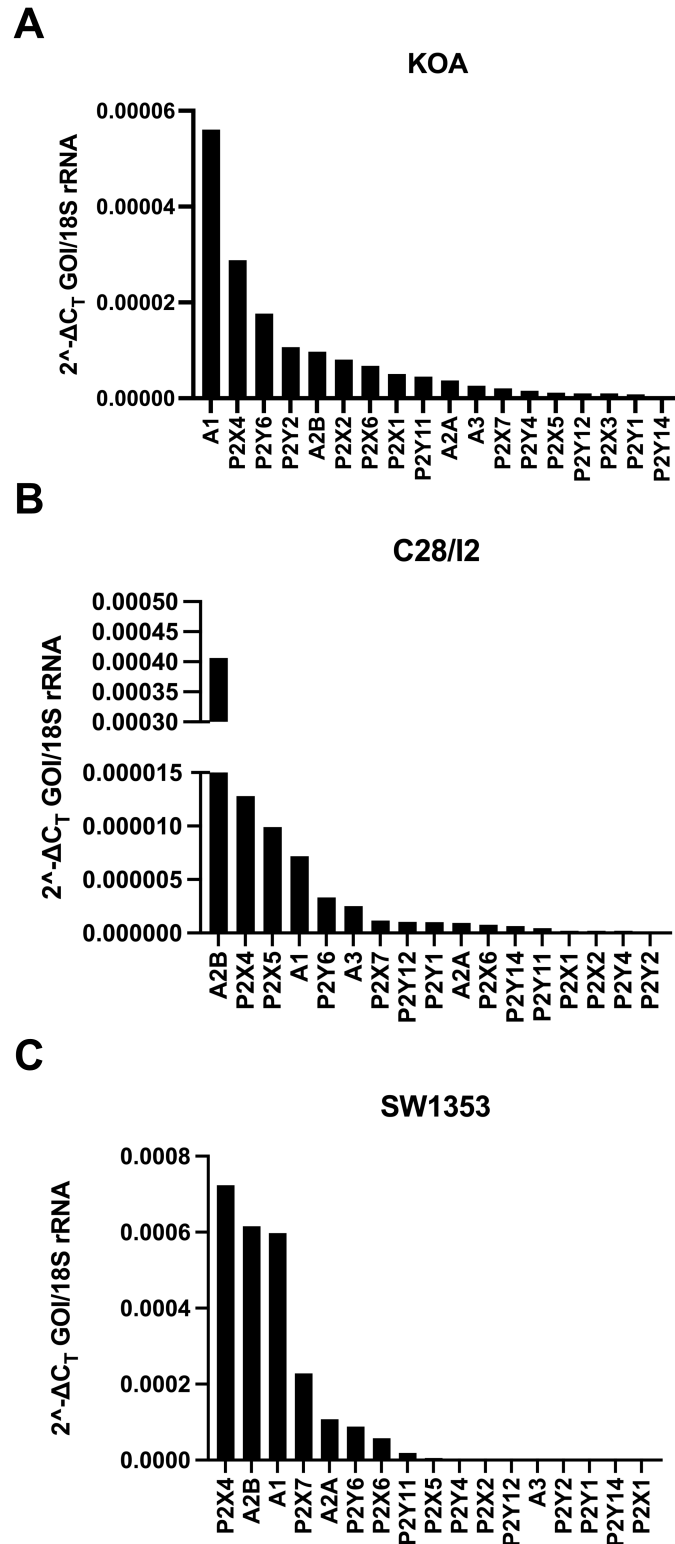


**Figure 3.1: mRNA Expression of Purinergic Receptors.** RNA was extracted from KOA PHC (A), C28/I2 (B) and SW1353 (C) followed by qRT-PCR for the purinergic receptors.  $C_T$  values  $>35$  were discounted and taken as non-specific amplification.  $N=3$  (separate patient isolates for PHC), data presented as mean.

**Table 3.1: mRNA Expression of Purinergic Receptors -  $C_T$  Values.** RNA was extracted from SW1353, C28/I2 and PHC, followed by qRT-PCR for the purinergic receptors.  $C_T$  values  $>35$  were discounted and taken as non-specific amplification. N=3 (separate patient isolates for PHC), data presented as mean  $C_T$  values with 18S housekeeper  $C_T$  values subtracted. NE = Not Expressed.

Receptor	KOA $C_T$ (SEM)	C28/I2 $C_T$ (SEM)	SW1353 $C_T$ (SEM)
<i>ADORA1</i>	14.1 (2.5)	17.1 (0.3)	10.7 (0.3)
<i>ADORA2A</i>	18 (0.9)	20 (0.3)	13.2 (0.3)
<i>ADORA2B</i>	16.7 (2.7)	11.3 (0.3)	10.7
<i>ADORA3</i>	18.7 (1.2)	18.6 (0.6)	18.5 (0.3)
<i>P2RX1</i>	17.6 (1.6)	22.1 (1.4)	20 (0.4)
<i>P2RX2</i>	16.9 (0.4)	22.2 (0.5)	18.4 (0.6)
<i>P2RX3</i>	19.9 (0.8)	NE	NE
<i>P2RX4</i>	15.1 (2.8)	16.3 (0.3)	10.4 (0.5)
<i>P2RX5</i>	19.7 (3.0)	16.6 (0.6)	17.5 (0.4)
<i>P2RX6</i>	17.2 (3.0)	20.3 (0.4)	14.1 (0.7)
<i>P2RX7</i>	18.9 (2.8)	19.7 (0.6)	12.1 (0.7)
<i>P2RY1</i>	20.3 (0.8)	19.9 (0.2)	19.8 (0.4)
<i>P2RY2</i>	16.5 (1.9)	24.1 (0.7)	19.8 (0.7)
<i>P2RY4</i>	19.3 (2.7)	22.2 (0.2)	18.0 (0.2)
<i>P2RY6</i>	15.8 (2.8)	18.2 (0.3)	13.5 (0.3)
<i>P2RY11</i>	17.8 (1.6)	21.1 (0.3)	15.7 (0.5)
<i>P2RY12</i>	19.9 (2.6)	19.9 (0.2)	18.5 (0.5)
<i>P2RY13</i>	NE	NE	NE
<i>P2RY14</i>	22.8 (3.2)	20.5 (0.6)	20 (0.3)

### 3.2.2 SkeletalVis reveals P2Y6 to be upregulated in OA

One indication as to whether a receptor might be important in disease processes is whether its expression levels change between disease states. This strategy was employed as it is a relatively easy and quick method of finding receptors that might be relevant to pathophysiology. In order to detect changes in purinergic receptor expression between healthy and diseased chondrocytes in existing datasets, an online transcriptomics database pertaining to musculoskeletal diseases was used. An analysis of five separate datasets contained within SkeletalVis [219], comparing chondrocytes from normal tissue to that from osteoarthritic tissue, found P2Y6 to be upregulated (Fig. 3.2). Its expression is 1.88-fold higher (SEM  $\pm 0.3$ ,  $p = 0.09$ ) in OA chondrocytes. The datasets collated by SkeletalVis were from these publications [220–224], and are summarised in Table 3.2.

**Table 3.2: Publications Collated by SkeletalVis.** SkeletalVis was used to interrogate existing transcriptomics data pertaining to musculoskeletal diseases. Data from the publications summarised in this table were analysed.

Reference	PMID	Author	Summary
[220]	22659600	Xu et al., 2012	NOF vs HOA n=9.
[221]	24361742	Snelling et al., 2014	Damaged vs undamaged from the same knee. Phenotype of anteromedial gonarthrosis. n=9.
[222]	29273645	Soul et al., 2018	KOA (n=44) vs NOF (n=10)
[223]	25054223	Ramos et al., 2014	Damaged vs undamaged from the same joint, both hip and knee n=33.
[224]	26973327	Dunn et al., 2016	Damaged vs undamaged from the same knee n=8.

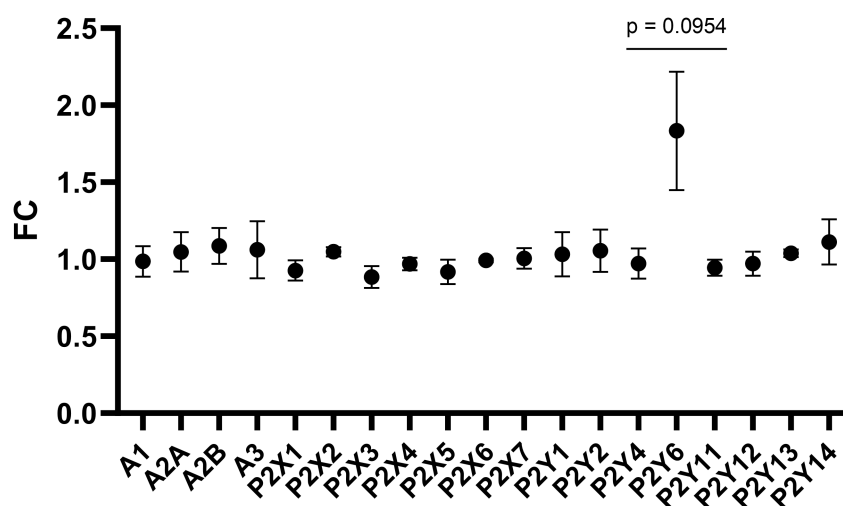


**Figure 3.2: Existing Dataset Analyses.** SkeletalVis [219] was used to interrogate purinergic receptor expression by chondrocytes from diseased and healthy cartilage, compiled from five separate experiments. A one sample t test was used to test for significance from a theoretical fold change of 1. Data represented as mean  $\pm$  SEM.

qRT-PCR was then used to detect *P2Y6* mRNA expression by chondrocytes isolated from hip or knee OA joints and NOF (neck of femur) healthy cartilage hip joints from patients who were undergoing surgery for non-OA pathology i.e. trauma. *P2RY6* is significantly increased in expression by OA chondrocytes compared to those isolated from NOF tissue (Fig. 3.3).

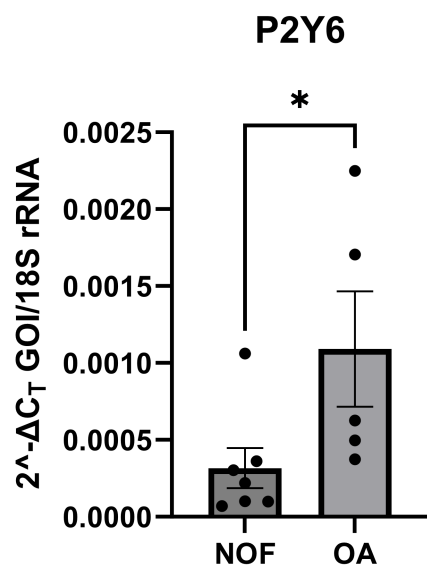


**Figure 3.3: *P2RY6* mRNA Expression by OA and NOF Chondrocytes.** cDNA was provided by Dr. Matt Barter (Newcastle University) from chondrocytes isolated from neck of femur (NOF) and osteoarthritis (OA) tissue. *P2RY6* mRNA was detected by qRT-PCR. Unpaired t-test, \* $p < 0.05$ . N=5/7 patient isolates. Data represented as mean  $\pm$  SEM.

### 3.2.3 Expression of functional P2Y6 in cell lines

It then became pertinent to understand whether P2Y6 was expressed in the primary cells and cell lines that were to be used for future experiments. To determine if PHC, SW1353 and C28/I2 express P2Y6 protein, cell lysates were probed with two different P2Y6 antibodies by SDS-PAGE. The first antibody, alomone APR-011, a polyclonal antibody, produced bands of around 150kD that were not at the expected weight of 37kD (Fig. 3.4), and so was deemed non-specific. Another antibody tested was a monoclonal antibody, abcam ab92504, which produced bands at the expected weight of 37kD (Fig. 3.5). Its specificity to P2Y6 was demonstrated with cell lysates from native and P2Y6-expressing 1321N1 astrocytoma cells. This shows that P2Y6 protein is expressed by all three cell types, with slightly darker bands produced from the SW1353 and C28/I2 cell lysates.

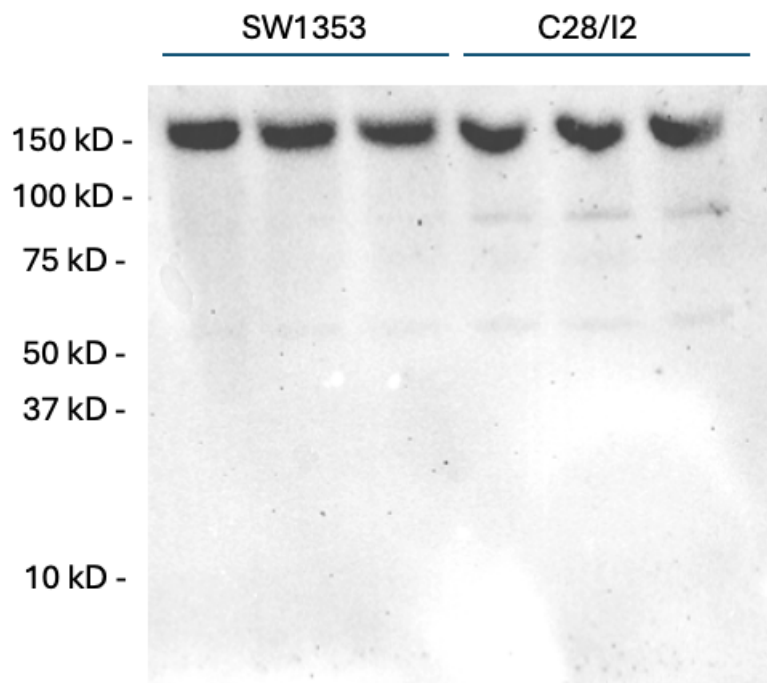


**Figure 3.4: SDS PAGE with Alomone P2Y6 Antibody.** SW1353 and C28/I2 cells were lysed and the proteins were solubilised RIPA buffer. Following quantification, 40µg total protein was loaded onto an acrylamide gel. Primary antibody was used at 1:550.

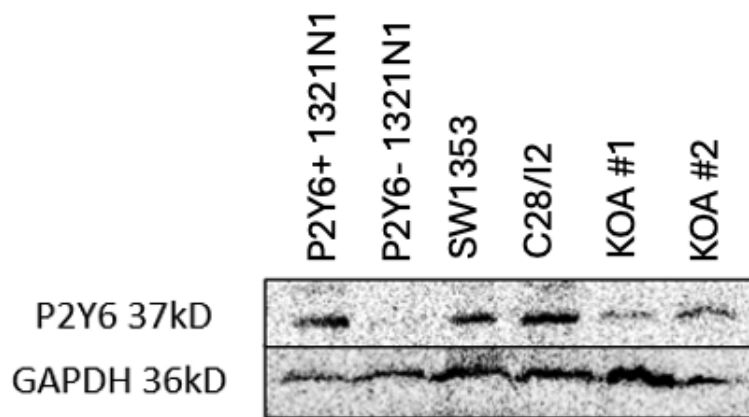


**Figure 3.5: SDS PAGE with Abcam P2Y6 Antibody.** Cell lysates from KOA, SW1353 and C28/I2 were solubilised with RIPA buffer and probed for P2Y6 protein. 40ug total protein was loaded onto an acrylamide gel, and the primary antibody was used at 1:10,000. From left to right; P2Y6 expressing 1321N1, parental 1321N1, SW1353, C28/I2, KOA 1, KOA 2.

Functionality of the expressed P2Y6 was then tested by measuring intracellular calcium changes elicited by UDP stimulation, as would be expected from a Gq coupled GPCR. Initially, SW1353 chondrosarcoma cells were stimulated with UDP over a range of doses (maximally 1mM). Despite expressing *P2RY6* mRNA and protein, there was no characteristic increase in intracellular calcium elicited by any dose of UDP nor ATP. Ionomycin, a  $Ca^{2+}$  ionophore, did elicit calcium release, showing that the cells were loaded with FURA-2 and the assay was working. This finding was the same for C28/I2 cells (Fig. 3.6), despite this being a different cell line in that it is non-neoplastic and costal in origin.

To understand why SW1353 may not have a UDP elicited response, thapsigargin was used to stimulate the cells to understand if they had intracellular calcium stores. Thapsigargin inhibits SERCA (sarco/endoplasmic reticulum  $Ca^{2+}$  ATPase), causing calcium to leak out of the endoplasmic reticulum, which did occur, meaning they contain intracellular calcium stores (Fig. 3.7A). SW1353 cells were then transfected with a P2Y6 over-expression plasmid (pcDNA3.1 backbone) and assayed again for a calcium response to UDP. SW1353 over-expressing P2Y6 did have a UDP-elicited calcium response, whilst transfection with an empty vector had no effect (Fig. 3.7B/C). Of note, cells that were seeded in a 96 well plate and then transfected in situ did not have this calcium response (data not shown),

only the cells that were transfected in the flask and then seeded did. Another hypothesis that could account for the lack of response was that the endogenously expressed P2Y6 was not trafficked to the cell surface, which would be required to elicit a calcium response. To prove or disprove this, membrane bound proteins from SW1353 were biotinylated and extracted using streptavidin agarose resin to capture the membrane bound proteins only, as shown in Fig. 3.8, and probed for P2Y6 using western blotting. There was no signal from the biotinylated proteins for P2Y6 nor actin. As a positive control, a sodium/potassium ATPase was also used to probe the biotinylated proteins, however this antibody produced bands that were not at the expected size of 112kD, but at approximately 27kD.

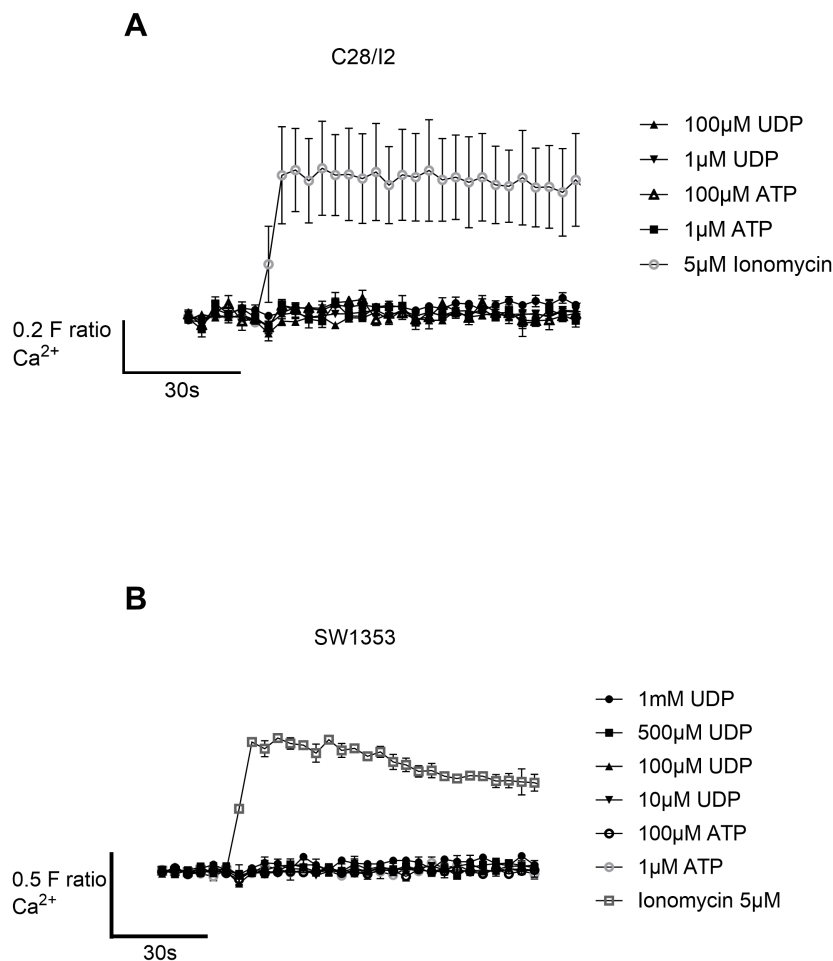


**Figure 3.6: Calcium responses in C28/I2 and SW1353.** C28/I2 (A) and SW1353 (B) cells were loaded with FURA-2 AM and changes in fluorescence were measured after stimulation with UDP and ionomycin. N=3, data presented as mean  $\pm$  SEM. F ratio is the fluorescence ratio of 340/380ex and 510em, scaled to a 0 baseline.

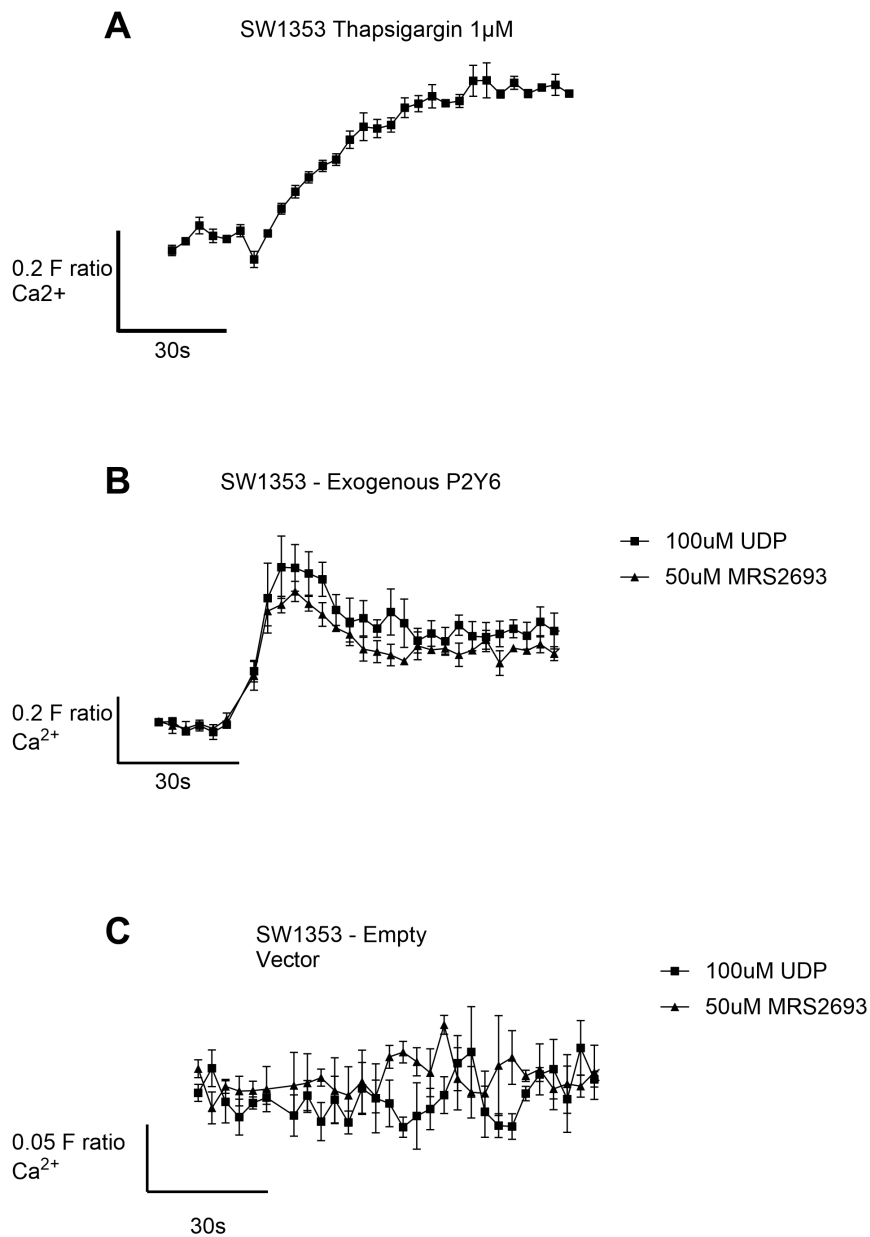


**Figure 3.7: Effect of thapsigargin and exogenous P2Y6 expression on UDP elicited calcium responses.** (A) SW1353 cells were incubated with FURA-2 and stimulated with thapsigargin. SW1353 cells were transfected with pcDNA3.1-DYK encoding the P2Y6 ORF (B) or empty vector (C) 48 hours prior to being incubated with FURA-2 AM and stimulated with UDP and MRS2693. N=3, data presented as mean  $\pm$  SEM. F ratio is the fluorescence ratio of 340/380ex and 510em, scaled to a 0 baseline.

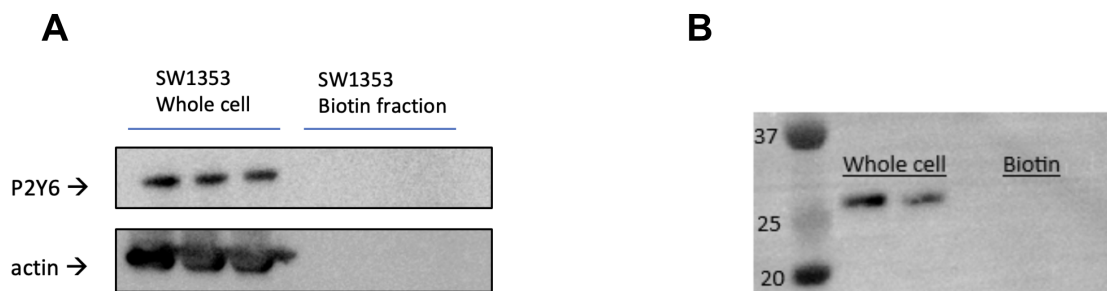


**Figure 3.8: SW1353 Biotinylated Proteins were probed by SDS-PAGE.** SW1353 cells were treated with biotin for 1 hour, followed by protein extraction with RIPA and extraction of the biotinylated proteins with streptavidin agarose resin. Proteins were then detected by SDS PAGE (A) P2Y6 and  $\beta$ -actin or (B) Sodium/Potassium ATPase.

### 3.2.4 Expression of functional P2Y6 in PHC

Following the lack of a UDP elicited calcium response in two chondrocyte cell lines, it became pertinent to understand if PHC also lacked this response. Some optimisation had to be carried out as the primary cells were showing signs of toxicity to FURA-2 during the incubation period, whereas the cell lines did not. This included being washed away during wash steps and morphological changes. Fig. 3.9 shows that the response to 10 $\mu$ M UDP as a percentage of the 1mM response was higher in cells that were incubated with FURA-2 for only 30 minutes compared to 1 hour. Moreover, initial fluorescent ratiometric values were the same, indicating that the cells were equally loaded with FURA-2 in both conditions. 30 minute FURA-2 incubations were then used for the subsequent experiments.

In contrast to SW1353 and C28/I2, UDP did elicit a calcium response in a dose dependent manner in KOA PHC. This response was blocked maximally by 81% by 10 $\mu$ M MRS2578. KOA PHC also responded to other nucleotides, ATP and ADP, in similar dose-dependent manners. ATP had the lowest EC<sub>50</sub>, followed by ADP and UDP. These responses were also partially blocked by 10 $\mu$ M MRS2578 (Fig. 3.10 and Table 3.3). MRS2578 had the highest inhibitory effect on the 1mM UDP response, followed by ADP and ATP. The pharmacological dynamics of MRS2578 in PHC was also tested, in experimentally determining the IC<sub>50</sub> by varying the concentration of MRS2578 but keeping the concentration of UDP constant. The experimental IC<sub>50</sub> of MRS2578 with respect to the UDP response is 428nM  $\pm$  182nM (Fig. 3.11). The effect of MRS2578 on the ionomycin response and LDH release was also carried out as an indicator of toxicity of MRS2578 to PHC. It had no significant effects on the ionomycin calcium response, LDH (lactate dehydrogenase) release nor pre-stimulation fluorescence readings.

**Table 3.3: Nucleotide Elicited Calcium Responses in PHC.** PHC were incubated with FURA-2 and calcium responses were tracked in response to UDP, ATP and ADP. EC<sub>50</sub>  $\pm$  SEM and maximal inhibition  $\pm$  SEM by MRS2578 are shown.

Agonist	EC <sub>50</sub>	Inhibition by MRS2578 of 1mM Response
UDP	30.8 $\mu$ M $\pm$ 4.77	81.4% $\pm$ 5.2
ATP	3.35 $\mu$ M $\pm$ 1.32	71.3% $\pm$ 6.7
ADP	11.7 $\mu$ M $\pm$ 2.57	78.5% $\pm$ 4.3

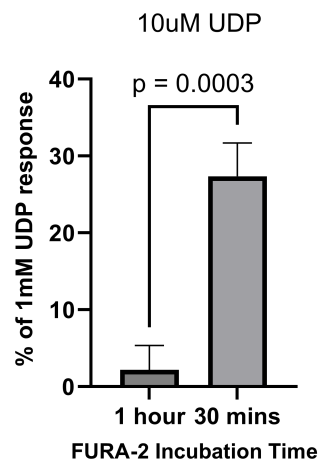


**Figure 3.9: PHC FURA-2 Incubation Time Optimisation.** PHC were seeded into a 96 well plate and incubated with FURA-2 for 1 hour or 30 minutes prior to stimulation with UDP and measurement of dual fluorescence excitation of 340/380nm and emission of 510nm in the Flexstation. The peak of the 10 $\mu$ M response was normalised to that of the 1mM response. N=3. T test was carried out.

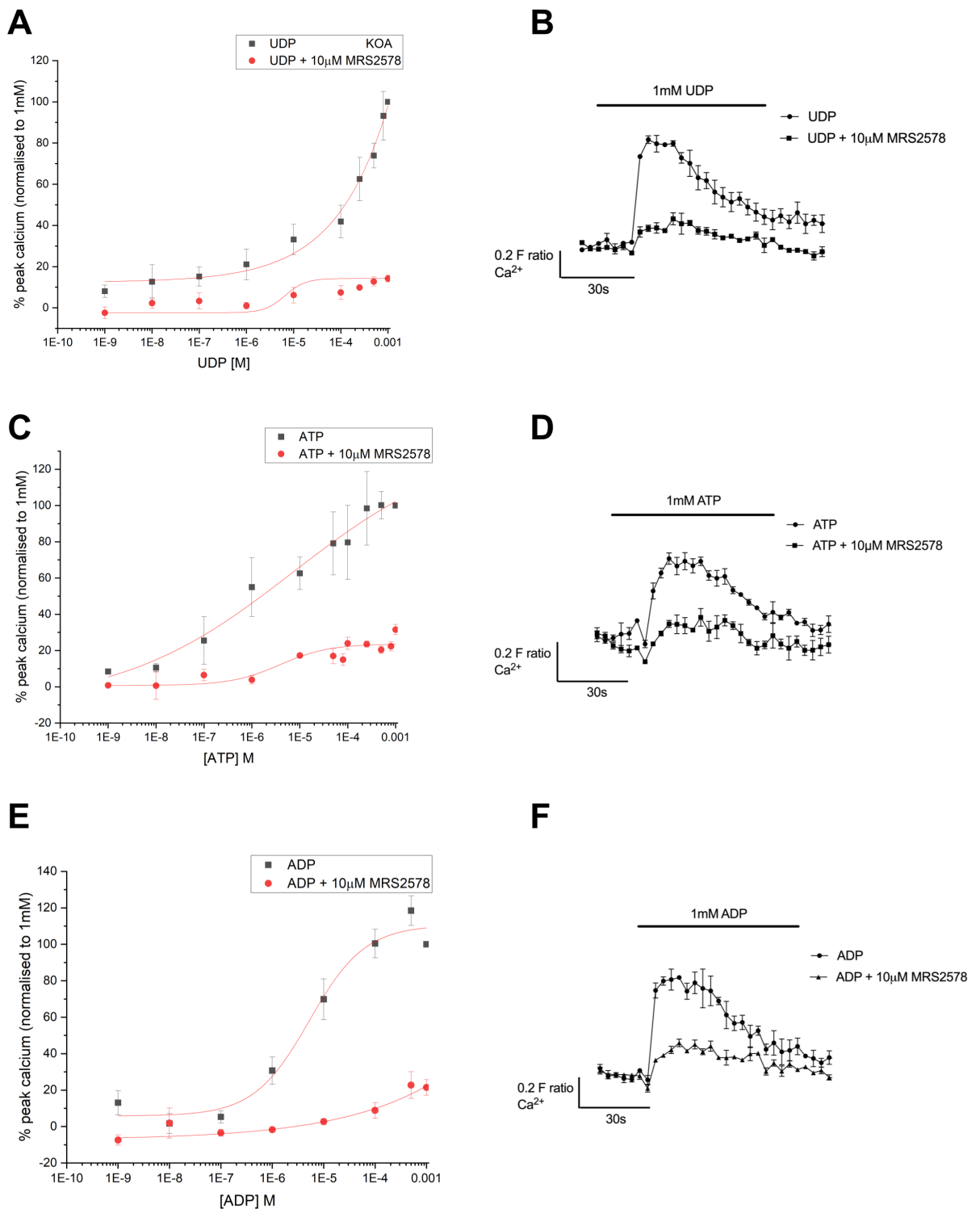


**Figure 3.10: UDP, ATP and ADP elicit a calcium response in PHC.** PHC were incubated with FURA-2 AM and intracellular calcium changes were measured in response to UDP (A,B), ATP (C,D) and ADP (E,F) stimulation,  $\pm$  10 $\mu$ M MRS2578. Data represented as mean  $\pm$  SEM. N=4 (separate patient isolates). Peak of the response F ratio (340/380ex and 510em) was normalised to 1mM response.

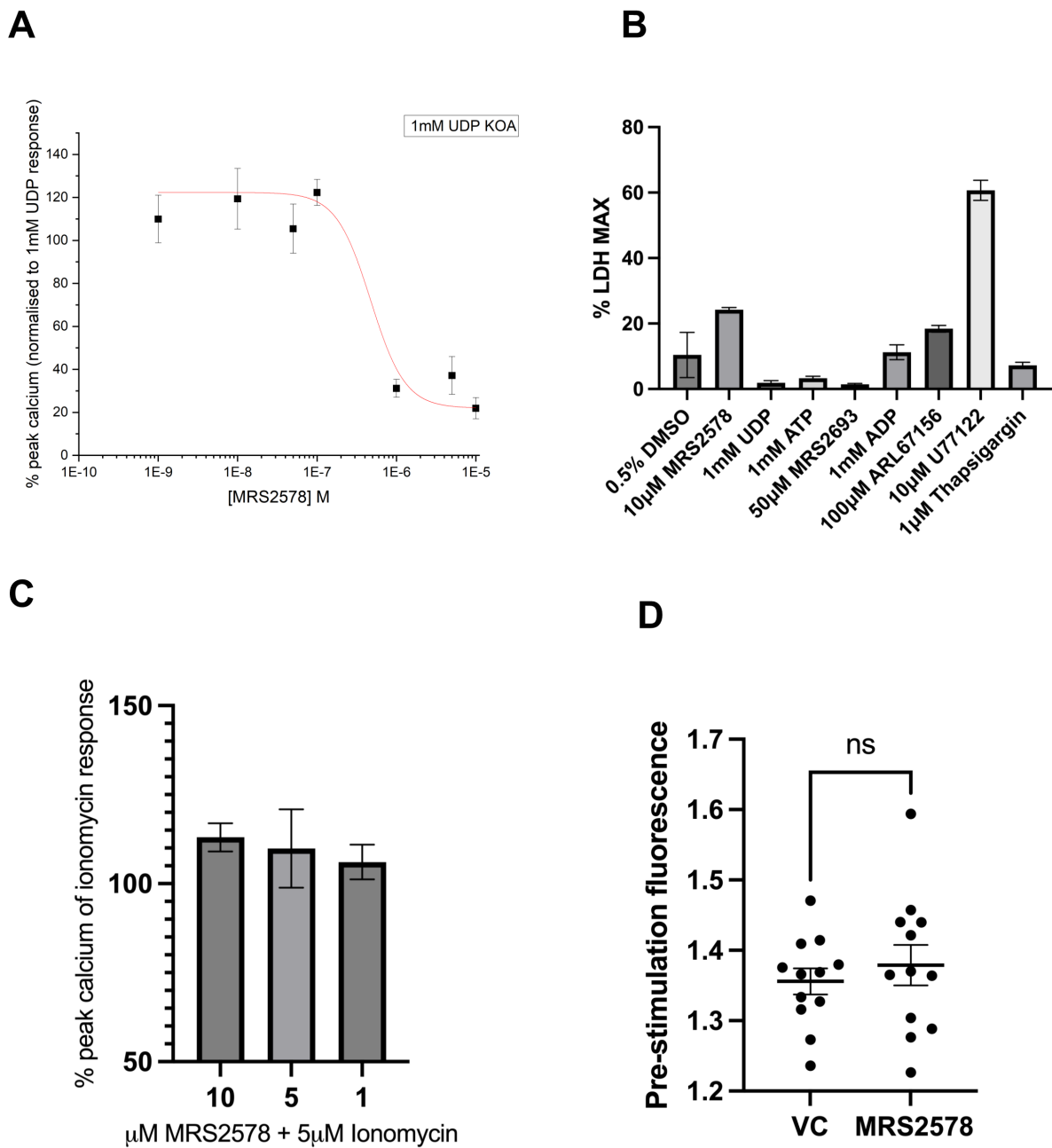


**Figure 3.11: MRS2578 Pharmacology & Toxicity.** MRS2578  $IC_{50}$  was determined (A) as well as its effect on LDH release for 30 minutes (B), the ionomycin response (C) and pre-stimulation fluorescence (D) in PHC. Data presented as mean  $\pm$  SEM. N=3.

### 3.2.5 The Function of P2Y6 in PHC

With the evidence that PHC express a functional P2Y6 receptor and that it is over-expressed in diseased chondrocytes, the next step was to try and understand why it is over-expressed by investigating how it can affect chondrocyte phenotype, if at all.

IL-1 $\beta$  is a cytokine commonly used in *in vitro* chondrocyte research as it is thought to mimic the inflammatory environment of OA and stimulates a lot of the pathways that are over-active. When stimulated with 5ng/mL recombinant human IL-1 $\beta$  for 6 hours, the expression of P2Y6 decreases significantly in PHC, but not in SW1353 nor C28/I2 cells, where it displays a trend to increased expression (Fig. 3.12).

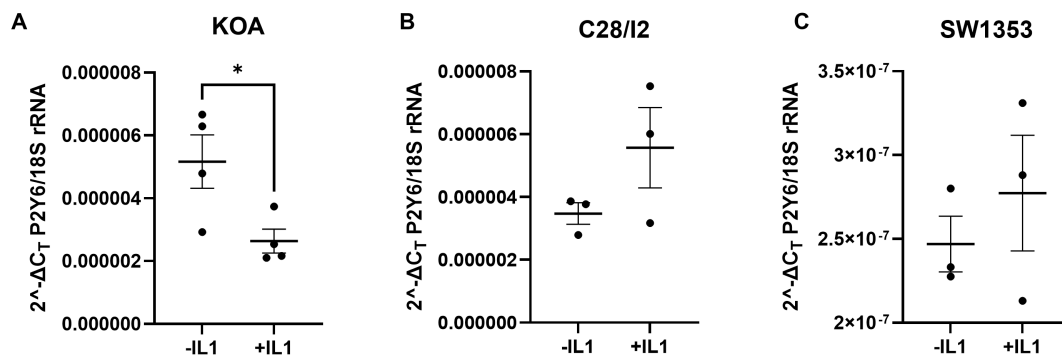


**Figure 3.12: Effect of IL-1 $\beta$  stimulation on P2RY6 mRNA.** P2RY6 mRNA levels were detected by qRT-PCR following stimulation with 5ng/mL IL-1 $\beta$  for six hours in KOA (A), C28/I2 (B) and SW1353 (C) cells. The P2RY6 primer set utilized a FAM/TAMRA based fluorescent probe for detection. Data represented  $\pm$  SEM, N=3/4, unpaired t-test \* $p$  < 0.05.

### 3.2.6 UDP- $\beta$ S nor MRS2578 has any effect on collagen deposition in PHC

The primary function of a chondrocyte is to produce the extracellular matrix that forms the cartilage tissue, of which one of the major components is collagen. Alteration of production and secretion of collagen fibres is relevant to OA as it is part of the remodelling and anabolic process of matrix turnover that becomes dysregulated. Initially, a Sirius Red staining protocol was tested in PHC, showing

that addition of ascorbic acid to the media increased collagen deposition and that TGF- $\beta$ 3 and apyrase increased and decreased it, respectively, over a period of 48 hours. UDP- $\beta$ S, a non-hydrolysable analogue of UDP, was used in longer term studies to agonise P2Y6 as UDP, as well as other nucleotides, are relatively unstable and can be metabolised by cellular ectonucleotidases [225]. As such, to avoid both the introduction of other nucleotides (as metabolites of UDP) and to ensure chronic UDP exposure, the non-hydrolysable agonist was used. When P2Y6 is activated with UDP- $\beta$ S or inhibited with MRS2578 over the same 48 hour period, there was no change in collagen deposition observed (Fig. 3.13).

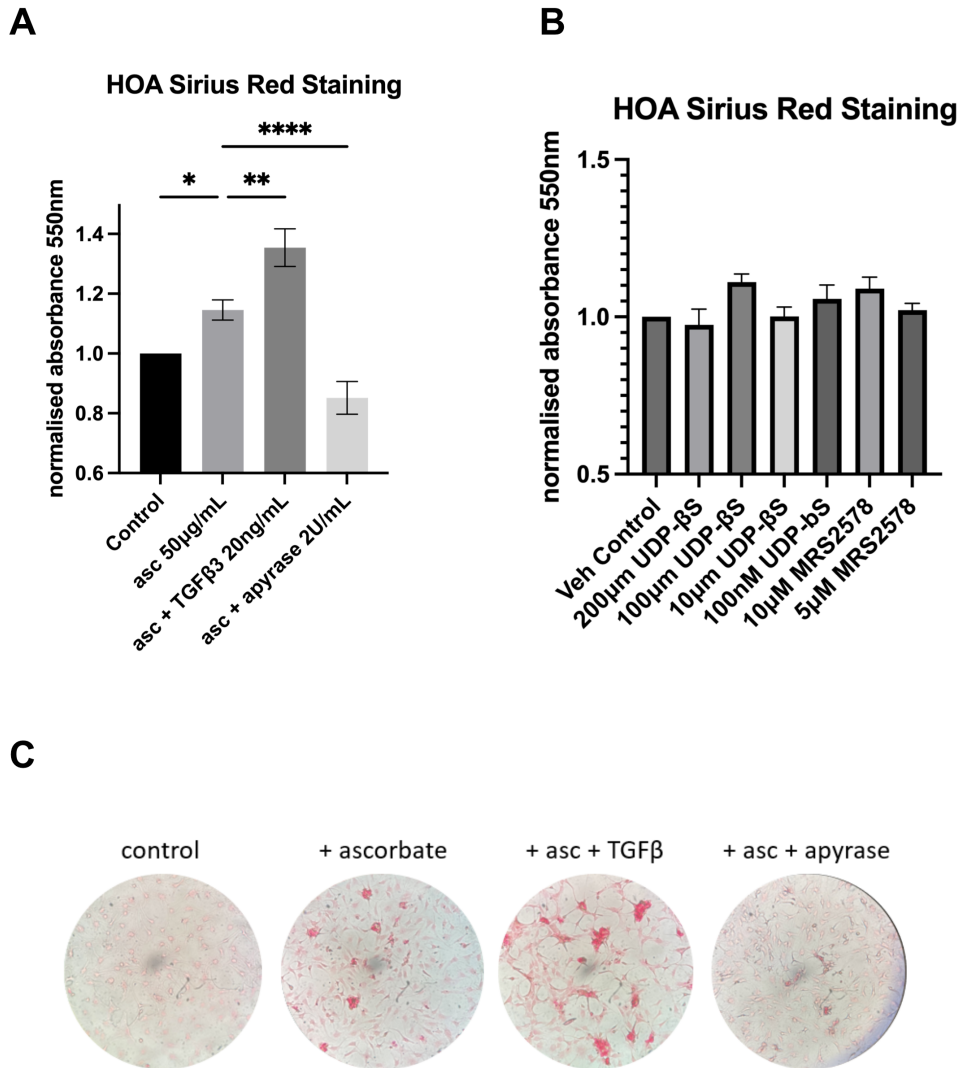


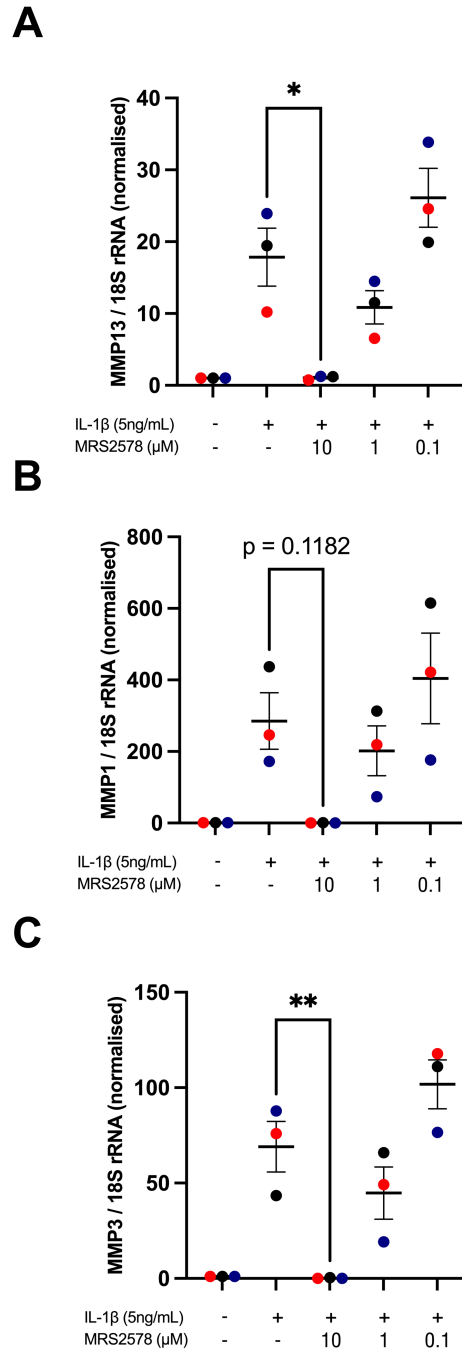
**Figure 3.13: Effect of UDP $\beta$ S and MRS2578 on Collagen Deposition.** HOA PHC were stimulated with 2-Phospho L-ascorbic acid (asc)  $\pm$  TGF $\beta$ -3  $\pm$  apyrase (A,C), UDP- $\beta$ S or MRS2578 (B) for 48 hours, followed by fixation and staining of the cell layer with sirius red. Data represented  $\pm$  SEM, N=3, one-way ANOVA with Tukey's post-hoc test, \* $p$  = < 0.05, \*\* $p$  = < 0.01, \*\*\* $p$  = < 0.001, \*\*\*\* $p$  = < 0.0001.

### 3.2.7 MRS2578 abrogates IL-1 $\beta$ induced MMP expression in PHC

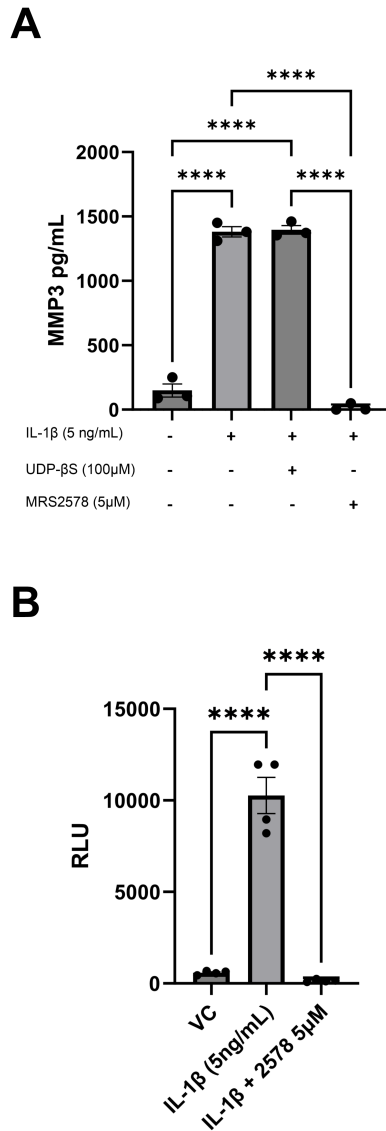
A hallmark of chondrocyte phenotype is the induction of expression of catabolic proteases, such as matrix metalloproteinases and ADAMTS', upon stimulation with cytokines, such as interleukin-1 $\beta$  or tumour necrosis factor  $\alpha$  (TNF $\alpha$ ). To assess the contribution of P2Y6 to this response, if any, HOA PHC were incubated with IL-1 $\beta$  in the presence and absence of varying concentrations of MRS2578 (P2Y6 antagonist)(Fig. 3.14). MRS2578 significantly inhibited the IL-1 $\beta$  induction

of *MMP13* and *MMP3* at 10 $\mu$ M in a dose-dependent manner at the mRNA level. The difference between 10 $\mu$ M and 0.1 $\mu$ M was statistically significant, as well as that between 1 $\mu$ M and 0.1 $\mu$ M for both *MMP13* and *MMP3*. *MMP1* showed a similar trend, albeit not statistically significant.

This alteration of MMP induction was also seen at the protein level, using an ELISA (Fig. 3.15). There was a significant reduction in the amount of MMP-3 protein secreted into the cell culture supernatant by PHC in the same 6 hour period with the addition of 5 $\mu$ M MRS2578, however the addition of the non-hydrolysable UDP analogue, UDP- $\beta$ S, had no effect. NF $\kappa$ B has long been established as a key mediator of interleukin signalling. To understand whether NF $\kappa$ B was mediating the inhibition of this response by MRS2578, a luciferase reporter plasmid was used. ATDC5 cells were used as they are easily transfectable, whereas primary cells are not. In ATDC5 cells transfected with the NF $\kappa$ B luciferase reporter plasmid, there was significantly less luciferase activity when cells were incubated with IL-1 $\beta$  and 5 $\mu$ M MRS2578 for 6 hours (Fig. 3.15B) compared to IL-1 $\beta$  alone.

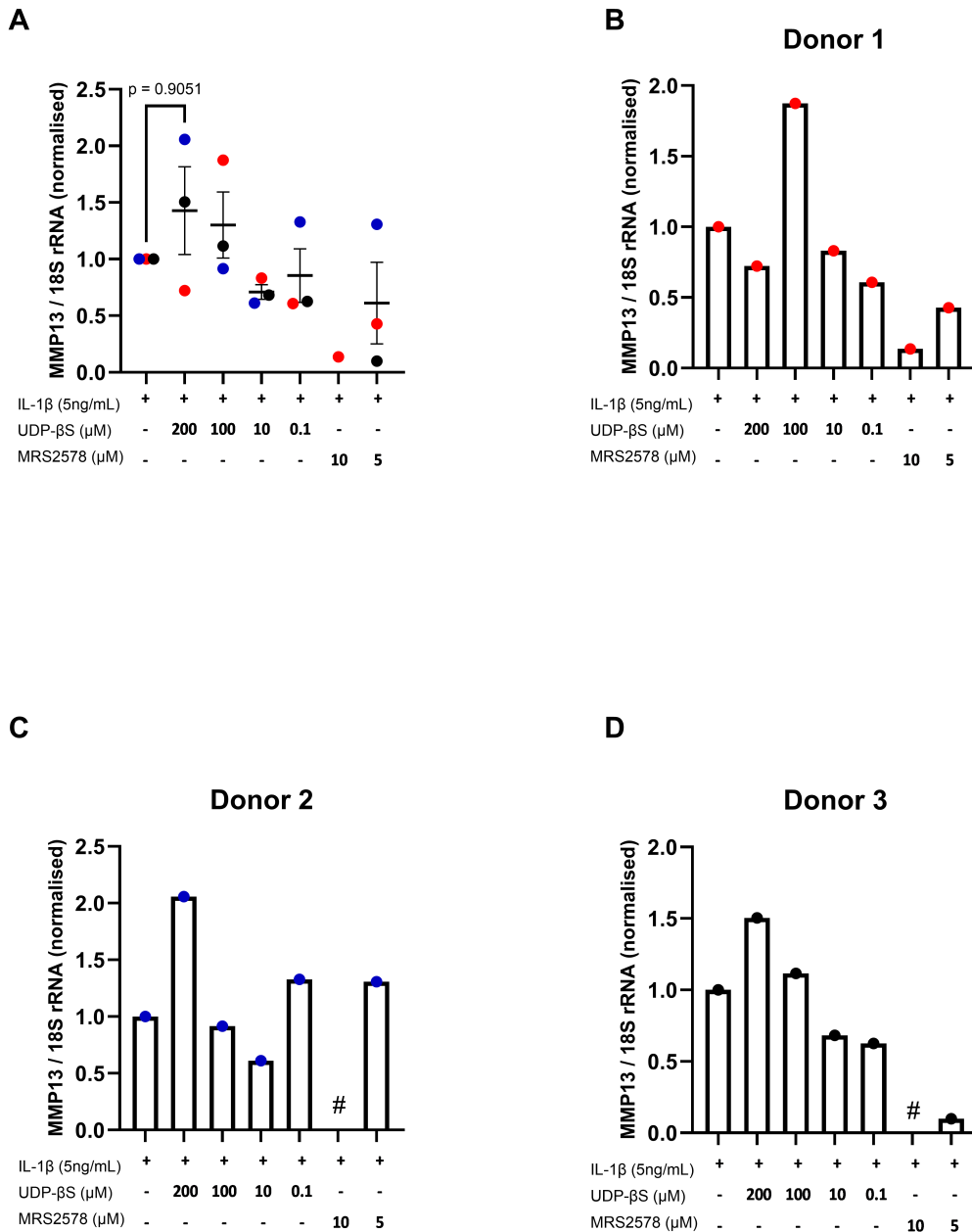


**Figure 3.14: Effect of MRS2578 on IL-1 $\beta$  induced MMP expression.** HOA PHC were stimulated IL-1 $\beta$   $\pm$  MRS2578 for 6 hours, followed by qRT-PCR for *MMP13* (A), *MMP1* (B) and *MMP3* (C). Data represented  $\pm$  SEM, N=3, one-way ANOVA with Tukey's post-hoc test, \* $p$  = < 0.05, \*\* $p$  = < 0.01, \*\*\* $p$  = < 0.001, \*\*\*\* $p$  = < 0.0001.

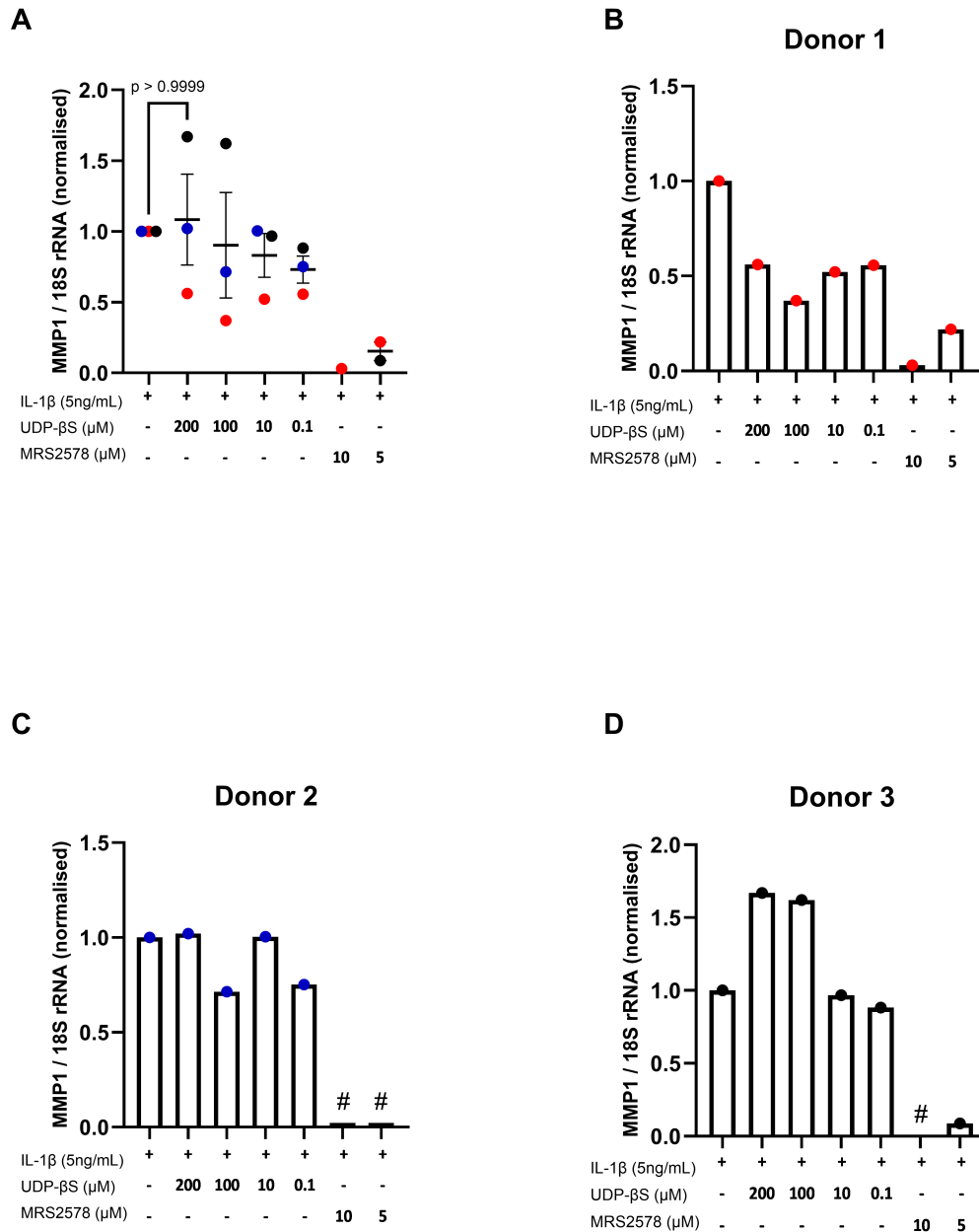


**Figure 3.15: Effect of MRS2578 on MMP secretion and NF $\kappa$ B Activity.** (A) PHC were stimulated IL-1 $\beta$   $\pm$  MRS2578 or UDP- $\beta$ S for 6 hours. MMP-3 secretion was detected in culture supernatants by ELISA. (B) ATDC5 cells were transfected with an NF $\kappa$ B luciferase plasmid and treated with IL-1 $\beta$   $\pm$  MRS2578 for 6 hours, followed by detection of luciferase activity. Data represented  $\pm$  SEM, N=4, one-way ANOVA with Tukey's post-hoc test, \* $p$  = < 0.05, \*\* $p$  = < 0.01, \*\*\* $p$  = < 0.001, \*\*\*\* $p$  = < 0.0001.

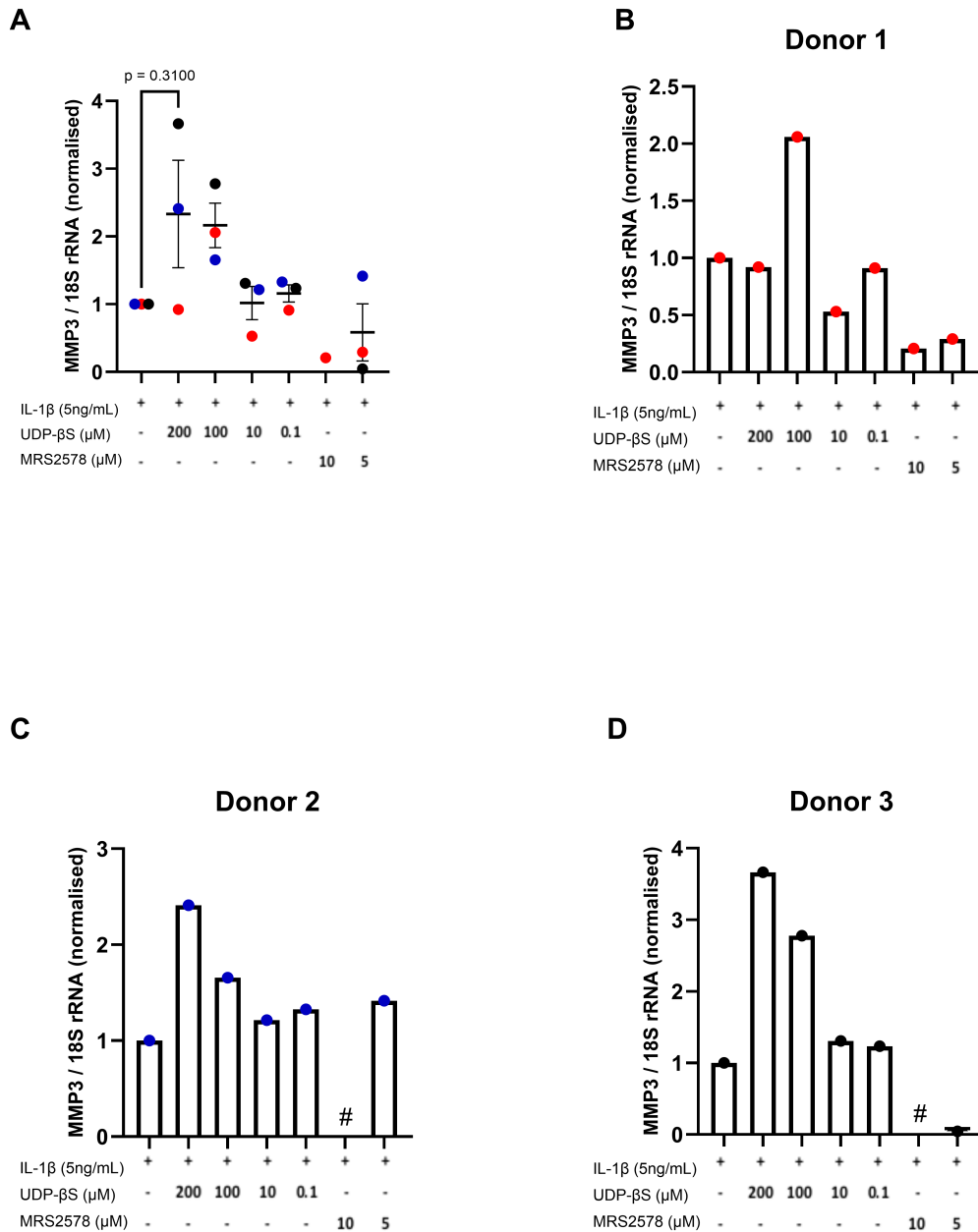
The hypothesis that followed from these data was that if inhibiting P2Y6 with MRS2578 reduced the IL-1 $\beta$  induced MMP expression, that activating with UDP- $\beta$ S should increase it. As such, PHC were incubated with IL-1 $\beta$   $\pm$  MRS2578 and UDP- $\beta$ S (0.1 $\mu$ M - 200 $\mu$ M) for 6 hours (Fig. 3.18). There was no significant increase in *MMP13*, *MMP3* nor *MMP1* expression with UDP- $\beta$ S compared to IL-1 $\beta$  alone. There was also relatively high inter-donor variability. Some donors did have increased MMP expression with UDP- $\beta$ S, for example donor 2 and *MMP13*, however this was not in a dose-dependent manner. Donor 3 does seem to have a dose-dependent increase in MMP expression with UDP- $\beta$ S, which is most clearly seen with *MMP3*. However, this was not repeated across donors and is not statistically significant as it is only 1 biological replicate. As such, this data cannot prove the hypothesis that UDP- $\beta$ S increases IL-1 $\beta$  induced MMP expression.



**Figure 3.16: Effect of MRS2578 and UDP- $\beta$ S on IL-1 $\beta$  stimulated *MMP13* expression.** HOA PHC were stimulated IL-1 $\beta$   $\pm$  MRS2578 or UDP- $\beta$ S for 6 hours, followed by RNA extraction and qRT-PCR for *MMP13*. Data represented  $\pm$  SEM, N=3, one-way ANOVA with Tukey's post-hoc test. Where no transcript was amplified within 40 cycles, this is represented by #. A represents all donors combined. B,C and D are the three donors separated.



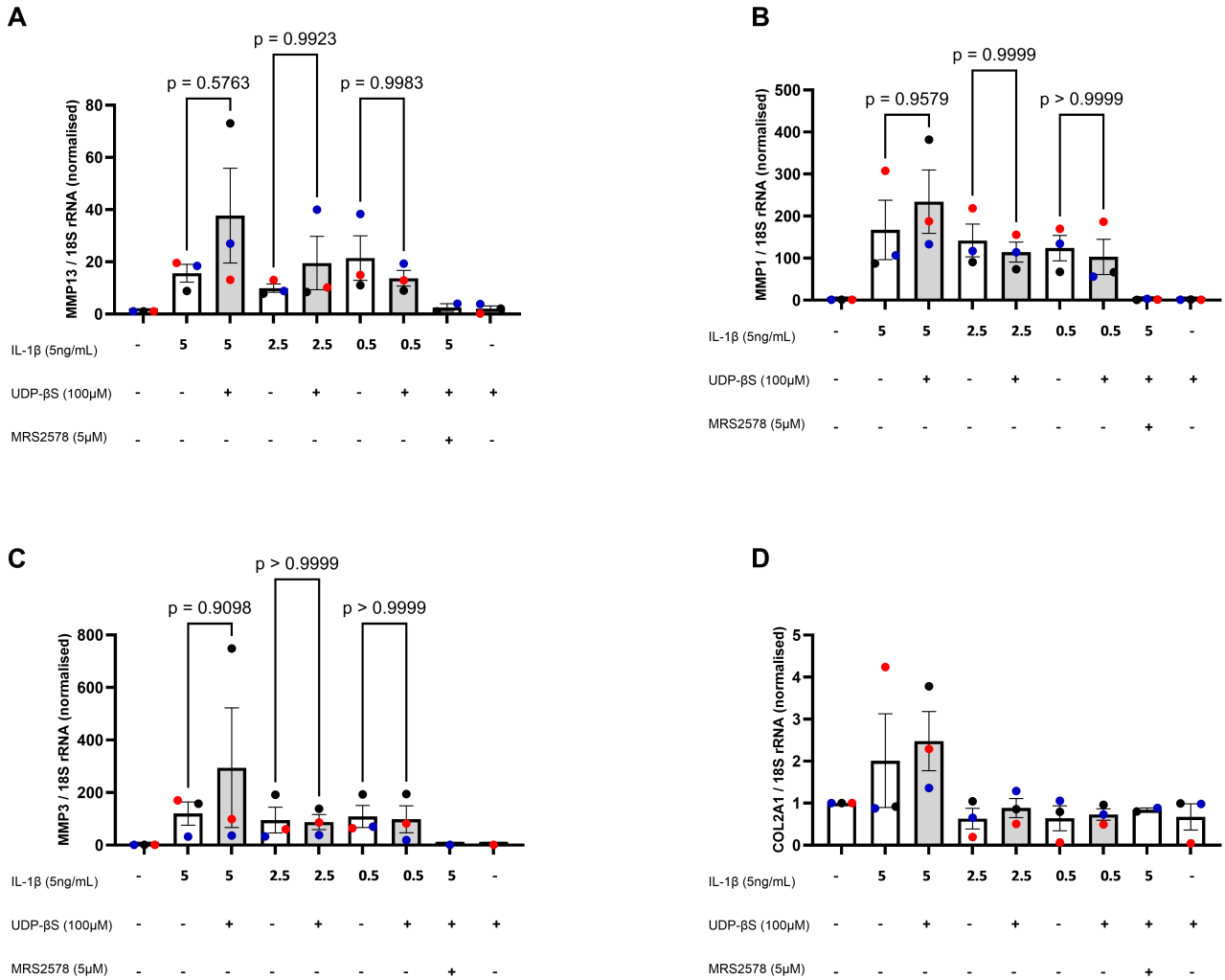
**Figure 3.17: Effect of MRS2578 and UDP-βS on IL-1β stimulated MMP1 expression.** HOA PHC were stimulated IL-1β ± MRS2578 or UDP-βS for 6 hours, followed by RNA extraction and qRT-PCR for MMP1. Data represented ± SEM, N=3, one-way ANOVA with Tukey's post-hoc test. Where no transcript was amplified within 40 cycles, this is represented by #. A represents all donors combined. B,C and D are the three donors separated.



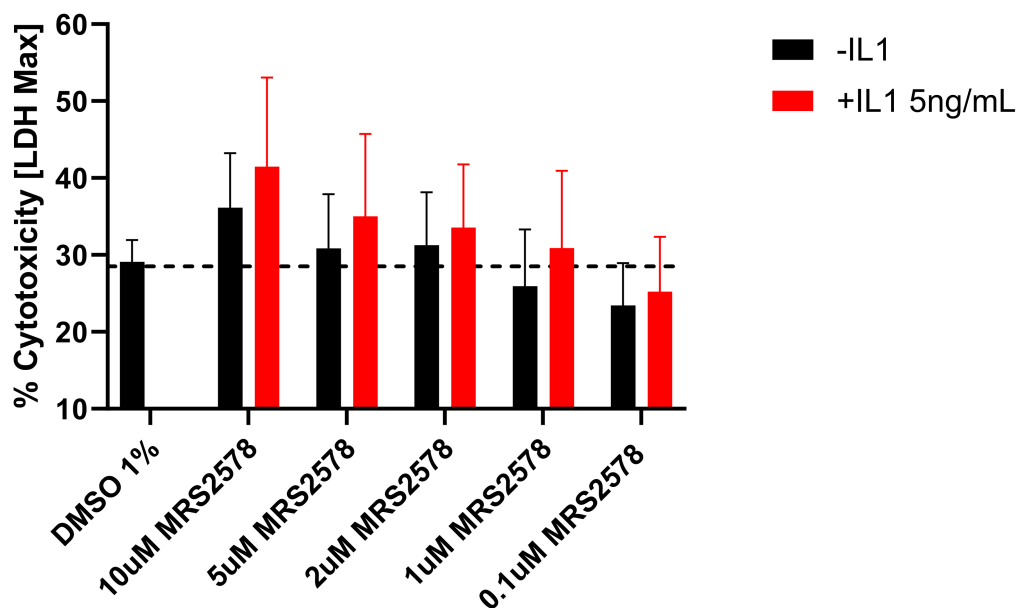
**Figure 3.18: Effect of MRS2578 and UDP- $\beta$ S on IL-1 $\beta$  stimulated *MMP3* expression.** HOA PHC were stimulated IL-1 $\beta$   $\pm$  MRS2578 or UDP- $\beta$ S for 6 hours, followed by RNA extraction and qRT-PCR for *MMP3*. Data represented  $\pm$  SEM, N=3, one-way ANOVA with Tukey's post-hoc test. Where no transcript was amplified within 40 cycles, this is represented by #. A represents all donors combined. B,C and D are the three donors separated.

One possible reason for the lack of induction of MMP responses by UDP- $\beta$ S is that the interleukin signalling system is already maximally activated at 5ng/mL, and so to test whether this hypothesis, lower concentrations of IL-1 $\beta$  (0.5ng/mL - 5ng/mL) were used to stimulate  $\pm$  UDP- $\beta$ S at 100 $\mu$ M (Fig. 3.19). There was no significant induction of *MMP13*, 1 or 3 at any concentration of IL-1 $\beta$ , and again there was relatively high inter-donor variability. The donor depicted with the black dots does show an induced MMP response with 5ng/mL IL-1 $\beta$  and UDP- $\beta$ S, compared to IL-1 $\beta$  alone, that is seen across all three matrix metalloproteinases measured.

Moreover, the donor depicted by the blue dot does show a trend of induction of *MMP13* with 200 $\mu$ M UDP- $\beta$ S at a concentration of 2.5ng/mL IL-1 $\beta$ . However, these responses are not significant, not repeated across donors and not robust. Collagen II was also measured as an indicator of toxicity, and it shows that there was a slight induction with 5ng/mL IL-1 $\beta$  but no significant changes across the experimental groups. LDH release was also measured from PHC with the addition of MRS2578  $\pm$  IL-1 $\beta$  for six hours (Fig. 3.20), showing an approximate increase of 10% above vehicle control with 10 $\mu$ M of MRS2578, that increases further by about 5% with the addition of IL-1 $\beta$ . This toxicity reduces in a dose dependent manner.



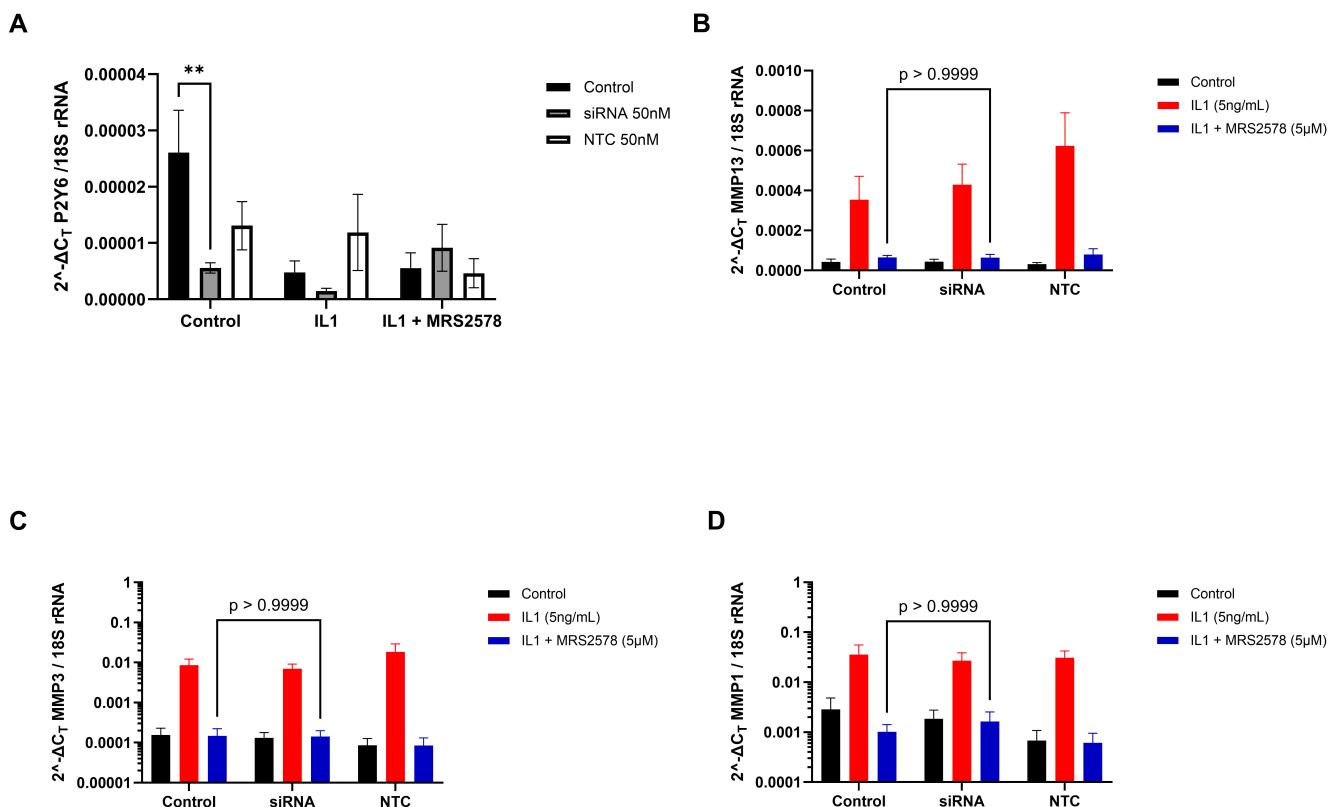
**Figure 3.19: Effect of MRS2578 and UDP- $\beta$ S on IL-1 $\beta$  stimulated MMP expression.** HOA PHC were stimulated IL-1 $\beta$   $\pm$  MRS2578 or UDP- $\beta$ S for 6 hours, followed by RNA extraction and qRT-PCR for *MMP13* (A), *MMP1* (B), *MMP3* (C) and *COL2A1* (D) as a measure of toxicity. Data represented  $\pm$  SEM, N=3, one-way ANOVA with Tukey's post-hoc test.



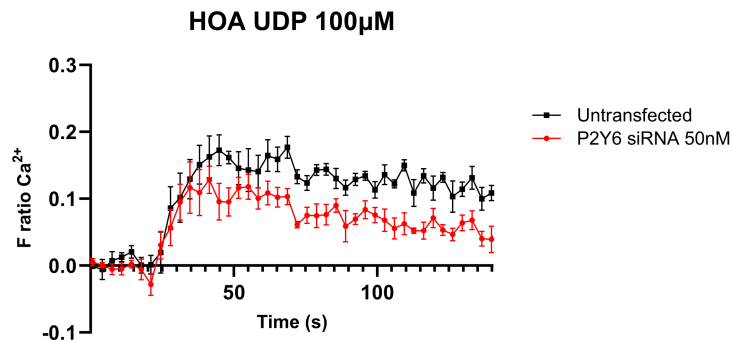
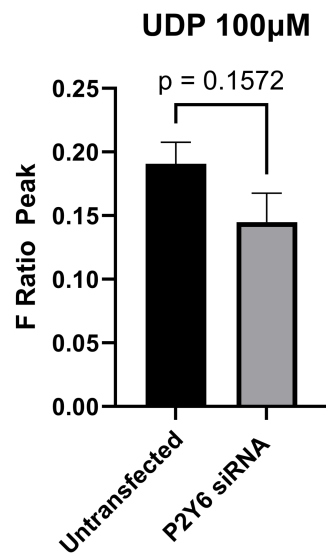
**Figure 3.20: Effect of MRS2578 on LDH release by PHC.** HOA PHC were stimulated with IL-1 $\beta$   $\pm$  MRS2578 for 6 hours, and lactate dehydrogenase release into cell culture supernatants was measured as a function of cytotoxicity. Data represented  $\pm$  SEM, N=3.

To ensure the specificity of the assay and MRS2578, the dependency of MRS2578 on P2Y6 expression was deemed important to understand. To test the hypothesis that MRS2578 is not acting via P2Y6 to facilitate this response, *P2RY6* expression was reduced with a small interfering RNA (siRNA). Fig. 3.21 shows that the siRNA was successful in reducing *P2Y6* expression significantly at the mRNA level. Fig. 3.22 shows the functional impact of this reduction in *P2RY6* transcript by assessing the UDP-elicited calcium response. Whilst the reduction in mRNA is statistically significant, the reduction in peak size of the calcium response is not. In the P2Y6-knockdown cells, there was no alteration in the action of MRS2578 in reducing the IL-1 $\beta$  induction of *MMP13*, 1 nor 3 between the control and knockdown cells. The control siRNA mix (depicted as NTC) also showed that the transfection had a slight effect on the expression of *P2RY6*, but not significantly compared to control. The action of MRS2578 on IL-1 $\beta$  induced genes was also tested in SW1353 as they did not have a UDP-elicited calcium response (Fig. 3.23) and would therefore provide further data on the reliance of this response on functional P2Y6 expression. MRS2578 had a similar effect in SW1353 compared to PHC. Although not significant, there was a similar trend of a re-

duction in *MMP13*, 3 and 1 expression and a lack of induction by UDP- $\beta$ S. This effect was also seen when stimulating with another cytokine, TNF $\alpha$ . With this inflammatory mediator, there was a significant reduction in MMP expression with MRS2578 and a lack of significant induction with UDP- $\beta$ S. This response was also tested in 1321N1 cells, both parental and P2Y6 expressing. Similarly to SW1353 cells, parental 1321N1 do not mount any calcium responses to nucleotides, and a P2Y6 expressing 1321N1 cell line had been previously made and characterised. Fig. 3.24 shows that this response is dependent on P2Y6 expression and function, as the reduction in IL-1 $\beta$  induced *MMP13* expression, catalysed by MRS2578, is only significant in the P2Y6 expressing cells.



**Figure 3.21: Effect of siRNA knockdown of P2Y6 on MRS2578 mediated inhibition of IL-1 $\beta$  response.** PHC were transfected with two P2Y6 targeting siRNA (25nM each) and a non-targeting control (NTC). Cells were then stimulated with IL-1 $\beta$   $\pm$  MRS2578 for 6 hours, followed by qRT-PCR for *P2RY6* (A), *MMP13* (B), *MMP1* (C), *MMP3* (D). Data represented  $\pm$  SEM, N=3. One-way ANOVA with Tukey's post-hoc test, \* $p$  < 0.05, \*\* $p$  < 0.01.

**A****B**

**Figure 3.22: Effect of siRNA knockdown of P2Y6 on UDP elicited calcium response.** HOA PHC were transfected with two siRNA targeting P2Y6 (25nM each). 48 hours later, the cells were assayed for UDP calcium responses using the flexstation. A: trace showing calcium response, B: bar chart showing peaks. Data represented  $\pm$  SEM, N=1, student's t test.

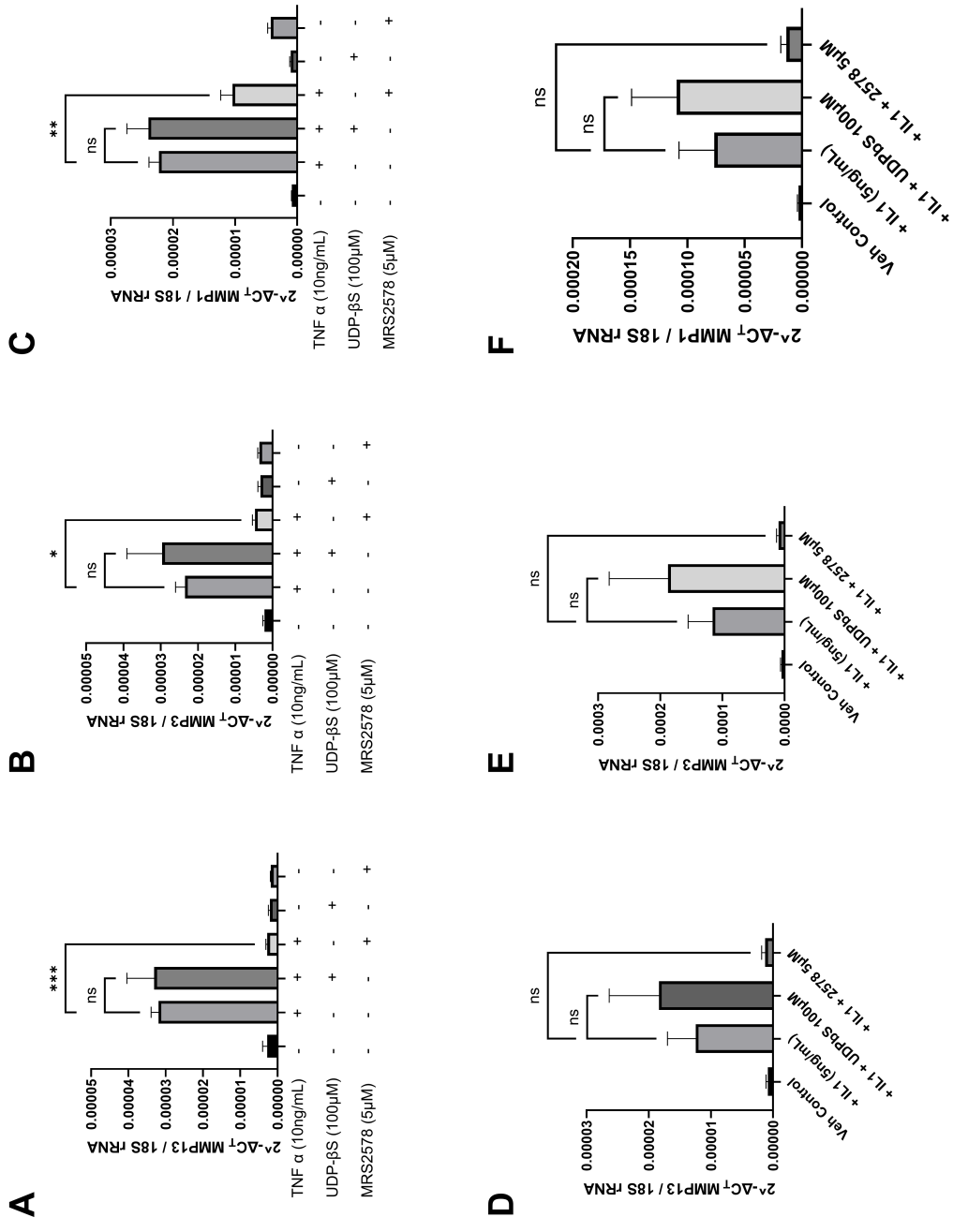


**Figure 3.23: Effect of UDPbS and MRS2578 on IL-1 $\beta$  response in SW1353 cells.** SW1353 were stimulated with TNF- $\alpha$  (A-C) IL-1 $\beta$  (D-F)  $\pm$  UDP- $\beta$ S and MRS2578 for 6 hours. RNA extracted and qRT-PCR was performed. Data represented  $\pm$  SEM, N=3, one way ANOVA with Tukey's post-hoc test \* $p < 0.05$ , \*\* $p < 0.01$ , \*\*\* $p < 0.001$ .

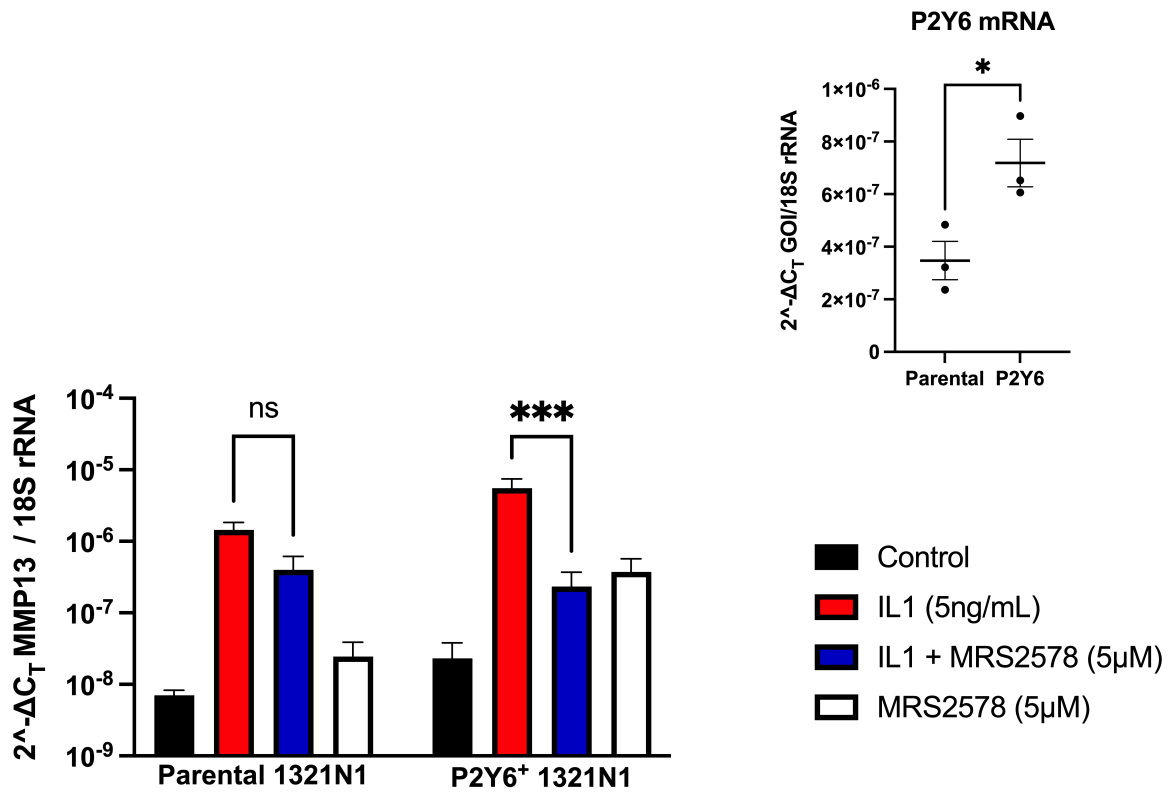


**Figure 3.24: Effect of MRS2578 on IL-1 $\beta$  response in P2Y6 expressing and parental 1321N1 cells.** Parental and P2Y6 expressing 1321N1 cells were seeded into a 24 well plate and stimulated with IL-1 $\beta$   $\pm$  MRS2578 for 6 hours. RNA was extracted and qRT-PCR was performed. Data represented  $\pm$  SEM, N=3, one way ANOVA with Tukey's post-hoc test \* $p$  = < 0.05, \*\* $p$  = < 0.01, \*\*\* $p$  = < 0.001.

## 3.3 Discussion

### 3.3.1 Two commonly used chondrocyte cell lines have phenotypic differences to PHC.

As well as primary human chondrocytes, two cell lines were used. These are a fibroblast-like chondrosarcoma cell, SW1353 and an SV40-immortalised costal chondrocyte line, C28/I2 [226]. Both of these cell lines have been used extensively in chondrocyte research, and the literature contains numerous examples of how they are similar to PHC, often pertaining to the upregulation of matrix metalloproteinases in response to IL-1 $\beta$  stimulation [227]. However, gene expression profiling revealed that whilst SW1353 do have an IL-1 $\beta$  response, there were some differences to PHC, including key mediators like bone morphogenetic proteins (BMPs) not being induced by IL-1 $\beta$  [228]. Owing to the relatively little known about the role of purinergic signalling in chondrocytes, it was also unknown how these two commonly utilised cell lines differ from each other and PHC in their purinergic expression profile and functionality.

Initially, mRNA expression of the purinergic receptors was tested with a comparative quantitative RT-PCR approach. To ensure robustness and validity, Ct values over 35 were discounted as non-specific/unreliable amplification as a relatively high amount of cDNA, 12.5ng, was used across all samples. None of the cells tested express *P2RY13*, showing consistency between the cell types. Moreover, generally speaking, the expression was relatively similar across cell types. *P2RX3* was only expressed by PHC. *P2RX4* was one of the most highly expressed transcripts across all three cell types, as well as *ADORA2B*. Moreover, there was larger variability in the KOA cell type as evidenced by larger SEM values. This is to be expected as a result of donor heterogeneity.

Where the cell lines and PHC differ more starkly is in their nucleotide-elicited calcium responses. PHC, along with most cell types, respond to ATP, UDP and ADP with a characteristic dose-dependent and transient intracellular calcium elevation. However, neither C28/I2 nor SW1353 mounted such responses, despite expressing multiple purinergic receptors. There has been no documented

nucleotide-elicited calcium response in the literature in SW1353 cells, however a calcium response to 2-ABP, an activator of orai store-operated calcium entry channel, has been shown [229]. Intracellular calcium transients have been demonstrated in response to histamine and cannabidiol in C28/I2 cells as well [230, 231]. SW1353 were sensitive to thapsigargin, showing that they do have intracellular calcium stores and so the reason for their lack of nucleotide-elicited calcium responses is not clear. To test if it was as a result of a lack of membrane localisation of P2Y6, membrane proteins were biotinylated and extracted using streptavidin. There was no detection of P2Y6 in the biotin extracted fraction of the cell lysate, however this data is weakened by the lack of a positive control. The cells also did not respond to ATP, which would activate multiple P2X receptors, so it would be unlikely that none of these receptors were being expressed at the cell surface despite there being mRNA expression. Moreover, when SW1353 overexpress P2Y6 by means of transfection of exogenous DNA, they did have a UDP-elicited calcium response. It is therefore possible that the endogenous *P2RY6* expressed does not function as expected, it is not trafficked to the membrane or that simply the expression is not high enough.

Another area where the cells differ from PHC is in how *P2RY6* expression changes in response to IL-1 $\beta$  stimulation. *P2RY6* is significantly downregulated with a 6h stimulation of 5ng/mL IL-1 $\beta$  in PHC, whereas there was no significant change in either C28/I2 nor SW1353. This indicates that there are differences to the pathways activated by IL-1 $\beta$ , despite all the cells mounting a classical induction of MMPs.

### **3.3.2 P2Y6 is over-expressed in OA**

With an initial focus on understanding how the purinergic system affects chondrocyte phenotype in the context of OA, existing data was analysed using SkeletalVis [219], which is an accessible online transcriptomics database pertaining to musculoskeletal physiology and disease. Analysis of five separate experiments showed a trend of higher expression in OA chondrocytes compared to phenotypically normal chondrocytes, with a fold change of 1.88 ( $\pm$  0.3 SEM). This is not significant at the level of 0.05, but is at the level of 0.1. The five experi-

ments were somewhat heterogeneous, for example, between hip and knee OA, as well as across different subtypes of OA such as anteromedial gonarthrosis. However, each study explores a facet of the OA vs normal chondrocyte transcriptome, and the heterogeneity adds confidence to the finding as it is reproducible across multiple experimental variables. cDNA kindly provided by Dr. Matt Barter (Newcastle University) from isolated chondrocytes of OA joints and NOF (neck of femur) healthy joints were assayed for *P2RY6* by qRT-PCR and showed significantly higher expression of *P2RY6* from OA chondrocytes. Studies looking at UDP concentrations in synovial fluid found it to be significantly higher in rheumatoid arthritis but not OA, and stimulated proliferation and IL-6 secretion in RA fibroblast-like synoviocytes [232]. Using chondrocytes from patients undergoing arthroplasty secondary to OA always presents large variability as the criteria for surgical intervention is often pain, which does not always correlate with histological or radiographic measures of severity. As such, there can be high inter-donor variability.

### **3.3.3 Functionality of P2Y6 in PHC**

Initially, detection of P2Y6 protein was determined by western blotting. Two antibodies were tested - an Alomone polyclonal antibody and an Abcam monoclonal antibody. The polyclonal antibody produced bands that were much higher than expected, which can happen if the protein is modified in some way eg glycosylated, or if the conditions were not reducing/denaturing. However, the bands produced were over 100kD larger than expected, so it was deemed that this antibody was non-specific, which can happen with a polyclonal antibody. The other antibody produced bands at the expected weight and was confirmed using a parental and P2Y6-expressing astrocytoma cell line, showing that both PHC isolates express P2Y6 protein. KOA PHC cells were then tested for a UDP, ATP and ADP-elicited calcium response using FURA-2 AM to determine that the protein expressed was functional. Initially, cells were incubated for 1 hour with the dye, but this resulted in high cytotoxicity, necessitating a reduction in the incubation time to 30 minutes. This led to lower cytotoxicity but equally efficient loading

of the dye into the cells as assessed by unstimulated fluorescence values (loading values). PHC mounted a dose-dependent calcium response to UDP, ATP and ADP with an  $EC_{50}$  of 30.8  $\mu$ M, 3.35  $\mu$ M and 11.7  $\mu$ M, respectively. The contribution of P2Y6 to these responses was tested by incubation of cells with MRS2578 10 $\mu$ M for 20 minutes prior to nucleotide stimulation. 10 $\mu$ M was chosen as the inhibitory concentration from the literature as a commonly used concentration to achieve maximal inhibition [232–234]. MRS2578 is a diisothiocyanate antagonist of P2Y6, that is described as insurmountable, meaning it both depresses the maximal response and causes a rightward shift in the dose response curve. It has shown to be potent at P2Y6, with a reported  $EC_{50}$  of 37nM, and demonstrated to be selective to this receptor, with the exception of showing approximately 20% inhibition of the 2-MeSADP response at the P2Y1 receptor [235]. MRS2578 inhibited the response to UDP, ATP and ADP at a maximal concentration by 81%, 71% and 78%, respectively. As expected, it inhibited the UDP response to the largest extent but somewhat unexpectedly also inhibited the ATP and ADP response by  $\geq 50\%$ . The main agonist of P2Y6 is UDP, with ADP as a partial agonist. This may explain why MRS2578 inhibited the ADP response as much as it did. Furthermore, the rapid metabolism of ATP by ectonucleotidases to ADP may also have meant that a proportion of the ATP calcium response was in fact caused by ADP stimulation of P2Y6, which is why the ATP response was also blocked by MRS2578. Another possibility is that the concentration of MRS2578 used was too high. Experimentally, the  $IC_{50}$  of MRS2578 was determined to be 428nM with respect to UDP, and so at 10 $\mu$ M the antagonist may have been acting non-specifically to inhibit the ATP and ADP response. These dose response experiments could not be repeated at a lower concentration of MRS2578 to test this hypothesis owing to the lack of supply of primary chondrocytes. The inhibition seen with MRS2578 was unlikely to be as a result of toxicity, as MRS2578 had no effect on the magnitude of the cells' response to ionomycin nor caused significant LDH release within the 30 minute time period.

### 3.3.4 MRS2578 inhibits the inflammatory response to IL-1 $\beta$ in PHC

IL-1 $\beta$  has long been identified as a mediator of inducing inflammatory responses in chondrocytes, owing to its overproduction in OA tissues and ability to overwhelm the balance of anabolic and catabolic factors towards catabolism of the extracellular matrix that forms the cartilage tissue[236]. It is therefore often used to recapitulate the OA environment in *in vitro* research, despite its utility for this purpose being questioned, as discussed in 1.3.2. Nevertheless, it is a potent inducer of matrix degrading enzymes that are thought to contribute to the OA pathology of thinned cartilage. *MMP13*, *MMP3* and *MMP1* mRNA were chosen to be the measured outcomes of IL-1 $\beta$  stimulation as they are disease relevant [237] and thought to be differentially regulated [238]. The contribution of P2Y6 to the induction of these genes by IL-1 $\beta$  was tested by addition of MRS2578 for the full time period of six hours. MRS2578 at 10 $\mu$ M brought expression levels of *MMP13*, *MMP1* and *MMP3* down to basal levels, which was statistically significant in the case of *MMP13* and *MMP3*. It did this in a dose dependent manner and was a robust response seen across donor heterogeneity. This significant inhibitory effect was also seen at the MMP-3 protein level as determined by ELISA, and in NF $\kappa$ B activity in ATDC5 cells with the use of a luciferase construct. MRS2578 inhibition of NF $\kappa$ B activity has been demonstrated in HMEC-1 cells at similar concentrations and stimulation times [239]. Within the classical model of agonism and antagonism, the next hypothesis to be tested was that if MRS2578 inhibited the response, agonising UDP would magnify it. To add confidence to this data, PHC were co-stimulated with IL-1 $\beta$  and UDP- $\beta$ S, and the concentration of MRS2578 was reduced to 5 $\mu$ M. 5 $\mu$ M MRS2578 still largely maintained a significant inhibition, however UDP- $\beta$ S (200 $\mu$ M - 0.1 $\mu$ M) did not robustly increase the expression of *MMP13*, *MMP1* nor *MMP3* above that seen from induction by IL-1 $\beta$ . There was high inter-donor variability, and one donor did have slightly induced expression above IL-1 $\beta$  levels, but not significantly. Moreover, where  $C_T$  values were returned undetermined, it was inferred that this is as a result of lower than detectable transcript within the 40 cycles, rather than technical fault.

One approach that can be taken is to use a value of 40 as the cycle threshold, however this has been shown to introduce substantial bias in normalised gene expression [240]. To this end, non-detects have been represented with symbols. It is possible that the reason for the lack of induction by UDP is as a result of the system being maximally activated by a concentration of 5ng/mL IL-1 $\beta$  and therefore cannot be induced any further. Concentrations commonly used in other studies range between 5 and 10ng/mL [9, 241]. As such, MMPs were induced by lower concentrations of IL-1 $\beta$  (0.5-5 ng/mL) with or without the addition of 100 $\mu$ M UDP- $\beta$ S. There was no significant induction at any concentration of IL-1 $\beta$ , meaning it is unlikely that the IL-1 $\beta$  system being already maximally activated is the reason as to why there is no induction. Collagen II was also measured as an indicator of whether any combinations of IL-1 $\beta$ , UDP- $\beta$ S or MRS2578 were toxic as the mRNA levels of collagen II should not change in response to any of these treatments. Whilst there was slight induction with IL-1 $\beta$  at 5ng/mL, the other conditions did not change the levels of expression. LDH release was also measured to assess the toxicity of IL1 and/or MRS2578 to PHC, with a maximal concentration of DMSO at 1% (v/v), although 0.5% was more commonly used in experiments. There was toxicity above the vehicle control at 10 $\mu$ M that increased further with IL-1 $\beta$ , however at 5 $\mu$ M the toxicity above vehicle control is negligible. Whilst there is around 30-40% cell death, this is still unlikely to be the reason for the transcriptomic changes detected by qRT-PCR, especially since more often than not, the final concentration of DMSO was half as much.

MRS2578 has been assessed to be specific to P2Y6 according to the literature, with some activity at P2Y1. To understand if MRS2578 is mediating its effects through P2Y6 or another mechanism, an siRNA to P2Y6 was used to assess the impact of P2Y6 knock-down on the MRS2578 inhibition of IL-1 $\beta$  induced MMP expression. P2Y6-targeting siRNA at 50nM significantly reduced P2Y6 transcript, however did not significantly reduce the UDP-induced calcium response, meaning there was still functional P2Y6 being expressed. There was no change or reduction of sensitivity to MRS2578 with respect to its ability to reduce IL-1 $\beta$  induced *MMP13*, *MMP3* and *MMP1* expression in PHC. It is hard to prove nor disprove the hypothesis that MRS2578 is acting in a mechanism independent of P2Y6 because of

the lack of complete knockout. Whilst it would be expected that there might be a small reduction in sensitivity if the hypothesis was incorrect, it is possible that qPCR is not sensitive enough to detect those small changes and/or it may not reach significance. The effect of MRS2578 on IL-1 $\beta$  induced gene expression was also tested in the SW1353 cell line as they do not have a UDP elicited calcium response, and it can therefore be assumed that they do not express functional P2Y6. MRS2578 was able to reduce the IL-1 $\beta$  and TNF- $\alpha$  induced MMP expression in these cells, which may also be because this effect is facilitated independent of P2Y6, but again, cannot prove nor disprove the hypothesis. The only way to definitively know if MRS2578 is acting independently of P2Y6 would be with a validated knockout cell line or animal model. UDP- $\beta$  also did not induce the expression of MMPs in these cells above IL-1 $\beta$  levels, which is consistent with what was seen in PHC. Conversely, in P2Y6 or parental 1321N1 cells, which do and do not mount a UDP calcium response (data not shown, cells previously validated by Fountain lab, UEA), respectively, the ability of MRS2578 to inhibit the IL-1 response was only significantly present in the P2Y6 expressing cells, suggesting that the mechanism of inhibition is dependent on P2Y6. More work would need to be done, likely with a P2Y6 knockout, to fully elucidate the dependence of functional P2Y6 expression on this pathway and MRS2578's ability to inhibit it.

# Chapter 4

## Investigating Role of P2Y6 in Chondrogenesis

### 4.1 Introduction

The previous chapter explored the effects of P2Y6 signalling on one facet of chondrocyte hallmark phenotype - the ability to upregulate matrix degrading genes in response to inflammatory cytokines. As well as the impact on mature chondrocyte phenotype, any effects of P2Y6 signalling processes on the differentiation of precursors into chondrocytes would be pertinent. Not only because it might affect the differentiation fate of cells, but also because there are many similarities between events that occur in chondrogenesis and OA (discussed in section 1.3.1), meaning it may also be disease relevant. Chondrogenesis is the process by which mesenchymal stem cells differentiate into chondrocytes, which is mainly orchestrated by SOX9 expression. MSCs are multipotent and can differentiate into bone cell types and adipocytes. During this process, the precursors express more ECM components, such as collagen II and aggrecan, as well as SOX9/SOX6. This process can be modelled with human bone marrow or adipose derived stem cells as well as a murine teratocarcinoma cell line, ATDC5, both of which are commonly used in the field. This approach is often taken to understand the determining factors in this process, for example, P2Y6 was shown to enhance osteogenic differentiation of rat BM-MSC in combination with titanium dioxide nanotubes [206]. The aims of this chapter were to;

- To establish chondrogenesis from an *in vitro* model.
- To understand how P2Y6 might affect key aspects of the process.
- To create a P2Y6 knockout cell line to validate experimental data obtained with antagonists.

## 4.2 Results

Initially, bone marrow derived mesenchymal stem cells (BM-MSC) were provided by Dr. Matt Barter (Newcastle University). They were isolated from mixed populations of bone marrow derived cells and had been passaged a number of times and cryopreserved prior to this experiment. They were expanded, pelleted and induced with chondrogenic medium (see section 2.1.5 for methods) for a total of 14 days. RNA was extracted at regular intervals over the time course and qRT-PCR was carried out to verify that increases in characteristic marker gene expression had occurred. Figure 4.1 shows that there were not sustained increases in two chondrogenesis gene markers, *SOX9* and *collagen X*. There was an increase in *collagen X* in the differentiated cells up to day 7, however this was not sustained across the time course. There was no characteristic increase in *SOX9* expression. As a result of a lack of availability of other BM-MSC isolates, we employed a more accessible ATDC5 model, which is also widely used and has been well established to model chondrogenesis well [242]. ATDC5 are a murine teratocarcinoma cell line that can differentiate into a chondrocyte phenotype when stimulated with insulin, transferrin and selenium as well as ascorbic acid. ATDC5 were cultured in monolayer and induced with chondrogenic medium for 21 days. qRT-PCR showed that the cells had increased transcription of chondrogenic gene markers, such as *COL2*, *SOX9*, *aggrecan* and *collagen X*. *Collagen II* showed the greatest increase between day 0 and 21. *RUNX2* mRNA expression increased between day 0 and 12, but then decreased between day 12 and 21. *SOX9* also seemed to plateau after day 16. Two purinergic genes were also measured, *P2RY6*, because of its over-expression in OA, and *ADORA2B* as data from a collaborator suggested this receptor may be important in chondrogenesis (data not shown). This data showed that *P2RY6* increased in expression between day 16 and day

21, whilst *ADORA2B* did not change in expression across the time course (Fig. 4.2B).

#### 4.2.1 Human BM-MSC failed to undergo chondrogenesis

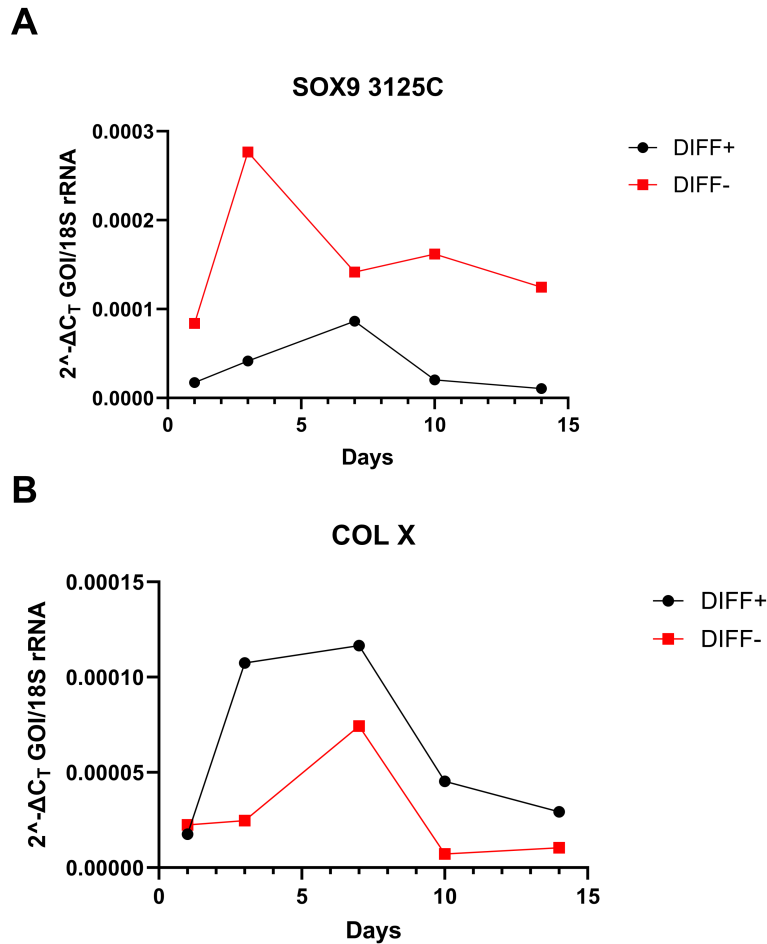


**Figure 4.1: Human BM-MSC Chondrogenesis.** Isolated human BM-MSC were maintained in DMEM with 5ng/mL FGF-2. To induce chondrogenesis,  $1 \times 10^5$  cells were pelleted by centrifugation in a round-bottom 96 well plate and cultured in chondrogenic induction media for 14 days, with media changes every 3 days. Subsequently, RNA was extracted and qRT-PCR was carried out for chondrogenesis markers *SOX9* (A) and *COLX* (B). 1 isolate, n=4.

## 4.2.2 ATDC5 cells follow a process analogous to chondrogenesis

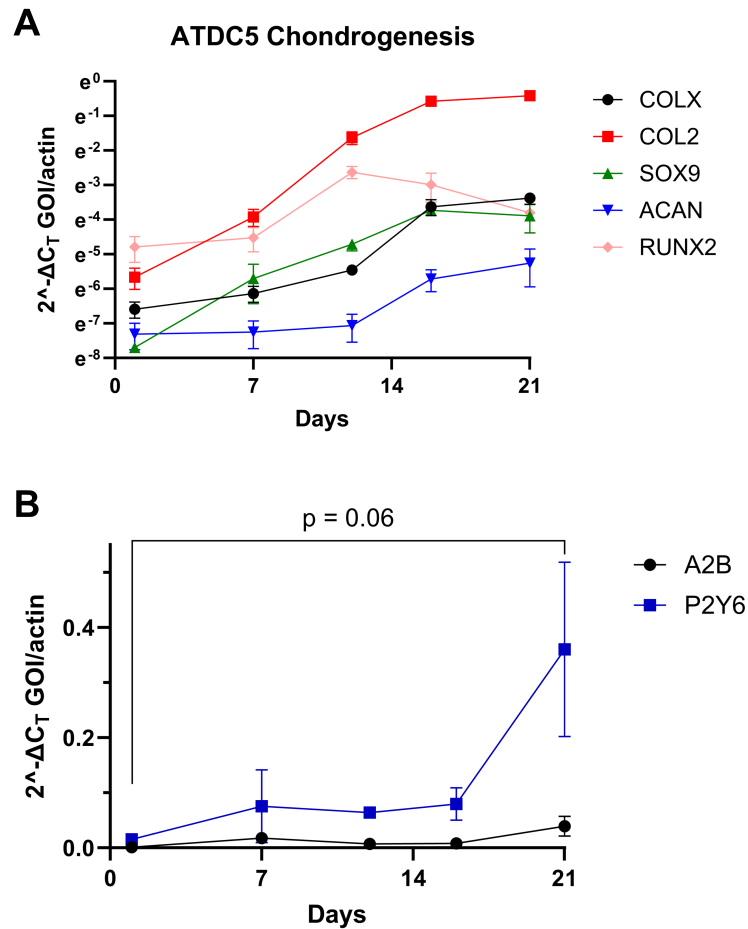


**Figure 4.2: ATDC5 Chondrogenesis.**  $5 \times 10^4$  ATDC5 cells were seeded in a 24 well plate and allowed to adhere overnight. Subsequently, they were cultured in induction media (DMEM supplemented with  $50 \mu\text{g}/\text{mL}$  ascorbate and 1X ITS) for 21 days, with media changes every 3 days, being careful not to disrupt the monolayer. This was followed by RNA extraction and qRT-PCR for chondrogenesis markers (A) as well as *ADORA2B* and *P2RY6* (B).  $\beta$ -actin was used as the house-keeping gene. Student's t test.  $N=4$ .

### 4.2.3 MRS2578 inhibits ATDC5 chondrogenesis at low concentrations

Once the chondrogenic model had been validated, it became pertinent to then assess whether P2Y6 contributed to the chondrogenic process. ATDC5 cells were induced with chondrogenic media in the presence or absence of MRS2578 at either 2 $\mu$ M or 500nM. These concentrations were chosen to balance toxicity, as it is a long term experiment, with efficacy. Previous experiments had shown that 10 $\mu$ M was possibly too high, and effects on primary chondrocytes were maintained at 5 $\mu$ M. These two concentrations were also chosen to try and establish dose dependency.

MRS2578 inhibited differentiation at the last time point of the 21 day experiment. It dose-dependently inhibited expression of *collagen X*, *collagen II* and *aggrecan* at day 21 (Fig. 4.3). It also inhibited proteoglycan staining by alcian blue at day 16 and day 21, again, in a dose dependent manner. It had non-dose dependent effects on SOX9 and *RUNX2* expression. 500nM MRS2578 seemed to induce SOX9 expression at day 21, however 2 $\mu$ M had no effect. Similarly, 500nM seemed to inhibit *RUNX2* expression whilst 2 $\mu$ M had no effect. An LDH assay showed that these effects were unlikely to be mediated by toxicity (Fig. 4.4B).

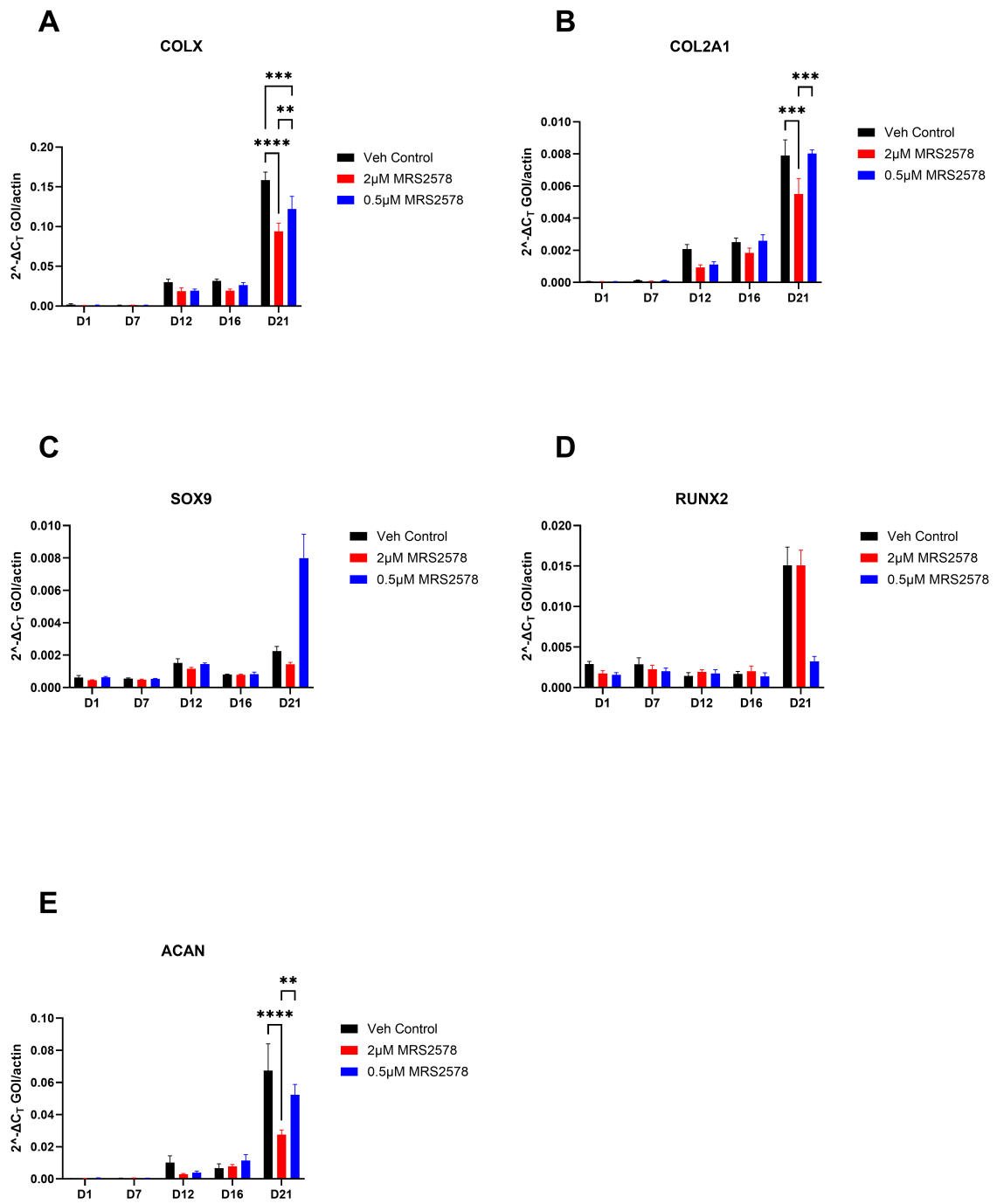


**Figure 4.3: ATDC5 Chondrogenesis** ATDC5 cells were seeded in a 24 well plate and put in induction media  $\pm$  MRS2578 for 21 days, followed by RNA extraction and qRT-PCR. Two-way ANOVA with Tukey's post-hoc test. N=4. \* $p < 0.05$ , \*\* $p < 0.01$ , \*\*\* $p < 0.001$ , \*\*\*\* $p < 0.0001$ .

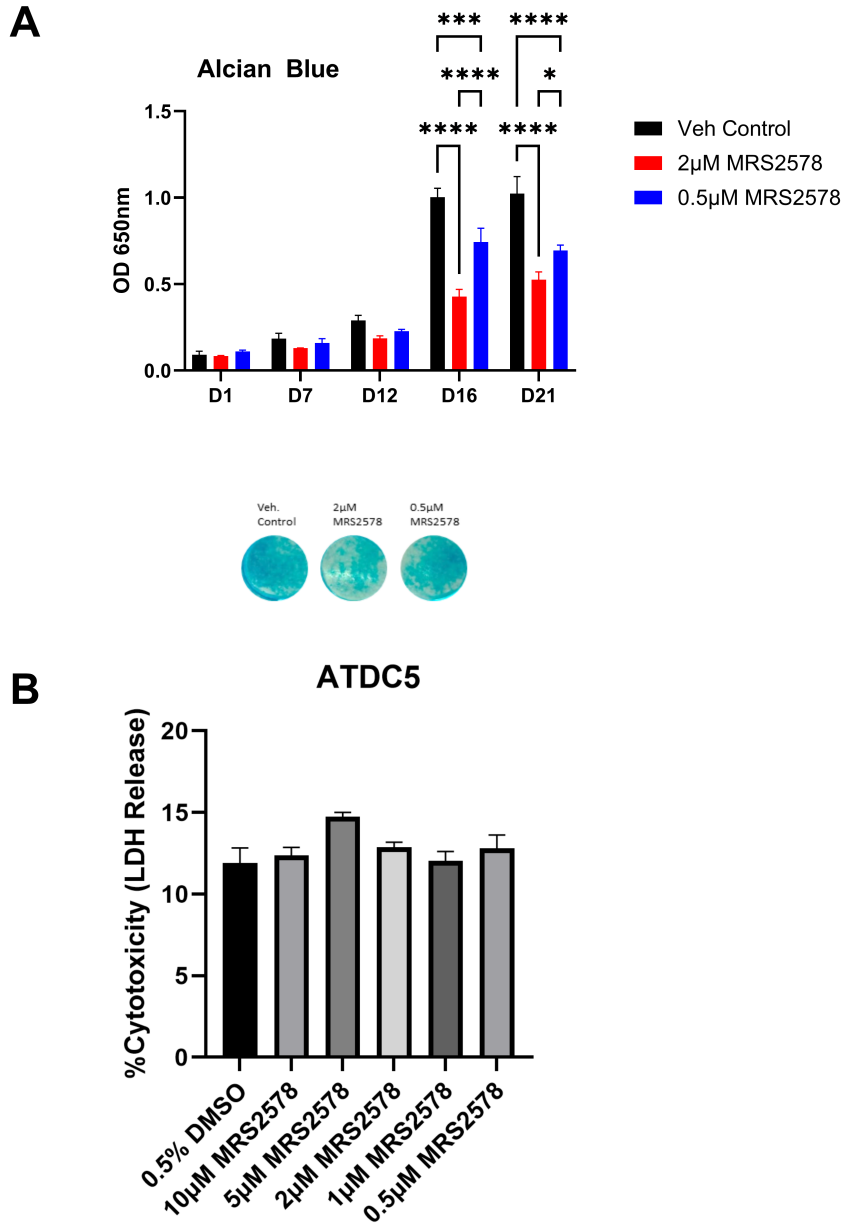
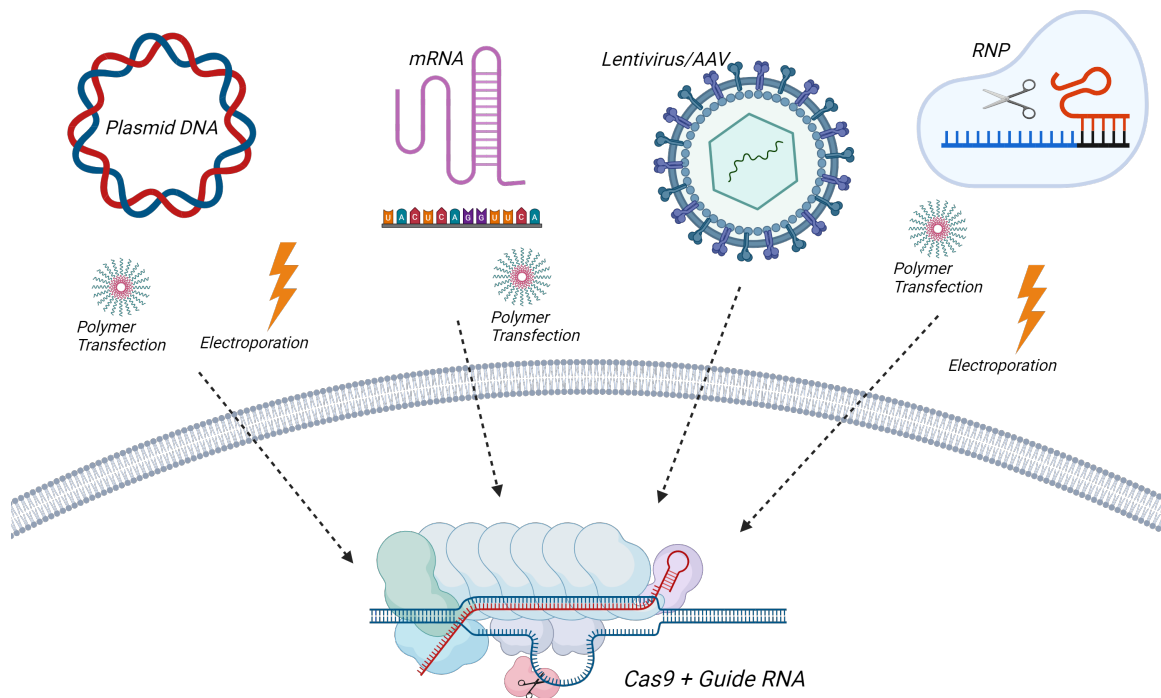


**Figure 4.4: ATDC5 Chondrogenesis** ATDC5 cells were seeded in a 24 well plate and put in induction media  $\pm$  MRS2578 for 21 days, followed by alcian blue staining (A). (C) ATDC5 were stimulated with MRS2578 and LDH activity in the cell culture supernatant was measured after 1 hour. Two-way ANOVA with Tukey's post-hoc test. N=4. \* $p$  = < 0.05, \*\* $p$  = < 0.01, \*\*\* $p$  = < 0.001, \*\*\*\* $p$  = < 0.0001.

#### 4.2.4 Knockout of P2Y6 in ATDC5 cell line

In the previous chapter, the specificity of MRS2578 was questioned, with no conclusive answer able to be drawn. As such, to add confidence to data collected with P2Y6 antagonist MRS2578, CRISPR-Cas9 was utilised to attempt to knock out P2Y6 from the ATDC5 cell line. CRISPR-Cas9 utilises a bacterial defence mechanism whereby double stranded breaks are created and indels are formed by non-homologous end joining (NHEJ). There are a number of ways in which the system can be delivered into cells, which are summarised in the figure below. Initially, the ribonucleoprotein (RNP) method was utilised, which involves transfecting recombinant Cas9 complexed with synthetic guide RNAs targeting the P2Y6 gene. This method has the advantage in that all of the components are already active and only need to successfully get inside the cell to work.



**CRISPR/Cas9 Delivery Methods.** The components of the CRISPR-Cas9 system can be delivered into cells in a number of ways. This includes as plasmid DNA encoding the guide RNA and Cas9 either together or in separate plasmids, mRNA encoding those components, as a lentivirus or already functional RNP. Plasmid DNA and RNP can also either be transfected with cationic polymers or liposomal transfection reagents or by electroporation. Created with biorender.com.

## 4.2.5 Ribonucleoprotein (RNP) Delivery

In the first instance, the RNP delivery method was chosen as it was thought that the ATDC5 cell line were easily transfectable, and delivery already active components (unlike DNA, which has to be transcribed and translated) would confer higher editing activity. Three guide RNAs targeting P2Y6 were chosen using Integrated DNA Technologies' (IDT) algorithm to provide highest on target activity whilst reducing off target activity. This is represented in the Doench score, which estimates the efficiency of knockout using this guide RNA. The base mismatches to off-target effects (OTE) metric is an estimation of how many bases need to be replaced for the guide RNA to recognise a different sequence to the one intended, and as such, is a measure of specificity.

Multiple transfection reagents and conditions were used to try and transfect the RNP into the ATDC5 cells. Two protocols were used, one following that recommended by IDT and that from the Lipofectamine CrisprMAX protocol. As well as this, the mass of Cas9 and gRNA transfected was varied, but the ratio of the two components was maintained. The outcome measure was analysis of Sanger sequencing data of a PCR amplicon spanning the cut sites (primers in appendix), whereby deconvolution algorithms were used to detect alterations in the sequences. Four algorithms were used; SeqScreener (Thermo Fisher), TIDE (Tracking of Insertion and Deletion Events) [215], DECODR (Deconvolution of Complex DNA Repair) [216] and ICE (Inference of CRISPR Edits, Synthego) [217]. These work to deconvolute the traces from the sanger sequencing and identify different sequences from a mixed population. From this, it can estimate what percentage of the cells in that population have any indels. This is a useful step as it allows for verification before moving on with the lengthy process of clonal dilution and also provides an estimate of how many clones need to be isolated. Table 4.2 shows the output of the deconvolution software from each of the transfection conditions, showing that the transfection was not successful enough to carry forward these mixed populations in any of the conditions. It also allows for comparison of the deconvolution software. Seqscreener estimated that 100% of the cells in the population had an indel, however the sequence was clearly the same as wild type, so this was deemed a false positive. TIDE seemed to consis-

tently return an estimation of  $\sim 4\%$ , which was assumed to be background, and DECODR and ICE seemed to be most accurate, giving the lowest percentages. For one transfection group, AA HI, ICE and DECODR were consistent in that they estimated a very small percentage had indels, however this was too low to continue forward. Interestingly, all three deconvolution algorithms did detect higher than background indel levels. An HPRT gRNA was also purchased from IDT and transfected as recommended from the manufacturer to see if it was an issue with the guide RNA sequences, but transfection of RNP with this complex did not produce indels either (Table 4.2).

Another verification method was used to see if indels were created, which is the T7E1 assay. In this assay, amplicons spanning the cut sites from transfected cells were heated and cooled to create heterodimers (if indels had been formed), which were then cleaved by the T7E1 enzyme, producing multiple bands when run on an agarose gel. The T7E1 assay for the HPRT positive control aligned with the deconvolution algorithm output in that the transfection was not successful. To test if the crRNA and tracrRNA were combining to form a functional guide RNA and that the Cas9 was active, an in vitro simulation of what should be happening inside the cell was carried out. This shows that the guide RNA and Cas9 system was working, as it cut the amplicon, producing two bands (Fig. 4.5). Another transfection reagent, TransIT-X2 (Mirus Bio) was also tested to transfect the RNP complex, and a T7E1 assay was carried out to see if the transfection had been successful, gel electrophoresis showed that it was not in either the P2Y6-targeting guide RNAs nor the HPRT positive control when transfected following manufacturers guidelines.

**Table 4.1: RNP gRNA Doench scores [243].** OTA = on-target activity, OTE = off-target effects.

	Doench OTA Score	Base Mismatches to OTE
gRNA 1 (AA)	0.629	3
gRNA 2 (AB)	0.619	2
gRNA 3 (AC)	0.497	3

**Table 4.2: Optimisation of RNP lipofection conditions.** ATDC5 cells were seeded into 6 well plates and Crispr/Cas9 RNP was transfected into the cells with varying conditions. Genomic DNA was then extracted and the amplicon surrounding the cut sites was amplified and sequenced by sanger sequencing. It was then entered into deconvolution algorithms to estimate the efficiency of indel formation. SS: SeqScreener; D: DECODR; FT : Forward Transfection; RT : Reverse Transfection. AA, AB, AC are the three guide RNAs. LO: 500ng Cas9/120ng gRNA. MED: 1.25 $\mu$ g Cas9/260ng gRNA. HI: 2 $\mu$ g Cas9/420ng gRNA. IDT protocol uses 6 $\mu$ L of lipofectamine, lipofectamine protocol uses 1.5 $\mu$ L for a 24 well plate.

	Protocol	FT/RT	gRNA/Cas9	SS %	ICE %	TIDE %	D %
P2Y6 RNP	IDT	FT	ALL3	100	0	4	0
		RT	ALL3	100	0	4	0
	Lipo	FT	AA LO		0	2	0
		FT	AA MED		0	2.5	0
		FT	AA HI		1	13.5	3.1
		FT	AB LO		0	2	0
		FT	AB MED		0	2.4	0
		FT	AB HI		0	1.5	0
		FT	AC LO		0	2.4	0
		FT	AC MED		0	2.3	0
		FT	AC HI		2	1.5	0
		FT	ALL3 LO		0	2.7	0
		FT	ALL3 MED		0	7.3	0
		FT	ALL3 HI		0	3.9	0
		HPRT RNP	IDT	FT	LO		0
FT	MED				0	3.8	0
FT	HI				0	5.9	0

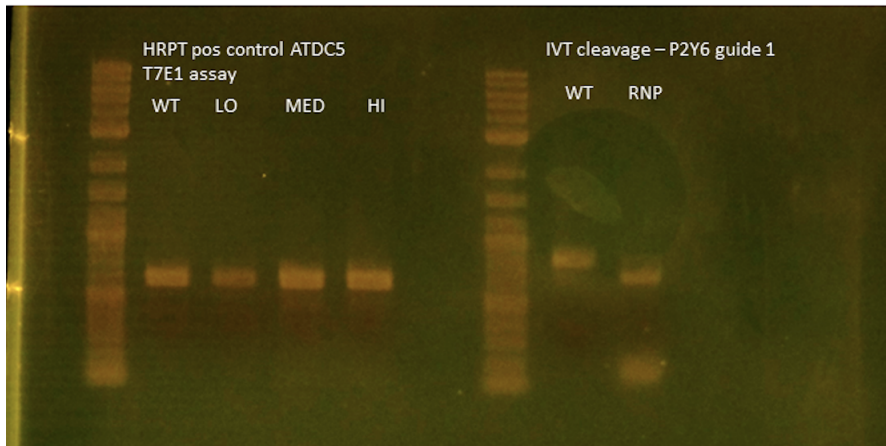


**Figure 4.5:** .

**T7E1 Assay from HPRT RNP transfection and in vitro cleavage test.** L: ATDC5 cells were transfected with HPRT targeting RNP using Lipofectamine CrisprMAX. gDNA was extracted and PCR was used to amplify amplicon spanning cut site, which was then incubated with T7E1 enzyme. R: AA P2Y6 gRNA was complexed with Cas9 and incubated with a cut-site spanning amplicon at 37 °C and run on a gel.

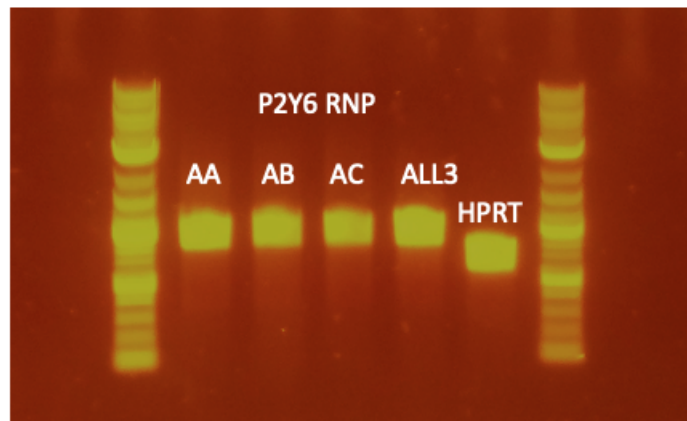


**Figure 4.6: T7E1 Assay from RNP transfection with TransIT-X2.** ATDC5 cells were transfected with P2Y6 targeting RNP complexes using TransIT-X2 (Mirus Bio), followed by gDNA extraction, amplification of region spanning cut sites by PCR and incubation with the T7E1 enzyme.

## 4.2.6 All-in-one Plasmid Delivery

The RNP method was not able to induce indels in these cells. An in vitro test had shown that the Cas9 was active and the gRNA was able to target the Cas9, so it was assumed that it was a transfection issue. The next strategy employed was an all-in-one plasmid that encoded Cas9 enzyme and the guide RNA. Two separate plasmids encoding two guide RNA sequences detailed in Table 4.3 were cloned into the PX459 plasmid and were about 9 kilobases in size. They were transfected into ATDC5 using Turbofect, which had previously been optimised for these cells (see 2.1) and electroporated using previously optimised conditions for these cells, using 5µg of high concentration (1µg/µL) DNA and a square wave form pulse of 280V for 15ms. The deconvolution algorithms showed that the transfection of plasmids with Turbofect was not successful. With electroporation, ICE and TIDE were unable to detect alignment between the WT and experimental sequences, however DECODR identified 10% of the cells to have an indel in the mixed population (Table 4.4). A T7E1 assay showed multiple bands in cells transfected with both guide RNAs, indicating the presence of indels (Fig. 4.7). Theoretically, there should have been three bands; one wild type (assuming there was not 100% efficiency), and one from either side of the cut site, which cannot clearly be seen from this gel. For the first guide RNA, the amplicons either side of the cut site would have been 163 and 656bp, so should have been easily distinguishable. Nevertheless, from these cells, populations that had been selected with puromycin for 48 hours post transfection were clonally diluted to isolate homogeneous cell populations. From single cell isolates, many of the clones did not expand once transferred out of the 96 well plate. 8 single cell clones were isolated, however sanger sequencing showed them to have wild type sequences (data not shown).

**Table 4.3: Plasmid gRNA Doench Scores [243].** OTA = on-target activity, OTE = off-target effects.

	Doench OTA Score	Base Mismatches to OTE
gRNA 1	0.763	3
gRNA 2	0.661	3

**Table 4.4: Deconvolution algorithm output from CRISPR plasmid transfection.** ATDC5 cells were electroporated and transfected with PX459 plasmids encoding Cas9 and two separate gRNAs. Post transfection, gDNA was extracted, an amplicon spanning the cut sites was amplified by PCR and sanger sequenced. NA = No Alignment.

	gRNA	ICE %	TIDE %	D %
Turbofect Transfection	1	0	6	0
	2	0	2	0
Electroporation square wave 280V 15ms	1	NA	NA	10
	2	NA	NA	0

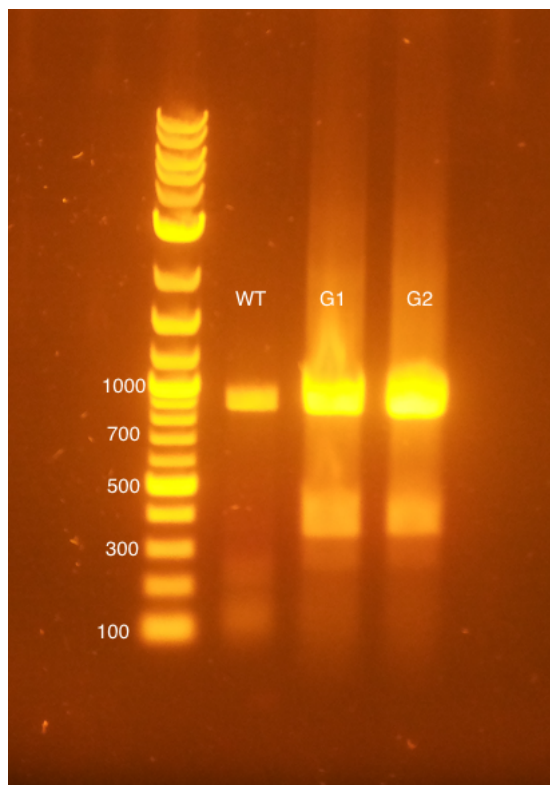


**Figure 4.7: T7E1 assay from electroporation of CRISPR plasmids.** PX459 plasmids encoding Cas9 and two separate gRNA sequences were electroporated into ATDC5 cells using a square-wave form pulse of 280V for 15ms. The cells were selected with 1 $\mu$ g/mL puromycin for 48h. gDNA was extracted and an amplicon spanning the cut sites was amplified using PCR, heated and cooled to form heterodimers and was subsequently incubated with the T7E1 enzyme to detect indels.

## 4.2.7 Lentiviral Delivery of Cas9 and transient transfection of gRNA.

The next strategy that was employed was creation of a stable Cas9 expressing ATDC5 cell line and subsequent transient transfection of the small RNA guides that were used in RNP formation. This strategy was employed because it alleviated the need for being able to transfect large constructs into cells by transient transfection. Lentiviral transduction often has much higher efficiency than transient transfection and also is a two-step process that can be verified at each stage to prevent wastage of time. Initially, ATDC5 cells were transduced with Cas9-encoding lentiviral particles and selected with 200 $\mu$ g/mL Hygromycin B for 10 days (a time point where all control/untransduced cells had died). Resistant cells were then expanded and insertion of the Cas9 gene into the genomic DNA was verified by PCR. Figure 4.8 shows the insertion to be successful. The next stage was to transfect the Cas9 positive cells with the P2Y6-targeting guide RNAs. The three guide RNAs, along with the HPRT-targeting positive control, were transfected both separately and together at a final concentration of 30nM. Figure 4.9 is a T7E1 assay from transfection of the synthetic guide RNAs in the Cas9+ ATDC5. It shows more than one band in the AA group and the ALL3 group, although the distribution of bands is not entirely clear. Theoretically, there should be three bands - the wild type, and the two amplicons either side of the cut site.

The deconvolution algorithms revealed that the majority of cells had indels in all of the groups that were transfected with the small RNAs. AC and all three of the guides transfected together had the highest efficiency, with DECODR and ICE estimating that a similar percentage of these indels produced a frame shift in the genomic sequence. DECODR even estimated that the AC group had 100% indel efficiency and 100% of the cells had a frame shift mutation that was likely to lead to non-functional protein. Interestingly, TIDE seemed to estimate lower indel percentages in this case than ICE and DECODR, whereas when the transfection was not working, it seemed to overestimate. One disadvantage to TIDE is that it also does not have the capability to estimate the percentage of cells that have a frame shift.

From these populations of cells, clonal dilution was carried out to isolate colonies originating from a single cell, and therefore genetically homogeneous. Again, many of the cells would not expand out from single cell colonies, however five single cell isolates from the AC group and three from the ALL3 group were isolated. Initially, the AC group clones were sanger sequenced and entered into the DECODR algorithm for clonal analysis. Figure 4.10 shows the mutated sequences of each clone. Three of the five clones had mutated sequences, and for one (not shown), DECODR could not produce statistical alignment between the experimental and control sequences. AC.1.2 had wild type sequence and AC2.2 had a one base pair deletion. AC.5.2 and AC.7.2 had more than one corresponding sequence, meaning it is likely that the population originated from more than one cell, however each sequence had at least a one base pair deletion or insertion i.e. there was no wild type sequence detected in these groups. RT-PCR for *P2RY6* mRNA in the AC.5.2 clone (Fig. 4.11 showed a band at the same size as the wild type band, at around 500bp, but also had a band slightly higher that was not in the wild type sample. This made it hard to interpret what this band was, but did show a difference between the two. Western blot, however, showed that the clones all still expressed wild type P2Y6. There were bands that were much higher than the expected weight of P2Y6, between 150 and 250kD that were present in the wild type and not in the transfected cell populations, but was determined to be too high to be P2Y6. Clones from the A3 group also expressed wild type P2Y6 as detected by western blot (Fig. 4.12B).

**Table 4.5: Deconvolution Algorithm Output.** Amplicons spanning cut sites from Cas9+ ATDC5 cells transfected with guide RNAs were amplified by PCR and sanger sequenced, followed by analysis by deconvolution algorithms. D = DECODR.

Guide	ICE % (Indel/Frame Shift)	TIDE %	D % (Indel/Frame Shift)
AA	40/31	38	48/38
AB	47/41	33	50/45
AC	75/75	79	100/100
ALL3	87/80	57	77/20
HPRT	79/75	74	85/77

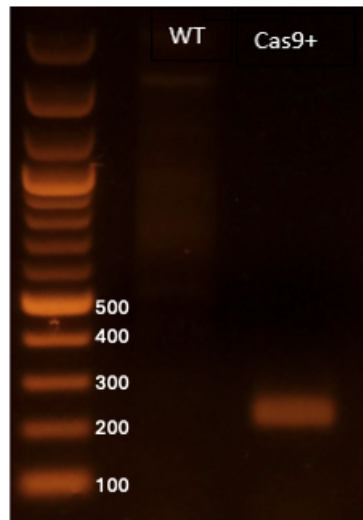


**Figure 4.8: Cas9 Genomic PCR.** ATDC5 cells that had been transduced with Cas9 encoding lentivirus were selected with 200 $\mu$ g/mL Hygromycin B. Genomic DNA was extracted and PCR was carried out to check for integration of the Cas9 gene.

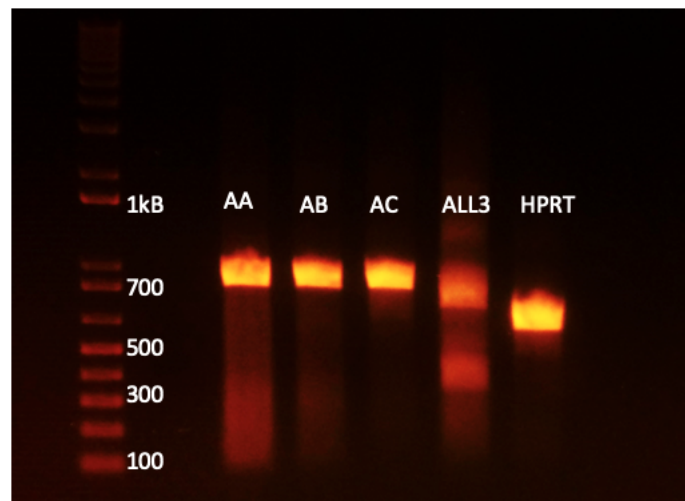


**Figure 4.9: T7E1 assay from lentiviral Cas9 delivery and transient transfection of guide RNAs.** ATDC5 cells that had confirmed Cas9 expression by PCR and were Hygromycin resistant were transfected with guide RNAs for P2Y6 and HPRT as a positive control. Subsequently, an amplicon spanning cut sites was amplified by PCR and incubated with T7E1 enzyme.



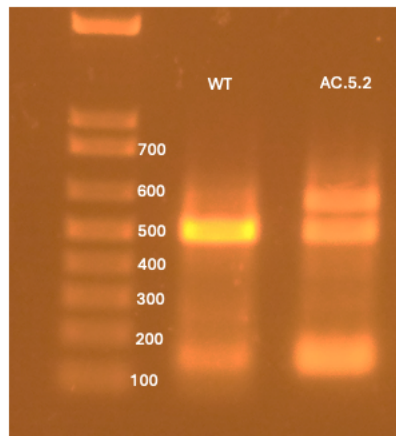


**Figure 4.11: AC.5.2 mRNA Expression of *P2RY6*.** RNA was extracted from AC.5.2 clone and reverse transcribed to cDNA. End point PCR was carried out for *P2RY6* on both wild type and AC.5.2 transfected clones and run on an agarose gel.

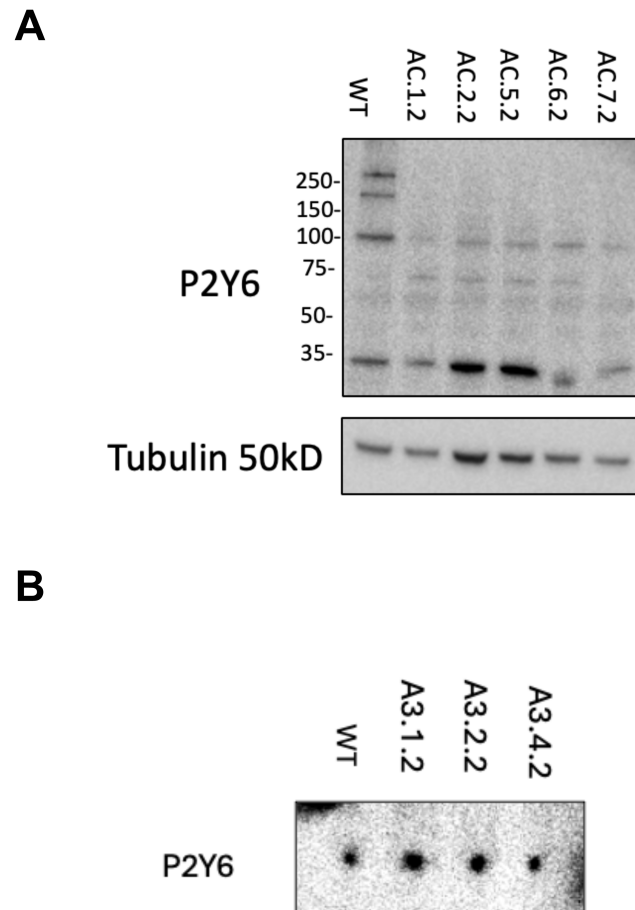


**Figure 4.12: Western blot for P2Y6 in AC and ALL3 (A3) group clones.** ATDC5 Cas9+ cells that were transfected with AC gRNA or all three of the gRNAs targeting P2Y6 were seeded in 6 well plates post transfection. Proteins were solubilised in RIPA buffer and SDS PAGE was carried out to detect P2Y6 using Invitrogen PA5-106912. A shows the WT protein lysates as well as that from clones transfected with the AC guide RNA, B shows the WT protein lysates as well as that from clones transfected with all three P2Y6 targeting guide RNAs.

## 4.3 Discussion

### 4.3.1 Establishment of Chondrogenesis Model

Initially, human bone marrow derived mesenchymal stem cells (BM-MSC) gifted from Dr. Matt Barter were tested to model chondrogenesis. However, markers of chondrogenesis, namely SOX9 and collagen X, did not increase in a characteristic way when induced to differentiate. Collagen X did increase between day 1 and 7, but then decreased after this time point. There are a number of possible reasons why they failed to undergo the chondrogenic process. Firstly, the cells were isolated from a mixed population of bone marrow derived cells and selected for stemness based on their expression profile. As such, they may not be a pure population of cells with the ability to differentiate, and may be contaminated with immune cells or other precursor cells. Moreover, these cells have been cultured in monolayer previously, cryopreserved and passaged seven times, so it is possible that they had phenotypic shift and lost their ability to differentiate. Doing this again, it would be pertinent to use a better isolated group of cells that had not been passaged nor cryopreserved to retain their stemness. Owing to the lack of availability of more primary cells and the high cost of commercially available BM-MSC cells, a cell line murine model of chondrogenesis was used. ATDC5 cells are a good model of the early stages of chondrogenesis [244, 245], whereby progenitors condense and begin to produce ECM components, such as collagen II and aggrecan. ATDC5 cells successfully underwent this process in monolayer over a time course of 21 days. qRT-PCR showed characteristic increases in *collagen X*, *collagen II*, *SOX9* and *aggrecan*. Looking to purinergic expression, *ADORA2B* and *P2RY6* were measured by qRT-PCR as collaborators' data (Dr. Matt Barter, Newcastle University) showed that *ADORA2B* may be regulated in chondrogenesis (data not shown) and *P2RY6* increases in expression in OA. Over this time course, *ADORA2B* expression remained stable but *P2RY6* increased in expression over the time course, especially between day 16 and 21, and almost reached statistical significance between day 1 and day 21 ( $p=0.06$ ).

### 4.3.2 MRS2578 inhibits ATDC5 Chondrogenesis

With the knowledge that P2Y6 is overexpressed in OA chondrocytes, and its expression was regulated during the chondrogenic process in ATDC5 cells, it became pertinent to see what effect inhibiting P2Y6 has on this process. As such, ATDC5 cells were differentiated in the presence or absence of MRS2578, which has activity at mouse P2Y6 [239] and has been used for murine *in vivo* studies [246, 247]. Two concentrations (2 $\mu$ M and 500nM) were chosen to try and establish dose dependency. These were chosen to be low enough to not cause toxicity but high enough to have an effect, as the IC<sub>50</sub> in PHC was approximately 400nM, and in the literature was found to be 37nM [235]. MRS2578 affected the differentiation process towards the latter end of the assay, where *P2RY6* expression was highest. It dose dependently inhibited proteoglycan deposition as detected by Alcian blue staining at day 16 and 21, as well as inhibited *collagen X*, *collagen II* and *aggrecan* mRNA expression at day 21 dose dependently. It had less predictable and clear effects on *SOX9* and *RUNX2*. 500nM MRS2578 seemed to increase *SOX9* expression at day 21, whereas it seemed to decrease *RUNX2* expression also at day 21, however these effects were not dose dependent. Moreover, MRS2578 was not toxic to ATDC5 cells as measured by LDH release when incubated for 1 hour with the antagonist at any concentration. Whilst this is only an indicative assay as in the chondrogenesis time course, the cells were exposed to MRS2578 for 21 days, the effects are still unlikely to be mediated by cellular toxicity as not all of the markers measured decrease in the same way.

Figure 3.15B shows MRS2578 to inhibit NF $\kappa$ B signalling, as has been shown by others in the literature [151, 248], irrespective of whether this effect is mediated by P2Y6. The inhibition of chondrogenesis markers in ATDC5 cells by MRS2578 would also be consistent with inhibition of NF $\kappa$ B. NF $\kappa$ B has been shown to regulate aspects of the process and its activation is a prerequisite for many of the hallmarks of chondrogenesis [207, 249]. However, somewhat inconsistently, *SOX9* has also been shown to be regulated by NF $\kappa$ B [250], but was not affected in a dose dependent manner by MRS2578. It is possible that at higher doses this would have been the case. Collagen II, X and aggrecan are also under control of TGF $\beta$  signalling, and it is possible that this is the mechanism by which MRS2578 ex-

erts these effects [251]. Overall, these data suggest that the blockade of P2Y6 by MRS2578 has a detrimental effect on the expression of ECM components, specifically collagen X, collagen II and aggrecan. To strengthen this data, it would be pertinent to repeat the ATDC5 chondrogenesis assay in the presence of UDP- $\beta$ S to provide evidence that the opposite phenotype is also seen i.e. that activation of P2Y6 positively regulates ECM components. From the inhibitory data produced by MRS2578 in this experiment, the hypothesis would be that agonising P2Y6 would accelerate chondrogenesis, with increased expression of key chondrogenic markers and increased proteoglycan deposition as assessed by Alcian blue staining. However, it would be comprehensible that in a similar way to the results from the IL-1 induction of MMPs in PHC, it can be inhibited but not induced, which could be explained for a number of reasons. This might be because the system is already maximally activated, or that P2Y6 in the process is not the limiting factor and only has cross-talk or tonic regulation of the key pathways.

### **4.3.3 Failure of CRISPR-Cas9 Knockout of P2Y6 in ATDC5 cells**

CRISPR-Cas9 is a very versatile system that has been harnessed from the bacterial defense system of *S. Pyrogenes* to edit genomic DNA. Its use in editing genomic DNA in eukaryotic cells was first described in 2013 [252] and consists of two major components - Cas9, the nuclease and a guide RNA, which directs the Cas9 to the genomic site intended to be cleaved. Design of guide RNAs is limited to sites which contain a protospacer adjacent motif (PAM) site of NGG, as this is required for Cas9 to function. There are also many ways with which to deliver the components of the Cas9 system, such as plasmid DNA, mRNA, ribonucleoprotein (RNP), lentiviral and AAV (adeno-associated virus). Often one of the biggest challenges arising from this system is being able to get the components of the system into the cell. For hard-to-transfect cells, transfecting a 10kB+ plasmid or large protein cargo into a cell can be challenging. Moreover, the validation of genomic cutting experimentally can be a lengthy process.

Initially, the RNP method was chosen to deliver the Cas9 components. RNP has the advantage over other methods in that it does not rely on the endogenous cellular machinery to produce the active components, unlike transfection

with plasmid DNA, as it utilises recombinant Cas9 protein and synthetic guide RNAs. There are not many commercial transfection reagents that are optimised for use with RNP transfection, but the two that were used here were Lipofectamine CrisprMAX (Thermo Fisher) and TransIT-X2 (Mirus Bio). Lipofectamine CrisprMAX is a lipid nanoparticle formulation and Transit-X2 is a lipid and polymer mix transfection reagent. Two methods were used for outcome measurement; the first being a deconvolution algorithm assessment of sanger sequencing traces and the second is a T7E1 assay. In the first method, genomic DNA is extracted from transfected cells and a region spanning the cut sites is amplified by PCR, followed by sanger sequencing. The traces are then entered into a deconvolution algorithm which estimates the percentage of cells in that population that have an indel. The advantage to this is that it allows for a measurement of success in a mixed pool before clonally isolating them. The second method is more crude; it involves a similar process of amplifying a region of DNA spanning cut sites, but then involves heating and cooling the DNA slowly to form heterodimers where there is sequence mismatch caused by indels. The heterodimers are then incubated with the T7E1 enzyme, which cuts the DNA at any mismatch sites. The disadvantage to this method is that the T7E1 enzyme cannot detect 1 base pair mismatches, and that it is more qualitative in nature.

Both outputs show that the RNP was ineffective in creating indels at the cut sites, despite efforts to optimise the transfection. This included following different protocols (IDT or Thermo Fisher) and altering the amounts of Cas9/gRNA, single or co-transfection and forward or reverse transfection. Some HI (2µg Cas9/420ng gRNA) groups had 1% or 2% indel creation as estimated by ICE, indicating that the higher amounts of Cas9 and guide RNA were more effective, however, isolating that percentage of cells in a mixed population would not be practical. An in-vitro test (i.e where the reaction is carried out outside of a cell) showed the Cas9 and guide RNA to be active when complexed together, highlighting that is is likely an issue with the transfection itself. Moreover, an experimentally validated guide RNA positive control (HPRT) was not able to produce indels either, meaning it was unlikely to be an issue with the guide RNA sequences. In using four different deconvolution algorithms, a comparison is able to be drawn between

them. SeqScreener (Thermo Fisher) was discounted early on as it estimated that 100% of the cells in the population had an indel, however this was assumed to be a false positive because the sequence was clearly the same as wild-type and the other deconvolution algorithms did not concur. TIDE seemed to consistently return a value of between 2-5%, so is likely to overestimate that amount over any true indels, but ICE and DECODR seemed to more accurately deliver a 0% value where it did not detect any sequence variations. As tools, ICE was easiest to use and allowed for the input of 3 guide sequences, whereas DECODR allowed for the input of only 2.

The next method used was to try a plasmid delivery option, with the additional benefit of being able to use electroporation to transfer it into the cell as well as lipofection methods. Previously used electroporation parameters and previously validated transfection conditions in these cells were used. The downfall of this method is that it still requires large cargo to be delivered into cells. Transient transfection with Turbofect failed to induce indels as determined by deconvolution algorithms and electroporation of the plasmids produced less clear results. ICE and TIDE were not able to find good statistical alignment between the control and transfected sequences, however DECODR estimated 10% indel formation for the first guide sequence when cells were electroporated with that plasmid. Moreover, the T7E1 assay produced multiple bands. Theoretically, there should be three bands - one wild type, and the two fragments either side of the cut site in the wild type sequence. The fragment sizes for guide 1 should have been 183bp and 656bp, and for guide 2 they should have been 371bp and 468bp. These fragments are large enough that they should be distinguishable on a gel, however there is only two clear bands on the T7E1 gel. Moreover, they are at the same size for each guide, so are unlikely to be the cut fragments. As expected, the eight clones isolated all had wild type sequences. If this method were to be developed further, it would be useful to verify Cas9 expression with a western blot post transfection to ensure that the plasmid was getting inside the cell and that it was being expressed sufficiently. It would also help to optimize the electroporation further and/or try different transfection reagents.

The third method utilised a different strategy to contain multiple phases for which

there were checkpoints to validate the process, thus saving time and money. It also does not rely on the inefficient delivery of large cargo into seemingly transfection resistant cells. This involved creating a Cas9+ stably expressing ATDC5 cell line, and transient transfection of synthetic guide RNAs. PCR from genomic DNA showed that the integration of the Cas9 gene into the Hygromycin B resistant cells was successful post transduction, and that they were likely to be expressing Cas9. Following expansion and freezing of this cell line, the synthetic guide RNAs that were used with the RNP method were transfected into these cells using Turbofect. Deconvolution algorithms suggested that this method was successful in creating indels and did so very efficiently, with the third guide sequence, AC, showing the highest indel percentage alone or the three combined being most efficient at 87%, according to ICE. Both ICE and DECODR also estimated that at least 20% (in most cases, higher) of these cells had a frame shift induced by the indel, which is what would be needed to induce a loss of transcription and therefore a knockout cell line. The T7E1 assay did not show the same result as clearly. For AB, AC and HPRT gRNA transfected cells, there seems to be nothing other than the wild type band. For AA transfected cells, there is a "smudge" at a low molecular weight, and for all three co-transfected (A3/ALL3), there is a clear lower band and seems as though the wild type band is slightly lower than expected, however this is difficult to interpret and there would be more than 5 fragments created from all three guide RNAs. Following clonal dilution of the cells through serial dilution, 8 clones expanded successfully from the AC and ALL3 transfected cell populations. Sanger sequencing showed that AC.1.2 had only wild type sequence, but AC.2.2, AC.5.2 and AC.7.2 contained no wild type sequence. DECODR did estimate, however, that they did not originate from a single cell but from three in the case of AC.5.2 and AC.7.2. Nevertheless, they did not contain any wild-type sequence. DECODR could not find sequence alignment for AC.6.2 and whilst the base-called sequence from Sanger sequencing was not wild-type, there may have been some wild type within as this can only be determined from deconvolution of the peaks. A western blot, however, showed all of these cells to still express *P2RY6*. The band from AC.6.2 did seem slightly fainter, however this was assumed to be due to incomplete transfer. On

this blot, there were two bands at around 200kD that were only present in the wild type sample and not in the transfected cell lysates. It is possible this is an artefact of the wild type sample going through two freeze-thaw cycles as it was collected prior to the transfected samples, and is highly unlikely to be P2Y6 due to its size. To prove this, an siRNA or blocking peptide to P2Y6 could be used to see if this band changes in the wild type sample, or to repeat it with a lysate that has not been subjected to freeze/thaw cycles.

In terms of method development, it is clear that the lentiviral delivery of Cas9 and transient transfection of guide RNAs was the best method as it did not rely on transient transfection of large cargo. However, it still failed to produce a knockout, and unfortunately there was not enough time nor money to continue to develop this method. There are a number of reasons why this might be the case. The first, which might be the simplest, is that the antibody used is not specific and is not detecting wild-type P2Y6, as this antibody has not been knockout validated. With more time and funds, other antibodies would have been tested using a positive and negative control (or blocking peptide) to see if they also detected P2Y6 protein. Another explanation is that the deconvolution algorithms estimated incorrectly or overestimated, and there were no indels formed, or the indels formed did not lead to the production of a non-functional protein or a lack of transcription. Moreover, it is also possible that more clones needed to be isolated to find the knockout, and strategies could have been employed to increase the number of cells that were able to expand out of the 96 well plate, for example, using pre-conditioned media or cloning rings. There are also specialist machines that can dispense 1 cell into each well of a 96 well plate.

# Chapter 5

## Transcriptomics

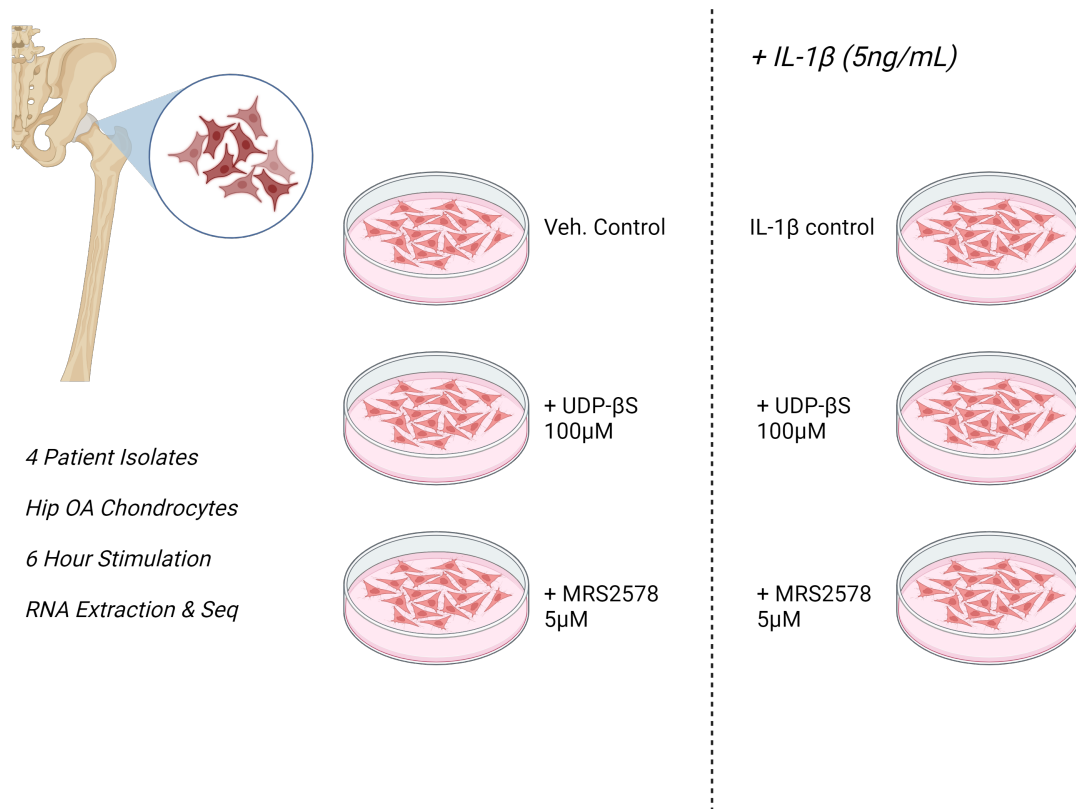
### 5.1 Introduction

To obtain a more global picture of how P2Y6 signalling affects chondrocyte phenotype, a transcriptome-wide approach was used. The overarching aim is to understand why *P2Y6* is overexpressed in OA and how its signalling may contribute to or oppose pathophysiological phenotypic changes. As such, total RNA was extracted from PHC from tissue isolated from OA hips. These hips originated from four patient donors and the extracted cells were stimulated with UDP- $\beta$ S or MRS2578 with and without IL-1 $\beta$  for six hours. This time point was chosen as it had proven to be effective in previous experiments, and is short enough to result in primary effects but long enough to allow a large enough response. In published phenotypic assays using both compounds, stimulation times can vary from 1 hour [234] to 24 hours [232], commonly using MRS2578 at 10 $\mu$ M, whereas a concentration of 5  $\mu$ M was used for this experiment. UDP- $\beta$ S has been shown to be more potent than UDP [253] with an EC<sub>50</sub> of 3 $\mu$ M in a vascular smooth muscle cell model [225], and as such 100 $\mu$ M was chosen as a maximal concentration. This concentration has also been used by others in similar phenotypic studies [200]. The aim of this transcriptomic approach was to answer the following questions;

- How does MRS2578 inhibit the IL-1 induced expression of MMPs - which genes may be mediating this effect?
- What effect does UDP- $\beta$ S have on both IL-1 stimulated and unstimulated

gene expression in PHC?

- Is it possible to infer the specificity of MRS2578 by analysing the reciprocity of differentially expressed genes resulting from UDP- $\beta$ S and MRS2578 stimulation?



**RNASeq Experimental Design.** Four hip OA chondrocyte patient isolates were stimulated with IL-1 $\beta$  5ng/mL  $\pm$  UDP- $\beta$ S  $\pm$  MRS2578 for six hours prior to RNA extraction, library prep and Illumina mRNA sequencing. Figure made with biorender.com.

## 5.2 Results

### 5.2.1 MRS2578 induces differential expression of over 6,000 genes whilst UDP- $\beta$ S causes differential expression of less than 300 genes in non-stimulated cells.

In this experiment, there were four direct comparisons made, comparing the effect of UDP- $\beta$ S and MRS2578 in both unstimulated and IL-1 $\beta$  stimulated cells on

differential gene expression. There were many fold more significantly differentially expressed genes (DEG) by p value in the MRS2578 groups compared to the UDP- $\beta$ S groups (Fig. 5.1), with fewer than 100 genes overlapping in both stimulated and non-stimulated comparisons.

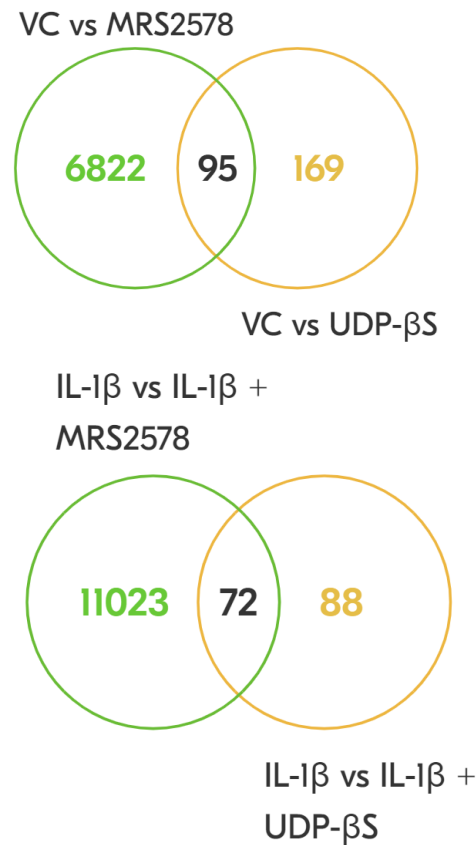
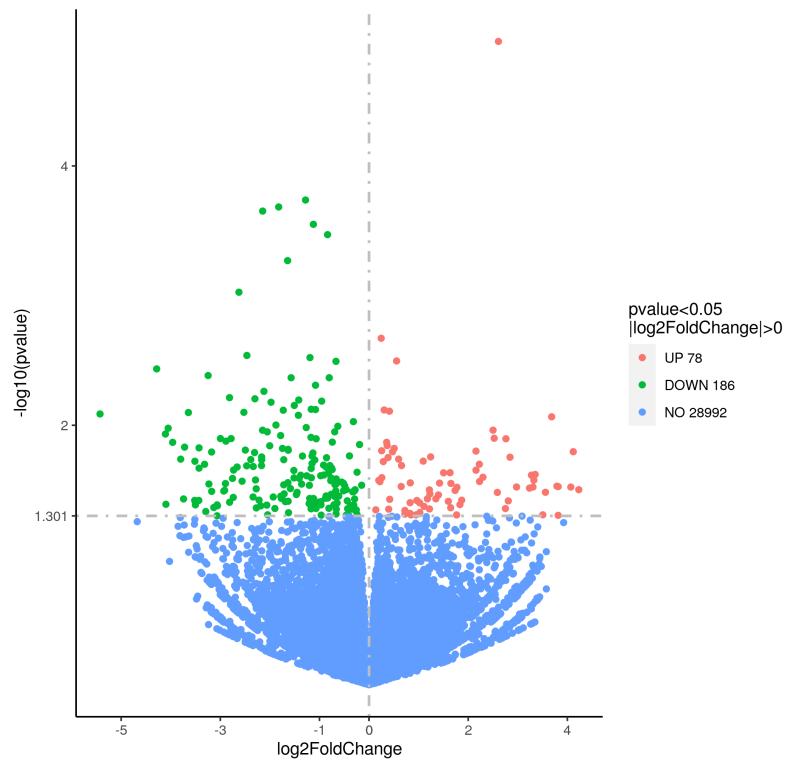
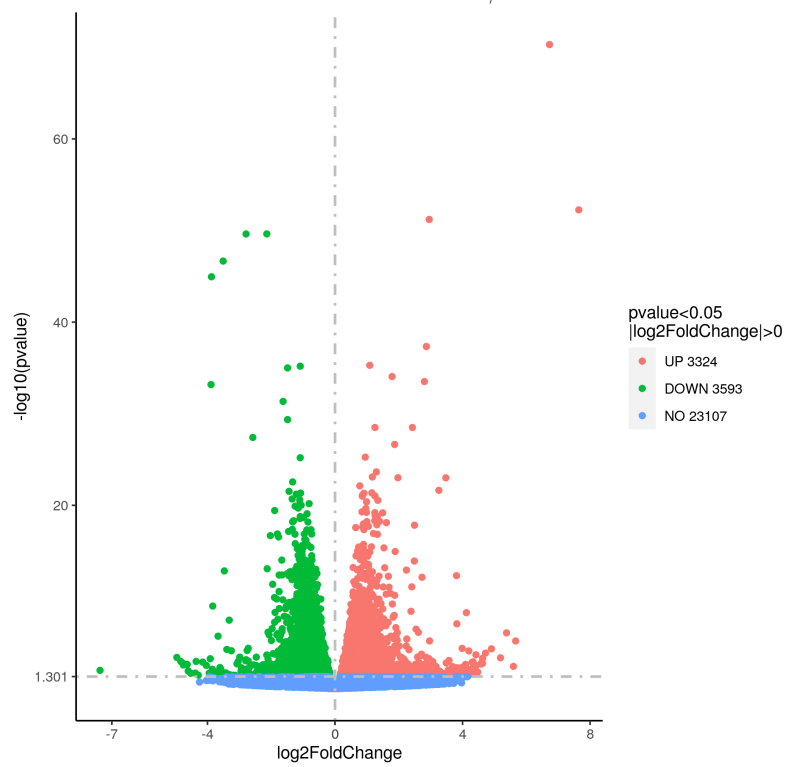


**Figure 5.1: Venn diagram showing DEG between experimental groups.** Four comparisons were made for differential gene expression analysis between vehicle control and UDP- $\beta$ S or MRS2578 in unstimulated and IL1- $\beta$  (5ng/mL) stimulated cells using DESeq2. DEG quoted here are significant by p value, as none of the UDP- $\beta$ S comparison groups remained significant after adjustment using the Benjamini-Hochberg false discovery rate method.

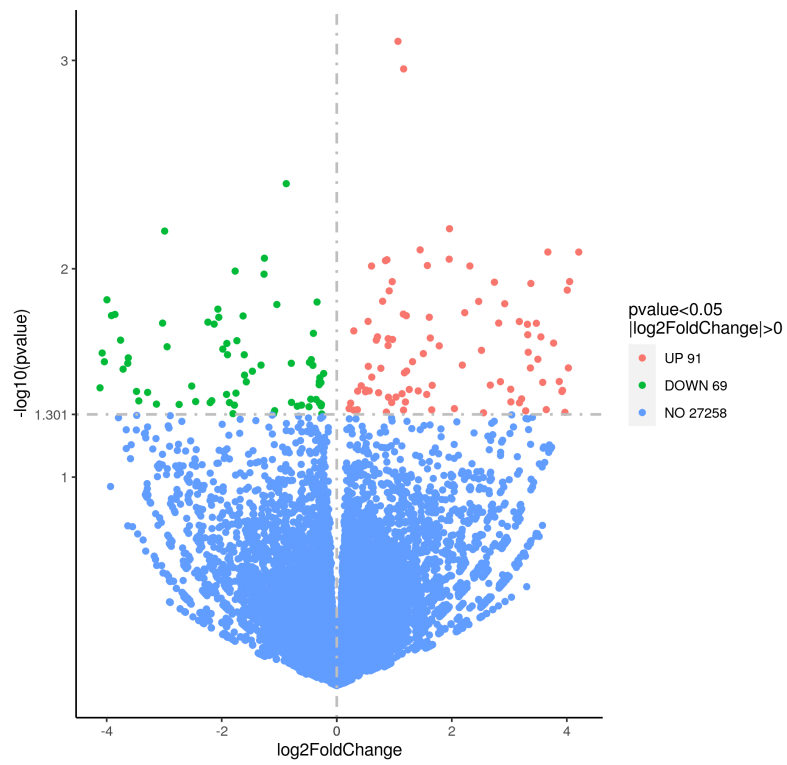


**A - VC vs UDP- $\beta$ S**

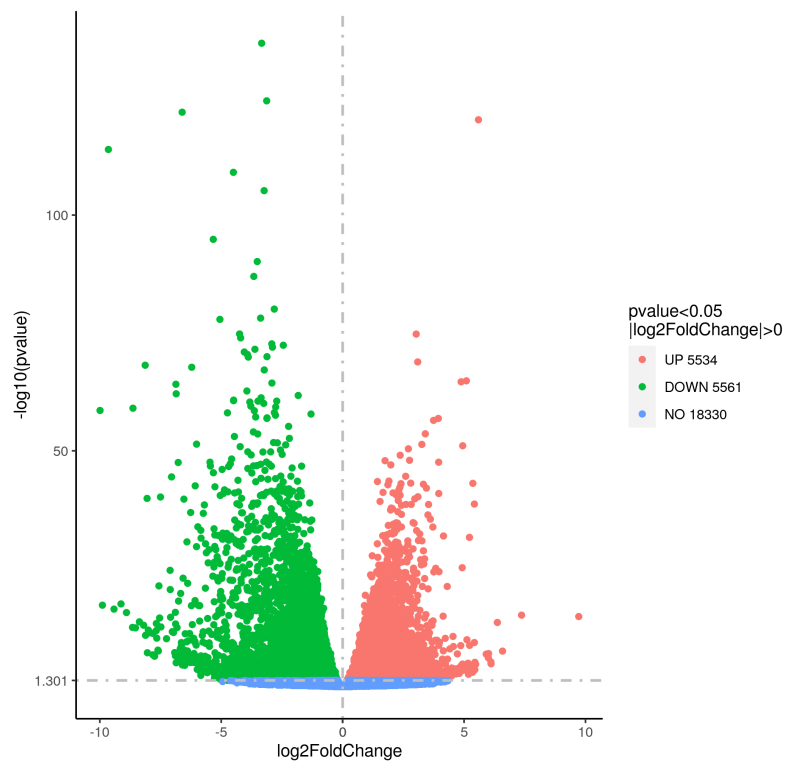


**B - VC vs MRS2578**

**Figure 5.2: Volcano Plot showing DEG in non-stimulated PHC.**



**A - IL-1 $\beta$  vs IL-1 $\beta$  + UDP- $\beta$ S**



**B - IL-1 $\beta$  vs IL-1 $\beta$  + MRS2578**

**Figure 5.3: Volcano Plot showing DEG in IL-1 $\beta$  stimulated PHC.**

## 5.2.2 UDP- $\beta$ S causes reduced expression of multiple pro-inflammatory mediators.

When comparing the vehicle control group and the cells treated with UDP- $\beta$ S, there was reduced transcription of a number of inflammatory mediator genes. This includes facets of NF $\kappa$ B signalling, such as *RELB*, *NF $\kappa$ BIA*, which encodes the I $\kappa$ B- $\alpha$  protein, and *IRAK2*, which is an interleukin-1 receptor associated kinase. Elements of TNF signalling are also downregulated, namely *TNFAIP8/3* and *TIFA*, which has a TRAF6 binding domain [254]. Some of the genes targeted by NF $\kappa$ B are also downregulated, such as *IL-6*, *MMP9*, *ADAMTS9/7*, *PTGES* and *NOD2*. The downregulation of these genes caused by P2Y6 agonism are all in opposition to the action of IL-1, and as shown by blank spaces on the heat map, were often not differentially expressed in the MRS2578 group (Fig. 5.4). These genes were significantly different by p value, but were not significant when adjusted for multiple testing using the Benjamini-Hochberg method (Table 5.1).

Analysing all of the genes that were significantly differentially expressed by p value, Gene Ontology (GO) [255], Reactome [256] and Kyoto Encyclopedia of Genes and Genomes (KEGG) pathway analysis [257] was performed to provide a more standardised view of how these genes might affect the chondrocyte phenotype. Both gene ontology and reactome analysis highlighted cytokine/chemokine receptor binding, as well as the cellular response to interleukins and toll-like receptor signalling as being impacted based on the full DEG list (Fig. 5.6). GO term analysis also flagged chemotaxis of immune cells (neutrophils/granulocytes) and the response to interferon-gamma and interleukin-1 (Fig. 5.5). These GO and Reactome terms have been found to be significantly enriched by p adjusted value, by comparing the background distribution of annotation to that of the differentially expressed gene list. The KEGG pathway analysis maps show the genes already mentioned involved in NF $\kappa$ B signalling, chemokine signalling and NOD-like receptor signalling, and where in their respective pathways they lie.

To understand what might be mediating these responses or if the genes have a common regulator or transcription factor, Enrichr [258] was used to probe for predicted transcription factors. Four different analyses were used, three of which

returned RELA, an NF $\kappa$ B protein, as a predicted controlling factor (Fig. 5.10). Others predicted include c-Jun, STAT1, IRF8 and NFAT. qRT-PCR was then used to validate some of the differentially expressed genes in the same RNA that was used for sequencing. Of those tested, *IRAK2* and *CX3CL1* showed a similar trend of downregulation to the sequencing data, but not significantly. qRT-PCR was not able to verify the sequencing data for *NOD2*, *CCL8* and *BDKRB1* with regards to UDP- $\beta$ S stimulation (Fig. 5.11). qRT-PCR was also used to test these responses in ATDC5 cells and *CCL8*, *CXCL2* and *IL6* showed a similar trend of downregulation to the sequencing, yet again, not statistically significant. An NF $\kappa$ B luciferase construct was then used to see if any change in NF $\kappa$ B activity could be seen with UDP- $\beta$ S stimulation. There were no significant changes in luciferase activity across the six hour time course (Fig. 5.12). There was no significant GO term enrichment in the IL-1 vs IL-1 + UDP group (Fig. 5.13), and the genes that are differentially expressed have a less clear impact on phenotype. These genes were not significantly differentially expressed by adjusted p value (Table 5.2).

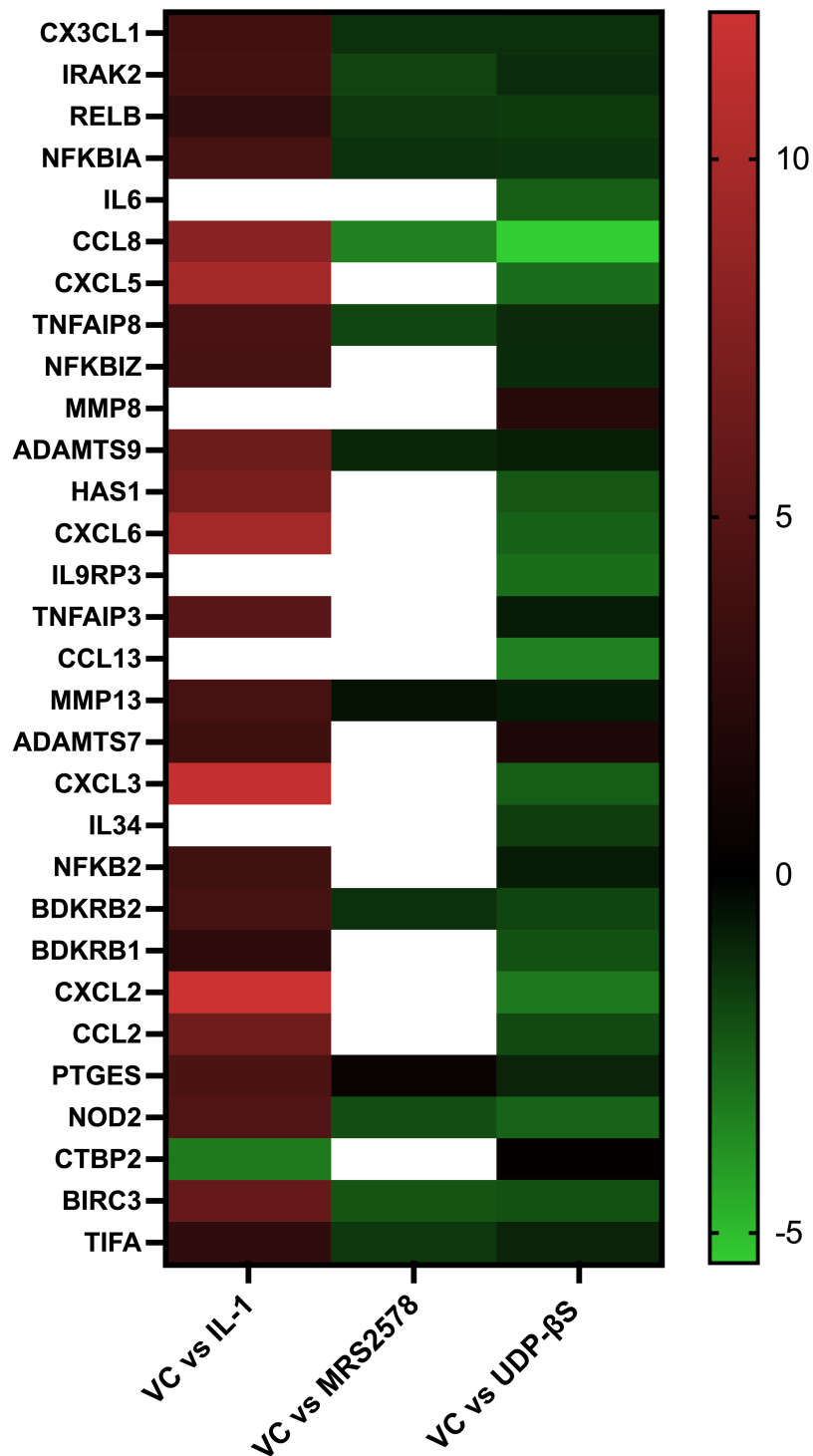


**Figure 5.4: Heat map.** Disease relevant genes were extracted from the DEG gene list in the unstimulated groups, whilst comparing to the action of IL1- $\beta$  alone. Blank spaces infer that the gene was not significantly differentially expressed in this group.

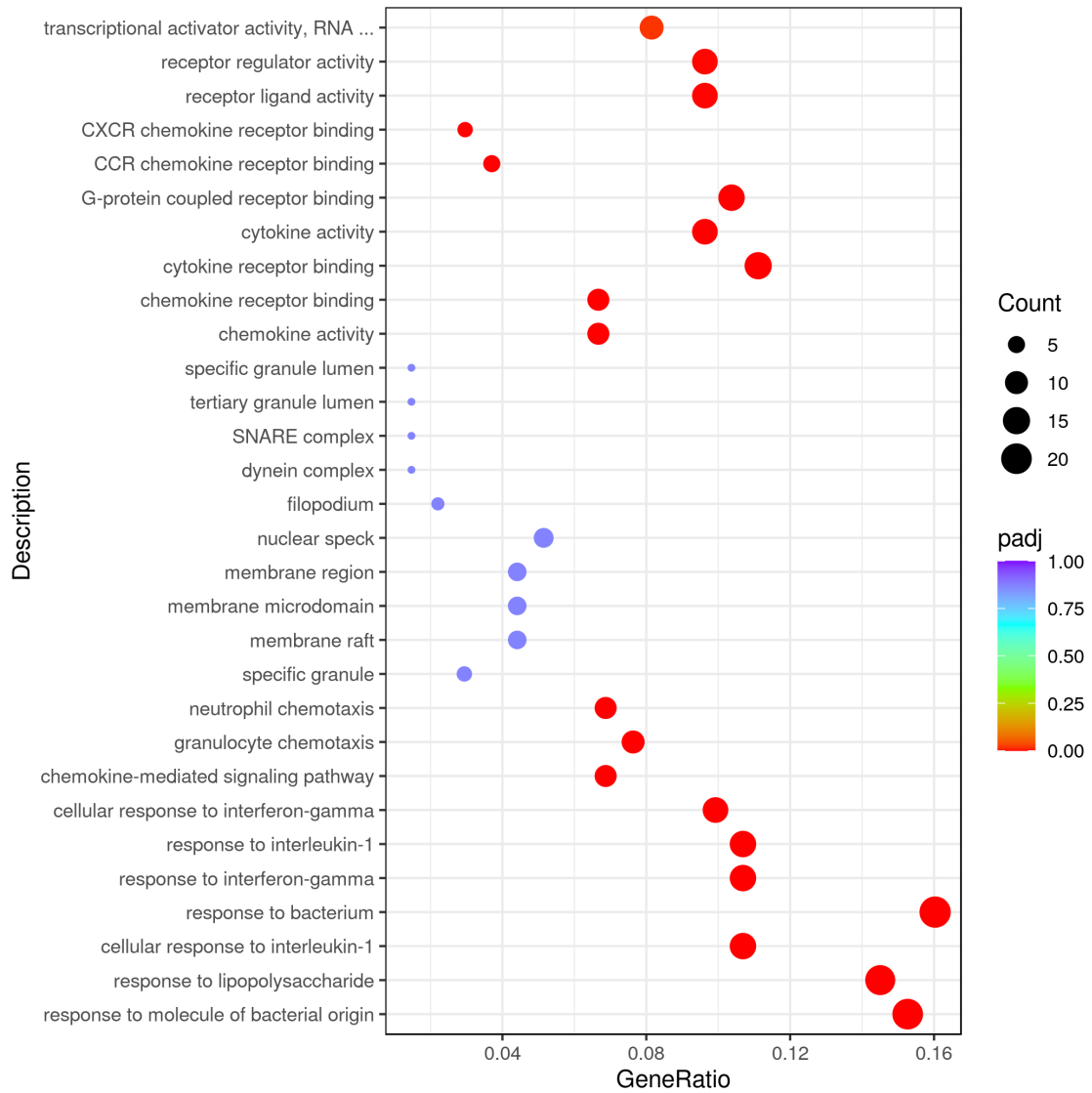


**Figure 5.5: Gene Ontology Enrichment Analysis - VC vs UDP- $\beta$ S.** Gene Ontology [255] term enrichment analysis was performed on the DEG list, whereby grouping of genes were analysed for significant enrichment.

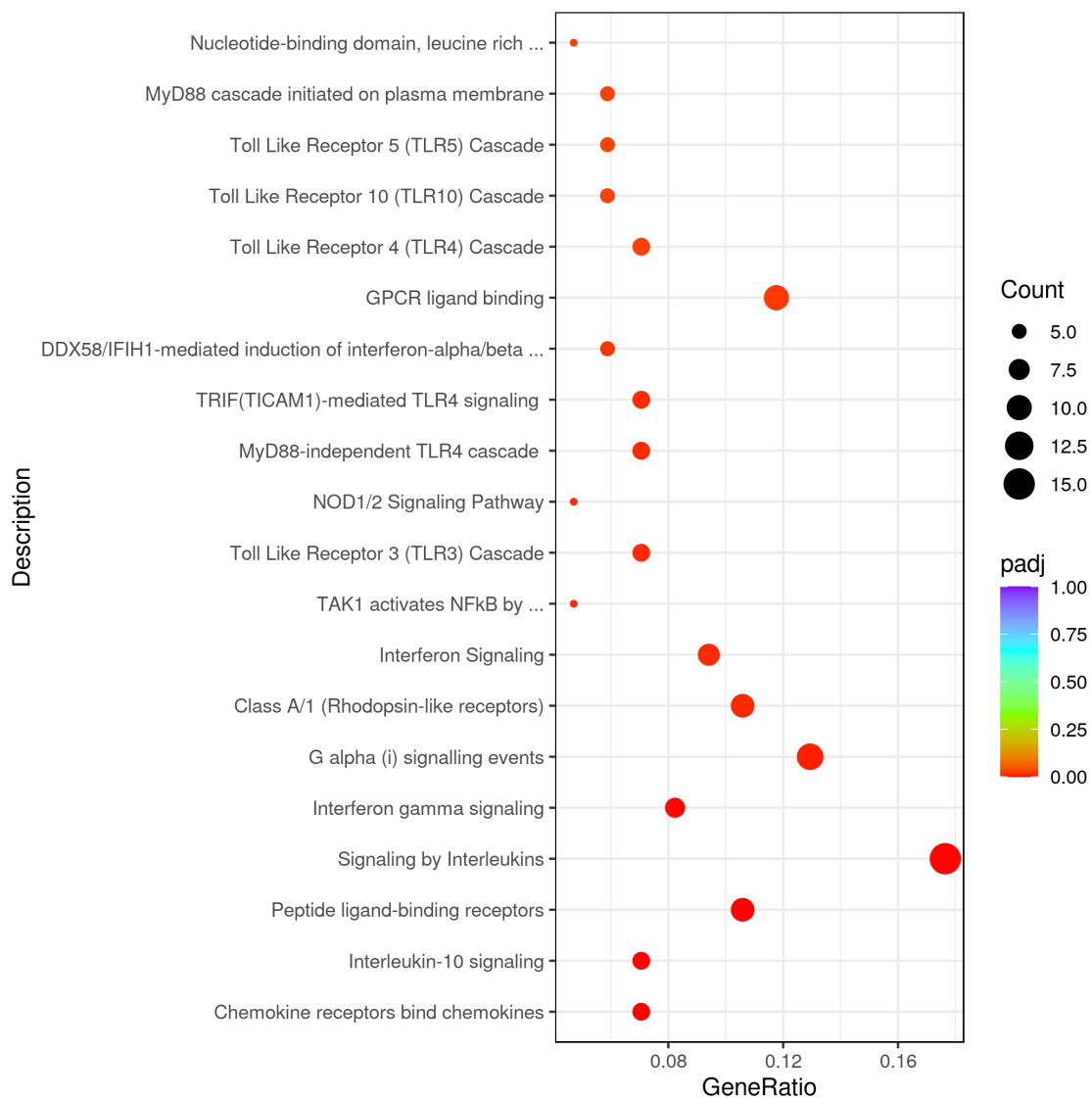


**Figure 5.6: Reactome Enrichment Analysis - VC vs UDP- $\beta$ S.** Reactome[256] enrichment analysis was performed on the DEG list, whereby grouping of genes were analysed for significant enrichment.

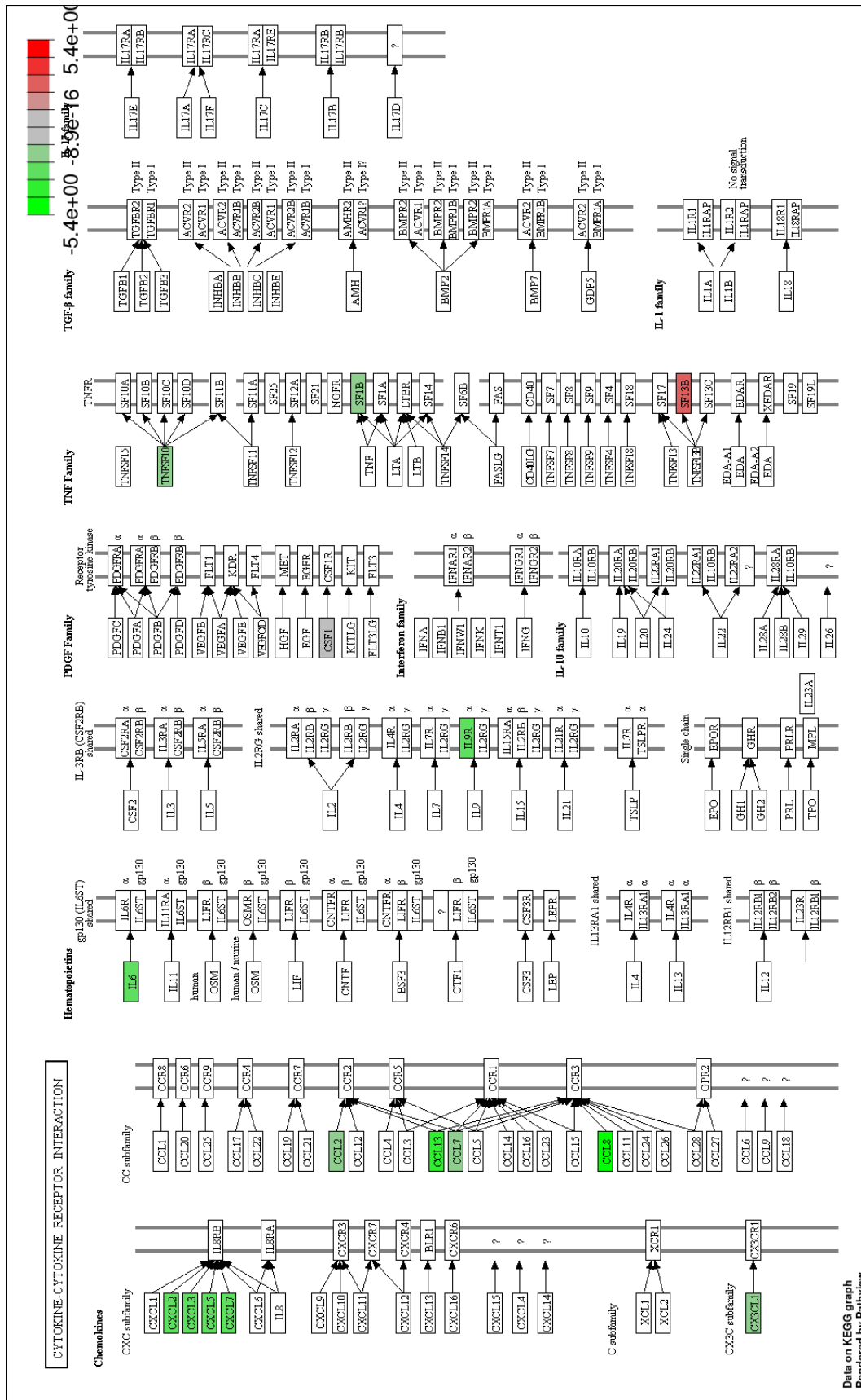


**Figure 5.7: KEGG Analysis - VC vs UDP-βS.** Kyoto encyclopedia of genes and genomes [257] enrichment pathway analysis was performed on the DEG list, whereby grouping of genes were analysed for significant enrichment and how they fit into their respective pathways.

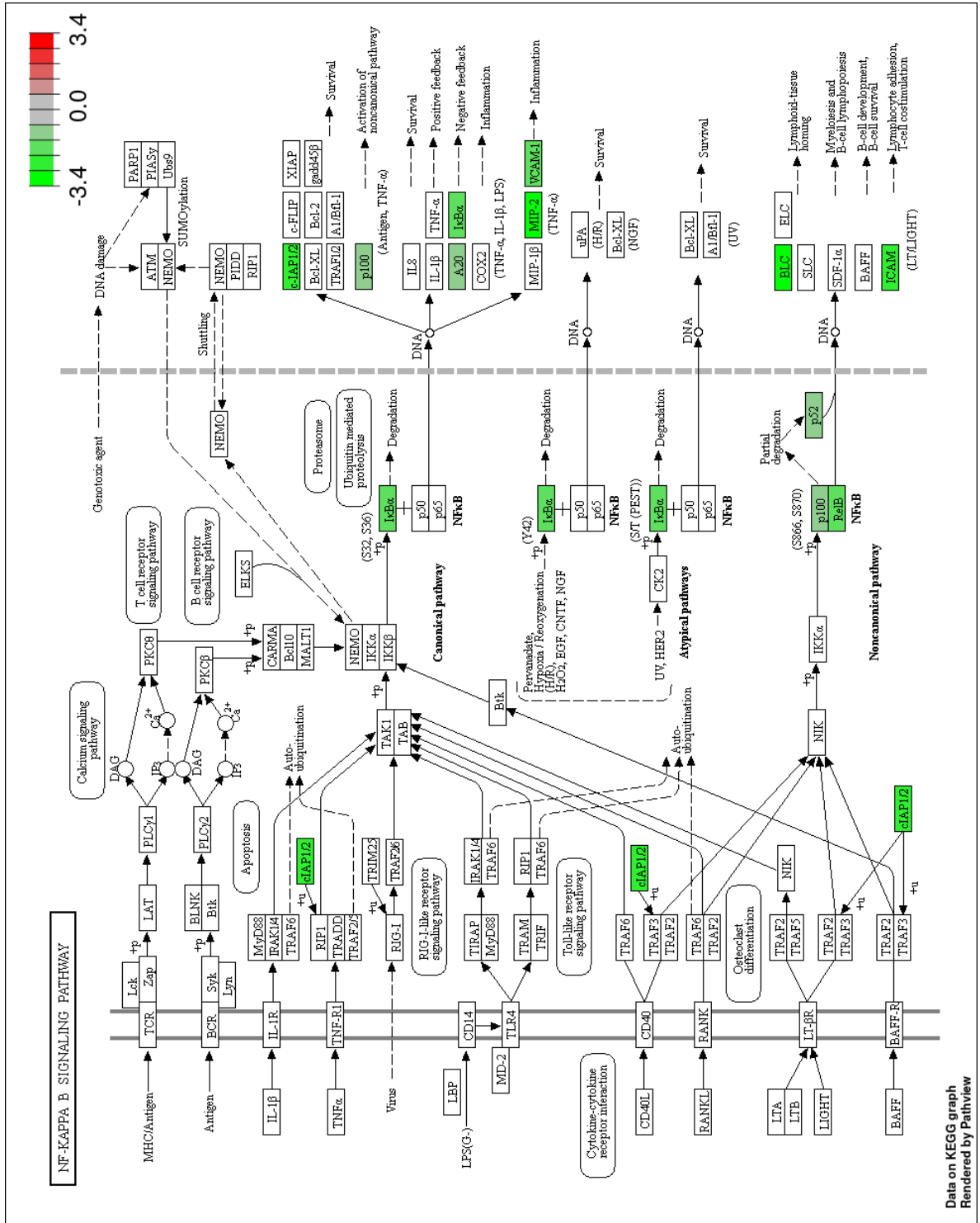
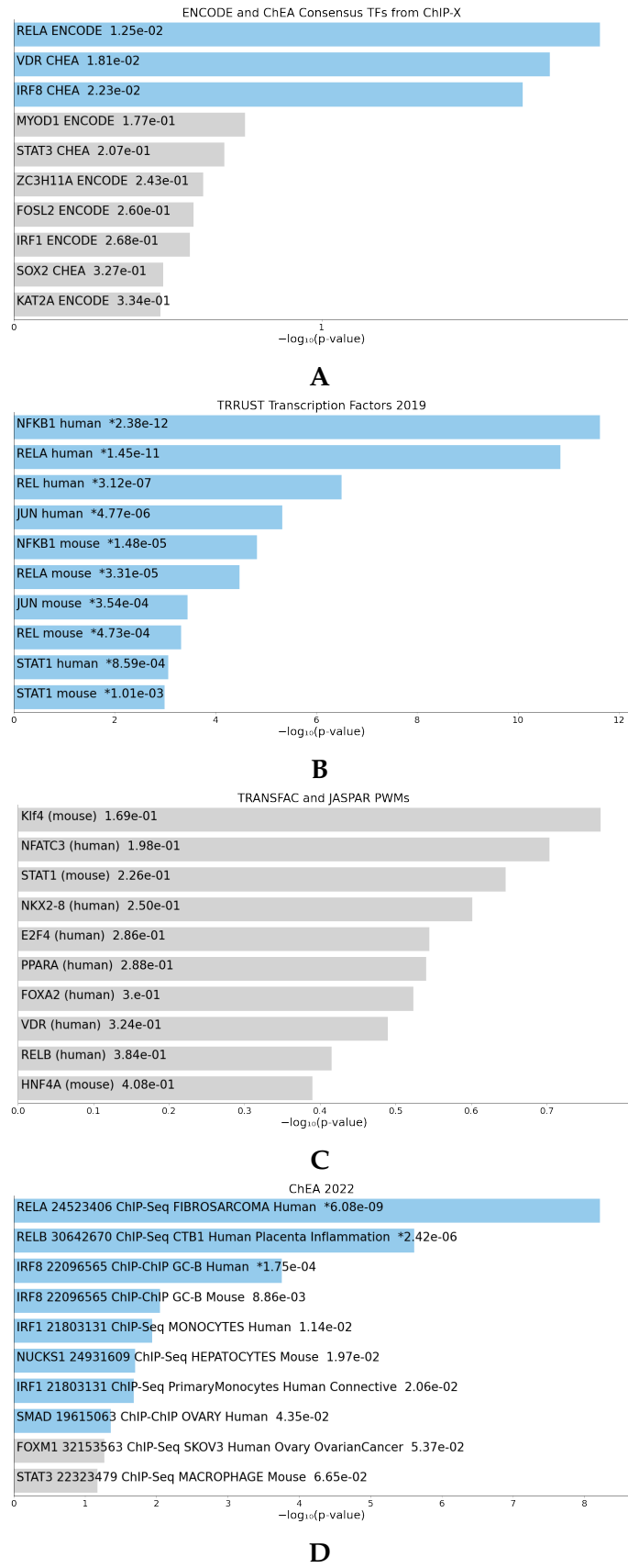
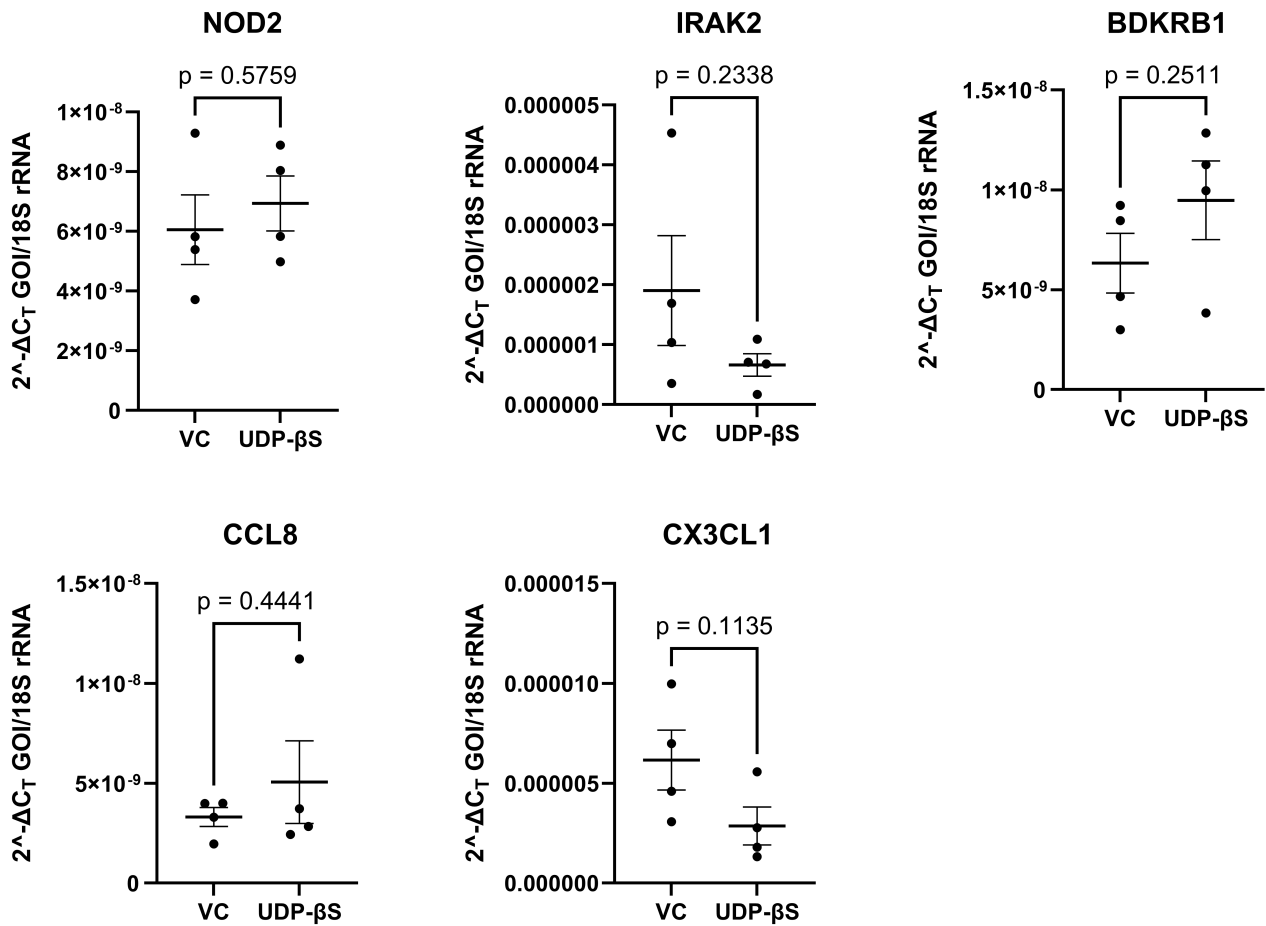


Figure 5.8: KEGG Pathway Analysis for VC vs UDP-βS. Kyoto encyclopedia of genes and genomes [257] enrichment pathway analysis was performed on the DEG list, whereby grouping of genes were analysed for significant enrichment and how they fit into their respective pathways.

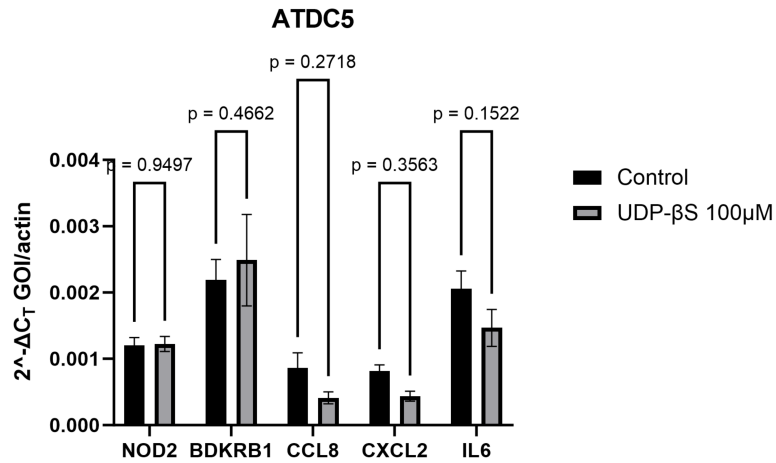
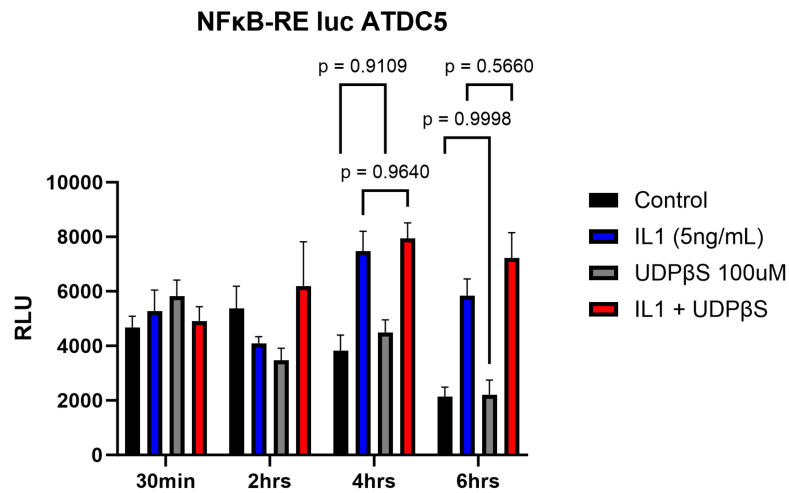




**Figure 5.10: Predicted Transcription Factors of DEG.** Enrichr [258] was used to predict common transcription factors of DEGs in the VC vs UDP- $\beta$ S comparison.



**Figure 5.11: qRT-PCR Verification in PHC.** Reserved RNA that was sent for sequencing was reverse transcribed and qRT-PCR was used to assess changes in gene expression as detected by mRNA sequencing. Data presented as mean  $\pm$  SEM. Student's t test. N=4.

**A****B**

**Figure 5.12: ATDC5 qRT-PCR and NF $\kappa$ B Luciferase.** ATDC5 cells were treated with UDP- $\beta$ S for six hours and RNA was extracted and reverse transcribed. qRT-PCR was carried out (A). (B) ATDC5 cells were transfected with NF $\kappa$ B luciferase construct and treated with UDP- $\beta$ S, followed by measurement of firefly luciferase activity upon cell lysis.

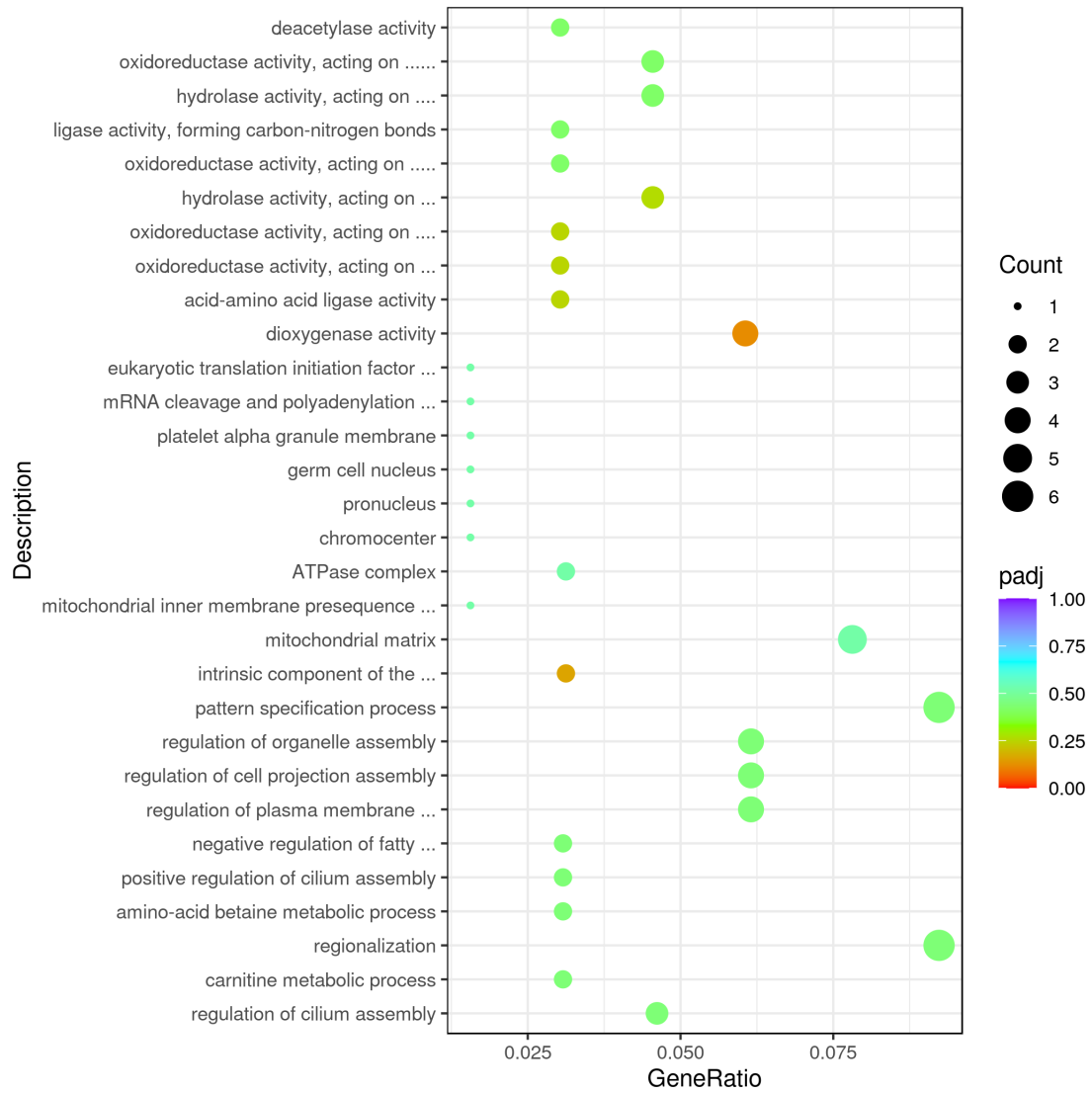


**Figure 5.13: Gene Ontology Enrichment Analysis - IL-1 vs IL-1 + UDP- $\beta$ S.** Gene Ontology [255] term enrichment analysis was performed on the DEG list, whereby grouping of genes were analysed for significant enrichment.

**Table 5.1:** VC vs UDP Top 50 DEG by p value

FC	p value	p adj	Gene	Description
2.61	1.1E-05	0.32002	<i>SMIM11A</i>	small integral membrane protein 11A
-1.28	1.8E-04	0.99997	<i>CX3CL1</i>	C-X3-C motif chemokine ligand 1
-1.82	2.1E-04	0.99997	<i>BDKRB2</i>	bradykinin receptor B2
-2.15	2.2E-04	0.99997	<i>BDKRB1</i>	bradykinin receptor B1
-1.12	2.8E-04	0.99997	<i>CMPK2</i>	cytidine/uridine monophosphate kinase 2
-0.84	3.4E-04	0.99997	<i>TBC1D3D</i>	TBC1 domain family member 3D
-1.64	5.4E-04	0.99997	<i>SERF1B</i>	small EDRK-rich factor 1B
-2.62	9.4E-04	0.99997	<i>NOD2</i>	nucleotide binding oligomerization domain containing 2
0.24	2.1E-03	0.99997	<i>ARHGEF17</i>	Rho guanine nucleotide exchange factor 17
-1.19	3.0E-03	0.99997	<i>IRAK2</i>	interleukin 1 receptor associated kinase 2
0.56	3.2E-03	0.99997	<i>ZFN704</i>	zinc finger protein 704
-0.67	3.2E-03	0.99997	<i>DDX60</i>	DExH/H-box helicase 60
-4.28	3.7E-03	0.99997	<i>MIR3132</i>	microRNA 3132
-3.25	4.1E-03	0.99997	<i>NSFP1</i>	N-ethylmaleimide-sensitive factor pseudogene 1
-0.80	4.3E-03	0.99997	<i>CYP7B1</i>	cytochrome P450 family 7 subfamily B member 1
-1.57	4.3E-03	0.99997	<i>RELB</i>	RELB proto-oncogene, NF-kB subunit
-1.08	4.9E-03	0.99997	<i>BCL3</i>	B cell CLL/lymphoma 3
-2.12	5.5E-03	0.99997	<i>AIRE</i>	autoimmune regulator
-2.81	6.1E-03	0.99997	<i>CABP7</i>	calcium binding protein 7
-1.42	6.4E-03	0.99997	<i>NFκBIA</i>	NFκB inhibitor alpha
-0.96	6.5E-03	0.99997	<i>NPL</i>	N-acetylneuraminase pyruvate lyase
-1.98	6.6E-03	0.99997	<i>MAGED4B</i>	MAGE family member D4B
-1.51	7.0E-03	0.99997	<i>SCO2</i>	SCO2, cytochrome c oxidase assembly protein
-1.08	7.6E-03	0.99997	<i>CSF1</i>	colony stimulating factor 1
0.31	7.6E-03	0.99997	<i>PXDC1</i>	PX domain containing 1
-1.73	7.7E-03	0.99997	<i>FP565260.3</i>	Homo sapiens ICOS ligand, mRNA
0.41	7.8E-03	0.99997	<i>PPCDC</i>	phosphopantothienoylcysteine decarboxylase
-2.52	7.9E-03	0.99997	<i>IL6</i>	interleukin 6
-3.64	8.0E-03	0.99997	<i>C15orf48</i>	chromosome 15 open reading frame 48
-5.43	8.2E-03	0.99997	<i>CCL8</i>	C-C motif chemokine ligand 8
-1.43	8.4E-03	0.99997	<i>ZC3H12A</i>	zinc finger CCCH-type containing 12A
-0.32	9.4E-03	0.99997	<i>CCNL1</i>	cyclin L1
-1.88	1.0E-02	0.99997	<i>CCL7</i>	C-C motif chemokine ligand 7
-0.63	1.0E-02	0.99997	<i>EPSTI1</i>	epithelial stromal interaction 1
-1.27	1.0E-02	0.99997	<i>TNFRSF1B</i>	TNF receptor superfamily member 1B
-4.05	1.1E-02	0.99997	<i>GNGT2</i>	G protein subunit gamma transducin 2
2.50	1.1E-02	0.99997	<i>DUOX2</i>	dual oxidase 2
-2.15	1.1E-02	0.99997	<i>BIRC3</i>	baculoviral IAP repeat containing 3
-0.69	1.1E-02	0.99997	<i>RARRES3</i>	retinoic acid receptor responder 3
-1.78	1.2E-02	0.99997	<i>HIST2H4B</i>	histone cluster 2 H4 family member b
-1.17	1.2E-02	0.99997	<i>IRF1</i>	interferon regulatory factor 1
2.52	1.3E-02	0.99997	<i>BISPR</i>	BST2 interferon stimulated positive regulator
-3.00	1.3E-02	0.99997	<i>HAVCR1</i>	hepatitis A virus cellular receptor 1

**Table 5.2:** IL-1 vs IL-1 + UDP- $\beta$ S Top 50 DEG by p value

FC	p value	p adj	Gene	Gene Description
1.06	0.0008	0.9999	<i>SCAI</i>	suppressor of cancer cell invasion
1.16	0.0011	0.9999	<i>EIF3C</i>	eukaryotic translation initiation factor 3 subunit C
-0.88	0.0039	0.9999	<i>PSMC1P1</i>	proteasome 26S subunit, ATPase 1 pseudogene 1
1.96	0.0064	0.9999	<i>SNHG22</i>	small nucleolar RNA host gene 22
-2.99	0.0066	0.9999	<i>SIRT4</i>	sirtuin 4
3.67	0.0083	0.9999	<i>AL162430.1</i>	ribosomal protein S2 (RPS2) pseudogene
-1.26	0.0089	0.9999	<i>RASA4</i>	RAS p21 protein activator 4
1.95	0.0090	0.9999	<i>AL136981.2</i>	novel zinc finger protein pseudogene
0.85	0.0091	0.9999	<i>FGD4</i>	FYVE, RhoGEF and PH domain containing 4
1.58	0.0096	0.9999	<i>CBWD4P</i>	COBW domain containing 4 pseudogene
2.31	0.0097	0.9999	<i>AC090912.1</i>	novel transcript, antisense to RBBP8
0.60	0.0097	0.9999	<i>AC022167.2</i>	novel transcript, antisense to CARHSP1
-1.77	0.0103	0.9999	<i>FSIP1</i>	fibrous sheath interacting protein 1
-1.26	0.0106	0.9999	<i>TEX22</i>	testis expressed 22
0.96	0.0115	0.9999	<i>AC120114.3</i>	novel transcript, sense intronic to KCTD13
2.74	0.0116	0.9999	<i>POLQ</i>	DNA polymerase theta
3.37	0.0118	0.9999	<i>SALL1</i>	spalt like transcription factor 1
4.01	0.0127	0.9999	<i>STPG4</i>	sperm-tail PG-rich repeat containing 4
0.91	0.0128	0.9999	<i>BCO2</i>	beta-carotene oxygenase 2
0.80	0.0143	0.9999	<i>37226</i>	deleted in esophageal cancer 1
-0.34	0.0144	0.9999	<i>ZNF581</i>	zinc finger protein 581
2.92	0.0147	0.9999	<i>IGSF6</i>	immunoglobulin superfamily member 6
-1.04	0.0148	0.9999	<i>SMG1P5</i>	SMG1 pseudogene 5
-2.07	0.0156	0.9999	<i>NEURL3</i>	neuralized E3 ubiquitin protein ligase 3
1.16	0.0165	0.9999	<i>AC024075.3</i>	novel transcript, antisense C19orf42
-3.86	0.0166	0.9999	<i>OTOA</i>	otoanchorin
-3.92	0.0168	0.9999	<i>AC079630.1</i>	novel transcript, antisense to LRRK2
1.21	0.0168	0.9999	<i>Z98884.2</i>	novel transcript, sense intronic to VAMP3
-1.63	0.0168	0.9999	<i>TIGD3</i>	tigger transposable element derived 3
1.61	0.0171	0.9999	<i>FBXL16</i>	F-box and leucine rich repeat protein 16
-2.05	0.0171	0.9999	<i>AL163540.1</i>	COBW domain containing protein pseudogene
0.54	0.0179	0.9999	<i>SEC61A2</i>	Sec61 translocon alpha 2 subunit
-2.24	0.0180	0.9999	<i>PRAM1</i>	PML-RARA regulated adaptor molecule 1
2.82	0.0182	0.9999	<i>PRH1</i>	proline rich protein HaeIII subfamily 1
3.47	0.0183	0.9999	<i>LINC00987</i>	long intergenic non-protein coding RNA 987
3.32	0.0185	0.9999	<i>EAF1-AS1</i>	EAF1 antisense RNA 1
0.30	0.0199	0.9999	<i>HECTD2</i>	HECT domain E3 ubiquitin protein ligase 2
-0.41	0.0204	0.9999	<i>SS18L2</i>	SS18 like 2
0.71	0.0212	0.9999	<i>BRCA1</i>	BRCA1, DNA repair associated
3.55	0.0212	0.9999	<i>AC004594.1</i>	novel transcript, antisense to CADPS2
1.63	0.0215	0.9999	<i>AC233968.1</i>	aminopeptidase puromycin sensitive pseudogene
0.89	0.0217	0.9999	<i>BNC1</i>	basonuclin 1
0.97	0.0218	0.9999	<i>ACVR1C</i>	activin A receptor type 1C
0.69	0.0220	0.9999	<i>AC093162.2</i>	retinol saturase pseudogene
-3.76	0.0220	0.9999	<i>MESP2</i>	mesoderm posterior bHLH transcription factor 2

### 5.2.3 Some of the DEG caused by UDP- $\beta$ S also change at the protein level.

Owing to the lack of statistical power to use the Benjamini-Hochberg method to validate true findings as well as to add weight to what is seen at the mRNA level, a proteomic solid-phase array was used to detect changes in cytokine secretion in PHC following UDP- $\beta$ S stimulation. A longer time course was chosen as it takes longer for a cell to transcribe, translate and secrete the protein than produce the mRNA, so time points of 24 and 48 hours were chosen. The same concentration of UDP- $\beta$ S was used (100 $\mu$ M), and the media was replaced at the beginning of the stimulation to create a basal or 0 starting point. A pooling approach was taken due to the prohibitive cost of the membranes - as such, whilst the samples contained the variation of 3 different donors, the variation cannot be measured. Shown in Figs. 5.14 and 5.15 is the densitometric analysis of the arrays, pictures can be seen in the appendix. At the 24 hour time point, many of the cytokines detected were below background levels in the control group but not in the stimulated group, including IL-2,3,4,5,6 and 7 as well as CCL1 and IL-10,12,13 and 15. CCL2 detection was higher in the stimulated group, as well as CXCL8, CCL4 and angiogenin. The detection of some cytokines was also lower in the stimulated group, including NT-3 and NT-4, CXCL7, TGF- $\beta$ 2/3 and CXCL10. At the 48 hour time point, many similar trends are also seen. CCL2 detection is also higher in the stimulated group. The same is true for many of the interleukins. However, detection in the stimulated group is also lower for many of the cytokines, including TGF- $\beta$ 2/3, PLGF, PARC, SPP1, NT-3, CCL13, CX3CL1, CCL26, CXCL1 and CCL22.

## 24 Hours

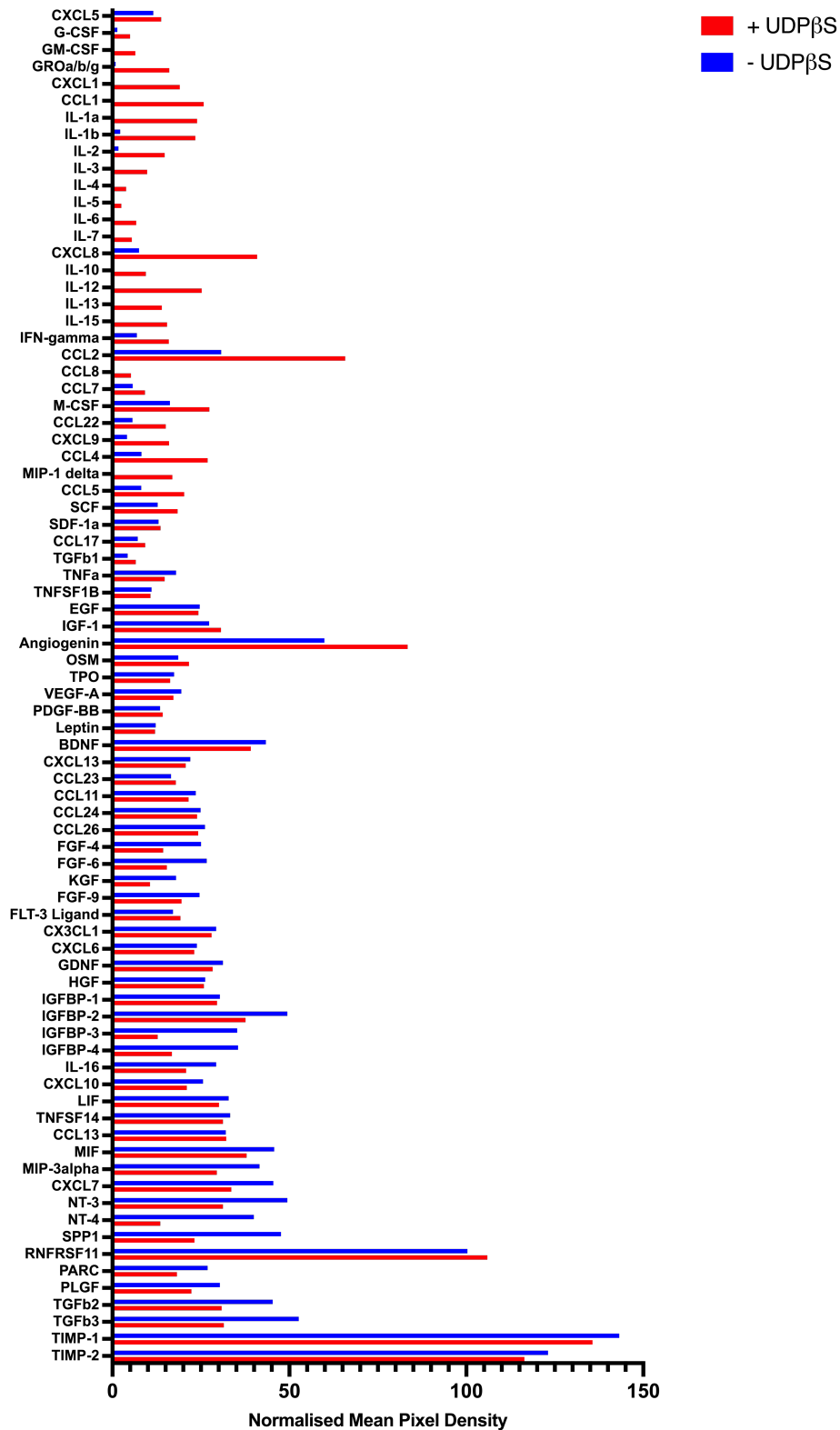


**Figure 5.14: Proteomic Array in PHC 24hr post UDP-βS stimulation.** 3 PHC isolates were incubated were plated into a 12 well plate, serum starved for 24 hours and stimulated with UDP-βS 100μM for 24 hours, followed by detection of cytokines in cell culture supernatant with a solid-phase proteomic array. Densitometry analysis was performed in Fiji/Image-J. N=1.

### 48 Hours

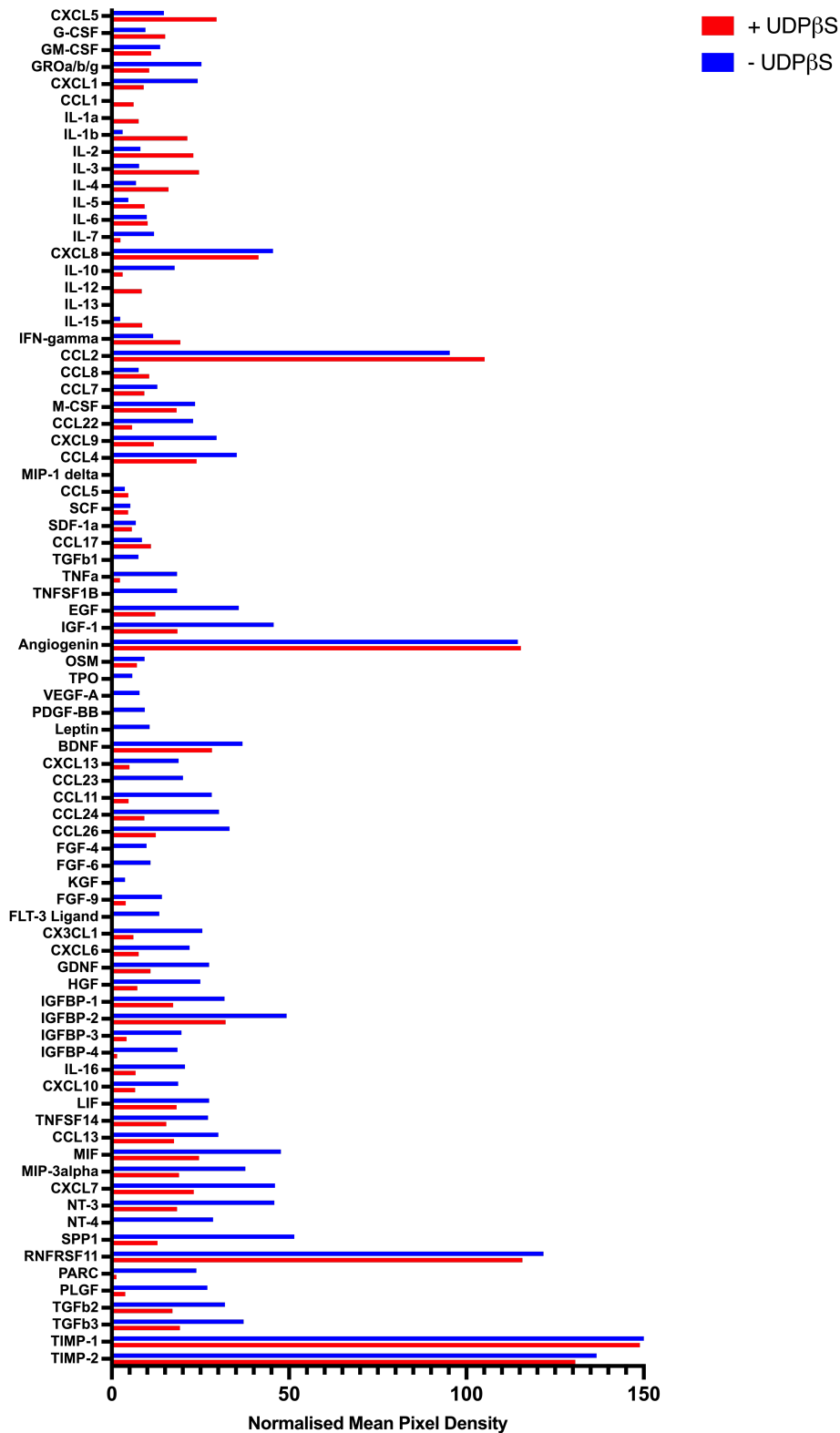


**Figure 5.15: Proteomic Array in PHC 24hr post UDP-βS stimulation.** 3 PHC isolates were incubated were plated into a 12 well plate, serum starved for 24 hours and stimulated with UDP-βS 100μM for 48 hours, followed by detection of cytokines in cell culture supernatant with a solid-phase proteomic array. Densitometry analysis was performed in Fiji/Image-J. N=1.

#### 5.2.4 UDP- $\beta$ S may mediate these effects via inhibition of STAT6.

To understand which proteins may mediate downstream effects of P2Y6 activation, a solid phase protein array detecting phosphorylated proteins was carried out. Following UDP- $\beta$ S stimulation, cells were lysed and proteins were solubilised (with phosphatase and protease inhibitors) at three time points - 15 minutes, 30 minutes and 60 minutes, as kinases can act very quickly to phosphorylate proteins [259]. Again, a pooling approach was taken, so that the samples contain the variation from three PHC donors, but the variance cannot be measured. There were five membranes, detecting phosphorylation of proteins from different families - namely NF $\kappa$ B, MAPK, AKT, JAK/STAT and TGF. Densitometric analysis of the detection of phosphorylated proteins is shown in Figs. 5.16 - 5.20, and images of the membranes are in the appendix. Data are shown as fold change from a control, basal phosphorylation membrane and adjusted for intra-membrane variability with a positive control spot on each individual membrane. Of the NF $\kappa$ B proteins, many of the proteins' phosphorylation remain unchanged between control and UDP- $\beta$ S stimulated groups. At 15 minutes, however, TAK1 and TBK1 are higher in the stimulated group, as is ATM at 30 minutes. Of the MAPK proteins, at 30 minutes post stimulation, detection of phosphorylated p38 is higher in the stimulated group, but that of ERK1/2 and MSK2 is higher in the control group. Of the AKT proteins, at 15 minutes, detection of phosphorylated PRAS40 is higher in the control group. At 30 minutes, that of PRAS40 reverses and is higher in the stimulated group, as does that of PTEN. The most stark change is that of STAT6, part of the JAK/STAT family of proteins. The detection of phosphorylated STAT6 is lower in the stimulated group at all three time points, and becomes lower than that of basal control at 30 and 60 minutes, with a negative fold change. As well as this, EGFR phosphorylation is lower than the untreated control and basal control at 60 minutes. At 30 and 60 minutes, the detection of phosphorylated JAK1, STAT5, TYK2 and SHP1 are also lower in the UDP- $\beta$ S stimulated groups than control. Phosphorylation of many of the TGF proteins also changes with UDP- $\beta$ S stimulation. At 15 minutes, detection of phosphorylated SMAD, ATF2 and c-Fos/c-Jun is higher in the stimulated group. This effect is not maintained at the 30 minute and 60 minute time points, and SMAD1 shows reduced phosphoryla-

tion in the stimulated group at the 30 and 60 minute time points. That of SMAD2 and SMAD5 then becomes lower at the 60 minute time point.

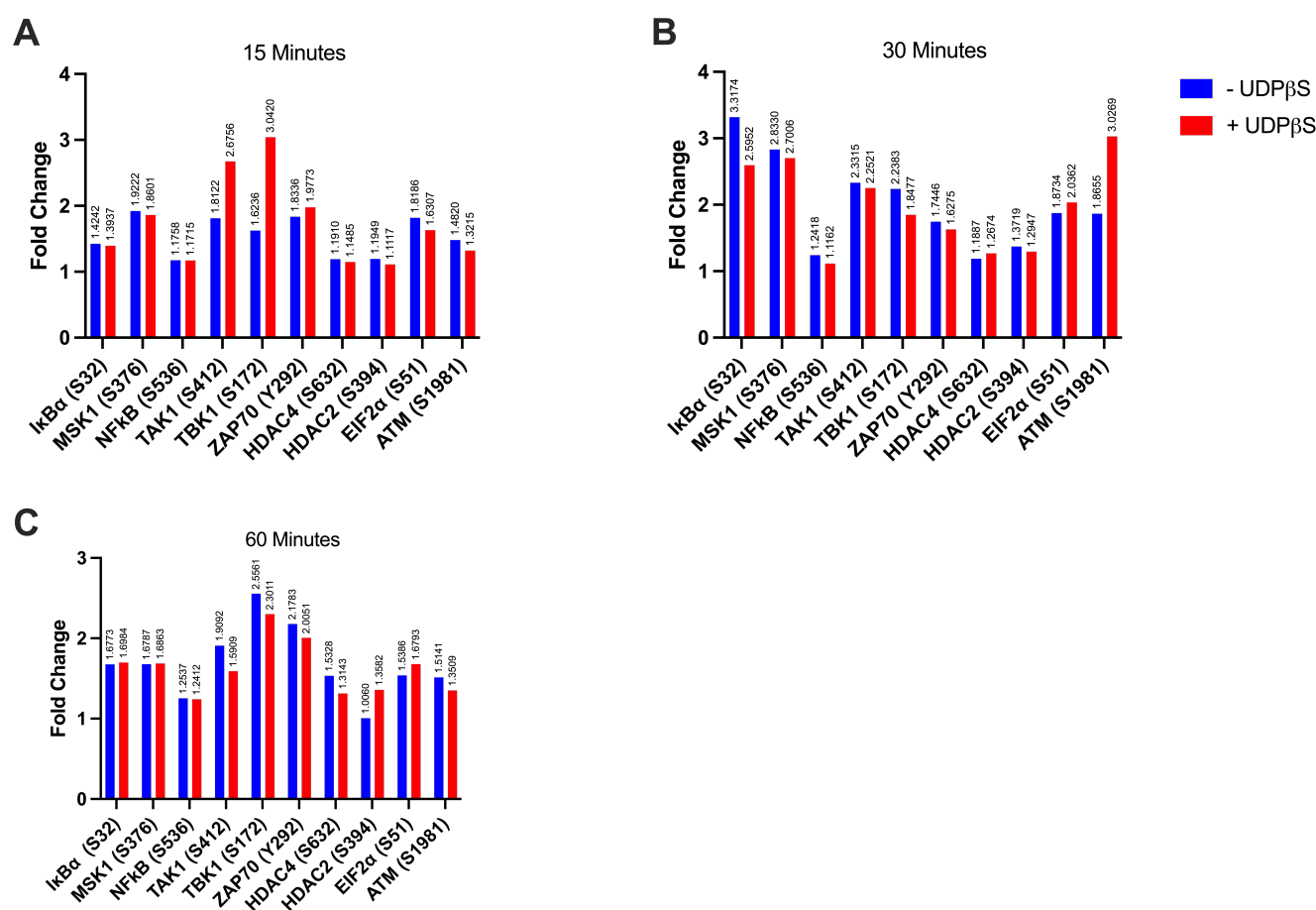


**Figure 5.16: Proteomic Array NFκB.** PHC were seeded into a 12 well plate, serum starved for 24 hours and stimulated with UDP-βS for the time indicated on the individual graph. Following this, phosphorylated proteins were detected by a solid phase proteomic array and densitometric analysis was carried out with Fiji/ImageJ. N=1.

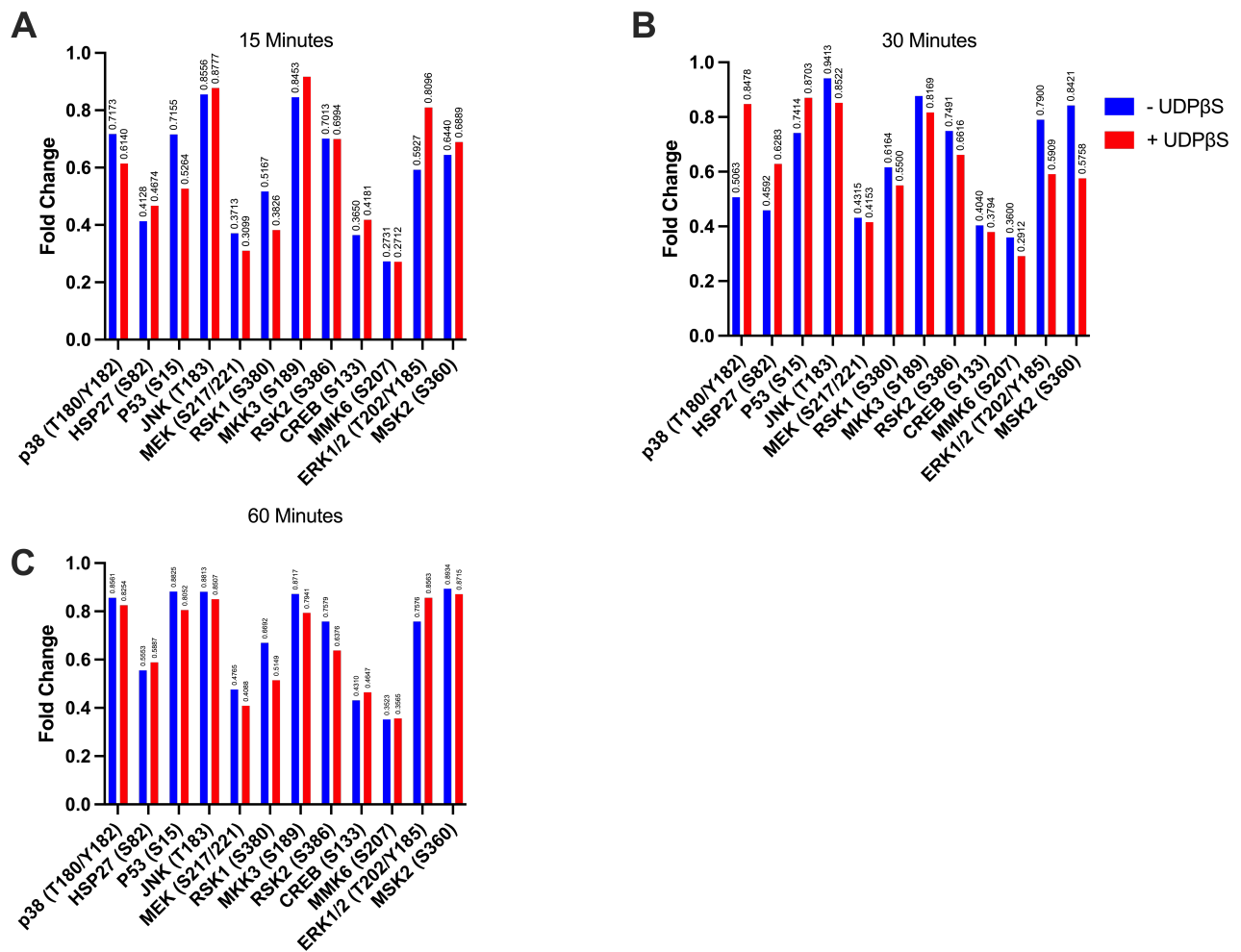


**Figure 5.17: Proteomic Array MAPK.** PHC were seeded into a 12 well plate, serum starved for 24 hours and stimulated with UDP-βS for the time indicated on the individual graph. Following this, phosphorylated proteins were detected by a solid phase proteomic array and densitometric analysis was carried out with Fiji/ImageJ. N=1.

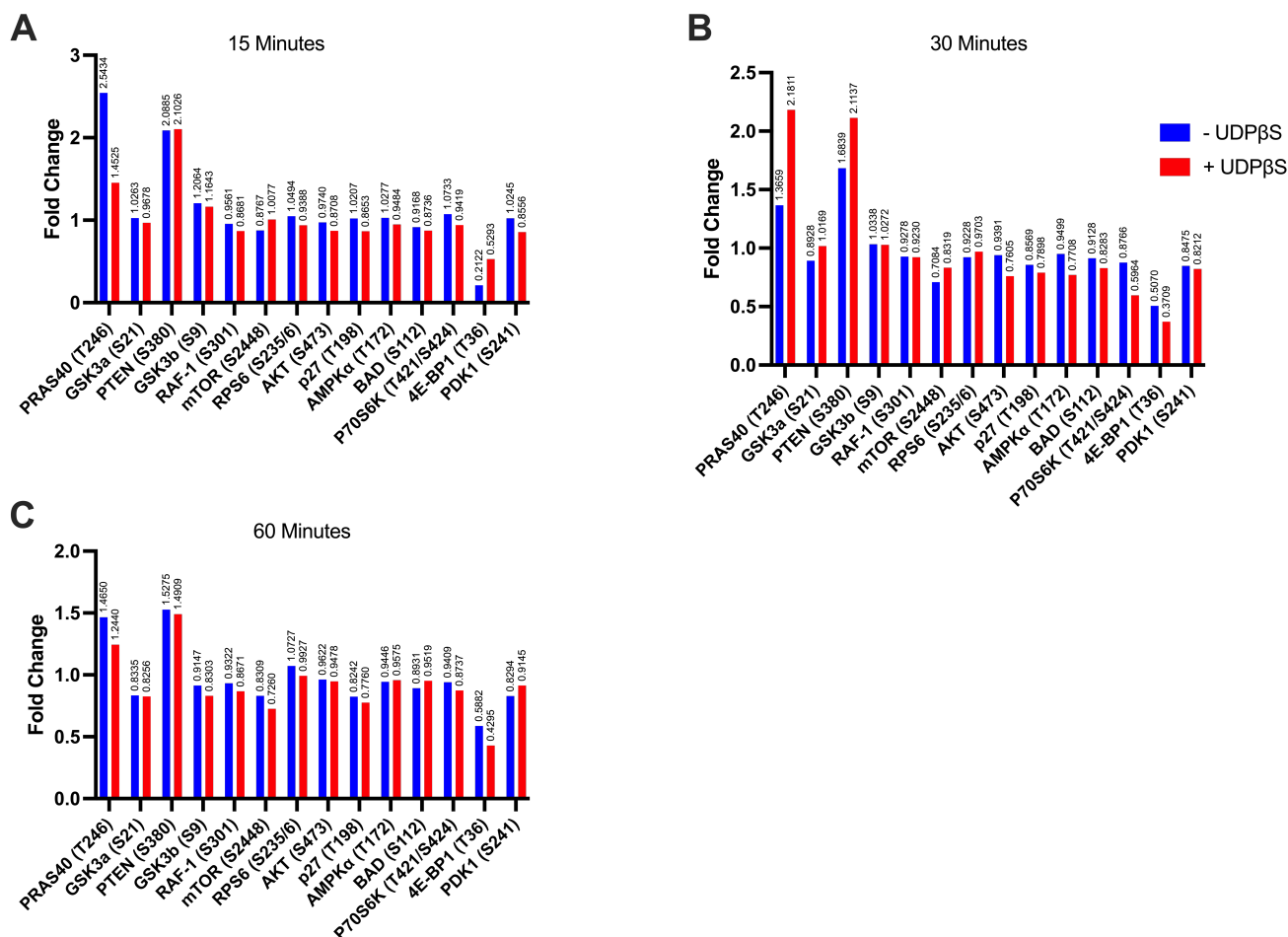


**Figure 5.18: Proteomic Array AKT.** PHC were seeded into a 12 well plate, serum starved for 24 hours and stimulated with UDP- $\beta$ S for the time indicated on the individual graph. Following this, phosphorylated proteins were detected by a solid phase proteomic array and densitometric analysis was carried out with Fiji/ImageJ. N=1.

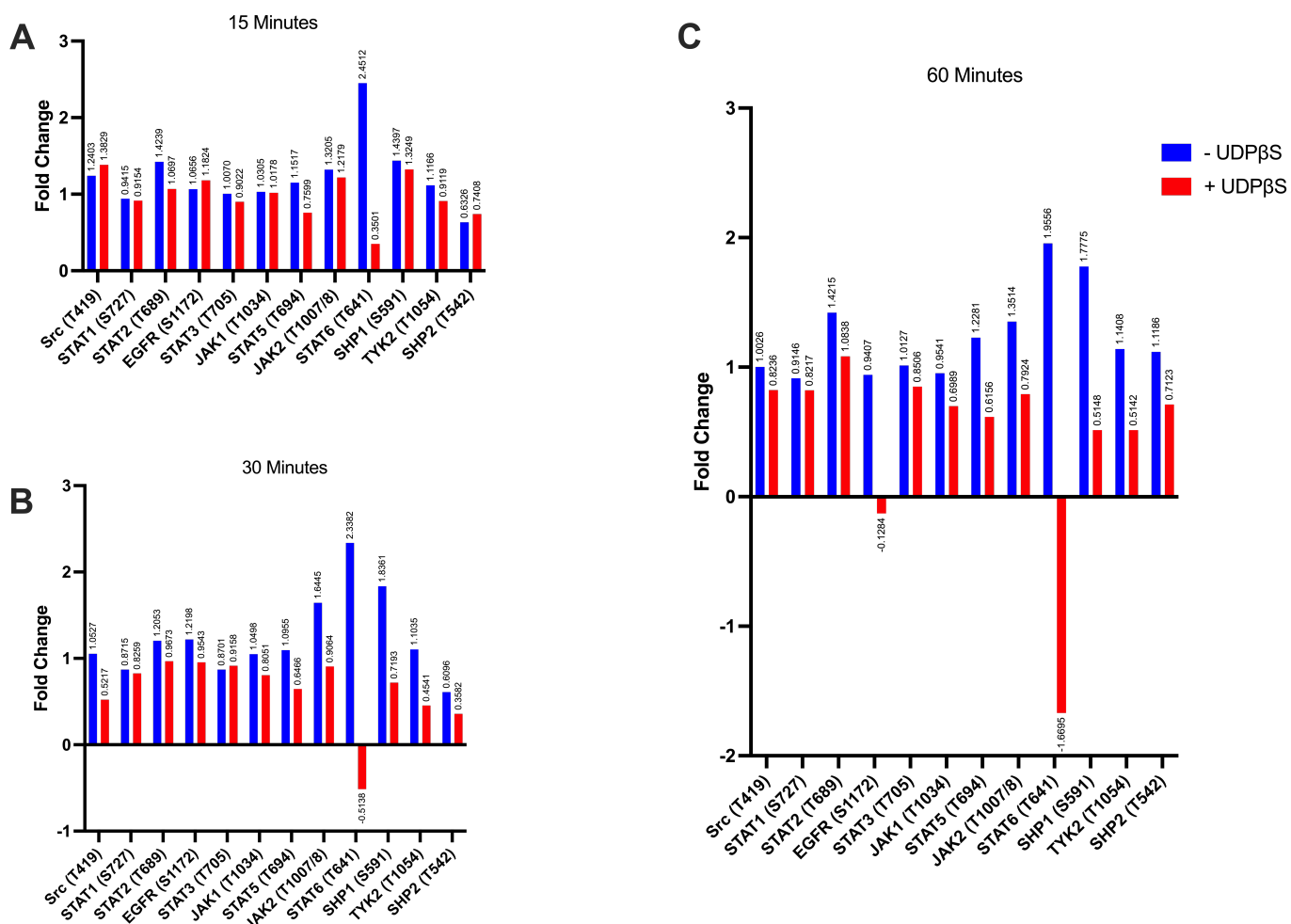


**Figure 5.19: Proteomic Array JAK/STAT.** PHC were seeded into a 12 well plate, serum starved for 24 hours and stimulated with UDP-βS for the time indicated on the individual graph. Following this, phosphorylated proteins were detected by a solid phase proteomic array and densitometric analysis was carried out with Fiji/ImageJ. N=1.

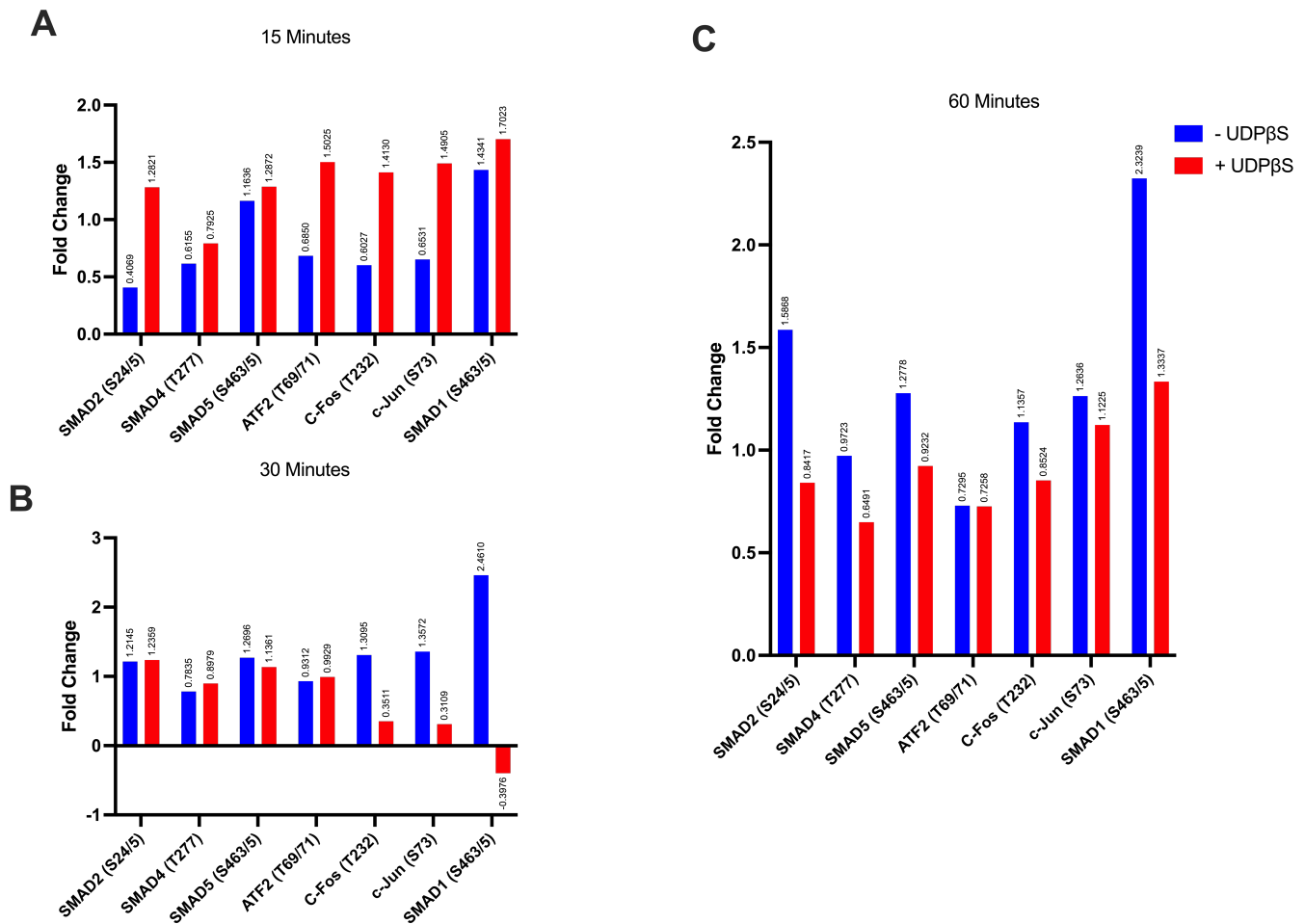


**Figure 5.20: Proteomic Array TGF.** PHC were seeded into a 12 well plate, serum starved for 24 hours and stimulated with UDP- $\beta$ S for the time indicated on the individual graph. Following this, phosphorylated proteins were detected by a solid phase proteomic array and densitometric analysis was carried out with Fiji/ImageJ. N=1.

### 5.2.5 UDP- $\beta$ S and MRS2578 cause differential gene expression often in the same direction of change.

There were a lot of genes in which UDP- $\beta$ S and MRS2578 both elicited reduced transcription in PHC compared to vehicle control. Fig. 5.21 highlights the top 30 genes, by p value, in the form of a heat map that are reciprocally differentially expressed in non-stimulated PHC. Many of the genes are involved in inflammatory processes. These include chemokines (*CX3CL1*, *CCL8/7*) and inflammatory signalling factors (*TNFAIP8*, *NOD2*, *NF $\kappa$ BIA*, *VCAM1*, *TNFSF10*), whose expression was repressed by MRS2578. Conversely, MRS2578 did induce some genes, including *HES7*, *EGR1*, and *CCL1*.

In the IL-1 $\beta$  stimulated PHC, UDP- $\beta$ S and MRS2578 also caused differential gene expression in the same direction of change, although this trend is less clear. Fig. 5.22 shows the top 30 genes by p value that are reciprocally differentially expressed in the IL-1 $\beta$  stimulated group. There is a wider range of genes in this list, and there is not a clear grouping of function. Of the genes that are expressed reciprocally in differing directions, these include *MESP2*, which is a type of bHLH transcription factor, *NKILA*, which is an NF $\kappa$ B lncRNA, and *TEX22*.

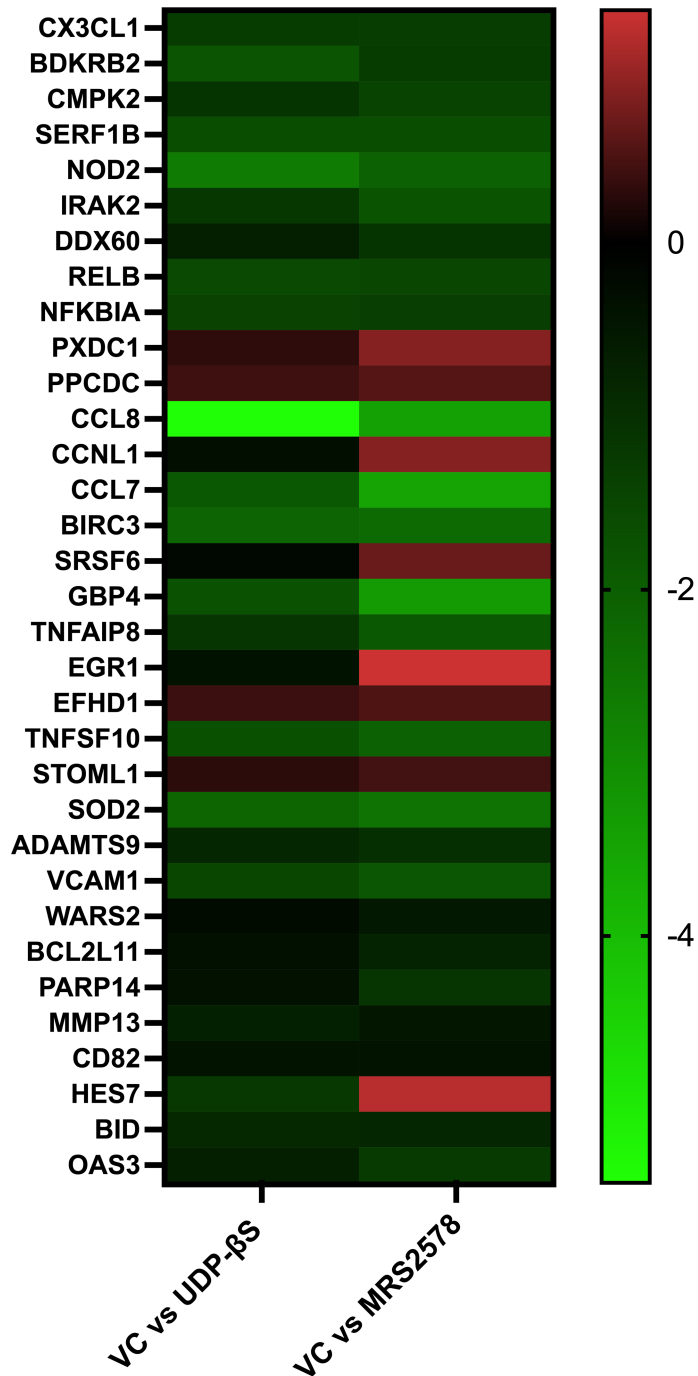


**Figure 5.21: Non-stimulated Reciprocal Heatmap.** Genes that were reciprocally differentially expressed and significant by p value in the UDP- $\beta$ S and MRS2578 groups were extracted and graphically presented in a heat map.

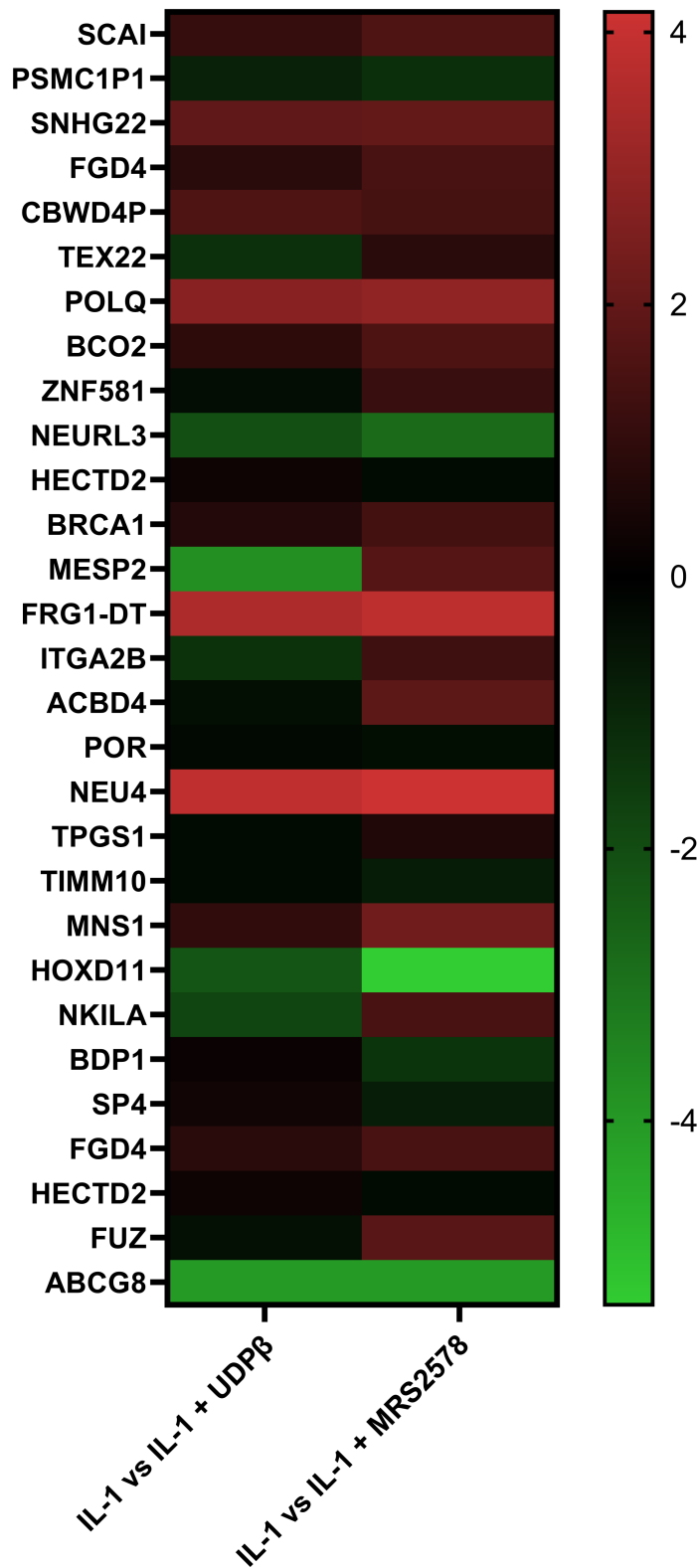


**Figure 5.22: IL-1 $\beta$  Stimulated Heatmap.** Genes that were reciprocally differentially expressed and significant by p value in the IL-1 $\beta$  stimulated UDP- $\beta$ S and MRS2578 groups were extracted and graphically presented in a heat map.

## 5.2.6 MRS2578 may inhibit the IL-1 induced expression of MMPs through likely more than one mechanism.

There were many more differentially expressed genes in the MRS2578 groups in both the IL-1 $\beta$  stimulated and unstimulated PHC (Fig. 5.1) than the UDP- $\beta$ S groups, showing it to be a highly potent molecule. The majority of these genes are significant by both p value and adjusted p value in both groups. The genes that are induced or repressed encode proteins that are from different families and have wide ranging cellular functions. This includes mitochondrially encoded metabolic genes and many heat shock genes in the unstimulated group. In the stimulated group, genes from many key pathways, such as MAPK, Wnt and JAK/STAT are differentially expressed. Enriched GO terms include interferon signalling, toll-like receptor signalling and deubiquitination. In the unstimulated group, the enriched GO terms include various aspects of ubiquitination, facets of cell-cell juxtacrine communication and protein/RNA catabolic processes (Fig. 5.24). KEGG pathway analysis revealed that the most enriched pathways from the IL-1 vs IL-1 + MRS2578 groups were the MAPK and JAK/STAT pathways. From the MAPK pathway, activators of the pathway such as growth factors and their tyrosine receptor kinases are downregulated, as well as NF $\kappa$ B and c-Jun. Heat shock proteins that inhibit JNK are upregulated (Fig. 5.25). JAK/STAT signalling factors are also downregulated, as are many of the genes whose expression is influenced by this pathway, such as *Bcl2* and *SOCS* (Fig. 5.26). The most enriched KEGG pathways from the VC vs MRS2578 groups are protein processing in the endoplasmic reticulum, phosphatidylinositol signaling system and the FoxO pathway (not shown).

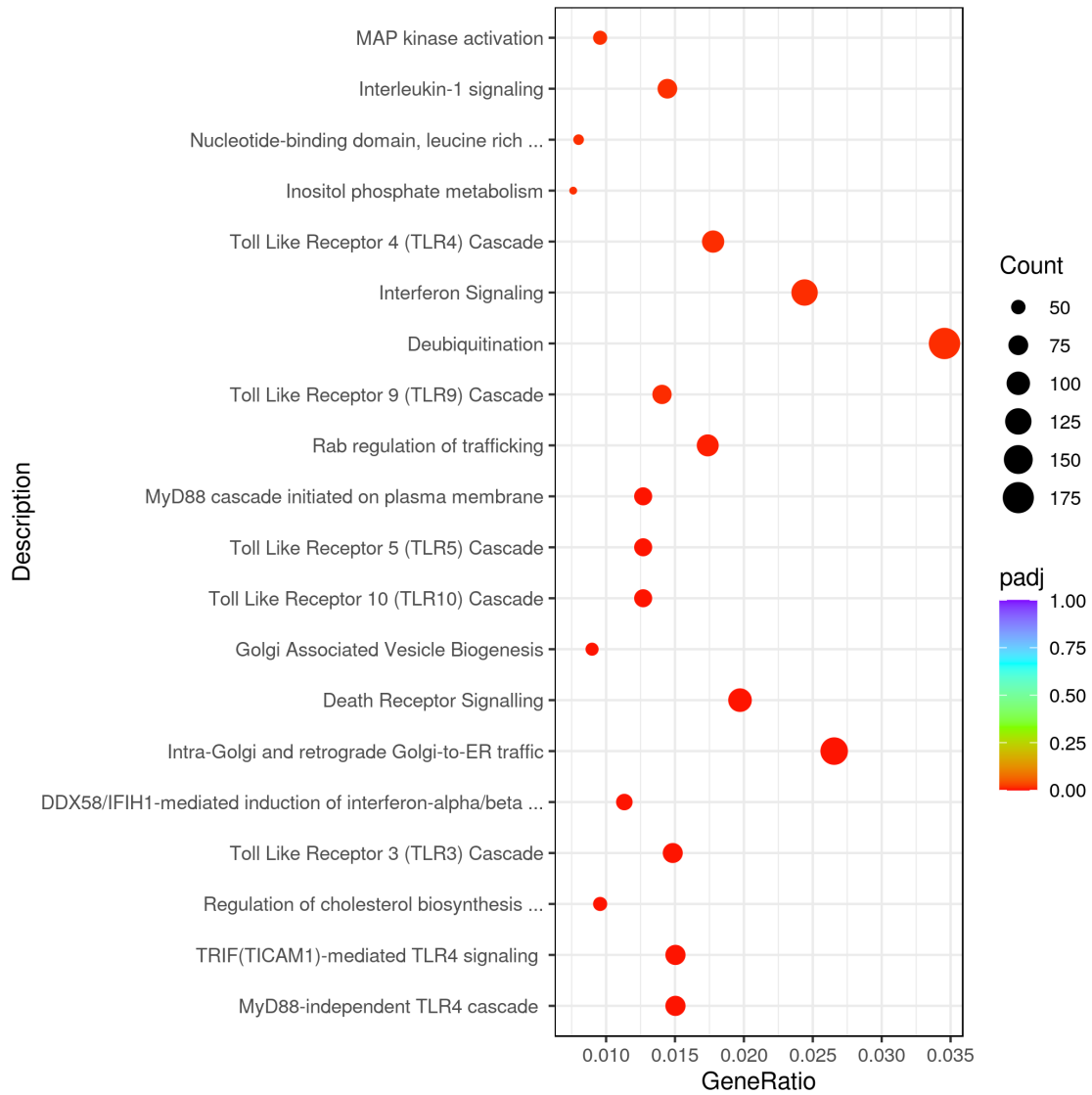


**Figure 5.23: Reactome Enrichment Analysis - IL-1 vs IL-1 + MRS2578.** Reactome[256] enrichment analysis was performed on the DEG list, whereby grouping of genes were analysed for significant enrichment.

**Table 5.3:** VC vs MRS2578 Top 50 DEG by p value

FC	p value	p adj	Gene	Description
6.73	5.02E-71	9.50E-67	<i>HSPA6</i>	heat shock protein family A (Hsp70) member 6
7.64	5.59E-53	5.28E-49	<i>HSPA7</i>	heat shock protein family A (Hsp70) member 7
2.95	6.22E-52	3.92E-48	<i>CIART</i>	circadian associated repressor of transcription
-2.14	2.35E-50	9.01E-47	<i>MT-ND5</i>	mitochondrially encoded NADH:ubiquinone oxidoreductase core subunit 5
-2.79	2.38E-50	9.01E-47	<i>MT-ND6</i>	mitochondrially encoded NADH:ubiquinone oxidoreductase core subunit 6
-3.51	2.17E-47	6.83E-44	<i>MT-TN</i>	mitochondrially encoded tRNA asparagine
-3.88	1.12E-45	3.03E-42	<i>MT-TC</i>	mitochondrially encoded tRNA cysteine
2.86	4.65E-38	1.10E-34	<i>HSPA1A</i>	heat shock protein family A (Hsp70) member 1A
1.09	5.21E-36	1.10E-32	<i>CLASRP</i>	CLK4 associating serine/arginine rich protein
-1.09	6.49E-36	1.23E-32	<i>IFNAR1</i>	interferon alpha and beta receptor subunit 1
-1.49	1.00E-35	1.73E-32	<i>ATXN1</i>	ataxin 1
2.80	3.09E-34	4.50E-31	<i>HSPA1B</i>	heat shock protein family A (Hsp70) member 1B
-3.89	6.62E-34	8.95E-31	<i>MT-TY</i>	mitochondrially encoded tRNA tyrosine
-1.63	4.53E-32	5.71E-29	<i>FAM217B</i>	family with sequence similarity 217 member B
-1.49	4.40E-30	5.21E-27	<i>ZBTB41</i>	zinc finger and BTB domain containing 41
1.25	3.20E-29	3.37E-26	<i>IER2</i>	immediate early response 2
2.43	3.20E-29	3.37E-26	<i>DNAJB1</i>	DnaJ heat shock protein family (Hsp40) member B1
-2.58	3.88E-28	3.87E-25	<i>LDLRAD4</i>	low density lipoprotein receptor class A domain containing 4
1.87	2.28E-27	2.15E-24	<i>PER1</i>	period circadian regulator 1
0.95	5.55E-26	5.00E-23	<i>DMTF1</i>	cyclin D binding myb like transcription factor 1
-1.09	6.39E-26	5.50E-23	<i>MIB1</i>	E3 ubiquitin protein ligase 1
1.30	2.28E-24	1.88E-21	<i>CCDC84</i>	coiled-coil domain containing 84
1.17	8.12E-24	6.40E-21	<i>KPTN</i>	kaptin, actin binding protein
1.97	9.77E-24	7.32E-21	<i>IER5</i>	immediate early response 5
3.47	1.01E-23	7.32E-21	<i>NR4A1</i>	nuclear receptor subfamily 4 group A member 1
-1.33	2.79E-23	1.96E-20	<i>ITGAV</i>	integrin subunit alpha V
0.78	7.56E-23	5.11E-20	<i>SELENOW</i>	selenoprotein W
3.26	2.32E-22	1.51E-19	<i>FOS</i>	Fos proto-oncogene, AP-1 transcription factor
-1.44	2.99E-22	1.88E-19	<i>LRRC58</i>	leucine rich repeat containing 58
1.15	4.35E-22	2.66E-19	<i>DDX39A</i>	DExD-box helicase 39A
-1.08	4.69E-22	2.77E-19	<i>CHM</i>	CHM, Rab escort protein 1
0.91	4.85E-22	2.78E-19	<i>BAX</i>	BCL2 associated X, apoptosis regulator
-1.21	6.11E-22	3.40E-19	<i>PTAR1</i>	protein prenyltransferase alpha subunit repeat containing 1
0.87	7.12E-22	3.85E-19	<i>RBM39</i>	RNA binding motif protein 39
1.25	9.58E-22	5.04E-19	<i>SRSF7</i>	serine and arginine rich splicing factor 7
0.86	1.03E-21	5.26E-19	<i>SLC12A4</i>	solute carrier family 12 member 4
-1.34	2.03E-21	1.01E-18	<i>NORAD</i>	non-coding RNA activated by DNA damage
-1.11	2.62E-21	1.27E-18	<i>GTF3C4</i>	general transcription factor IIIC subunit 4
1.34	2.83E-21	1.34E-18	<i>EGR1</i>	early growth response 1
0.99	4.23E-21	1.95E-18	<i>ULK3</i>	unc-51 like kinase 3
-0.81	6.62E-21	2.98E-18	<i>MTPN</i>	myotrophin
-1.12	8.66E-21	3.81E-18	<i>SEL1L</i>	SEL1L, ERAD E3 ligase adaptor subunit
-1.06	9.73E-21	4.18E-18	<i>PPARA</i>	peroxisome proliferator activated receptor alpha

**Table 5.4:** IL-1 vs IL-1 + MRS2578 Top 50 DEG by p value

FC	p value	p adj	Gene	Description
-3.34	3.60E-137	8.31E-133	<i>SMS</i>	spermine synthase
-3.13	5.92E-125	6.85E-121	<i>KPNA2</i>	karyopherin subunit alpha 2
-6.61	1.53E-122	1.18E-118	<i>CCL5</i>	C-C motif chemokine ligand 5
5.59	6.20E-121	3.58E-117	<i>ID3</i>	inhibitor of DNA binding 3, HLH protein
-9.65	1.22E-114	5.66E-111	<i>ESM1</i>	endothelial cell specific molecule 1
-4.50	8.71E-110	3.35E-106	<i>GPR68</i>	G protein-coupled receptor 68
-3.23	6.68E-106	2.21E-102	<i>TNIP1</i>	TNFAIP3 interacting protein 1
-5.33	1.42E-95	4.10E-92	<i>CSF1</i>	colony stimulating factor 1
-3.52	7.36E-91	1.89E-87	<i>NFκB2</i>	nuclear factor kappa B subunit 2
-3.66	1.03E-87	2.37E-84	<i>TLNRD1</i>	talin rod domain containing 1
-2.82	8.73E-81	1.83E-77	<i>EHD1</i>	EH domain containing 1
-3.38	7.16E-79	1.38E-75	<i>ISG20</i>	interferon stimulated exonuclease gene 20
-5.05	1.33E-78	2.37E-75	<i>BDKRB1</i>	bradykinin receptor B1
3.03	1.75E-75	2.69E-72	<i>PLEKHG2</i>	pleckstrin homology and RhoGEF domain containing G2
-4.20	1.12E-74	1.61E-71	<i>C1QTNF1</i>	C1q and TNF related 1
-2.92	2.07E-73	2.82E-70	<i>CACHD1</i>	cache domain containing 1
-2.44	4.07E-73	5.23E-70	<i>A4GALT</i>	alpha 1,4-galactosyltransferase (P blood group)
-2.89	1.05E-72	1.28E-69	<i>NMI</i>	N-myc and STAT interactor
-3.61	2.91E-72	3.37E-69	<i>MCC</i>	MCC, WNT signaling pathway regulator
-3.92	3.67E-71	3.86E-68	<i>MT-TC</i>	mitochondrially encoded tRNA cysteine
-3.12	1.08E-70	1.09E-67	<i>DENND5A</i>	DENN domain containing 5A
-3.89	1.32E-70	1.27E-67	<i>MAP3K8</i>	mitogen-activated protein kinase kinase kinase 8
3.09	1.42E-69	1.31E-66	<i>PIK3IP1</i>	phosphoinositide-3-kinase interacting protein 1
-8.13	7.10E-69	6.31E-66	<i>CXCL6</i>	C-X-C motif chemokine ligand 6
-6.22	1.90E-68	1.62E-65	<i>TSLP</i>	thymic stromal lymphopoietin
-3.23	7.03E-68	5.80E-65	<i>PDPN</i>	podoplanin
5.09	1.45E-65	1.15E-62	<i>DBP</i>	D-box binding PAR bZIP transcription factor
4.88	2.34E-65	1.80E-62	<i>DEPP1</i>	DEPP1, autophagy regulator
-2.91	4.24E-65	3.16E-62	<i>SERPINB8</i>	serpin family B member 8
-6.87	7.66E-65	5.54E-62	<i>GPR37L1</i>	G protein-coupled receptor 37 like 1
-3.94	2.06E-63	1.44E-60	<i>FGF2</i>	fibroblast growth factor 2
-6.86	8.11E-63	5.51E-60	<i>MIR3142HG</i>	MIR3142 host gene
-1.83	1.84E-62	1.22E-59	<i>TNKS1BP1</i>	tankyrase 1 binding protein 1
-3.36	5.66E-62	3.63E-59	<i>PLPP3</i>	phospholipid phosphatase 3
-4.49	1.79E-61	1.12E-58	<i>NFκB1</i>	nuclear factor kappa B subunit 1
-4.49	2.35E-61	1.43E-58	<i>VCAM1</i>	vascular cell adhesion molecule 1
-2.71	2.87E-61	1.70E-58	<i>SLC7A1</i>	solute carrier family 7 member 1
-3.49	2.95E-61	1.71E-58	<i>RNF144B</i>	ring finger protein 144B
-3.82	4.55E-61	2.56E-58	<i>GFPT2</i>	glutamine-fructose-6-phosphate transaminase 2
-3.25	8.84E-61	4.87E-58	<i>ABHD17C</i>	abhydrolase domain containing 17C
-3.78	3.36E-60	1.81E-57	<i>STAT5A</i>	signal transducer and activator of transcription 5A
-2.76	5.09E-60	2.67E-57	<i>MT-ND6</i>	mitochondrially encoded NADH:ubiquinone oxidoreductase core subunit 6
-8.64	9.19E-60	4.72E-57	<i>CXCL5</i>	C-X-C motif chemokine ligand 5
-9.99	2.76E-59	1.39E-56	<i>IL36G</i>	interleukin 36 gamma
-3.64	3.16E-59	1.55E-56	<i>ID2</i>	inhibitor of DNA binding 2

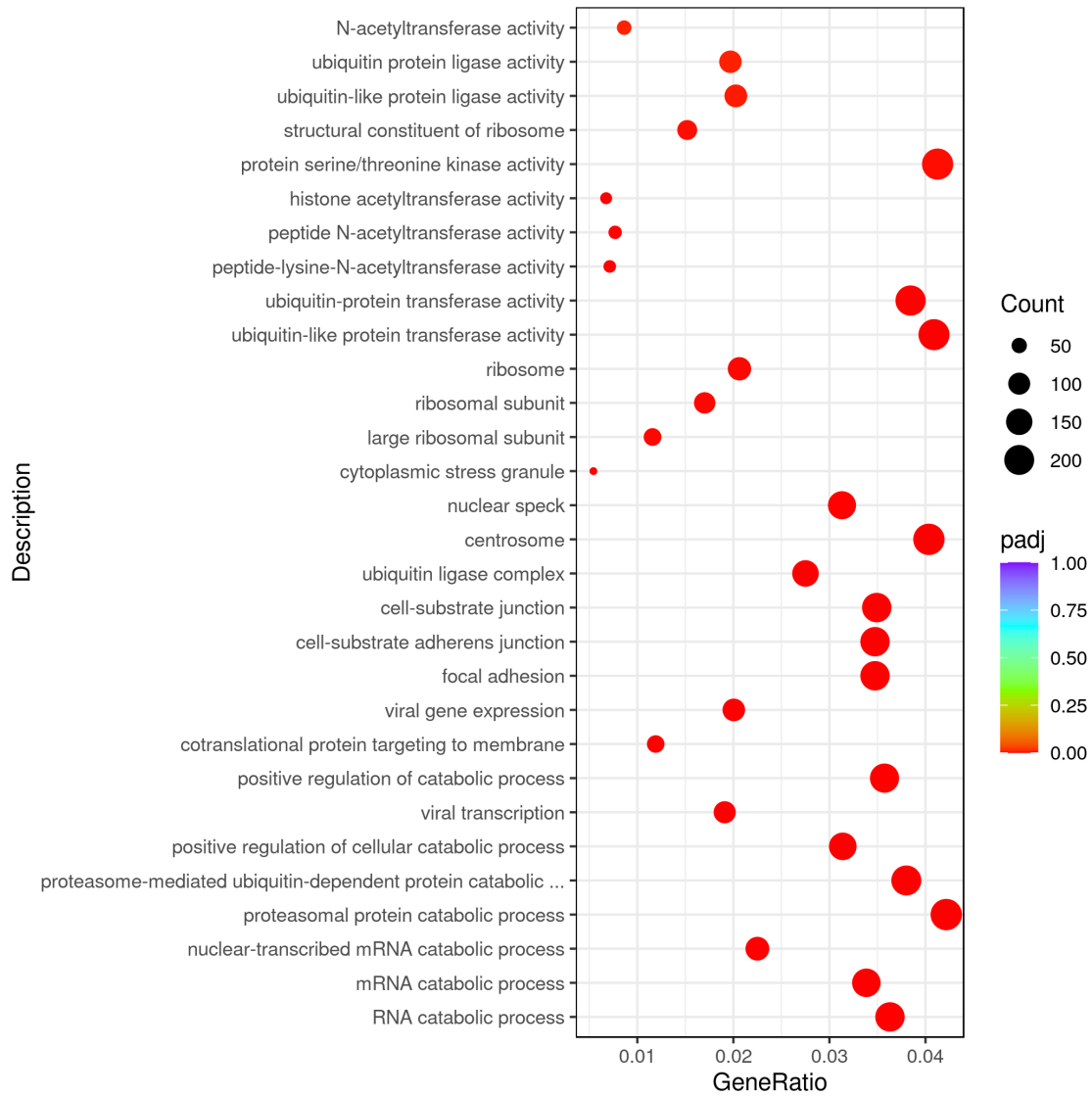


**Figure 5.24: Gene Ontology Enrichment Analysis - VC vs MRS2578.** Gene Ontology [255] term enrichment analysis was performed on the DEG list, whereby grouping of genes were analysed for significant enrichment.

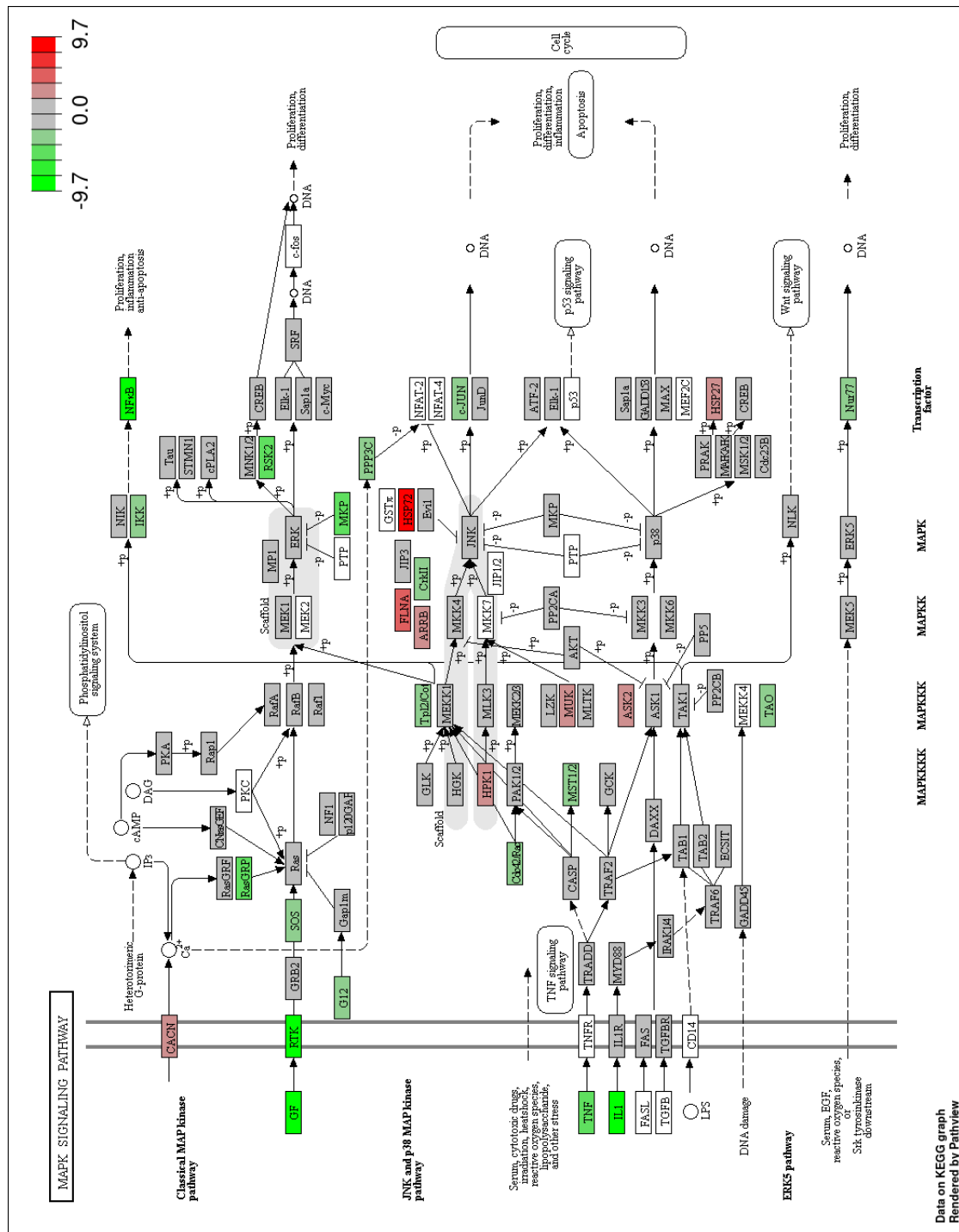


Figure 5.25: KEGG Pathway Analysis for IL-1 vs IL-1 + MRS2578 - MAPK. Kyoto encyclopedia of genes and genomes [257] enrichment pathway analysis was performed on the DEG list, whereby grouping of genes were analysed for significant enrichment and how they fit into their respective pathways.

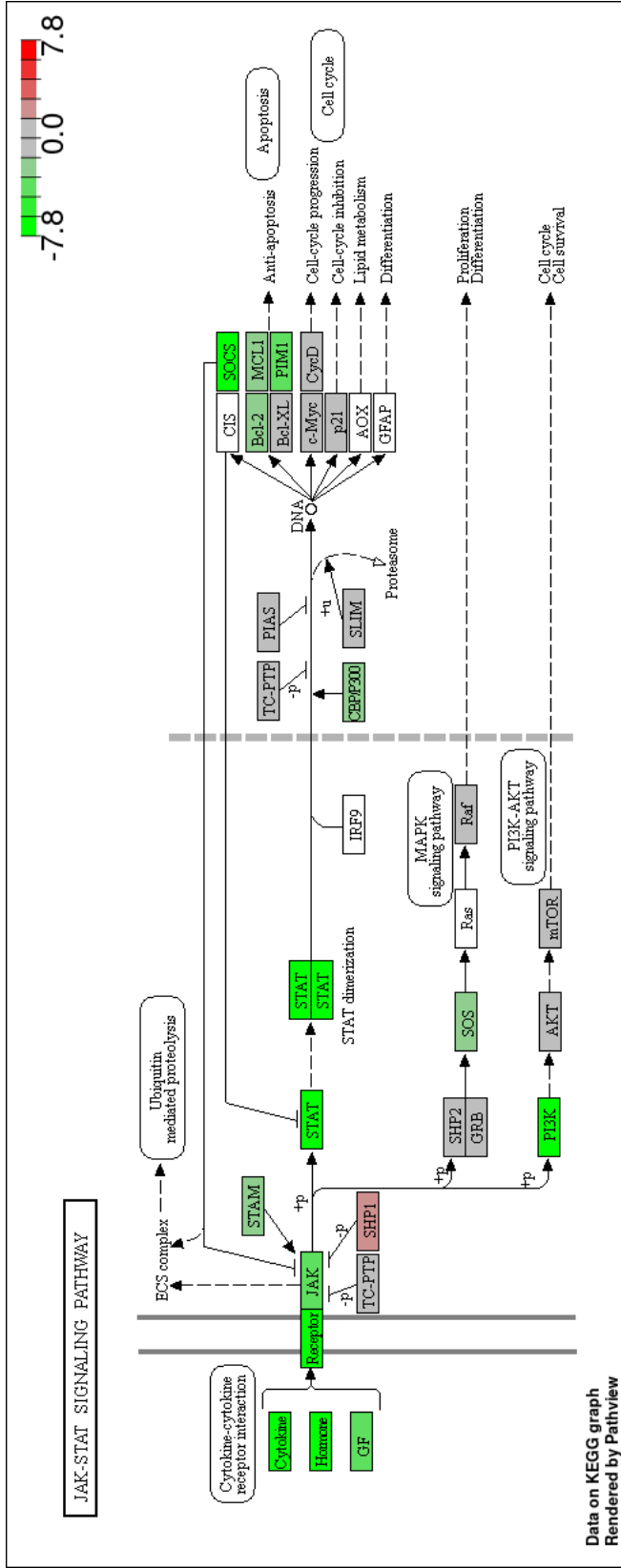


Figure 5.26: KEGG Pathway Analysis for IL-1 vs MRS2578 - JAK/STAT. Kyoto encyclopedia of genes and genomes [257] enrichment pathway analysis was performed on the DEG list, whereby grouping of genes were analysed for significant enrichment and how they fit into their respective pathways.

## 5.3 Discussion

### 5.3.1 Analysis Methods for RNAseq Data.

DESeq2 [213] was used to analyse the raw data from the Illumina sequencing by synthesis (SBS). There are a number of quality control measures that are taken to ensure the data is robust. Initially, variation within groups is examined using principal component plot analysis, and outliers are removed. Moreover, the raw reads are normalised based on gene length and total number of mapped reads, producing an FPKM (fragments per kilobase of transcript per million mapped reads). This FPKM is then used to calculate fold change between control and treated groups. DESeq2 normalises data across samples to account for varying sequencing depth and is a robust and accurate method for reducing bias. From this analysis, a Wald test is used to test for significance of a logarithmic fold change from 0, producing a p value. An adjusted p value is then produced to account for the issue of multiple testing using the Benjamini-Hochberg method. The adjusted p value takes into consideration the large number of genes that are being tested in an NGS experiment and tests the hypothesis that the significant genes are false positives. None of the DEG in the UDP- $\beta$ S groups are significant by the adjusted p value and so false positives cannot be excluded from these gene lists. However, excluding all of the values would also exclude true positives and so it becomes harder to distinguish between true and false positives.

Some of the genes that were significant by p value were measured by qRT-PCR to try and validate whether they are true findings or by chance. Some genes, namely CX3CL1 and IRAK2 showed a trend of expression that is similar to the that found by NGS, but not significantly by t test at the 0.05 level. There are a number of reasons why this might be the case. Firstly, PCR uses primers that only amplify a small section of the gene (~100 base pairs) and therefore might not be capturing the full expression due to sequence variations like splice variants. There may also be an element of reverse transcription bias, although this step is also part of the NGS workflow, albeit with different enzymes used. Moreover, more technical replicates would give higher accuracy and more statistical power, likely resulting

in significance by qPCR. The precision and sensitivity of NGS is also higher than qPCR because of the depth of sequencing [260], meaning qPCR might not be able to detect smaller differences with the same accuracy. That said, it might also be because the difference is not a true finding and that the q value estimation of false positives is accurate.

There is also some confidence that the NGS findings are not all false positives provided in the types of genes that are differentially expressed. For example, in the VC vs UDP- $\beta$ S group, a lot of the genes that are in the DEG list and are significant by p value are from a similar gene grouping, eg cytokines and mediators of inflammation. This is reflected in the significantly enriched (by adjusted p value) GO terms and KEGG pathway analyses. On the other hand, the genes in the IL-1 vs IL-1 + UDP comparison, there are no significantly enriched GO terms and no clear grouping of the genes. This does not mean that they are any more likely to be false positives, but it could be argued that one way of differentiating between false and true positives in the lack of quantitative data is looking at the relationship of the genes to each other i.e it is likely that more than one gene in a group of genes would be differentially expressed if their regulation was altered. For example, there are many genes under transcriptional control of NF $\kappa$ B, and so alterations in NF $\kappa$ B activity would likely lead to differential expression of more than one target of it.

Another potential reason for the lack of statistical power, and therefore significance by p adjusted value, might be the high variability between donor groups. PHC from OA patients are always heterogeneous between donors because of the stage of disease often being different. This is due to the critical factor for joint replacement being pain, not histological or other more quantitative methods of disease scoring. Since pain is not a good measure of disease severity as it is very dependent on the individual, disease progression will be different and this would have implications on the isolated chondrocytes' phenotype. It may have been pertinent to conduct a power calculation to alleviate the question of whether sample size is a factor in the lack of significance.

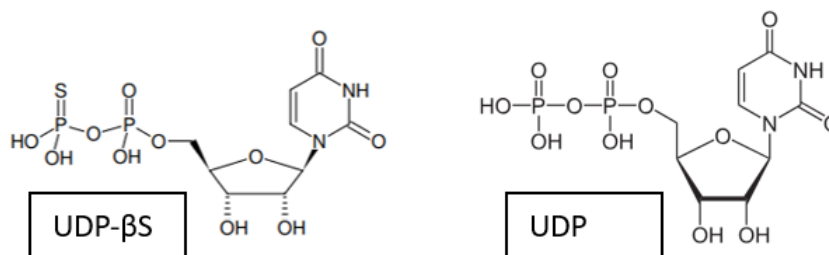


**Figure 5.27:** Structure of UDP and UDP- $\beta$ S.

### 5.3.2 UDP- $\beta$ S vs UDP and receptor desensitisation

Uridine-5'-O-2'-thiodiphosphate (UDP- $\beta$ S) is a non-hydrolysable analogue of UDP that is a potent agonist of P2Y<sub>6</sub> and has a lower EC<sub>50</sub> than UDP when measuring contractility in the rat basilar artery [253]. The modification of the phosphate to a thiophosphate group prevents ectonucleotidases from degrading the nucleotide but allows it to retain its activity at P2Y<sub>6</sub>. In 1321N1 astrocytoma cell culture, UDP was completely degraded after 2 hours, whereas UDP- $\beta$ S remained stable [225]. As such, UDP- $\beta$ S was used to create sustained activation of P2Y<sub>6</sub> in PHC, and prevent degradation into other agonists of purinergic receptors. The pitfall with this approach is that the receptor may become desensitised and in extremes, the agonist may start to have an antagonistic effect. It could also be argued that the chronic exposure to agonist is not what happens physiologically, as there would be more transient signalling. However, even exaggerated effects would be useful to understand how P2Y<sub>6</sub> signals in this system. Moreover, P2Y<sub>6</sub> has been shown to be slow to desensitise, with a peak response maintained for at least 3 hours as measured by IP<sub>3</sub> accumulation in 1321N1 cells [261]. As such, it is unlikely that any response seen is due to receptor desensitisation in the six hour time period. It would also take time for any downstream signalling to occur after that three hour period, so a six hour period is appropriate to see downstream effects. There is also no evidence to suggest that the modification of the phosphate group confers any off-target activity.

### 5.3.3 Action of UDP- $\beta$ S

In the cells treated with UDP- $\beta$ S, there were no significant differentially expressed genes when p values were adjusted using the Benjamini-Hochberg method. As such, any discussion of the differentially expressed genes needs to be in the context of this lack of significance and resulting inability to prove or disprove a hypothesis. With that said, the following discussion details the differentially expressed genes that were significant by unadjusted p value, and would require further validation to be able to draw any conclusions from. UDP- $\beta$ S may alter the expression of a number of genes that are disease relevant and important to inflammatory processes in non-IL-1 $\beta$ -stimulated PHC that are from OA patients. In the IL-1 vs Il-1 + UDP- $\beta$ S group, there was not a clear effect of the stable P2Y6 agonist, with no significantly enriched GO terms. It is also important to note that the PHC cells were from osteoarthritic tissues and so would have a level of these inflammatory pathways already activated.

Of the differentially expressed genes in the VC vs UDP- $\beta$ S group, there are many cytokines of the CX and CC families that were reduced in expression. These include *CCL8*, *CX3CL1*, *IL6*, *CCL8*, *CXCL5*, *CXCL6*, *CCL13*, *CXCL3*, *IL34*, *CXCL2* and *CCL2*. These cytokines have the action of recruiting immune cells, for example *CX3CL1* is a membrane-bound chemokine that when bound to its receptor, *CX3CL1R* found on effector T cells and macrophages, initiates inflammatory cascades. It also has a soluble domain which causes the chemotaxis of leukocytes [262]. Many of the proteins that these genes encode were found less abundantly in the cell culture supernatant of PHC incubated with UDP- $\beta$ S compared to control, albeit at N=1. These include *CX3CL1*, *CXCL7*, *CCL22* and *CXCL6*. Interestingly, the proteomic array showed UDP- $\beta$ S to increase *CCL2* release compared to control at 24 and 48 hours. However, whilst this data contains the variation of three PHC isolates, they are only at N=1 and were used to validate the findings at the mRNA level.

*CX3CL1* concentrations have been shown to be elevated in both serum and synovial fluid from OA patients [263] and it is transcriptionally regulated by IL-1 $\beta$  [264]. The expression of many other chemokines by chondrocytes is also upregulated in OA [265] and can act in an autocrine way to induce expression of MMPs

[90]. It has been shown that many chemokines are under transcriptional control of  $\text{NF}\kappa\text{B}$  and as well as upregulating MMPs, can cause chondrocyte apoptosis [266]. The action of CCL2 at CCR2 on chondrocytes activates p38 MAPK and ERK signalling to induce expression of *MMP1*, *MMP3*, *MMP13* and *TIMP1* in healthy chondrocytes and in OA chondrocytes, only *MMP1* and *MMP3* with longer exposure times [107]. CCL2 has also been found to mediate OA-related pain *in vivo* [105]. IL-6 is also highly disease relevant, as it causes inflammatory pain and cartilage degeneration [267]. As such, it is clear that these molecules are very relevant to the pathophysiology of OA, but exactly how P2Y6 signalling may modulate their expression is yet to be understood. Transcription factor analysis estimated that from the list of differentially expressed genes caused by UDP- $\beta\text{S}$ , many of the genes are regulated transcriptionally by  $\text{NF}\kappa\text{B}$ . It is possible that P2Y6 inhibits  $\text{NF}\kappa\text{B}$  activity to reduce transcription of inflammatory mediators, such as cytokines. Whilst this was not the case in the ATDC5 cell line as tested with a luciferase construct, it might be the case in the primary PHC. Downstream from P2Y6 signalling is calcium release, and there is literature surrounding the role of calcium signals in the canonical  $\text{NF}\kappa\text{B}$  pathway, with complex interplay between PKC, PI3K and calmodulin [268]. Whilst NFAT is more commonly thought of as the calcium-dependent transcription factor, in T-cells with defective calcium entry, constitutive calcineurin activity reverses the inhibition of  $\text{NF}\kappa\text{B}$  activity caused by dysregulated calcium signalling. Moreover, constitutive calmodulin kinase II activity rescues I $\kappa$ B $\alpha$  degradation [269].

There is a small amount of evidence linking P2Y6 to  $\text{NF}\kappa\text{B}$ . In rabbit osteoclasts, UDP and a stable analogue (INS48823) induced  $\text{NF}\kappa\text{B}$  activation and increased survival, an effect that was sensitive to lactacystin (a proteasome inhibitor) [151]. Moreover, in a macrophage cell line, UTP induced the LPS-induced  $\text{NF}\kappa\text{B}$  response, although the receptor was not identified [270]. In mouse intestinal epithelial cells, UDP induced *CXCL10* expression [271] as well as *CXCL8* [272]. Conversely, in skeletal muscle cells, UDP and MRS2693 (an agonist of P2Y6) protected against  $\text{TNF-}\alpha$  induced apoptosis through attenuation of  $\text{NF}\kappa\text{B}$  activation and ERK1/2 phosphorylation [273]. As such, the literature has conflicting evidence but these data support the idea that there is cross-talk between signalling in some

way.

As well as many of the genes that are differentially expressed being targets of  $\text{NF}\kappa\text{B}$ , there are also facets of the canonical  $\text{NF}\kappa\text{B}$  pathway itself that have altered expression with UDP- $\beta\text{S}$  stimulation, namely *IRAK2* (interleukin-1 receptor associated kinase 2), *NF $\kappa$ BIZ/A* ( $\text{NF}\kappa\text{B}$  inhibitor zeta/alpha), *RELB* (p100/52) and *NF $\kappa$ B2* (subunit p100/p52 precursor). *IRAK2* is a kinase involved in the transduction of TLR and IL-1R signalling in association with MyD88, and can phosphorylate TRAF6 to affect the ubiquitination and degradation of I $\kappa$ B $\alpha$ . Downregulation of *IRAK2* along with direct  $\text{NF}\kappa\text{B}$  subunits *RELB* and *p100* (p52 precursor) would reduce transcription of target genes. Somewhat inconsistently, inhibitors of  $\text{NF}\kappa\text{B}$  signalling are also downregulated. *NF $\kappa$ BIA* encodes the I $\kappa$ B $\alpha$  protein which sequesters  $\text{NF}\kappa\text{B}$  subunits in the cytoplasm and prevents them from entering the nucleus. *NF $\kappa$ BIZ* is slightly different in that it is an atypical inhibitor; it resides in the nucleus and has an ankyrin-repeat domain on the C-terminus [274]. In the nucleus, it binds  $\text{NF}\kappa\text{B}$  dimers and prevents them from binding to promoter regions. The reduced transcription of the inhibitors may be as a direct consequence of reduced transcription of cytokines and other molecules that can activate the  $\text{NF}\kappa\text{B}$  pathway, as the *NF $\kappa$ BIZ/A* genes are transcriptionally regulated by  $\text{NF}\kappa\text{B}$  themselves [275], rather than as a consequence of P2Y6 signalling. Moreover, regulation at the phosphorylation or cellular localisation level, rather than mRNA, will also play a factor and is not captured in this data.

A proteomic array was also used to understand what signalling factors may be involved in the functional effects of P2Y6 activation by looking at changes to phosphorylation of key mediators. Interestingly, this revealed that the phosphorylation of many  $\text{NF}\kappa\text{B}$  proteins do not change with UDP- $\beta\text{S}$  stimulation. 15 minutes post addition, detection of phosphorylated TAK1 and TBK1 were slightly higher. These are proteins involved in the cascade of activating the canonical  $\text{NF}\kappa\text{B}$  pathway, but can also interact with other signalling pathways, such as the TGF- $\beta$  pathway [276]. Another transcription factor that was highlighted to potentially regulate the genes in the differentially expressed gene list was interferon regulatory factor 8 (IRF8). IRF8 is a transcription factor that binds the IFN-stimulated response element (ISRE) in gene promoters to initiate transcription, of which is

found in the promoters of many cytokines [277]. In chondrocytes, IRF8 is upregulated in OA chondrocytes, and is involved in the IL-1 stimulation of MMP-13 via janus kinase 2 (JAK2) [278], and in other cell types, has been shown to crosstalk with NF $\kappa$ B signals [279].

UDP- $\beta$ S also caused reduced transcription of nucleotide-oligomerisation domain 2 (NOD2), which is an intracellular pattern recognition receptor (PRR) that recognises PAMPs and DAMPs (pathogen/damage associated molecular patterns). NOD2 and other PRRs have been implicated in OA pathophysiology as release of DAMPs from breakdown of the ECM can initiate inflammatory cascades through these receptors [280]. In chondrocytes, fibronectin fragments have been shown to activate NOD2 and stimulate MMP and IL-6 expression via MAPK and NF $\kappa$ B activation, in synergism with TLR2 [281]. Also downregulated by UDP- $\beta$ S are the bradykinin receptors 1 and 2 (*BDKRB1/2*), of which their agonist, bradykinin, has long long been associated with pain in OA [282]. In human chondrocytes, bradykinin stimulates IL-6 and IL-8 release via p38 MAPK and NF $\kappa$ B activation [283], and SNPs in the *BDKRB2* gene correlate with OA severity [284]. It is clear that UDP- $\beta$ S has effects on many disease relevant genes and signalling processes. The proteomic arrays also assayed the phosphorylation status of proteins from many other signalling families. The most prominent change was of STAT6, which may be how UDP- $\beta$ S signals to reduce cytokine expression. At 60 minutes post stimulation, the detection of phosphorylated STAT6 was 1.6X lower than the basal control, whereas the control group was 1.9X higher than the basal control. STAT6 is part of the JAK/STAT family, which are mediators of inflammatory responses, commonly being activated by cytokine and interleukin receptors, and contain a classical SH2 domain. Upon phosphorylation, STAT proteins form homodimers and initiate transcription of target genes. There is very little described about any functional effect of STAT6 in chondrocytes. It is most commonly activated by IL-4 [285], which binds to the IL-4R, a tyrosine kinase, and phosphorylates STAT6 in human chondrocytes [286]. More generally, JAK/STAT signalling has been implicated in OA as the cytokines that are found more abundantly in OA joints, such as IL-6, can activate JAK/STAT signalling and propagate inflammation [287]. In canine chondrocytes, IL-4 is anti-inflammatory, reducing the effects of IL-1- $\beta$  and

TNF- $\alpha$  [288] and in a rat model, IL-4 over-expression mediated by an adenovirus reduced inflammation and cytokine production in an arthritis model [289]. The anti-inflammatory effect of IL-4 was also shown in human chondrocytes, by inhibiting the IL1- $\beta$  induced expression of MMP-13 and CCL5. IL-4 was also shown to be less abundant in OA joints [290] and protect against blood-induced damage in human cartilage explants, reducing IL-1 $\beta$  and TNF $\alpha$  production [291]. Interestingly, STAT6 does not change in expression between OA and normal chondrocytes and a STAT6-independent IL-4 signalling pathway has been established [286]. There is also an association between IL-4 SNPs and susceptibility to OA [292]. There is a disconnect between the anti-inflammatory effect of IL-4, which serves to increase phosphorylation of STAT6, and the anti-inflammatory effect of reduced phosphorylation of STAT6 that is seen in this data. It is possible that IL-4 is mediating its effects through another pathway or that IL-4 actually serves to reduce phosphorylation of STAT6. It may also be the case that STAT6 has a dual role that when phosphorylated, serves to reduce MMP expression, but also can reduce cytokine expression. However, the exact signalling is still unclear.

There was also detection of more phosphorylated TGF- $\beta$  family protein members at the 15 minute time point that only occurs transiently. These include SMAD2, ATF2, c-Fos and c-Jun. TGF- $\beta$  is often discussed in the context of development, as it is crucial for chondrogenesis and growth plate proliferation. These proteins all facilitate TGF- $\beta$  signalling, which in development, regulates proliferation, condensation and differentiation of chondrocytes [251]. In an OA context, TGF- $\beta$  signalling can prevent chondrocyte hypertrophy [293] and in experimental OA models, inhibition of TGF- $\beta$  signalling reduced OA severity, indicating that its effects are deleterious [294].

#### **5.3.4 Action of MRS2578**

MRS2578 was first described by Mamedova et al. in 2004 [235] as a diisothiocyanate derivative that had potent action at human P2Y6 with an IC<sub>50</sub> of 37nM as measured by inositol phosphate accumulation. MRS2578 was found to have no activity at P2Y2, P2Y4 or P2Y11 with around 20% inhibition of the maximal response at P2Y1. It also reversed the effects of UDP on TNF $\alpha$ -induced cell death

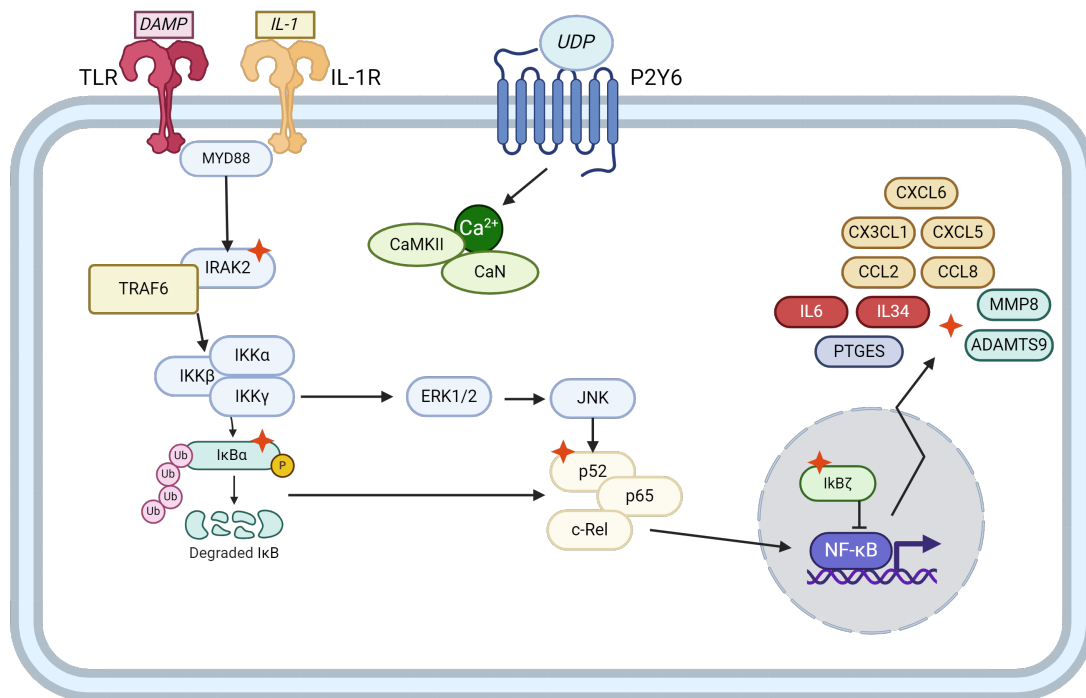


**Figure 5.28: NF $\kappa$ B signalling genes that may be regulated by P2Y6.** Red stars indicate where RNAseq data showed that activation of P2Y6 with UDP- $\beta$ S induced downregulation of the associated gene by p value only. At the mRNA level, when chondrocytes are stimulated with UDP- $\beta$ S, there is reduced expression at the mRNA level of many targets of NF $\kappa$ B signalling, as well as signal mediators of inflammation, such as P52, IRAK2 and I $\kappa$ B $\alpha$ . Many of the genes that are transcriptionally regulated by NF $\kappa$ B signalling, such as IL-6, CCL2 and ADAMTS9, are also downregulated. Created with biorender.com

[235]. Since then, there have been 92 publications mentioning its use (Pubmed) and has been used extensively to study the effects of P2Y6 both *in vivo* and *in vitro*. It is also the only commercial selective P2Y6 antagonist available in the UK. Initially, our aim was to understand how MRS2578 inhibits the IL-1 $\beta$  response in PHC, but secondarily, to attempt to infer its specificity from these data.

In unstimulated cells (i.e without IL-1 $\beta$ ), GO enrichment analysis revealed that it has effects on some of the most basic cellular functions, including serine/threonine kinase activity, ubiquitination, (m)RNA catabolism and focal adhesion. The genes with the highest fold change of approximately 7 were heat shock protein family A 6/7 (*HSPA6/7*). Many mitochondrially encoded metabolic genes were also very significantly differentially expressed, such as NADH:ubiquinone oxidoreductase (*MT-ND5*). In stimulated cells, the activity was related more to inflammatory

processes, such as TLR cascades, interferon signalling and MAP kinase activation, according to GO enrichment analysis.

In answering the question of how does MRS2578 inhibit the action of IL-1 $\beta$ , it is clear that it is likely through a number of mechanisms. As highlighted by KEGG pathway enrichment analysis, many of the components of the MAPK signalling pathway are downregulated, including NF $\kappa$ B components, c-Jun, IL-1 and TNF. As well as this, transcription of members of the STAT and JAK family of genes are downregulated, which may explain how MRS2578 can inhibit the response to IL-1 as this pathway is a key regulator. It is also likely that the alteration of some of the most basic functions, like ubiquitination, can interfere with activation of inflammatory cascades. For example, inhibiting the ubiquitination of I $\kappa$ B can prevent NF $\kappa$ B from becoming able to translocate to the nucleus. It is also evident that MRS2578 has a large impact on phenotype, based on the sheer number of genes that are differentially regulated and the extent to which they change.

There are a number of instances in the literature documenting a similar effect of MRS2578. Genetos et al. showed in osteoblasts that MRS2578 (10 $\mu$ M) increased I $\kappa$ B levels, serving to inhibit NF $\kappa$ B activity, an effect that was not reversed by UDP [295]. Additionally, MRS2578 reduced both UDP and toxin-induced NF $\kappa$ B dependent IL-8 release in an epithelial cell line [296]. Morioka et al. attribute UTP-induced NF $\kappa$ B dependent CCL2 release in microglia to P2Y6 because it was inhibited by MRS2578 (5  $\mu$ M) [297], and Riegel et al. also found MRS2578 to inhibit both basal and TNF- $\alpha$  induced NF $\kappa$ B activity in endothelial HMEC cells [239]. Similarly, MRS2578 inhibits the poly(I:C) (TLR agonist) induced CXCL10 expression in mouse intestinal epithelial cells (IEC). MRS2578 was not able to have this effect in P2Y6 KO IEC, showing that in this instance, this is dependent on P2Y6 expression [271].

In the PHC system, MRS2578 induced the differential expression of many thousands of genes, and often in the same direction as UDP- $\beta$ S where genes are reciprocally differentially expressed. This does not fit with the classical model of agonist/antagonist behaviour, and draws into question the specificity of MRS2578. Both UDP- $\beta$ S and MRS2578 reduce inflammatory mediators and cytokines, in opposition to the effect of IL-1 $\beta$  and as such, the role of P2Y6 is not entirely clear.

As discussed above, it is unlikely that there is receptor desensitisation from the six hour chronic exposure. The fact that MRS2578 had an effect alone would also suggest that there is constitutive activity that can be inhibited at basal levels, although the lack of change in initial FURA-2 fluorescence with incubation with MRS2578, prior to UDP stimulation, does not support this (Fig. 3.11D). It is clear that MRS2578 does block the UDP-elicited calcium response, and there are likely to be functional effects of this. It also seems likely that MRS2578 has P2Y6-independent effects and it therefore becomes difficult to distinguish between these without a knockout model. There are, however, some genes that are reciprocally differentially expressed in opposing directions by UDP- $\beta$ S and MRS2578 which may indicate that the effect is P2Y6-dependent. One example is *HES7* in non-IL-1 $\beta$  stimulated cells, which is upregulated with MRS2578 and downregulated with UDP- $\beta$ S. *HES7* is a bHLH (basic helix loop helix) transcription factor that is itself regulated by the Notch pathway. It negatively regulates transcription of target genes and may be involved in hypertrophy and chondrogenesis [298]. In IL-1 stimulated cells, *MESP2* is differentially regulated, going down with UDP and up with MRS2578, which is the same direction as *HES7*. *MESP2* is a direct target of *HES7*, and produces oscillations in expression during somite development [299]. *MESP2* is another bHLH transcription factor that is required for normal somite formation in the developing embryo [300]. The involvement of these genes in development may also be relevant to OA, as notch signalling has been shown to regulate a number of key genes like *MMP13* [301]. Also reciprocally regulated in stimulated cells is *NKILA*, which encodes an NF $\kappa$ B long non-coding RNA. It has been shown to interact with and suppress the translocation of NF $\kappa$ B dimers to the nucleus [302]. Its transcription goes up with UDP and down with MRS2578, which contradicts initial findings that MRS2578 inhibits NF $\kappa$ B activation, as reduced *NKILA* expression would reduce its inhibition. However, *NKILA* is only one facet of NF $\kappa$ B regulation and may not have that large of an effect on overall activation. *ITGA2B* is also reciprocally regulated in stimulated cells, which codes for integrin  $\alpha$ 2 $\beta$ 1. Integrins are important receptors for chondrocytes to interact with the ECM, and integrin  $\alpha$ 2 $\beta$ 1 has been shown to influence how a chondrocyte can respond to mechanical stress, MMP

expression and proliferation [303].

### 5.3.5 Next Steps

There are a number of experiments that would be able to provide further evidence as to how P2Y6 affects chondrocyte phenotype. Initially, this would be to increase n numbers to provide more statistical power to allow for accurate detection of false positives by the Benjamini-Hochberg method. It would also be useful to repeat this experiment in undiseased chondrocytes and/or better stratified OA chondrocytes that were grouped according to histological or other quantitative measures of disease. It may also be useful to align each donor group with the expression of P2Y6 to understand to what extent P2Y6 is overexpressed and how that affects the phenotypic outcome. As well as this, refinement of the time period and concentration of MRS2578 and UDP could also be useful. This would involve doing a time course experiment, ideally every hour up to the six hour mark and possibly up to 24 hours. Testing a concentration above and below those tested here would also help to establish whether these effects had dose dependency. On the goal of trying to infer the specificity of MRS2578, the use of a P2Y6 knockout cell line or primary cell would illuminate which of these effects are P2Y6 dependent and which are not. Without this, there cannot be a conclusive answer, only inferences and assumptions.

# Chapter 6

## Discussion

### 6.1 Methods Development

Immortalised cell lines are so often used in *in vitro* research because of their unlimited proliferative potential, relatively stable phenotype and accessibility. Three were used here - SW1353, C28/I2 and ATDC5. ATDC5 are more commonly used to model the pre-differentiated chondrocyte phenotype, whilst SW1353 and C28/I2 are used to model the differentiated, but non-hypertrophic chondrocyte. SW1353 originate from a chondrosarcoma, so are neoplastic in type, whereas C28/I2 are non-neoplastic costal chondrocytes that have been immortalised with an SV40 large T antigen expression construct. There are numerous examples in the literature of where they have been used to model primary chondrocytes, detailing how they are similar and distinct, often pertaining to their response to IL-1 $\beta$ .

Initially, the expression of purinergic receptors by primary chondrocytes and two cell lines was investigated and found to be relatively similar with the exception of a few receptors. This indicated that the cell lines were a good model in this respect for primary chondrocytes. However, progress was halted when it was discovered that neither SW1353 nor C28/I2 mounted a UDP nor ATP elicited calcium response despite mRNA expression of many purinergic receptors. Steps were taken to eliminate the chance that it was a technical fault with the assay. This included plating the cells at different densities, using probenecid to reduce efflux of the dye from cells, using multiple batches of nucleotides, asking a col-

league to complete the assay and in C28/I2, trying to re-differentiate the phenotype using agarose culture to no avail. An ATP elicited calcium response is robust across many cell types and is often used as a positive control for calcium signalling, even where purinergic signalling isn't the focus. Efforts were made to try and understand why SW1353 lacked this response to any nucleotide. It was concluded that they contain the cellular machinery to mount a calcium response, namely by having intracellular calcium stores. It is possible that it is as a result of a lack of sufficient expression and/or the receptor does not get trafficked to the cell surface, but no definite explanation was discovered. It is also puzzling that neither cell line, SW1353 nor C28/I2, which are very different in origin, have a nucleotide elicited calcium response, especially when primary chondrocytes do. This is an important finding for the both the purinergic research field, but also the chondrocyte research field, as any processes relating to calcium signalling will not be modelled very well in these cell lines.

Another area where there was substantial method development was in the CRISPR-Cas9 knockout of P2Y6 in the ATDC5 cell line. The main outcome from this development is the understanding that ATDC5, in this instance, were very resistant to transfection of large cargo, both plasmid and protein. Others have used large plasmids and other cargo in ATDC5 with success, including the exact plasmid that was used here [304], so there is no clear explanation as to why it did not work. A more robust method of delivering Cas9 stably into the genome using a lentivirus did produce a Cas9-expressing cell line. Deconvolution algorithms also suggested that transient transfection of synthetic guide RNAs did produce indels successfully, despite the lack of isolation of a true knockout. Unfortunately, this method was not able to be developed any further but use of other strategies to deliver the guide RNAs (such as small plasmids) and other clonal isolation strategies (e.g. FACS) may have led to successful isolation of a knockout clone.

## 6.2 What functional effect does P2Y6 have on chondrocyte phenotype?

OA is a highly debilitating disease with poor treatment options, despite its high prevalence. It is characterised by joint pain, reduced mobility, thinned cartilage and underlying bone changes. It often results in surgical replacement of the joint, which is costly and results in a long recovery period. To this end, it is important that more efficacious and disease slowing or modifying treatments for OA are found. The aim of this project was to understand how any purinergic receptors may influence chondrocyte phenotype with a view to better understanding their role in OA pathophysiology. Initial analysis of existing transcriptomic datasets comparing facets of OA vs normal chondrocyte expression revealed that P2Y6 is more highly expressed by OA chondrocytes compared to normal. Changes in expression during disease states is an indication that its signalling is important in the pathophysiology.

The endogenous ligand for P2Y6 is UDP, with UTP and ADP also having activity at this receptor, albeit with lower potency [305]. Whilst the source of ATP, as the universal energy molecule, is clear in the extracellular milieu, the origins of UTP/UDP are more complex. Extracellular UTP concentrations (1-5nM) have been measured to be about one third of that of extracellular ATP, and it has been postulated that there is constitutive release to counteract the constant metabolism by ectonucleotidases [306]. It has also shown to be released from cells as a result of mechanical stimulation [307], and potentially via pannexin channels in a similar way to ATP [125]. Theoretically, UDP can be released from a cell in this form, or can be released as UTP and metabolised to UDP outside the cell. UTP and UDP are involved in the glycogen metabolic pathway. UDP-glucose is formed from the activity of UDP-glucose pyrophosphorylase from UTP and glucose 1-phosphate. Glycogen is then synthesised from UDP-glucose by glycogen synthase, releasing UDP from the reaction [308].

This body of work cannot provide a conclusive answer as to why P2Y6 is over-expressed, how it might affect or contribute to the osteoarthritic phenotype or whether it is a useful avenue with which to pursue further research. However,

there are some key findings. Assuming that all effects mediated by MRS2578 are mediated through the inhibition of P2Y6, it was found that there is constitutive P2Y6 signalling in chondrocytes, it contributes to the IL-1 response and is necessary for the induction of MMPs in response to IL-1. MRS2578 inhibited the IL-1 stimulated induction of *MMP13*, *MMP1* and *MMP3* mRNA in primary human chondrocytes, as well as SW1353 cells in a dose dependent manner, which was also seen at the protein level. The lack of agonism in this experiment suggests that there is constitutive P2Y6 activity for which to inhibit, alluding to a stable concentration of UDP in the extracellular space. Moreover, this inhibition suggests that P2Y6 signalling is required for IL-1 signalling, potentially involving NF $\kappa$ B, as MMP expression levels were brought down to baseline levels with MRS2578. However, P2Y6 agonism was not able to induce IL-1 responses robustly, which may mean that the P2Y6 downstream signalling is a prerequisite for IL-1 signalling but only acts in this way. For example, one hypothesis might be that intracellular calcium transients downstream of P2Y6 are required for NF $\kappa$ B signalling, but the NF $\kappa$ B activation is the rate-limiting step and so more P2Y6 signalling does not transduce this any further. These data elude to P2Y6 being pro-inflammatory and may explain why it is over-expressed. In OA chondrocytes, the IL-1 pathway (amongst others) is more highly activated and so if P2Y6 signalling is required for this, that would explain why it is more highly expressed. However, interestingly, IL-1 stimulation itself seemed to negatively regulate *P2Y6* mRNA expression in PHC, which would not fit with this hypothesis, and also does not correlate with the data suggesting it is over-expressed in OA, where IL-1 concentrations are higher.

As well as being over-expressed in OA, there was increased P2Y6 transcript expressed towards the end of the 21-day ATDC5 chondrogenesis time course, suggesting that it is regulated in this process and might have functional signalling effects. MRS2578, at low concentrations, inhibited markers of chondrogenesis in these cells, including mRNA expression of ECM components such as *collagen II* as well as Alcian Blue staining of proteoglycans. These data suggest that P2Y6 signalling may also be important to the regulatory processes in chondrogenesis. Owing to the similarities between some of the pathophysiological changes that

occur in OA to the events of chondrogenesis, it would follow that P2Y6 may be involved in the tight regulation of the processes facilitating both these phenotypic changes. For example, MMP-13 is expressed both in OA, where it pathologically degrades the matrix, and during terminal differentiation and chondrocyte hypertrophy, where it degrades the matrix to allow for neovascularisation and calcification. If P2Y6 does in fact regulate the expression of MMPs, it makes sense that this regulation would occur both in an inflammatory setting and in chondrogenesis. Calcium signalling has been shown to be important in chondrogenesis, specifically oscillations in ATP and calcium signals being a prerequisite for prechondrogenic condensation [309]. Modulation of calcium signalling, downstream from P2Y6, may be the mechanism by which these effects are mediated. Repeating this experiment with a calcium chelator, such as BAPTA, would provide insights into the role of calcium signalling, albeit not specific to P2Y6. More work would be needed to understand exactly how this signalling from P2Y6 would affect this change, with the use of a knockout cell line or mouse.

Alongside use of the P2Y6 inhibitor MRS2578, UDP- $\beta$ S (a non-hydrolysable analogue) was used to agonise the receptor. The use of a non-hydrolysable analogue ensures that it is not metabolised to other nucleotides that can activate other purinergic receptors, but also to ensure that the agonist is present in the media long enough to activate the receptor. UDP- $\beta$ S has shown to have higher potency at P2Y6 compared to unmodified UDP and there is no evidence of off-target effects [253]. RNAseq was used to understand globally how P2Y6 agonism and antagonism affected gene expression in both inflammatory (IL-1 $\beta$  stimulated) and basal environments. This revealed that UDP- $\beta$ S induced a reduction in the transcription of a number of genes that mediate inflammation, such as cytokines and elements of the NF $\kappa$ B pathway, and would have an anti-inflammatory effect *in vivo*. This chondroprotective role would work to reduce inflammation in the joint, as reduced transcription of cytokines would lead to less secretion and subsequently reduced activation of inflammatory cascades that catalyse ECM destruction and recruit other immune cells. This effect of P2Y6 may be mediated by STAT6, as less phosphorylated protein was detected following UDP- $\beta$ S stimulation in PHC. STAT6 is commonly activated by IL-4 and IL-13, which have been

shown to have chondroprotective effects in reducing the effects of inflammatory cytokines. It is possible that there is cross-talk and/or dependence between these two pathways. Whilst there is a disconnect between IL-4 and P2Y6 both having the same anti-inflammatory effect whilst either inducing or reducing the phosphorylation of STAT6, respectively, this is preliminary data and provides a starting point for further investigation.

### 6.3 Is MRS2578 a reliable tool?

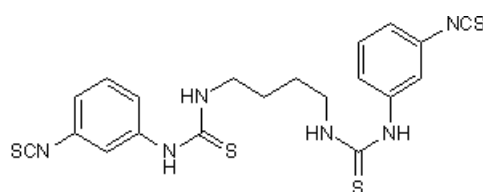


**Figure 6.1: Structure of MRS2578**

MRS2578 is the most commonly used selective P2Y6 antagonist in the field, and is, at present, the only commercially available antagonist in the UK. It is a diisothiocyanate that was first described in 2004 by Mamedova et al., [235]. It was described as insurmountable, meaning that the maximal agonist response is depressed and is thought to be semi-irreversible (i.e. it releases from the receptor slowly). It was also described to be specific to P2Y6 with no activity at P2Y4 or P2Y11 and around 20% inhibition at P2Y1. It was also tested in both the context of pharmacological (IP3 accumulation) and functional effects (reversal of UDP induced protection against cell death in P2Y6 expressing 1321N1 cells). Some of the effects of MRS2578 in this body of work call into question whether it is always mediating these effects through inhibition of P2Y6. Firstly, it significantly inhibited the IL-1 induction of *MMP13*, *MMP3* and *MMP1* in PHC, down to basal levels at a concentration of 10 $\mu$ M, albeit a concentration that is much higher than the EC<sub>50</sub> of 37nM, but a concentration commonly used in the literature at which it is claimed to have specific effects. This inhibition would suggest that there is constitutive P2Y6 activity for which to inhibit. Theoretically, this makes sense as there is likely to be maintenance of an extracellular concentration of UDP, as has been shown with UTP and ATP [306], however this is not supported by the

lack of change of intracellular calcium concentrations when PHC were incubated with MRS2578 prior to being stimulated with UDP. Moreover, MRS2578, again at 10 $\mu$ M, inhibited the UDP-elicited calcium response, but also the ATP and ADP response. It is possible that the concentration is too high, and that a lower concentration would have maintained the inhibition of the UDP response but lost the inhibition of the ATP and ADP response. It is also possible that some of the activity of ATP and ADP is attributed to P2Y6. ADP is a partial agonist of P2Y6, and ATP could be metabolised very rapidly by ectonucleotidases to have activity at P2Y6, however the extent of inhibition (71% and 78% for ATP and ADP, respectively) would suggest that this is not the case. It would be expected that the percentage of ATP and ADP signalling that would be facilitated by P2Y6 would be smaller, with P2X or other P2Y receptors being the predominant responders. Furthermore, in many cases, the effects of MRS2578 were not able to be reversed by agonists of P2Y6 and so do not fit the classical model of agonist/antagonist behaviour. UDP- $\beta$ S was not able to reverse or induce the inhibition of IL-1 induced MMP expression, despite changes to experimental conditions, such as reducing stimulating concentrations of IL-1 or the concentration of UDP- $\beta$ S. This was also seen in the sequencing data. Not only was MRS2578 far more potent than the agonist, there was differential expression of many more fold genes in the MRS2578 group compared to the UDP- $\beta$ S group. Moreover, where there was reciprocal differential expression between these groups, they were often in the same direction of change. MRS2578 also catalysed effects that were very diverse, such as cellular metabolism, mitochondrially encoded enzyme genes and serine/threonine kinase activity, according to GO term analysis - whereas none of these GO terms were returned from analysis of the DEG list from the UDP- $\beta$ S group. This might lead to the conclusion that MRS2578 was having P2Y6 independent effects, even at 5 $\mu$ M. When P2Y6 expression was knocked-down using an siRNA and the inhibition of IL-1 induced MMP expression was tested, there was no difference between the knockdown and control cell groups. Whilst this might be due to insufficient knockdown, there was not even a small difference, indicating that the response is not dependent on the level of P2Y6 expression. Nevertheless, there are some data suggesting that MRS2578 does require P2Y6 to elicit its ef-

fects. From the literature, Salem et al., showed that in their intestinal epithelial cells, MRS2578 activity on CXCL10 induction was absent in cells lacking P2Y6 [271]. In addition, the ability of MRS2578 to inhibit IL-1 induced MMP expression was tested in parental/non-expressing and P2Y6 expressing 1321N1 astrocytoma cells. Similarly, MRS2578 was only able to significantly exert this effect in the P2Y6 expressing cells. As such, these data provides convincing evidence that MRS2578 is a useful and specific tool, but further exploration would be required to understand why some of the effects of MRS2578 do not fit with the classical model of agonism and antagonism. The use of a P2Y6 knockout cell line would be able to definitively answer these research questions.

## 6.4 Future Directions

There are lots of next steps that would follow on from this body of work. Initially, being able to link P2Y6 signalling to STAT6 would be useful in showing that it is a direct cause and effect. This would involve initially using a western blot or ELISA to verify the findings of the multiplex array. Verification of the RNAseq findings would also be useful to increase n numbers and/or better stratify donors in their histological scoring and/or P2Y6 expression. This would provide more statistical power and would allow the Benjamini-Hochberg method to remove false positives. Exploring the dynamics of the UDP- $\beta$ S/STAT6 response, including assessing whether it is dose dependent and the time frame within which it occurs, would shed light on its robustness. Then, to try and understand what specifically downstream is causing this effect - such as calcium signalling, which could be interrogated with the use of thapsigargin to deplete calcium stores, or another facet like PKC or calmodulin kinase. Inhibitors of these proteins could help to determine if they are needed for and therefore involved in the response. The functional outcomes of STAT6 in chondrocytes could also be interrogated through knockdown or overexpression and assessing the effects on chondrocyte phenotype. Should these data continue to highlight the anti-inflammatory effects of UDP- $\beta$ S, moving to an *in vivo* model whereby the effect of UDP- $\beta$ S as an intra-articular or intraperitoneal injection on outcomes of DMM surgery would

be interesting to understand whether the impact of reduced cytokine expression would be able to improve pain, histological or mobility outcomes.

What would also be important to know for the field and to help interpret results using MRS2578 in this body of work would be to use a P2Y6 knockout cell line to understand whether the effects of this antagonist are truly as a result of inhibition of P2Y6. If I were to continue my attempts to use CRISPR-Cas9 to knockout P2Y6 in the ATDC5 cell line, it would be pertinent to validate Cas9 protein expression in the transduced cells to ensure successful transcription of the integrated gene. Optimisation of the transfection of guide RNAs would also be useful, as well as a more precise method to clonally dilute cells. This could be through the use of cloning rings in a 100mm dish, FACS or a single cell sorter and seeder specifically designed for this purpose. Using a validated antibody would also help to ensure that detection of P2Y6 protein was robust. With a knockout cell line, assessing the ability of MRS2578 to inhibit the IL-1 induction of MMPs in the knockout and expressing cells would allow an assessment of its specificity in this cell line. Moreover, using RNAseq to get a global picture of gene expression changes in response to MRS2578 in the knockout cells would help to understand the effects that are mediated by P2Y6 and those that aren't. Being able to use another inhibitor of P2Y6, such as TIM-38 [310], would add confidence to any data seen with MRS2578 if the effects were similar.

In summary, this project has provided an initial exploration of the expression and functional role of P2Y6 in chondrocyte biology. Initially, understanding its expression levels in existing datasets revealed it to be more highly expressed in osteoarthritic chondrocytes compared to normal. There was then exploration of the utility of two chondrocyte cell lines for purinergic signalling research, and functional effects of P2Y6 were determined using MRS2578, a specific P2Y6 antagonist. This highlighted that MRS2578 is able to fully inhibit the IL-1 $\beta$  induction of MMP expression. This work also revealed the anti-inflammatory effects of UDP- $\beta$ S by RNA sequencing data and called into question the utility of MRS2578 as a specific antagonist based on its potency and lack of classical agonist/antagonist behaviour. Moreover, work to optimize a CRISPR/Cas9 protocol in ATDC5 cells was undertaken.

# Chapter 7

## Bibliography

1. Sambrook, P. *The musculoskeletal system: basic science and clinical conditions* OCLC: 909892660. ISBN: 978-0-7020-4833-3 (2010).
2. Buckwalter, J. A., Mow, V. C. & Ratcliffe, A. Restoration of Injured or Degenerated Articular Cartilage. *The Journal of the American Academy of Orthopaedic Surgeons* **2**, 192–201. ISSN: 1940-5480 (July 1994).
3. Eschweiler, J. *et al.* The Biomechanics of Cartilage—An Overview. *Life* **11**, 302. ISSN: 2075-1729 (Apr. 1, 2021).
4. Mansfield, J., Bell, J. & Winlove, C. The micromechanics of the superficial zone of articular cartilage. *Osteoarthritis and Cartilage* **23**, 1806–1816. ISSN: 10634584 (Oct. 2015).
5. Zhang, W., Green, C. & Stott, N. S. Bone morphogenetic protein-2 modulation of chondrogenic differentiation in vitro involves gap junction-mediated intercellular communication. *Journal of Cellular Physiology* **193**, 233–243. ISSN: 0021-9541 (Nov. 2002).
6. Gao, Y. *et al.* The ECM-cell interaction of cartilage extracellular matrix on chondrocytes. *BioMed Research International* **2014**, 648459. ISSN: 2314-6141 (2014).
7. Loeser, R. F. Integrins and chondrocyte-matrix interactions in articular cartilage. *Matrix Biology: Journal of the International Society for Matrix Biology* **39**, 11–16. ISSN: 1569-1802 (Oct. 2014).

8. Lambert, C. *et al.* The Damage-Associated Molecular Patterns (DAMPs) as Potential Targets to Treat Osteoarthritis: Perspectives From a Review of the Literature. *Frontiers in Medicine* **7**, 607186. ISSN: 2296-858X (2020).
9. Zhang, J., Hao, X., Chi, R., Qi, J. & Xu, T. Moderate mechanical stress suppresses the IL-1 $\beta$ -induced chondrocyte apoptosis by regulating mitochondrial dynamics. *Journal of Cellular Physiology* **236**, 7504–7515. ISSN: 1097-4652 (Nov. 2021).
10. Liu, Q. *et al.* Effects of mechanical stress on chondrocyte phenotype and chondrocyte extracellular matrix expression. *Scientific Reports* **6**, 37268. ISSN: 2045-2322 (Nov. 17, 2016).
11. Nishida, T. & Kubota, S. Roles of CCN2 as a mechano-sensing regulator of chondrocyte differentiation. *The Japanese Dental Science Review* **56**, 119–126. ISSN: 1882-7616 (Nov. 2020).
12. Hendrickx, G. *et al.* Piezo1 Inactivation in Chondrocytes Impairs Trabecular Bone Formation. *Journal of Bone and Mineral Research: The Official Journal of the American Society for Bone and Mineral Research* **36**, 369–384. ISSN: 1523-4681 (Feb. 2021).
13. Knight, M. The role of primary cilia in cartilage health and disease. *Osteoarthritis and Cartilage* **21**, S2. ISSN: 10634584 (Apr. 2013).
14. Izadifar, Z., Chen, X. & Kulyk, W. Strategic design and fabrication of engineered scaffolds for articular cartilage repair. *Journal of Functional Biomaterials* **3**, 799–838. ISSN: 2079-4983 (Nov. 14, 2012).
15. Hall, A. C. The Role of Chondrocyte Morphology and Volume in Controlling Phenotype-Implications for Osteoarthritis, Cartilage Repair, and Cartilage Engineering. *Current Rheumatology Reports* **21**, 38. ISSN: 1534-6307 (June 15, 2019).
16. Lord, M. S. & Whitelock, J. M. Recombinant production of proteoglycans and their bioactive domains. *The FEBS journal* **280**, 2490–2510. ISSN: 1742-4658 (May 2013).

17. Fuentes-Mera, L., Camacho, A., Moncada-Saucedo, N. K. & Peña-Martínez, V. in *Mesenchymal Stem Cells - Isolation, Characterization and Applications* (ed Pham, P. V.) (InTech, Nov. 29, 2017). ISBN: 978-953-51-3615-6 978-953-51-3616-3.
18. Visweswaran, M. *et al.* Multi-lineage differentiation of mesenchymal stem cells – To Wnt, or not Wnt. *The International Journal of Biochemistry & Cell Biology* **68**, 139–147. ISSN: 13572725 (Nov. 2015).
19. Lim, J. *et al.* BMP-Smad4 signaling is required for precartilaginous mesenchymal condensation independent of Sox9 in the mouse. *Developmental Biology* **400**, 132–138. ISSN: 1095-564X (Apr. 1, 2015).
20. Akiyama, H., Chaboissier, M.-C., Martin, J. F., Schedl, A. & de Crombrughe, B. The transcription factor Sox9 has essential roles in successive steps of the chondrocyte differentiation pathway and is required for expression of Sox5 and Sox6. *Genes & Development* **16**, 2813–2828. ISSN: 0890-9369 (Nov. 1, 2002).
21. Yu, K. & Ornitz, D. M. FGF signaling regulates mesenchymal differentiation and skeletal patterning along the limb bud proximodistal axis. *Development (Cambridge, England)* **135**, 483–491. ISSN: 0950-1991 (Feb. 2008).
22. Davidson, D. *et al.* Fibroblast Growth Factor (FGF) 18 Signals through FGF Receptor 3 to Promote Chondrogenesis. *Journal of Biological Chemistry* **280**, 20509–20515. ISSN: 00219258 (May 2005).
23. Inada, M. *et al.* Critical roles for collagenase-3 (Mmp13) in development of growth plate cartilage and in endochondral ossification. *Proceedings of the National Academy of Sciences of the United States of America* **101**, 17192–17197. ISSN: 0027-8424 (Dec. 7, 2004).
24. Rabie, A. B. M. & Hägg, U. Factors regulating mandibular condylar growth. *American Journal of Orthodontics and Dentofacial Orthopedics: Official Publication of the American Association of Orthodontists, Its Constituent Societies, and the American Board of Orthodontics* **122**, 401–409. ISSN: 0889-5406 (Oct. 2002).
25. Yang, G. *et al.* Osteogenic fate of hypertrophic chondrocytes. *Cell Research* **24**, 1266–1269. ISSN: 1748-7838 (Oct. 2014).

26. NIH SEER NCI Training. *Bone Development & Growth*
27. Hunziker, E. B. Mechanism of longitudinal bone growth and its regulation by growth plate chondrocytes. *Microscopy Research and Technique* **28**, 505–519. ISSN: 1059-910X, 1097-0029 (Aug. 15, 1994).
28. Ballock, R. T. & O’Keefe, R. J. The biology of the growth plate. *The Journal of Bone and Joint Surgery. American Volume* **85**, 715–726. ISSN: 0021-9355 (Apr. 2003).
29. Minina, E. *et al.* BMP and Ihh/PTHrP signaling interact to coordinate chondrocyte proliferation and differentiation. *Development (Cambridge, England)* **128**, 4523–4534. ISSN: 0950-1991 (Nov. 2001).
30. Steinert, A. F. *et al.* Hypertrophy is induced during the in vitro chondrogenic differentiation of human mesenchymal stem cells by bone morphogenetic protein-2 and bone morphogenetic protein-4 gene transfer. *Arthritis Research & Therapy* **11**, R148. ISSN: 1478-6362 (2009).
31. Le Goff, C. & Cormier-Daire, V. Chondrodysplasias and TGF $\beta$  signaling. *BoneKEY Reports* **4**, 642. ISSN: 2047-6396 (2015).
32. Hata, K., Takahata, Y., Murakami, T. & Nishimura, R. Transcriptional Network Controlling Endochondral Ossification. *Journal of Bone Metabolism* **24**, 75–82. ISSN: 2287-6375 (May 2017).
33. Nilsson, A., Carlsson, B., Isgaard, J., Isaksson, O. G. & Rymo, L. Regulation by GH of insulin-like growth factor-I mRNA expression in rat epiphyseal growth plate as studied with in-situ hybridization. *The Journal of Endocrinology* **125**, 67–74. ISSN: 0022-0795 (Apr. 1990).
34. Ağirdil, Y. The growth plate: a physiologic overview. *EFORT open reviews* **5**, 498–507. ISSN: 2058-5241 (Aug. 2020).
35. Katsimbri, P. The biology of normal bone remodelling. *European Journal of Cancer Care* **26**, e12740. ISSN: 09615423 (Nov. 2017).
36. Mallorie, A. & Shine, B. Normal bone physiology, remodelling and its hormonal regulation. *Surgery (Oxford)* **40**, 163–168. ISSN: 02639319 (Mar. 2022).

37. Arias, C. F., Herrero, M. A., Echeverri, L. F., Oleaga, G. E. & López, J. M. Bone remodeling: A tissue-level process emerging from cell-level molecular algorithms. *PloS One* **13**, e0204171. ISSN: 1932-6203 (2018).
38. Michigami, T. Skeletal mineralization: mechanisms and diseases. *Annals of Pediatric Endocrinology & Metabolism* **24**, 213–219. ISSN: 2287-1012 (Dec. 2019).
39. Ali, N., Qadery, S., Narle, G. & Public Health England. *Musculoskeletal Health: A 5 year strategic framework for prevention across the lifecourse*. 2019.
40. Mohammed, A. *et al.* A comparison of risk factors for osteo- and rheumatoid arthritis using NHANES data. *Preventive Medicine Reports* **20**, 101242. ISSN: 2211-3355 (Dec. 2020).
41. Swain, S. *et al.* Trends in incidence and prevalence of osteoarthritis in the United Kingdom: findings from the Clinical Practice Research Datalink (CPRD). *Osteoarthritis and Cartilage* **28**, 792–801. ISSN: 1522-9653 (June 2020).
42. Losina, E. *et al.* Lifetime risk and age at diagnosis of symptomatic knee osteoarthritis in the US. *Arthritis Care & Research* **65**, 703–711. ISSN: 2151-4658 (May 2013).
43. Allen, K. D., Thoma, L. M. & Golightly, Y. M. Epidemiology of osteoarthritis. *Osteoarthritis and Cartilage* **30**, 184–195. ISSN: 1522-9653 (Feb. 2022).
44. Prieto-Alhambra, D. *et al.* Incidence and risk factors for clinically diagnosed knee, hip and hand osteoarthritis: influences of age, gender and osteoarthritis affecting other joints. *Annals of the Rheumatic Diseases* **73**, 1659–1664. ISSN: 0003-4967, 1468-2060 (Sept. 2014).
45. Dong, Q., Liu, H., Yang, D. & Zhang, Y. Diabetes mellitus and arthritis: is it a risk factor or comorbidity?: A systematic review and meta-analysis. *Medicine* **96**, e6627. ISSN: 1536-5964 (May 2017).
46. Osteoarthritis Research Society International. *Osteoarthritis: A Serious Disease, submitted to the U.S. Food and Drug Administration* 2016.
47. United States Bone and Joint Initiative. *The Burden of Musculoskeletal Diseases in the United States (BMUS)* 2018.

48. Swingler, T. E. *et al.* Degradome expression profiling in human articular cartilage. *Arthritis Research & Therapy* **11**, R96. ISSN: 1478-6362 (2009).
49. Wuelling, M. & Vortkamp, A. Chondrocyte proliferation and differentiation. *Endocrine Development* **21**, 1–11. ISSN: 1662-2979 (2011).
50. Barbero, A. *et al.* Age related changes in human articular chondrocyte yield, proliferation and post-expansion chondrogenic capacity. *Osteoarthritis and Cartilage* **12**, 476–484. ISSN: 1063-4584 (June 2004).
51. David, M. A. *et al.* Early, focal changes in cartilage cellularity and structure following surgically induced meniscal destabilization in the mouse. *Journal of Orthopaedic Research* **35**, 537–547. ISSN: 0736-0266, 1554-527X (Mar. 2017).
52. Van Der Kraan, P. M. & Van Den Berg, W. B. Osteophytes: relevance and biology. *Osteoarthritis and Cartilage* **15**, 237–244. ISSN: 10634584 (Mar. 2007).
53. Alliston, T., Hernandez, C. J., Findlay, D. M., Felson, D. T. & Kennedy, O. D. Bone marrow lesions in osteoarthritis: What lies beneath. *Journal of Orthopaedic Research: Official Publication of the Orthopaedic Research Society* **36**, 1818–1825. ISSN: 1554-527X (July 2018).
54. Priam, S. *et al.* Identification of soluble 14-3-3 as a novel subchondral bone mediator involved in cartilage degradation in osteoarthritis. *Arthritis and Rheumatism* **65**, 1831–1842. ISSN: 1529-0131 (July 2013).
55. Mobasheri, A. *et al.* The role of metabolism in the pathogenesis of osteoarthritis. *Nature Reviews. Rheumatology* **13**, 302–311. ISSN: 1759-4804 (May 2017).
56. Sokolove, J. & Lepus, C. M. Role of inflammation in the pathogenesis of osteoarthritis: latest findings and interpretations. *Therapeutic Advances in Musculoskeletal Disease* **5**, 77–94. ISSN: 1759-720X (Apr. 2013).
57. Dreier, R. Hypertrophic differentiation of chondrocytes in osteoarthritis: the developmental aspect of degenerative joint disorders. *Arthritis Research & Therapy* **12**, 216. ISSN: 1478-6354 (2010).
58. Ackers, I. & Malgor, R. Interrelationship of canonical and non-canonical Wnt signalling pathways in chronic metabolic diseases. *Diabetes & Vascular Disease Research* **15**, 3–13. ISSN: 1752-8984 (Jan. 2018).

59. Loughlin, J. *et al.* Functional variants within the secreted frizzled-related protein 3 gene are associated with hip osteoarthritis in females. *Proceedings of the National Academy of Sciences of the United States of America* **101**, 9757–9762. ISSN: 0027-8424 (June 29, 2004).
60. Zhu, M. *et al.* Activation of beta-catenin signaling in articular chondrocytes leads to osteoarthritis-like phenotype in adult beta-catenin conditional activation mice. *Journal of Bone and Mineral Research: The Official Journal of the American Society for Bone and Mineral Research* **24**, 12–21. ISSN: 1523-4681 (Jan. 2009).
61. Yuasa, T., Otani, T., Koike, T., Iwamoto, M. & Enomoto-Iwamoto, M. Wnt/beta-catenin signaling stimulates matrix catabolic genes and activity in articular chondrocytes: its possible role in joint degeneration. *Laboratory Investigation; a Journal of Technical Methods and Pathology* **88**, 264–274. ISSN: 1530-0307 (Mar. 2008).
62. Sabha, M., Siaton, B. C. & Hochberg, M. C. Lorecivivint, an intra-articular potential disease-modifying osteoarthritis drug. *Expert Opinion on Investigational Drugs* **29**, 1339–1346. ISSN: 1744-7658 (Dec. 2020).
63. Patel, S., Alam, A., Pant, R. & Chattopadhyay, S. Wnt Signaling and Its Significance Within the Tumor Microenvironment: Novel Therapeutic Insights. *Frontiers in Immunology* **10**, 2872. ISSN: 1664-3224 (Dec. 16, 2019).
64. D'Souza, B., Meloty-Kapella, L. & Weinmaster, G. Canonical and non-canonical Notch ligands. *Current Topics in Developmental Biology* **92**, 73–129. ISSN: 1557-8933 (2010).
65. Liu, Z. *et al.* A dual role for NOTCH signaling in joint cartilage maintenance and osteoarthritis. *Science Signaling* **8**, ra71. ISSN: 1937-9145 (July 21, 2015).
66. Ustunel, I. *et al.* The immunohistochemical localization of notch receptors and ligands in human articular cartilage, chondroprogenitor culture and ultrastructural characteristics of these progenitor cells. *Acta Histochemica* **110**, 397–407. ISSN: 0065-1281 (2008).

67. Hosaka, Y. *et al.* Notch signaling in chondrocytes modulates endochondral ossification and osteoarthritis development. *Proceedings of the National Academy of Sciences of the United States of America* **110**, 1875–1880. ISSN: 1091-6490 (Jan. 29, 2013).
68. Kobayashi, H. *et al.* Transcriptional Induction of ADAMTS5 Protein by Nuclear Factor- $\kappa$ B (NF- $\kappa$ B) Family Member RelA/p65 in Chondrocytes during Osteoarthritis Development. *Journal of Biological Chemistry* **288**, 28620–28629. ISSN: 00219258 (Oct. 2013).
69. Yan, C., Wang, H., Aggarwal, B. B. & Boyd, D. D. A novel homologous recombination system to study 92 kDa type IV collagenase transcription demonstrates that the NF $\kappa$ B motif drives the transition from a repressed to an activated state of gene expression. *The FASEB Journal* **18**, 540–541. ISSN: 0892-6638, 1530-6860 (Mar. 2004).
70. Ulivi, V., Giannoni, P., Gentili, C., Cancedda, R. & Descalzi, F. p38/NF- $\kappa$ B-dependent expression of COX-2 during differentiation and inflammatory response of chondrocytes. *Journal of Cellular Biochemistry* **104**, 1393–1406. ISSN: 07302312, 10974644 (July 1, 2008).
71. Catheline, S. E. *et al.* IKK $\beta$ -NF- $\kappa$ B signaling in adult chondrocytes promotes the onset of age-related osteoarthritis in mice. *Science Signaling* **14**, eabf3535. ISSN: 1937-9145 (Sept. 21, 2021).
72. Choi, M.-C., Jo, J., Park, J., Kang, H. K. & Park, Y. NF- $\kappa$ B Signaling Pathways in Osteoarthritic Cartilage Destruction. *Cells* **8**, 734. ISSN: 2073-4409 (July 17, 2019).
73. Xu, L. *et al.* Sam68 Promotes NF- $\kappa$ B Activation and Apoptosis Signaling in Articular Chondrocytes during Osteoarthritis. *Inflammation Research: Official Journal of the European Histamine Research Society ... [et Al.]* **64**, 895–902. ISSN: 1420-908X (Nov. 2015).
74. Yan, H. *et al.* Suppression of NF- $\kappa$ B activity via nanoparticle-based siRNA delivery alters early cartilage responses to injury. *Proceedings of the National Academy of Sciences* **113**. ISSN: 0027-8424, 1091-6490 (Oct. 11, 2016).

75. De Luca, F. Regulatory role of NF- $\kappa$ B in growth plate chondrogenesis and its functional interaction with Growth Hormone. *Molecular and Cellular Endocrinology* **514**, 110916. ISSN: 03037207 (Aug. 2020).
76. Wu, S., Fadoju, D., Rezvani, G. & De Luca, F. Stimulatory Effects of Insulin-like Growth Factor-I on Growth Plate Chondrogenesis Are Mediated by Nuclear Factor- $\kappa$ B p65. *Journal of Biological Chemistry* **283**, 34037–34044. ISSN: 00219258 (Dec. 2008).
77. Coimbra, I. B., Jimenez, S. A., Hawkins, D. F., Piera-Velazquez, S. & Stokes, D. G. Hypoxia inducible factor-1 alpha expression in human normal and osteoarthritic chondrocytes11Supported by NIH/NIAMS Program Project grant (AR-39740) to S.A.J. I. C. was supported by a fellowship from Fundacao de Amparo'a Ciencia do Estado de Sao Paulo. *Osteoarthritis and Cartilage* **12**, 336–345. ISSN: 10634584 (Apr. 2004).
78. Schrobback, K. *et al.* Effects of Oxygen on Zonal Marker Expression in Human Articular Chondrocytes. *Tissue Engineering Part A* **18**, 920–933. ISSN: 1937-3341, 1937-335X (May 2012).
79. Amarilio, R. *et al.* HIF1 $\alpha$  regulation of Sox9 is necessary to maintain differentiation of hypoxic prechondrogenic cells during early skeletogenesis. *Development* **134**, 3917–3928. ISSN: 1477-9129, 0950-1991 (Nov. 1, 2007).
80. Robins, J. C. *et al.* Hypoxia induces chondrocyte-specific gene expression in mesenchymal cells in association with transcriptional activation of Sox9. *Bone* **37**, 313–322. ISSN: 8756-3282 (Sept. 2005).
81. Duval, E. *et al.* Hypoxia-inducible factor 1 $\alpha$  inhibits the fibroblast-like markers type I and type III collagen during hypoxia-induced chondrocyte redifferentiation: Hypoxia not only induces type II collagen and aggrecan, but it also inhibits type I and type III collagen in the hypoxia-inducible factor 1 $\alpha$ -dependent redifferentiation of chondrocytes. *Arthritis & Rheumatism* **60**, 3038–3048. ISSN: 00043591, 15290131 (Oct. 2009).
82. Hu, S. *et al.* Stabilization of HIF-1 $\alpha$  alleviates osteoarthritis via enhancing mitophagy. *Cell Death & Disease* **11**, 481. ISSN: 2041-4889 (June 25, 2020).

83. Yudoh, K., Nakamura, H., Masuko-Hongo, K., Kato, T. & Nishioka, K. Catabolic stress induces expression of hypoxia-inducible factor (HIF)-1 alpha in articular chondrocytes: involvement of HIF-1 alpha in the pathogenesis of osteoarthritis. *Arthritis Research & Therapy* **7**, R904–914. ISSN: 1478-6362 (2005).
84. Markway, B. D., Cho, H. & Johnstone, B. Hypoxia promotes redifferentiation and suppresses markers of hypertrophy and degeneration in both healthy and osteoarthritic chondrocytes. *Arthritis Research & Therapy* **15**, R92. ISSN: 1478-6362 (Aug. 21, 2013).
85. Pfander, D. & Gelse, K. Hypoxia and osteoarthritis: how chondrocytes survive hypoxic environments. *Current Opinion in Rheumatology* **19**, 457–462. ISSN: 1040-8711 (Sept. 2007).
86. Saito, T. *et al.* Transcriptional regulation of endochondral ossification by HIF-2alpha during skeletal growth and osteoarthritis development. *Nature Medicine* **16**, 678–686. ISSN: 1546-170X (June 2010).
87. Yang, S. *et al.* Hypoxia-inducible factor-2alpha is a catabolic regulator of osteoarthritic cartilage destruction. *Nature Medicine* **16**, 687–693. ISSN: 1546-170X (June 2010).
88. Thoms, B. L., Dudek, K. A., Lafont, J. E. & Murphy, C. L. Hypoxia promotes the production and inhibits the destruction of human articular cartilage. *Arthritis and Rheumatism* **65**, 1302–1312. ISSN: 1529-0131 (May 2013).
89. Goldring, M. B. & Otero, M. Inflammation in osteoarthritis. *Current Opinion in Rheumatology* **23**, 471–478. ISSN: 1531-6963 (Sept. 2011).
90. Borzì, R. M. *et al.* Human chondrocytes express functional chemokine receptors and release matrix-degrading enzymes in response to C-X-C and C-C chemokines. *Arthritis and Rheumatism* **43**, 1734–1741. ISSN: 0004-3591 (Aug. 2000).
91. Da Silva, P. H. R. *et al.* Chemokines and the extracellular matrix: Set of targets for tumor development and treatment. *Cytokine* **144**, 155548. ISSN: 10434666 (Aug. 2021).

92. Orlowsky, E. W. & Kraus, V. B. The role of innate immunity in osteoarthritis: when our first line of defense goes on the offensive. *The Journal of Rheumatology* **42**, 363–371. ISSN: 0315-162X (Mar. 2015).
93. Aladal, M. *et al.* Insights into the implementation of Fibronectin 1 in the cartilage tissue engineering. *Biomedicine & Pharmacotherapy* **148**, 112782. ISSN: 07533322 (Apr. 2022).
94. Scanzello, C. R., Plaas, A. & Crow, M. K. Innate immune system activation in osteoarthritis: is osteoarthritis a chronic wound? *Current Opinion in Rheumatology* **20**, 565–572. ISSN: 1531-6963 (Sept. 2008).
95. Zhang, H., Cai, D. & Bai, X. Macrophages regulate the progression of osteoarthritis. *Osteoarthritis and Cartilage* **28**, 555–561. ISSN: 10634584 (May 2020).
96. Vincent, T. L. IL-1 in osteoarthritis: time for a critical review of the literature. *F1000Research* **8**, F1000 Faculty Rev–934. ISSN: 2046-1402 (2019).
97. Clements, K. M. *et al.* Gene deletion of either interleukin-1beta, interleukin-1beta-converting enzyme, inducible nitric oxide synthase, or stromelysin 1 accelerates the development of knee osteoarthritis in mice after surgical transection of the medial collateral ligament and partial medial meniscectomy. *Arthritis and Rheumatism* **48**, 3452–3463. ISSN: 0004-3591 (Dec. 2003).
98. Kloppenburg, M. *et al.* Phase IIa, placebo-controlled, randomised study of lutikizumab, an anti-interleukin-1 $\alpha$  and anti-interleukin-1 $\beta$  dual variable domain immunoglobulin, in patients with erosive hand osteoarthritis. *Annals of the Rheumatic Diseases* **78**, 413–420. ISSN: 1468-2060 (Mar. 2019).
99. Fleischmann, R. M. *et al.* A Phase II Trial of Lutikizumab, an Anti-Interleukin-1 $\alpha$ / $\beta$  Dual Variable Domain Immunoglobulin, in Knee Osteoarthritis Patients With Synovitis. *Arthritis & Rheumatology (Hoboken, N.J.)* **71**, 1056–1069. ISSN: 2326-5205 (July 2019).
100. Chevalier, X. *et al.* Intraarticular injection of anakinra in osteoarthritis of the knee: a multicenter, randomized, double-blind, placebo-controlled study. *Arthritis and Rheumatism* **61**, 344–352. ISSN: 0004-3591 (Mar. 15, 2009).

101. Cohen, S. B. *et al.* A randomized, double-blind study of AMG 108 (a fully human monoclonal antibody to IL-1R1) in patients with osteoarthritis of the knee. *Arthritis Research & Therapy* **13**, R125. ISSN: 1478-6362 (July 29, 2011).
102. Ryder, J. J. *et al.* Genetic associations in peripheral joint osteoarthritis and spinal degenerative disease: a systematic review. *Annals of the Rheumatic Diseases* **67**, 584–591. ISSN: 0003-4967 (Aug. 17, 2007).
103. Sherwood, J. *et al.* A homeostatic function of CXCR2 signalling in articular cartilage. *Annals of the Rheumatic Diseases* **74**, 2207–2215. ISSN: 0003-4967, 1468-2060 (Dec. 2015).
104. Scanzello, C. R. Chemokines and inflammation in osteoarthritis: Insights from patients and animal models. *Journal of Orthopaedic Research: Official Publication of the Orthopaedic Research Society* **35**, 735–739. ISSN: 1554-527X (Apr. 2017).
105. Miotla Zarebska, J. *et al.* CCL2 and CCR2 regulate pain-related behaviour and early gene expression in post-traumatic murine osteoarthritis but contribute little to chondropathy. *Osteoarthritis and Cartilage* **25**, 406–412. ISSN: 10634584 (Mar. 2017).
106. Wang, Z. *et al.* Chemokine (C-C Motif) Ligand 2/Chemokine Receptor 2 (CCR2) Axis Blockade to Delay Chondrocyte Hypertrophy as a Therapeutic Strategy for Osteoarthritis. *Medical Science Monitor: International Medical Journal of Experimental and Clinical Research* **27**, e930053. ISSN: 1643-3750 (Dec. 8, 2021).
107. Willcockson, H., Ozkan, H., Chubinskaya, S., Loeser, R. F. & Longobardi, L. CCL2 induces articular chondrocyte MMP expression through ERK and p38 signaling pathways. *Osteoarthritis and Cartilage Open* **3**, 100136. ISSN: 2665-9131 (Mar. 2021).
108. Kour, S. *et al.* IL-3 Decreases Cartilage Degeneration by Downregulating Matrix Metalloproteinases and Reduces Joint Destruction in Osteoarthritic Mice. *Journal of Immunology (Baltimore, Md.: 1950)* **196**, 5024–5035. ISSN: 1550-6606 (June 15, 2016).

109. Pan, D. *et al.* Holomycin, a novel NLRP3 inhibitor, attenuates cartilage degeneration and inflammation in osteoarthritis. *Biochemical and Biophysical Research Communications* **657**, 59–68. ISSN: 1090-2104 (May 21, 2023).
110. Gong, T., Liu, L., Jiang, W. & Zhou, R. DAMP-sensing receptors in sterile inflammation and inflammatory diseases. *Nature Reviews. Immunology* **20**, 95–112. ISSN: 1474-1741 (Feb. 2020).
111. Burnstock, G. Purinergic nerves. *Pharmacological Reviews* **24**, 509–581. ISSN: 0031-6997 (Sept. 1972).
112. Burnstock, G. in *Purinergic Signaling* (ed Pelegrín, P.) Series Title: Methods in Molecular Biology, 1–15 (Springer New York, New York, NY, 2020). ISBN: 978-1-4939-9716-9 978-1-4939-9717-6.
113. Webb, T. E. *et al.* Cloning and functional expression of a brain G-protein-coupled ATP receptor. *FEBS letters* **324**, 219–225. ISSN: 0014-5793 (June 14, 1993).
114. Burnstock, G. Purinergic Signalling: Therapeutic Developments. *Frontiers in Pharmacology* **8**, 661. ISSN: 1663-9812 (Sept. 25, 2017).
115. Dsouza, C., Moussa, M. S., Mikolajewicz, N. & Komarova, S. V. Extracellular ATP and its derivatives provide spatiotemporal guidance for bone adaptation to wide spectrum of physical forces. *Bone Reports* **17**, 101608. ISSN: 23521872 (Dec. 2022).
116. Young, K. A. *et al.* *Anatomy and Physiology* 1st. ISBN: 978-1-938168-13-0 (XanEdu Publishing, 2013).
117. Mizuno, Y., Kondo, T. & the Japanese Istradefylline Study Group. Adenosine A<sub>2A</sub> receptor antagonist istradefylline reduces daily OFF time in Parkinson's disease. *Movement Disorders* **28**, 1138–1141. ISSN: 0885-3185, 1531-8257 (July 2013).
118. Poole, R. *et al.* Coffee consumption and health: umbrella review of meta-analyses of multiple health outcomes. *BMJ*, j5024. ISSN: 0959-8138, 1756-1833 (Nov. 22, 2017).

119. Borea, P. A., Gessi, S., Merighi, S., Vincenzi, F. & Varani, K. Pharmacology of Adenosine Receptors: The State of the Art. *Physiological Reviews* **98**, 1591–1625. ISSN: 0031-9333, 1522-1210 (July 1, 2018).
120. Bragança, B. & Correia-de-Sá, P. Resolving the Ionotropic P2X4 Receptor Mystery Points Towards a New Therapeutic Target for Cardiovascular Diseases. *International Journal of Molecular Sciences* **21**, 5005. ISSN: 1422-0067 (July 15, 2020).
121. Di Virgilio, F., Vultaggio-Poma, V. & Sarti, A. C. P2X receptors in cancer growth and progression. *Biochemical Pharmacology* **187**, 114350. ISSN: 1873-2968 (May 2021).
122. Di Virgilio, F., Dal Ben, D., Sarti, A. C., Giuliani, A. L. & Falzoni, S. The P2X7 Receptor in Infection and Inflammation. *Immunity* **47**, 15–31. ISSN: 1097-4180 (July 18, 2017).
123. Markham, A. Gefapixant: First Approval. *Drugs* **82**, 691–695. ISSN: 1179-1950 (Apr. 2022).
124. Illes, P. *et al.* Update of P2X receptor properties and their pharmacology: IUPHAR Review 30. *British Journal of Pharmacology* **178**, 489–514. ISSN: 1476-5381 (Feb. 2021).
125. Lazarowski, E. R. & Harden, T. K. UDP-Sugars as Extracellular Signaling Molecules: Cellular and Physiologic Consequences of P2Y14 Receptor Activation. *Molecular Pharmacology* **88**, 151–160. ISSN: 1521-0111 (July 2015).
126. Delekate, A. *et al.* Metabotropic P2Y1 receptor signalling mediates astrocytic hyperactivity in vivo in an Alzheimer's disease mouse model. *Nature Communications* **5**, 5422. ISSN: 2041-1723 (Nov. 19, 2014).
127. Von Kügelgen, I. Pharmacology of P2Y receptors. *Brain Research Bulletin* **151**, 12–24. ISSN: 03619230 (Sept. 2019).
128. Orriss, I. R., Key, M. L., Hajjawi, M. O. R. & Arnett, T. R. Extracellular ATP Released by Osteoblasts Is A Key Local Inhibitor of Bone Mineralisation. *PLoS ONE* **8** (ed Malaval, L.) e69057. ISSN: 1932-6203 (July 9, 2013).

129. Hoebertz, A., Mahendran, S., Burnstock, G. & Arnett, T. R. ATP and UTP at low concentrations strongly inhibit bone formation by osteoblasts: a novel role for the P2Y2 receptor in bone remodeling. *Journal of Cellular Biochemistry* **86**, 413–419. ISSN: 0730-2312 (2002).
130. Xing, Y. *et al.* The roles of P2Y2 purinergic receptors in osteoblasts and mechanotransduction. *PloS One* **9**, e108417. ISSN: 1932-6203 (2014).
131. Wesselius, A. Role of purinergic receptor polymorphisms in human bone. *Frontiers in Bioscience* **16**, 2572. ISSN: 10939946, 10934715 (2011).
132. Agrawal, A. *et al.* Absence of P2Y2 Receptor Does Not Prevent Bone Destruction in a Murine Model of Muscle Paralysis-Induced Bone Loss. *Frontiers in Endocrinology* **13**, 850525. ISSN: 1664-2392 (2022).
133. Jørgensen, N. R. The purinergic P2X7 ion channel receptor—a ‘repair’ receptor in bone. *Current Opinion in Immunology* **52**, 32–38. ISSN: 1879-0372 (2018).
134. Li, J., Liu, D., Ke, H. Z., Duncan, R. L. & Turner, C. H. The P2X7 nucleotide receptor mediates skeletal mechanotransduction. *The Journal of Biological Chemistry* **280**, 42952–42959. ISSN: 0021-9258 (Dec. 30, 2005).
135. Cabahug-Zuckerman, P. *et al.* Potential role for a specialized  $\beta_3$  integrin-based structure on osteocyte processes in bone mechanosensation. *Journal of Orthopaedic Research* **36**, 642–652. ISSN: 0736-0266, 1554-527X (Feb. 2018).
136. Grol, M. W., Brooks, P. J., Pereverzev, A. & Dixon, S. J. P2X7 nucleotide receptor signaling potentiates the Wnt/ $\beta$ -catenin pathway in cells of the osteoblast lineage. *Purinergic Signalling* **12**, 509–520. ISSN: 1573-9538, 1573-9546 (Sept. 2016).
137. Sindhavajiva, P. R., Sastravaha, P., Arksornnukit, M. & Pavasant, P. Purinergic 2X7 receptor activation regulates WNT signaling in human mandibular-derived osteoblasts. *Archives of Oral Biology* **81**, 167–174. ISSN: 00039969 (Sept. 2017).
138. Varley, I. *et al.* Functional polymorphisms in the P2X7 receptor gene are associated with stress fracture injury. *Purinergic Signalling* **12**, 103–113. ISSN: 1573-9538, 1573-9546 (Mar. 2016).

139. Kara, F. M. *et al.* Adenosine A(1) receptors regulate bone resorption in mice: adenosine A(1) receptor blockade or deletion increases bone density and prevents ovariectomy-induced bone loss in adenosine A(1) receptor-knockout mice. *Arthritis and Rheumatism* **62**, 534–541. ISSN: 0004-3591 (Feb. 2010).
140. Mediero, A., Kara, F. M., Wilder, T. & Cronstein, B. N. Adenosine A2A Receptor Ligation Inhibits Osteoclast Formation. *The American Journal of Pathology* **180**, 775–786. ISSN: 00029440 (Feb. 2012).
141. Corciulo, C., Wilder, T. & Cronstein, B. N. Adenosine A2B receptors play an important role in bone homeostasis. *Purinergic Signalling* **12**, 537–547. ISSN: 1573-9546 (Sept. 2016).
142. Orriss, I. R. *et al.* The regulation of osteoblast function and bone mineralisation by extracellular nucleotides: The role of p2x receptors. *Bone* **51**, 389–400. ISSN: 1873-2763 (Sept. 2012).
143. Ellegaard, M., Hegner, T., Ding, M., Ulmann, L. & Jørgensen, N. R. Bone phenotype of P2X4 receptor knockout mice: implication of a P2X7 receptor mutation? *Purinergic Signalling* **17**, 241–246. ISSN: 1573-9546 (June 2021).
144. Orriss, I. R., Davies, B. K., Bourne, L. E. & Arnett, T. R. Modulation of osteoblast differentiation and function by the P2X4 receptor. *Purinergic Signalling* **19**, 367–378. ISSN: 1573-9538, 1573-9546 (June 2023).
145. Kim, H. *et al.* The purinergic receptor P2X5 regulates inflammasome activity and hyper-multinucleation of murine osteoclasts. *Scientific Reports* **7**, 196. ISSN: 2045-2322 (Mar. 15, 2017).
146. Kim, H. *et al.* Methylosome protein 50 associates with the purinergic receptor P2X5 and is involved in osteoclast maturation. *FEBS Letters* **594**, 144–152. ISSN: 0014-5793, 1873-3468 (Jan. 2020).
147. Wang, N., Agrawal, A., Jørgensen, N. R. & Gartland, A. P2X7 receptor regulates osteoclast function and bone loss in a mouse model of osteoporosis. *Scientific Reports* **8**, 3507. ISSN: 2045-2322 (2018).
148. Alvarenga, E. C. *et al.* Low-intensity pulsed ultrasound-dependent osteoblast proliferation occurs by via activation of the P2Y receptor: role of the P2Y1 receptor. *Bone* **46**, 355–362. ISSN: 1873-2763 (Feb. 2010).

149. Hoebertz, A., Meghji, S., Burnstock, G. & Arnett, T. R. Extracellular ADP is a powerful osteolytic agent: evidence for signaling through the P2Y(1) receptor on bone cells. *FASEB journal: official publication of the Federation of American Societies for Experimental Biology* **15**, 1139–1148. ISSN: 0892-6638 (May 2001).
150. Orriss, I. R. *et al.* The P2Y(6) receptor stimulates bone resorption by osteoclasts. *Endocrinology* **152**, 3706–3716. ISSN: 1945-7170 (Oct. 2011).
151. Korcok, J., Raimundo, L. N., Du, X., Sims, S. M. & Dixon, S. J. P2Y6 Nucleotide Receptors Activate NF- $\kappa$ B and Increase Survival of Osteoclasts. *Journal of Biological Chemistry* **280**, 16909–16915. ISSN: 00219258 (Apr. 2005).
152. Kong, Q., Quan, Y., Tian, G., Zhou, J. & Liu, X. Purinergic P2 Receptors: Novel Mediators of Mechanotransduction. *Frontiers in Pharmacology* **12**, 671809. ISSN: 1663-9812 (2021).
153. Su, X. *et al.* The ADP receptor P2RY12 regulates osteoclast function and pathologic bone remodeling. *The Journal of Clinical Investigation* **122**, 3579–3592. ISSN: 1558-8238 (Oct. 2012).
154. Syberg, S. *et al.* Clopidogrel (Plavix), a P2Y12 receptor antagonist, inhibits bone cell function in vitro and decreases trabecular bone in vivo. *Journal of Bone and Mineral Research: The Official Journal of the American Society for Bone and Mineral Research* **27**, 2373–2386. ISSN: 1523-4681 (Nov. 2012).
155. Jørgensen, N. R., Grove, E. L., Schwarz, P. & Vestergaard, P. Clopidogrel and the risk of osteoporotic fractures: a nationwide cohort study. *Journal of Internal Medicine* **272**, 385–393. ISSN: 1365-2796 (Oct. 2012).
156. Mikolajewicz, N. & Komarova, S. V. Role of UDP-Sugar Receptor P2Y14 in Murine Osteoblasts. *International Journal of Molecular Sciences* **21**, 2747. ISSN: 1422-0067 (Apr. 15, 2020).
157. Caswell, A. M., Leong, W. S. & Russell, R. G. G. Evidence for the presence of P2-purinoceptors at the surface of human articular chondrocytes in monolayer culture. *Biochimica et Biophysica Acta (BBA) - General Subjects* **1074**, 151–158. ISSN: 03044165 (May 1991).

158. Koolpe, M., Pearson, D. & Benton, H. P. Expression of both P1 and P2 purine receptor genes by human articular chondrocytes and profile of ligand-mediated prostaglandin E2 release. *Arthritis and Rheumatism* **42**, 258–267. ISSN: 0004-3591 (Feb. 1999).
159. Attur, M. *et al.* Prostaglandin E2 Exerts Catabolic Effects in Osteoarthritis Cartilage: Evidence for Signaling via the EP4 Receptor. *The Journal of Immunology* **181**, 5082–5088. ISSN: 0022-1767, 1550-6606 (Oct. 1, 2008).
160. Brown, C. J., Caswell, A. M., Rahman, S., Russell, R. G. & Buttle, D. J. Proteoglycan breakdown from bovine nasal cartilage is increased, and from articular cartilage is decreased, by extracellular ATP. *Biochimica et Biophysica Acta (BBA) - Molecular Basis of Disease* **1362**, 208–220. ISSN: 09254439 (Dec. 1997).
161. Croucher, L., Crawford, A., Hatton, P., Russell, R. & Buttle, D. Extracellular ATP and UTP stimulate cartilage proteoglycan and collagen accumulation in bovine articular chondrocyte pellet cultures. *Biochimica et Biophysica Acta (BBA) - Molecular Basis of Disease* **1502**, 297–306. ISSN: 09254439 (Oct. 2000).
162. Graff, R. D., Lazarowski, E. R., Banes, A. J. & Lee, G. M. ATP release by mechanically loaded porcine chondrons in pellet culture. *Arthritis and Rheumatism* **43**, 1571–1579. ISSN: 0004-3591 (July 2000).
163. Garcia, M. & Knight, M. M. Cyclic loading opens hemichannels to release ATP as part of a chondrocyte mechanotransduction pathway. *Journal of Orthopaedic Research: Official Publication of the Orthopaedic Research Society* **28**, 510–515. ISSN: 1554-527X (Apr. 2010).
164. Wann, A. *et al.* The primary cilium conducts chondrocyte mechanotransduction. *Cilia* **1**, P59, 2046–2530–1–S1–P59. ISSN: 2046-2530 (S1 Nov. 2012).
165. Ogawa, H., Kozhemyakina, E., Hung, H.-H., Grodzinsky, A. J. & Lassar, A. B. Mechanical motion promotes expression of Prg4 in articular cartilage via multiple CREB-dependent, fluid flow shear stress-induced signaling pathways. *Genes & Development* **28**, 127–139. ISSN: 1549-5477 (Jan. 15, 2014).

166. Hatori, M., Teixeira, C. C., Debolt, K., Pacifici, M. & Shapiro, I. M. Adenine nucleotide metabolism by chondrocytes in vitro: Role of ATP in chondrocyte maturation and matrix mineralization. *Journal of Cellular Physiology* **165**, 468–474. ISSN: 0021-9541, 1097-4652 (Dec. 1995).
167. Hung, C. T., Allen, F. D., Mansfield, K. D. & Shapiro, I. M. Extracellular ATP modulates  $[Ca^{2+}]_i$  in retinoic acid-treated embryonic chondrocytes. *The American Journal of Physiology* **272**, C1611–1617. ISSN: 0002-9513 (May 1997).
168. Koolpe, M. & Benton, H. P. Calcium-mobilizing purine receptors on the surface of mammalian articular chondrocytes. *Journal of Orthopaedic Research: Official Publication of the Orthopaedic Research Society* **15**, 204–212. ISSN: 0736-0266 (Mar. 1997).
169. Elfervig, M. K. *et al.* ATP induces  $Ca^{2+}$  signaling in human chondrons cultured in three-dimensional agarose films. *Osteoarthritis and Cartilage* **9**, 518–526. ISSN: 1063-4584 (Aug. 2001).
170. Caswell, A. M., Leong, W. S. & Russell, R. G. Interleukin- $1\beta$  enhances the response of human articular chondrocytes to extracellular ATP. *Biochimica et Biophysica Acta (BBA) - Molecular Cell Research* **1137**, 52–58. ISSN: 01674889 (Oct. 1992).
171. Corciulo, C. *et al.* Endogenous adenosine maintains cartilage homeostasis and exogenous adenosine inhibits osteoarthritis progression. *Nature Communications* **8**, 15019. ISSN: 2041-1723 (May 11, 2017).
172. Cronstein, B. N., Naime, D. & Ostad, E. The antiinflammatory mechanism of methotrexate. Increased adenosine release at inflamed sites diminishes leukocyte accumulation in an in vivo model of inflammation. *Journal of Clinical Investigation* **92**, 2675–2682. ISSN: 0021-9738 (Dec. 1, 1993).
173. Luo, H. *et al.* Prenatal caffeine exposure induces a poor quality of articular cartilage in male adult offspring rats via cholesterol accumulation in cartilage. *Scientific Reports* **5**, 17746. ISSN: 2045-2322 (Dec. 7, 2015).

174. Varani, K. *et al.* Characterization of adenosine receptors in bovine chondrocytes and fibroblast-like synoviocytes exposed to low frequency low energy pulsed electromagnetic fields. *Osteoarthritis and Cartilage* **16**, 292–304. ISSN: 10634584 (Mar. 2008).
175. Matta, C. *et al.* Purinergic signalling is required for calcium oscillations in migratory chondrogenic progenitor cells. *Pflügers Archiv - European Journal of Physiology* **467**, 429–442. ISSN: 0031-6768, 1432-2013 (Feb. 2015).
176. Shkhyan, R. *et al.* Genetic ablation of adenosine receptor A3 results in articular cartilage degeneration. *Journal of Molecular Medicine* **96**, 1049–1060. ISSN: 0946-2716, 1432-1440 (Oct. 2018).
177. Bai, H. *et al.* Activation of adenosine A3 receptor attenuates progression of osteoarthritis through inhibiting the NLRP3/caspase-1/GSDMD induced signalling. *Journal of Cellular and Molecular Medicine* **26**, 4230–4243. ISSN: 1582-4934 (Aug. 2022).
178. Corciulo, C. *et al.* Intraarticular injection of liposomal adenosine reduces cartilage damage in established murine and rat models of osteoarthritis. *Scientific Reports* **10**, 13477. ISSN: 2045-2322 (Aug. 10, 2020).
179. Castro, C. M. *et al.* Adenosine A2A receptor null chondrocyte transcriptome resembles that of human osteoarthritic chondrocytes. *Purinergic Signalling* **17**, 439–448. ISSN: 1573-9546 (Sept. 2021).
180. Castro, C. M. *et al.* Adenosine A2A receptor (A2AR) stimulation enhances mitochondrial metabolism and mitigates reactive oxygen species-mediated mitochondrial injury. *FASEB journal: official publication of the Federation of American Societies for Experimental Biology* **34**, 5027–5045. ISSN: 1530-6860 (Apr. 2020).
181. Friedman, B., Corciulo, C., Castro, C. M. & Cronstein, B. N. Adenosine A2A receptor signaling promotes FoxO associated autophagy in chondrocytes. *Scientific Reports* **11**, 968. ISSN: 2045-2322 (Jan. 13, 2021).
182. Friedman, B. *et al.* Adenosine A2A receptor activation reduces chondrocyte senescence. *The FASEB Journal* **37**, e22838. ISSN: 0892-6638, 1530-6860 (Apr. 2023).

183. Li, D., Cronstein, B. N., Cook, J., Bozynski, C. & Angle, S. *Intra-articular injections of two liposomal adenosine formulations provide significant pain relief and gain in function, improve comfortable range of motion and slowed radiologic progression in a preclinical canine model of osteoarthritis.* in *Scientific Abstracts EULAR 2023 European Congress of Rheumatology*, 31 May - 3 June. Milan, Italy (BMJ Publishing Group Ltd and European League Against Rheumatism, June 2023), 133.1–133.
184. Tan, L., Zhao, B., Ge, F.-T., Sun, D.-H. & Yu, T. Shockwaves Inhibit Chondrogenic Differentiation of Human Mesenchymal Stem Cells in Association with Adenosine and A2B Receptors. *Scientific Reports* **7**, 14377. ISSN: 2045-2322 (Oct. 30, 2017).
185. Carroll, S. H. *et al.* A2B Adenosine Receptor Promotes Mesenchymal Stem Cell Differentiation to Osteoblasts and Bone Formation in Vivo. *Journal of Biological Chemistry* **287**, 15718–15727. ISSN: 00219258 (May 2012).
186. Knight, M. M., McGlashan, S. R., Garcia, M., Jensen, C. G. & Poole, C. A. Articular chondrocytes express connexin 43 hemichannels and P2 receptors - a putative mechanoreceptor complex involving the primary cilium? *Journal of Anatomy* **214**, 275–283. ISSN: 1469-7580 (Feb. 2009).
187. Chowdhury, T. T. & Knight, M. M. Purinergic pathway suppresses the release of .NO and stimulates proteoglycan synthesis in chondrocyte/agarose constructs subjected to dynamic compression. *Journal of Cellular Physiology* **209**, 845–853. ISSN: 0021-9541 (Dec. 2006).
188. Pingguan-Murphy, B., El-Azzeh, M., Bader, D. L. & Knight, M. M. Cyclic compression of chondrocytes modulates a purinergic calcium signalling pathway in a strain rate- and frequency-dependent manner. *Journal of Cellular Physiology* **209**, 389–397. ISSN: 0021-9541 (Nov. 2006).
189. He, Z. *et al.* Strain-induced mechanotransduction through primary cilia, extracellular ATP, purinergic calcium signaling, and ERK1/2 transactivates CITED2 and downregulates MMP-1 and MMP-13 gene expression in chondrocytes. *Osteoarthritis and Cartilage* **24**, 892–901. ISSN: 10634584 (May 2016).

190. Rosenthal, A. K. *et al.* The progressive ankylosis gene product ANK regulates extracellular ATP levels in primary articular chondrocytes. *Arthritis Research & Therapy* **15**, R154. ISSN: 1478-6362 (Oct. 17, 2013).
191. Rosenthal, A. K. & Ryan, L. M. Calcium Pyrophosphate Deposition Disease. *The New England Journal of Medicine* **374**, 2575–2584. ISSN: 1533-4406 (June 30, 2016).
192. Gadjanski, I., Yodmuang, S., Spiller, K., Bhumiratana, S. & Vunjak-Novakovic, G. Supplementation of exogenous adenosine 5'-triphosphate enhances mechanical properties of 3D cell-agarose constructs for cartilage tissue engineering. *Tissue Engineering. Part A* **19**, 2188–2200. ISSN: 1937-335X (Oct. 2013).
193. Usprech, J., Chu, G., Giardini-Rosa, R., Martin, K. & Waldman, S. D. The Therapeutic Potential of Exogenous Adenosine Triphosphate (ATP) for Cartilage Tissue Engineering. *Cartilage* **3**, 364–373. ISSN: 1947-6035 (Oct. 2012).
194. Kwon, H. J. Extracellular ATP signaling via P2X(4) receptor and cAMP/PKA signaling mediate ATP oscillations essential for prechondrogenic condensation. *The Journal of Endocrinology* **214**, 337–348. ISSN: 1479-6805 (Sept. 2012).
195. Fodor, J. *et al.* Iontropic purinergic receptor P2X4 is involved in the regulation of chondrogenesis in chicken micromass cell cultures. *Cell Calcium* **45**, 421–430. ISSN: 01434160 (May 2009).
196. Adinolfi, E. *et al.* The P2X7 receptor: A main player in inflammation. *Biochemical Pharmacology* **151**, 234–244. ISSN: 1873-2968 (May 2018).
197. Tanigawa, H. *et al.* P2X7 ionotropic receptor is functionally expressed in rabbit articular chondrocytes and mediates extracellular ATP cytotoxicity. *Purinergic Signalling* **14**, 245–258. ISSN: 1573-9546 (Sept. 2018).
198. Li, Z. *et al.* P2X7 Receptor Induces Pyroptotic Inflammation and Cartilage Degradation in Osteoarthritis via NF- $\kappa$ B/NLRP3 Crosstalk. *Oxidative Medicine and Cellular Longevity* **2021**, 8868361. ISSN: 1942-0994 (2021).

199. Hu, H., Yang, B., Li, Y., Zhang, S. & Li, Z. Blocking of the P2X7 receptor inhibits the activation of the MMP-13 and NF- $\kappa$ B pathways in the cartilage tissue of rats with osteoarthritis. *International Journal of Molecular Medicine* **38**, 1922–1932. ISSN: 1107-3756, 1791-244X (Dec. 2016).
200. Szustak, M. & Gendaszewska-Darmach, E. Extracellular Nucleotides Selectively Induce Migration of Chondrocytes and Expression of Type II Collagen. *International Journal of Molecular Sciences* **21**. ISSN: 1422-0067 (July 23, 2020).
201. Kudirka, J. C., Panupinthu, N., Tesseyman, M. A., Dixon, S. J. & Bernier, S. M. P2Y nucleotide receptor signaling through MAPK/ERK is regulated by extracellular matrix: involvement of beta3 integrins. *Journal of Cellular Physiology* **213**, 54–64. ISSN: 0021-9541 (Oct. 2007).
202. Berenbaum, F., Humbert, L., Bereziat, G. & Thirion, S. Concomitant recruitment of ERK1/2 and p38 MAPK signalling pathway is required for activation of cytoplasmic phospholipase A2 via ATP in articular chondrocytes. *The Journal of Biological Chemistry* **278**, 13680–13687. ISSN: 0021-9258 (Apr. 18, 2003).
203. Xing, Y., Gu, Y., Gomes, R. R. & You, J. P2Y(2) receptors and GRK2 are involved in oscillatory fluid flow induced ERK1/2 responses in chondrocytes. *Journal of Orthopaedic Research: Official Publication of the Orthopaedic Research Society* **29**, 828–833. ISSN: 1554-527X (June 2011).
204. Garcia, A. E., Mada, S. R., Rico, M. C., Dela Cadena, R. A. & Kunapuli, S. P. Clopidogrel, a P2Y12 receptor antagonist, potentiates the inflammatory response in a rat model of peptidoglycan polysaccharide-induced arthritis. *PloS One* **6**, e26035. ISSN: 1932-6203 (2011).
205. Wang, D., Lin, N., Tang, Y. & Lu, H. Inhibition of P2Y11R ameliorated TNF- $\alpha$ -induced degradation of extracellular matrix in human chondrocytic SW1353 cells. *American Journal of Translational Research* **11**, 2108–2116. ISSN: 1943-8141 (2019).

206. Wang, C. *et al.* Titanium dioxide nanotubes increase purinergic receptor P2Y<sub>6</sub> expression and activate its downstream PKC $\alpha$ -ERK1/2 pathway in bone marrow mesenchymal stem cells under osteogenic induction. *Acta Biomaterialia* **157**, 670–682. ISSN: 17427061 (Feb. 2023).
207. Jimi, E., Fei, H. & Nakatomi, C. NF- $\kappa$ B Signaling Regulates Physiological and Pathological Chondrogenesis. *International Journal of Molecular Sciences* **20**, 6275. ISSN: 1422-0067 (Dec. 12, 2019).
208. Meyer, M. P., Swann, K., Burnstock, G. & Clarke, J. D. The extracellular ATP receptor, cP2Y(1), inhibits cartilage formation in micromass cultures of chick limb mesenchyme. *Developmental Dynamics: An Official Publication of the American Association of Anatomists* **222**, 494–505. ISSN: 1058-8388 (Nov. 2001).
209. Barter, M. J. *et al.* Genome-Wide MicroRNA and Gene Analysis of Mesenchymal Stem Cell Chondrogenesis Identifies an Essential Role and Multiple Targets for miR-140-5p. *Stem Cells (Dayton, Ohio)* **33**, 3266–3280. ISSN: 1549-4918 (Nov. 2015).
210. Schmittgen, T. D. & Livak, K. J. Analyzing real-time PCR data by the comparative C(T) method. *Nature Protocols* **3**, 1101–1108. ISSN: 1750-2799 (2008).
211. Pires, B. R. B. *et al.* NF-kappaB Regulates Redox Status in Breast Cancer Subtypes. *Genes* **9**, E320. ISSN: 2073-4425 (June 26, 2018).
212. Tabak, S., Schreiber-Avissar, S. & Beit-Yannai, E. Trabecular meshwork's collagen network formation is inhibited by non-pigmented ciliary epithelium-derived extracellular vesicles. *Journal of Cellular and Molecular Medicine* **25**, 3339–3347. ISSN: 1582-1838, 1582-4934 (Apr. 2021).
213. Love, M. I., Huber, W. & Anders, S. Moderated estimation of fold change and dispersion for RNA-seq data with DESeq2. *Genome Biology* **15**, 550. ISSN: 1474-760X (Dec. 2014).
214. Ran, F. A. *et al.* Genome engineering using the CRISPR-Cas9 system. *Nature Protocols* **8**, 2281–2308. ISSN: 1750-2799 (Nov. 2013).

215. Brinkman, E. K. & van Steensel, B. Rapid Quantitative Evaluation of CRISPR Genome Editing by TIDE and TIDER. *Methods in Molecular Biology (Clifton, N.J.)* **1961**, 29–44. ISSN: 1940-6029 (2019).
216. Bloh, K. *et al.* Deconvolution of Complex DNA Repair (DECODR): Establishing a Novel Deconvolution Algorithm for Comprehensive Analysis of CRISPR-Edited Sanger Sequencing Data. *The CRISPR Journal* **4**, 120–131. ISSN: 2573-1599, 2573-1602 (Feb. 1, 2021).
217. Hsiao, T. *et al.* *Inference of CRISPR Edits from Sanger Trace Data* preprint (Bioinformatics, Jan. 20, 2018).
218. Pinto-Cardoso, R. *et al.* Adenosinergic signalling in chondrogenesis and cartilage homeostasis: Friend or foe? *Biochemical Pharmacology* **174**, 113784. ISSN: 1873-2968 (Apr. 2020).
219. Soul, J., Hardingham, T. E., Boot-Handford, R. P. & Schwartz, J.-M. SkeletalVis: an exploration and meta-analysis data portal of cross-species skeletal transcriptomics data. *Bioinformatics (Oxford, England)* **35**, 2283–2290. ISSN: 1367-4811 (July 1, 2019).
220. Xu, Y. *et al.* Identification of the pathogenic pathways in osteoarthritic hip cartilage: commonality and discord between hip and knee OA. *Osteoarthritis and Cartilage* **20**, 1029–1038. ISSN: 1522-9653 (Sept. 2012).
221. Snelling, S. *et al.* A gene expression study of normal and damaged cartilage in anteromedial gonarthrosis, a phenotype of osteoarthritis. *Osteoarthritis and Cartilage* **22**, 334–343. ISSN: 1522-9653 (Feb. 2014).
222. Soul, J. *et al.* Stratification of knee osteoarthritis: two major patient subgroups identified by genome-wide expression analysis of articular cartilage. *Annals of the Rheumatic Diseases* **77**, 423. ISSN: 1468-2060 (Mar. 2018).
223. Ramos, Y. F. M. *et al.* Genes involved in the osteoarthritis process identified through genome wide expression analysis in articular cartilage; the RAAK study. *PloS One* **9**, e103056. ISSN: 1932-6203 (2014).
224. Dunn, S. L. *et al.* Gene expression changes in damaged osteoarthritic cartilage identify a signature of non-chondrogenic and mechanical responses. *Osteoarthritis and Cartilage* **24**, 1431–1440. ISSN: 1522-9653 (Aug. 2016).

225. Hou, M. *et al.* UDP acts as a growth factor for vascular smooth muscle cells by activation of P2Y(6) receptors. *American Journal of Physiology. Heart and Circulatory Physiology* **282**, H784–792. ISSN: 0363-6135 (Feb. 2002).
226. Goldring, M. B. Immortalization of human articular chondrocytes for generation of stable, differentiated cell lines. *Methods in Molecular Medicine* **100**, 23–36. ISSN: 1543-1894 (2004).
227. Goldring, M. B. *et al.* Interleukin-1 beta-modulated gene expression in immortalized human chondrocytes. *The Journal of Clinical Investigation* **94**, 2307–2316. ISSN: 0021-9738 (Dec. 1994).
228. Gebauer, M. *et al.* Comparison of the chondrosarcoma cell line SW1353 with primary human adult articular chondrocytes with regard to their gene expression profile and reactivity to IL-1beta. *Osteoarthritis and Cartilage* **13**, 697–708. ISSN: 1063-4584 (Aug. 2005).
229. Inayama, M. *et al.* Orai1–Orai2 complex is involved in store-operated calcium entry in chondrocyte cell lines. *Cell Calcium* **57**, 337–347. ISSN: 01434160 (May 2015).
230. Winklmayr, M. *et al.* Dose-Dependent Cannabidiol-Induced Elevation of Intracellular Calcium and Apoptosis in Human Articular Chondrocytes. *Journal of Orthopaedic Research: Official Publication of the Orthopaedic Research Society* **37**, 2540–2549. ISSN: 1554-527X (Dec. 2019).
231. Hammer, A. *et al.* Retrograde Analysis of Calcium Signaling by CaMPARI2 Shows Cytosolic Calcium in Chondrocytes Is Unaffected by Parabolic Flights. *Biomedicines* **10**, 138. ISSN: 2227-9059 (Jan. 8, 2022).
232. Wang, H., Wu, H., Fang, K. & Chang, X. Uridine Diphosphate Promotes Rheumatoid Arthritis Through P2Y6 Activation. *Frontiers in Pharmacology* **12**, 658511. ISSN: 1663-9812 (2021).
233. Ali, S., Turner, J. & Fountain, S. J. P2Y2 and P2Y6 receptor activation elicits intracellular calcium responses in human adipose-derived mesenchymal stromal cells. *Purinergic Signalling* **14**, 371–384. ISSN: 1573-9546 (Dec. 2018).

234. Sil, P. *et al.* P2Y6 Receptor Antagonist MRS2578 Inhibits Neutrophil Activation and Aggregated Neutrophil Extracellular Trap Formation Induced by Gout-Associated Monosodium Urate Crystals. *The Journal of Immunology* **198**, 428–442. ISSN: 0022-1767, 1550-6606 (Jan. 1, 2017).
235. Mamedova, L. K., Joshi, B. V., Gao, Z.-G., von Kügelgen, I. & Jacobson, K. A. Diisothiocyanate derivatives as potent, insurmountable antagonists of P2Y6 nucleotide receptors. *Biochemical Pharmacology* **67**, 1763–1770. ISSN: 0006-2952 (May 1, 2004).
236. Fan, Z., Söder, S., Oehler, S., Fundel, K. & Aigner, T. Activation of interleukin-1 signaling cascades in normal and osteoarthritic articular cartilage. *The American Journal of Pathology* **171**, 938–946. ISSN: 0002-9440 (Sept. 2007).
237. Elamir, A. M., Zahra, A., Senara, S. H., Ezzat, E. M. & El Sayed, H. S. Diagnostic value of matrix metalloproteinases-1, -3 and -13 in patients with primary knee osteoarthritis: Relation to radiological severity. *The Egyptian Rheumatologist* **45**, 17–20. ISSN: 11101164 (Jan. 2023).
238. Rawlings, N. D. & Salvesen, G. *Handbook of proteolytic enzymes* 3rd ed. ISBN: 978-0-12-382219-2 (Academic Press, Boston London, 2013).
239. Riegel, A.-K. *et al.* Selective induction of endothelial P2Y6 nucleotide receptor promotes vascular inflammation. *Blood* **117**, 2548–2555. ISSN: 1528-0020 (Feb. 24, 2011).
240. McCall, M. N., McMurray, H. R., Land, H. & Almudevar, A. On non-detects in qPCR data. *Bioinformatics (Oxford, England)* **30**, 2310–2316. ISSN: 1367-4811 (Aug. 15, 2014).
241. Lim, H. & Kim, H. P. Matrix metalloproteinase-13 expression in IL-1 $\beta$ -treated chondrocytes by activation of the p38 MAPK/c-Fos/AP-1 and JAK/STAT pathways. *Archives of Pharmacal Research* **34**, 109–117. ISSN: 1976-3786 (Jan. 2011).
242. Newton, P. T. *et al.* Chondrogenic ATDC5 cells: an optimised model for rapid and physiological matrix mineralisation. *International Journal of Molecular Medicine* **30**, 1187–1193. ISSN: 1791-244X (Nov. 2012).

243. Doench, J. G. *et al.* Optimized sgRNA design to maximize activity and minimize off-target effects of CRISPR-Cas9. *Nature Biotechnology* **34**, 184–191. ISSN: 1546-1696 (Feb. 2016).
244. Wilhelm, D., Kempf, H., Bianchi, A. & Vincourt, J.-B. ATDC5 cells as a model of cartilage extracellular matrix neosynthesis, maturation and assembly. *Journal of Proteomics* **219**, 103718. ISSN: 1876-7737 (May 15, 2020).
245. Atsumi, T., Miwa, Y., Kimata, K. & Ikawa, Y. A chondrogenic cell line derived from a differentiating culture of AT805 teratocarcinoma cells. *Cell Differentiation and Development: The Official Journal of the International Society of Developmental Biologists* **30**, 109–116. ISSN: 0922-3371 (May 1990).
246. Du, X. *et al.* The Role of a Selective P2Y6 Receptor Antagonist, MRS2578, on the Formation of Angiotensin II-Induced Abdominal Aortic Aneurysms. *BioMed Research International* **2020**, 1983940. ISSN: 2314-6141 (2020).
247. Wen, R.-X. *et al.* P2Y6 receptor inhibition aggravates ischemic brain injury by reducing microglial phagocytosis. *CNS Neuroscience & Therapeutics* **26**, 416–429. ISSN: 1755-5930, 1755-5949 (Apr. 2020).
248. Li, X. *et al.* Blockade of the LRP16-PKR-NF- $\kappa$ B signaling axis sensitizes colorectal carcinoma cells to DNA-damaging cytotoxic therapy. *eLife* **6**, e27301. ISSN: 2050-084X (Aug. 18, 2017).
249. Caron, M. M. J. *et al.* Activation of NF- $\kappa$ B/p65 Facilitates Early Chondrogenic Differentiation during Endochondral Ossification. *PLoS ONE* **7** (ed Beier, F.) e33467. ISSN: 1932-6203 (Mar. 12, 2012).
250. Rockel, J. S., Kudirka, J. C., Guzi, A. J. & Bernier, S. M. Regulation of Sox9 activity by crosstalk with nuclear factor- $\kappa$ B and retinoic acid receptors. *Arthritis Research & Therapy* **10**, R3. ISSN: 1478-6354 (2008).
251. Wang, W., Rigueur, D. & Lyons, K. M. TGF $\beta$  signaling in cartilage development and maintenance. *Birth Defects Research. Part C, Embryo Today: Reviews* **102**, 37–51. ISSN: 1542-9768 (Mar. 2014).
252. Cong, L. *et al.* Multiplex genome engineering using CRISPR/Cas systems. *Science (New York, N.Y.)* **339**, 819–823. ISSN: 1095-9203 (Feb. 15, 2013).

253. Malmjö, M., Hou, M., Pendergast, W., Erlinge, D. & Edvinsson, L. The stable pyrimidines UDP $\beta$ S and UTP $\gamma$ S discriminate between contractile cerebrovascular P2 receptors. *European Journal of Pharmacology* **458**, 305–311. ISSN: 00142999 (Jan. 2003).
254. Maubach, G. *et al.* TIFA has dual functions in Helicobacter pylori-induced classical and alternative NF- $\kappa$ B pathways. *EMBO reports* **22**, e52878. ISSN: 1469-3178 (Sept. 6, 2021).
255. Ashburner, M. *et al.* Gene Ontology: tool for the unification of biology. *Nature Genetics* **25**, 25–29. ISSN: 1061-4036, 1546-1718 (May 2000).
256. Milacic, M. *et al.* The Reactome Pathway Knowledgebase 2024. *Nucleic Acids Research* **52**, D672–D678. ISSN: 0305-1048, 1362-4962 (D1 Jan. 5, 2024).
257. Kanehisa, M. & Goto, S. KEGG: kyoto encyclopedia of genes and genomes. *Nucleic Acids Research* **28**, 27–30. ISSN: 0305-1048 (Jan. 1, 2000).
258. Chen, E. Y. *et al.* Enrichr: interactive and collaborative HTML5 gene list enrichment analysis tool. *BMC bioinformatics* **14**, 128. ISSN: 1471-2105 (Apr. 15, 2013).
259. Tarrant, M. K. & Cole, P. A. The chemical biology of protein phosphorylation. *Annual Review of Biochemistry* **78**, 797–825. ISSN: 1545-4509 (2009).
260. Zhao, S. *et al.* Next generation sequencing is a highly reliable method to analyze exon 7 deletion of survival motor neuron 1 (SMN1) gene. *Scientific Reports* **12**, 223. ISSN: 2045-2322 (Jan. 7, 2022).
261. Robaye, B., Boeynaems, J.-M. & Communi, D. Slow desensitization of the human P2Y6 receptor. *European Journal of Pharmacology* **329**, 231–236. ISSN: 00142999 (June 1997).
262. Imai, T. & Yasuda, N. Therapeutic intervention of inflammatory/immune diseases by inhibition of the fractalkine (CX3CL1)-CX3CR1 pathway. *Inflammation and Regeneration* **36**, 9. ISSN: 1880-8190 (Dec. 2016).
263. Yano, R. *et al.* Recruitment of CD16+ monocytes into synovial tissues is mediated by fractalkine and CX3CR1 in rheumatoid arthritis patients. *Acta Medica Okayama* **61**, 89–98. ISSN: 0386-300X (Apr. 2007).

264. Sandell, L. *et al.* Exuberant expression of chemokine genes by adult human articular chondrocytes in response to IL-1 $\beta$ . *Osteoarthritis and Cartilage* **16**, 1560–1571. ISSN: 10634584 (Dec. 2008).
265. Borzi, R. M. *et al.* Flow cytometric analysis of intracellular chemokines in chondrocytes in vivo: constitutive expression and enhancement in osteoarthritis and rheumatoid arthritis. *FEBS letters* **455**, 238–242. ISSN: 0014-5793 (July 23, 1999).
266. Zhang, Y. *et al.* CC chemokines and receptors in osteoarthritis: new insights and potential targets. *Arthritis Research & Therapy* **25**, 113. ISSN: 1478-6362 (July 3, 2023).
267. Liao, Y. *et al.* Interleukin-6 signaling mediates cartilage degradation and pain in posttraumatic osteoarthritis in a sex-specific manner. *Science Signaling* **15**, eabn7082. ISSN: 1945-0877, 1937-9145 (July 26, 2022).
268. Lilienbaum, A. & Israël, A. From calcium to NF-kappa B signaling pathways in neurons. *Molecular and Cellular Biology* **23**, 2680–2698. ISSN: 0270-7306 (Apr. 2003).
269. Berry, C. T., May, M. J. & Freedman, B. D. STIM- and Orai-mediated calcium entry controls NF- $\kappa$ B activity and function in lymphocytes. *Cell Calcium* **74**, 131–143. ISSN: 1532-1991 (Sept. 2018).
270. Chen, B. C. & Lin, W. W. Pyrimidinoceptor potentiation of macrophage PGE(2) release involved in the induction of nitric oxide synthase. *British Journal of Pharmacology* **130**, 777–786. ISSN: 0007-1188 (June 2000).
271. Salem, M., Tremblay, A., Pelletier, J., Robaye, B. & Sévigny, J. P2Y6 Receptors Regulate CXCL10 Expression and Secretion in Mouse Intestinal Epithelial Cells. *Frontiers in Pharmacology* **9**, 149. ISSN: 1663-9812 (2018).
272. Grbic, D. M., Degagné, É., Langlois, C., Dupuis, A.-A. & Gendron, F.-P. Intestinal Inflammation Increases the Expression of the P2Y6 Receptor on Epithelial Cells and the Release of CXC Chemokine Ligand 8 by UDP. *The Journal of Immunology* **180**, 2659–2668. ISSN: 0022-1767, 1550-6606 (Feb. 15, 2008).

273. Mamedova, L. K., Wang, R., Besada, P., Liang, B. T. & Jacobson, K. A. Attenuation of apoptosis in vitro and ischemia/reperfusion injury in vivo in mouse skeletal muscle by P2Y6 receptor activation. *Pharmacological Research* **58**, 232–239. ISSN: 1043-6618 (2008).
274. Trinh, D. V., Zhu, N., Farhang, G., Kim, B. J. & Huxford, T. The nuclear I kappaB protein I kappaB zeta specifically binds NF-kappaB p50 homodimers and forms a ternary complex on kappaB DNA. *Journal of Molecular Biology* **379**, 122–135. ISSN: 1089-8638 (May 23, 2008).
275. Feng, Y. *et al.* The central inflammatory regulator I $\kappa$ B $\zeta$ : induction, regulation and physiological functions. *Frontiers in Immunology* **14**, 1188253. ISSN: 1664-3224 (June 12, 2023).
276. Choi, M. E., Ding, Y. & Kim, S. I. TGF- $\beta$  signaling via TAK1 pathway: role in kidney fibrosis. *Seminars in Nephrology* **32**, 244–252. ISSN: 1558-4488 (May 2012).
277. Platanitis, E. & Decker, T. Regulatory Networks Involving STATs, IRFs, and NF $\kappa$ B in Inflammation. *Frontiers in Immunology* **9**, 2542. ISSN: 1664-3224 (Nov. 13, 2018).
278. Yang, Q. *et al.* Interferonregulatoryfactor-8(IRF-8) regulates the expression of matrix metalloproteinase-13 (MMP-13) in chondrocytes. *Cell Stress & Chaperones* **23**, 393–398. ISSN: 1466-1268 (May 2018).
279. Simon, P. S. *et al.* The NF- $\kappa$ B p65 and p50 homodimer cooperate with IRF8 to activate iNOS transcription. *BMC Cancer* **15**, 770. ISSN: 1471-2407 (Dec. 2015).
280. Xu, J. *et al.* NOD2 pathway via RIPK2 and TBK1 is involved in the aberrant catabolism induced by T-2 toxin in chondrocytes. *Osteoarthritis and Cartilage* **23**, 1575–1585. ISSN: 10634584 (Sept. 2015).
281. Hwang, H. S., Lee, M. H., Choi, M. H. & Kim, H. A. NOD2 signaling pathway is involved in fibronectin fragment-induced pro-catabolic factor expressions in human articular chondrocytes. *BMB reports* **52**, 373–378. ISSN: 1976-670X (June 2019).

282. Meini, S. & Maggi, C. A. Knee osteoarthritis: a role for bradykinin? *Inflammation Research* **57**, 351–361. ISSN: 1023-3830, 1420-908X (Aug. 2008).
283. Meini, S. *et al.* Bradykinin and B<sup>2</sup> receptor antagonism in rat and human articular chondrocytes. *British Journal of Pharmacology* **162**, 611–622. ISSN: 1476-5381 (Feb. 2011).
284. Chen, S., Zhou, Y., Li, J., Shan, L.-Q. & Fan, Q.-Y. The effect of bradykinin B2 receptor polymorphisms on the susceptibility and severity of osteoarthritis in a Chinese cohort. *Journal of Biomedicine & Biotechnology* **2012**, 597637. ISSN: 1110-7251 (2012).
285. Hebenstreit, D., Wirnsberger, G., Horejs-Hoeck, J. & Duschl, A. Signaling mechanisms, interaction partners, and target genes of STAT6. *Cytokine & Growth Factor Reviews* **17**, 173–188. ISSN: 1359-6101 (June 2006).
286. Millward-Sadler, S., Khan, N., Bracher, M., Wright, M. & Salter, D. Roles for the interleukin-4 receptor and associated JAK/STAT proteins in human articular chondrocyte mechanotransduction. *Osteoarthritis and Cartilage* **14**, 991–1001. ISSN: 10634584 (Oct. 2006).
287. Zhou, Q. *et al.* The potential roles of JAK/STAT signaling in the progression of osteoarthritis. *Frontiers in Endocrinology* **13**, 1069057. ISSN: 1664-2392 (2022).
288. Rachakonda, P. S., Rai, M. F., Manning, K. & Schmidt, M. F. G. Expression of canine interleukin-4 in canine chondrocytes inhibits inflammatory cascade through STAT6. *Cytokine* **44**, 179–184. ISSN: 1096-0023 (Oct. 2008).
289. Woods, J. M. *et al.* IL-4 adenoviral gene therapy reduces inflammation, proinflammatory cytokines, vascularization, and bony destruction in rat adjuvant-induced arthritis. *Journal of Immunology (Baltimore, Md.: 1950)* **166**, 1214–1222. ISSN: 0022-1767 (Jan. 15, 2001).
290. Assirelli, E. *et al.* Human Osteoarthritic Cartilage Shows Reduced In Vivo Expression of IL-4, a Chondroprotective Cytokine that Differentially Modulates IL-1 $\beta$ -Stimulated Production of Chemokines and Matrix-Degrading Enzymes In Vitro. *PLoS ONE* **9** (ed Tsilibary, E. C.) e96925. ISSN: 1932-6203 (May 12, 2014).

291. Van Meegeren, M. *et al.* IL-4 alone and in combination with IL-10 protects against blood-induced cartilage damage. *Osteoarthritis and Cartilage* **20**, 764–772. ISSN: 10634584 (July 2012).
292. Forster, T., Chapman, K. & Loughlin, J. Common variants within the interleukin 4 receptor alpha gene (IL4R) are associated with susceptibility to osteoarthritis. *Human Genetics* **114**, 391–395. ISSN: 0340-6717 (Mar. 2004).
293. Yang, X. *et al.* TGF-beta/Smad3 signals repress chondrocyte hypertrophic differentiation and are required for maintaining articular cartilage. *The Journal of Cell Biology* **153**, 35–46. ISSN: 0021-9525 (Apr. 2, 2001).
294. Van Der Kraan, P. M. Inhibition of transforming growth factor- $\beta$  in osteoarthritis. Discrepancy with reduced TGF $\beta$  signaling in normal joints. *Osteoarthritis and Cartilage Open* **4**, 100238. ISSN: 26659131 (Mar. 2022).
295. Genetos, D. C., Karin, N. J., Geist, D. J., Donahue, H. J. & Duncan, R. L. Purinergic signaling is required for fluid shear stress-induced NF- $\kappa$ B translocation in osteoblasts. *Experimental Cell Research* **317**, 737–744. ISSN: 1090-2422 (Apr. 1, 2011).
296. Hansen, A. *et al.* The P2Y6 receptor mediates Clostridium difficile toxin-induced CXCL8/IL-8 production and intestinal epithelial barrier dysfunction. *PloS One* **8**, e81491. ISSN: 1932-6203 (2013).
297. Morioka, N. *et al.* The activation of P2Y6 receptor in cultured spinal microglia induces the production of CCL2 through the MAP kinases-NF- $\kappa$ B pathway. *Neuropharmacology* **75**, 116–125. ISSN: 00283908 (Dec. 2013).
298. Mead, T. J. & Yutzey, K. E. Notch pathway regulation of chondrocyte differentiation and proliferation during appendicular and axial skeleton development. *Proceedings of the National Academy of Sciences* **106**, 14420–14425. ISSN: 0027-8424, 1091-6490 (Aug. 25, 2009).
299. Harima, Y. & Kageyama, R. Oscillatory links of Fgf signaling and Hes7 in the segmentation clock. *Current Opinion in Genetics & Development* **23**, 484–490. ISSN: 1879-0380 (Aug. 2013).

300. Takahashi, Y. *et al.* Transcription factors Mesp2 and Paraxis have critical roles in axial musculoskeletal formation. *Developmental Dynamics: An Official Publication of the American Association of Anatomists* **236**, 1484–1494. ISSN: 1058-8388 (June 2007).
301. Saito, T. & Tanaka, S. Molecular mechanisms underlying osteoarthritis development: Notch and NF- $\kappa$ B. *Arthritis Research & Therapy* **19**, 94. ISSN: 1478-6362 (Dec. 2017).
302. Hussen, B. M., Azimi, T., Hidayat, H. J., Taheri, M. & Ghafouri-Fard, S. NF-KappaB interacting LncRNA: Review of its roles in neoplastic and non-neoplastic conditions. *Biomedicine & Pharmacotherapy* **139**, 111604. ISSN: 07533322 (July 2021).
303. Kanamoto, T. *et al.* Integrin  $\alpha$ 2 $\beta$ 1 plays an important role in the interaction between human articular cartilage-derived chondrocytes and atelocollagen gel. *Scientific Reports* **11**, 1757. ISSN: 2045-2322 (Jan. 19, 2021).
304. Fahrner, J. A. *et al.* Precocious chondrocyte differentiation disrupts skeletal growth in Kabuki syndrome mice. *JCI insight* **4**, e129380, 129380. ISSN: 2379-3708 (Oct. 17, 2019).
305. Communi, D., Parmentier, M. & Boeynaems, J. M. Cloning, functional expression and tissue distribution of the human P2Y6 receptor. *Biochemical and Biophysical Research Communications* **222**, 303–308. ISSN: 0006-291X (May 15, 1996).
306. Lazarowski, E. R. & Boucher, R. C. UTP as an Extracellular Signaling Molecule. *Physiology* **16**, 1–5. ISSN: 1548-9213, 1548-9221 (Feb. 2001).
307. Lazarowski, E. R., Homolya, L., Boucher, R. C. & Harden, T. K. Direct Demonstration of Mechanically Induced Release of Cellular UTP and Its Implication for Uridine Nucleotide Receptor Activation. *Journal of Biological Chemistry* **272**, 24348–24354. ISSN: 00219258 (Sept. 1997).
308. Hames, B. D., Hooper, N. M. & Hames, B. D. *Biochemistry* 4. ed. 473 pp. ISBN: 978-0-415-60845-9 (Garland Science, New York London, 2011).

309. Kwon, H. J. *et al.* Synchronized ATP oscillations have a critical role in pre-chondrogenic condensation during chondrogenesis. *Cell Death & Disease* **3**, e278–e278. ISSN: 2041-4889 (Mar. 2012).
310. Ito, M. *et al.* Identification of novel selective P2Y6 receptor antagonists by high-throughput screening assay. *Life Sciences* **180**, 137–142. ISSN: 1879-0631 (July 1, 2017).
311. Kitagawa, A. *et al.* Genistein inhibits chondrogenic differentiation and mineralization of ATDC5 cells. *Biochemical and Biophysical Research Communications* **566**, 123–128. ISSN: 1090-2104 (Aug. 20, 2021).
312. Kashfi, S. *et al.* Purinergic Receptor Expression and Potential Association with Human Embryonic Stem Cell-Derived Oligodendrocyte Progenitor Cell Development. *Cell Journal* **19**, 386–402. ISSN: 2228-5806 (Oct. 2017).

# Chapter 8

## Appendix

### 8.1 Primer Sequences

**Table 8.1:** Mouse qPCR Primers SYBR. Primers 1-6 Taken from [311].

Gene	Sequence (5' → 3')	Amplicon Size
<i>β</i> -ACTIN	F: CTTGGGTATGGAATCCTGTGG R: GTACTTGCGCTCAGGAGGAG	214
AGGRECAN	F: GGTCACTGTTACCGCCACTT R: GCCAGATCATCACCACACAG	280
COL2A1	F: GGCTCCCAGAACATCACCTA R: GCCCCACTTACCAGTGTGTT	186
COL10A1	F: ATGCCCGTGTCTGCTTTTAC R: TGAGTCCCTTTCACATGCAC	182
SOX9	F: AATCTCCTGGACCCCTTCAT R: TCCTCGCTCTCCTTCTTCAG	194
RUNX2	F: GCCGGGAATGATGAGAACTA R: GGACCGTCCACTGTCACTTT	200
P2RY6	F: GGCAACCCACGATCTCTTA R: AAACACATTGCAGCCAGTGC	100
ADORA2B	F: CCATGCAGCTAGAGACGCAA R: TTGGTGGGGGTCTGTAATGC	130
BDKRB1	F: GGCAGCTTCTGATCTGGTGT R: GTCACTTCCAAAGGGCCAGT	88
NOD2	F: TCTGGAGGTTTGGCTTCGAG R: TCACAACAAGAGTCTGGCGT	85
IL6	F: GTCCTTCCTACCCCAATTTCCA R: TGGTCTTGGTCCTTAGCCAC	79
CCL8	F: TCCAGTCACCTGCTGCTTTC R: ACCCTGCTTGGTCTGGAAAA	124
CXCL2	F: GCTGTCCCTCAACGGAAGAA R: CAGGTACGATCCAGGCTTCC	72

**Table 8.2:** ATDC5 CRISPR sequencing primers

Gene	Sequence (5' → 3')	Amplicon Size
Plasmid Seq Primers	F: CTCTCCGAGCATAGGAAAGG R: GATGACCGTGAGGGCCATAC	630
RNP Seq Primers	F: GAAAGAACGGGGTTGCCAGT R: CTGTCTTGGTGATGTGGAAA	872
Cas9 Genomic DNA Primers	F: GACAATCTGACCAAGGCCGA R: CTTCCGGAAATCGGACACCA	213

**Table 8.3:** Human SYBR qPCR Primers. Taken from [312].

Gene	Sequence (5' → 3')	Amplicon Size
A1	F: CTTCTTTGTGTGGGTGCT R: CTGCTTGCGGATTAGGTAG	79
A2A	F: CCCAGAGGTGACATTTGAC R: GCAGCCAGAGAGTGAAAG	87
A2B	F: TCAGTAGTAGGCTCCAAG R: ACCATAAACAAGGCAGAC	133
A3	F: AAAGGCTGGGTATCGGCTGT R: AAGGAGGCAAACGGGAGAAG	134
P2X1	F: ATCTGTGCTCTCCGATGT R: AGTTCAGCCGAGGAATTG	98
P2X2	F: TGGGACTGTGACCTGGACCT R: ACCTGAAGTTGTAGCCTGACGAG	106
P2X3	F: CATCCTGCTCAACTTCCT R: TTCAGCGTAGTCTCATTCA	78
P2X4	F: CCTTCCCAACATCACCCTAC R: GTCCTGCGTTCTCCACTATT	107
P2X5	F: TGAATTGCCTCTGCTTACGTT R: TCCGTCCTGATGACCCCA	197
P2X6	F: CTTCTCTGGTGCTGTGAT R: GGGATAGGGAGGTGGATTA	82
P2X7	F: GCCACAACACTACACCACGAGA R: GCCCATTATCCGCCCTGA	161
P2Y1	F: GAATCTCCAAACACCTCTCTG R: GAAAGCAAACCCAAACAAGC	175
P2Y2	F: CTGGTAGCGAGAACACTAAGG R: GCACAAGTCCTGGTCCTCTA	98
P2Y4	F: GTGGAGCTGGACTGTTGGTT R: ATAGGGTTGGGGCGTTAAGG	106
P2Y6	F: AAACCATGCGGAGAATTAGAG R: AGAAGGGGCTGAAGAAATAGTT	100
P2Y11	F: GACTGGAGACGCAAGAACA R: CCTTGGCGACAGAAGACA	100
P2Y12	F: GTAAGAACGAGGGGTGTAGG R: GGTTTGGCTCAGGGTGTAAG	132
P2Y13	F: GCCGACTTGATAATGACACT R: TATGAGCCCTAACAGCACGAT	150
P2Y14	F: TAGCCGCAACATATTCAGCATCG R: GCAGCAGATAGTAGCAGAGTGA	165

**Table 8.4: Human qPCR Primers**

Gene	Sequence (5' → 3')	Amplicon Size
18S	F: GCCGCTAGAGGTGAAATTCTTG	66
	R: CATTCTTGGCAAATGCTTTTCG	
	Probe: FAM ACCGGCCGAAGACCGG TAMRA	
MMP13	F: AAATTATGGAGGAGATGCCCATTT	126
	R: TCCTTGGAGTGGTCAAGACCTAA	
	Probe: FAM CTACAACCTTGTCTTGTGCTGCCGATGA TAMRA	
MMP1	F: AAGATGAAAGGTGGACCAACAATT	79
	R: CCAAGAGAATGGCCGAGTTC	
	Probe: FAM CAGAGAGTACAACCTTACATCGTGTGGGGCTC TAMRA	
MMP3	F: TTCCGCCCTGTC AAGATGATAT	144
	R: AAAGGACAAAGCAGGATCACAGTT	
	Probe: FAM TCAGTCCCTCTATGGACCTCCCCCTGAC TAMRA	
P2RY6	F: GAAGAACCATGGCTTTGGAA	96
	R: CCAGGTGGGTTTCCTATGTTTC	
	Probe: UPL Probe #16	
COL2A1	F: TGGTGGCTTCCATTTACAGCT	77
	R: GGCGTAGGAAGGTCACTCTGG	
	Probe: UPL Probe #36	
CX3CL1	F: CCACCTTCTGCCATCTGACT	74
	R: GCTGCACGTGATGTTGCATT	
IRAK2	F: CGCGTATCTGCCAGAGGATT	130
	R: AACCGGGCTTCGGTTGTTAT	
BDKRB1	F: CCGCAAGGATAGCAAGACCA	157
	R: CAGGCCCAGGTCAATGAAGT	
NOD2	F: CGGCTCGCGGTTGTGAA	160
	R: TGGAAGCCCTCGTAGTCCTC	
CCL8	F: CATGCTGAAGCTCACACCCCT	95
	R: GTCCCTGAGGGCTGAAAGTG	

## 8.2 Proteomic Arrays

### ARRAY 1 (MAPK Pathway)

Each antibody is spotted in duplicate vertically		A	B	C	D	E	F	G	H
	1	POS	POS	NEG	NEG	IC	CREB (S133)	ERK1 (T202/Y204) ERK2 (Y185/Y187)	IC
	2								
	3	IC	HSP27 (S82)	JNK (T183)	MEK (S217/221)	MKK3 (S189)	MMK6 (S207)	MSK2 (S360)	IC
	4								
	5	p38 (T180/Y182)	P53 (S15)	IC	RSK1 (S380)	RSK2 (S386)	NEG	NEG	POS
6									

### ARRAY 2 (AKT Pathway)

Each antibody is spotted in duplicate vertically		A	B	C	D	E	F	G	H
	1	POS	POS	NEG	NEG	AKT (S473)	AMPKα (T172)	BAD (S112)	4E-BP1 (T36)
	2								
	3	IC	GSK3α (S21)	GSK3β (S9)	mTOR (S2448)	p27 (T198)	IC	P70S6K (T421/S424)	PDK1 (S241)
	4								
	5	PRAS40 (T246)	PTEN (S380)	RAF-1 (S301)	RPS6 (S235/236)	IC	IC	NEG	POS
6									

### ARRAY 3 (JAK/STAT Pathway)

Each antibody is spotted in duplicate vertically		A	B	C	D	E	F	G	H
	1	POS	POS	NEG	EGFR (Ser1172)	JAK1 (Tyr1034)	JAK2 (Tyr1007/1008)	SHP1 (Ser591)	SHP2 (Tyr542)
	2								
	3	Src (Tyr419)	Stat1 (Ser727)	Stat2 (Tyr689)	Stat3 (Tyr705)	Stat5 (Tyr694)	Stat6 (Tyr641)	TYK2 (Tyr1054)	POS
4									

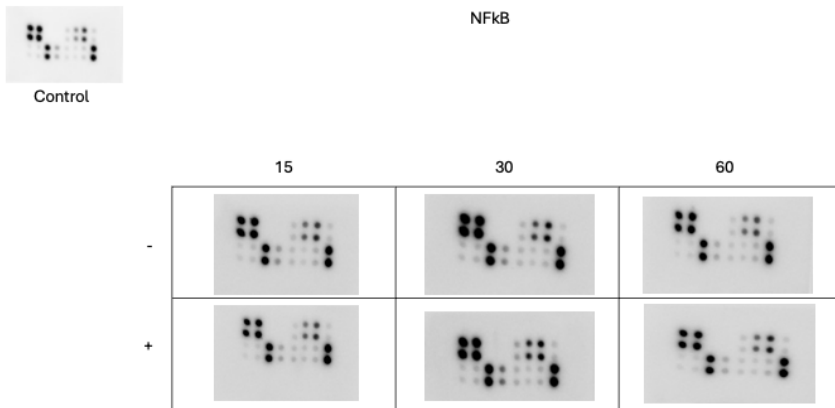
### ARRAY 4 (NFκB Pathway)

Each antibody is spotted in duplicate vertically		A	B	C	D	E	F	G	H
	1	POS	POS	NEG	NEG	ATM (S1981)	eIF2α (S51)	HDAC2 (S394)	HDAC4 (S632)
	2								
	3	IκBa (S32)	MSK1 (S376)	NFκB (S536)	IC	TAK1 (S412)	TBK1 (S172)	ZAP70 (Y292)	POS
4									

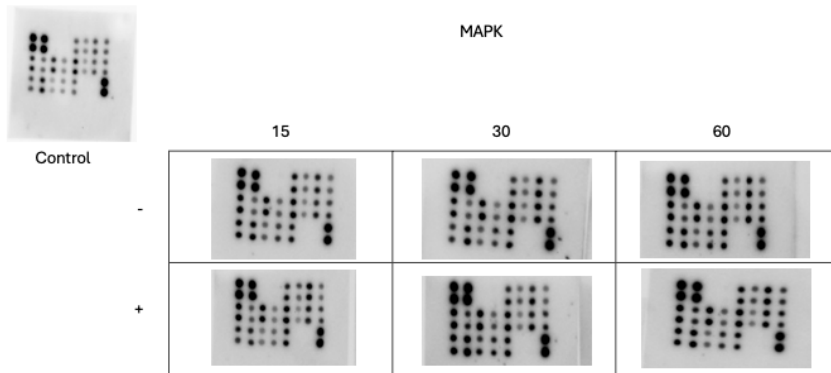
### ARRAY 5 (TGFβ Pathway)

Each antibody is spotted in duplicate vertically		A	B	C	D	E	F	G	H
	1	POS	POS	NEG	NEG	ATF2 (T69/71)	C-Fos (T232)	c-Jun (S73)	SMAD1 (S463/465)
	2								
	3	SMAD2(S245/250/255)	SMAD4 (T277)	SMAD5 (S463/465)	IC	NEG	NEG	NEG	POS
4									

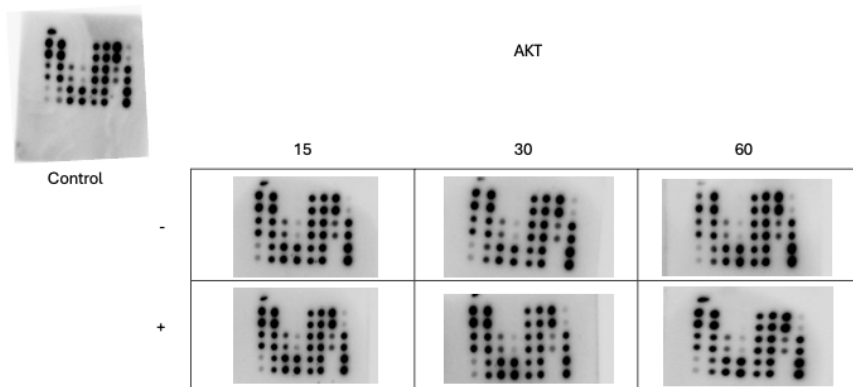
Figure 8.1: Array Maps. Taken from Raybiotech.com.



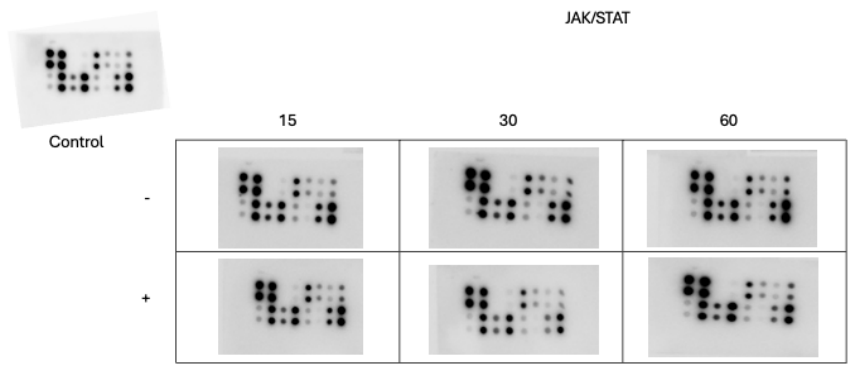
A



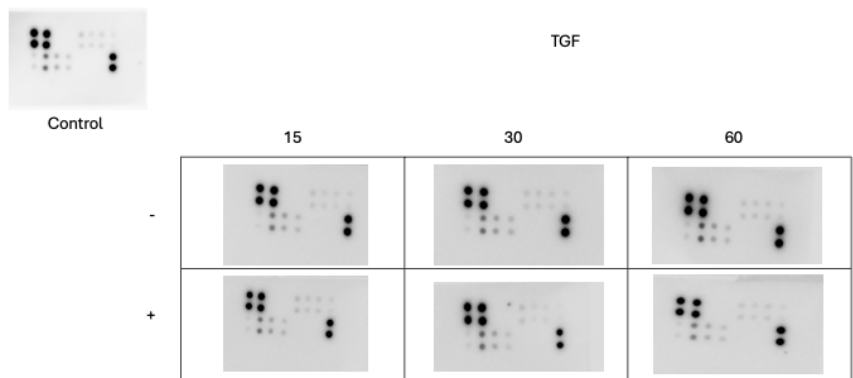
B



C



D

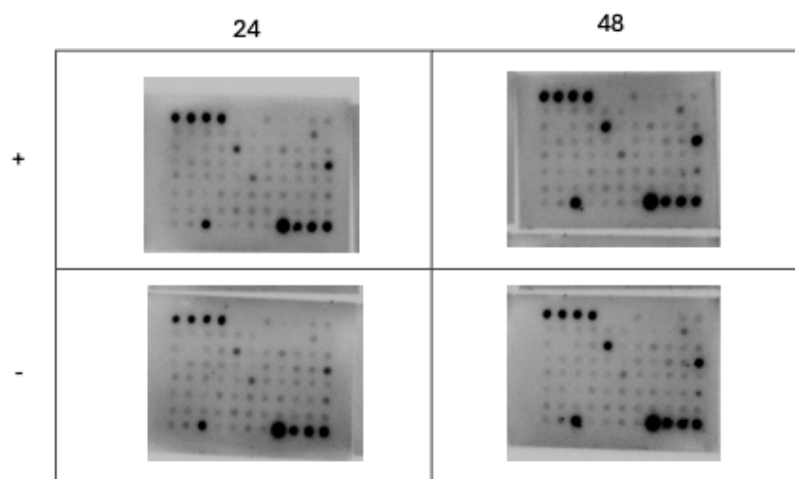


E

**Figure 8.2:** Phosphorylated Protein Pathway Arrays

	A	B	C	D	E	F	G	H	I	J	K
1	POS	POS	POS	POS	NEG	NEG	ENA-78 (CXCL5)	G-CSF	GM-CSF	GRO a/b/g	GRO alpha (CXCL1)
2	I-309 (CCL1)	IL-1 alpha (IL-1 F1)	IL-1 beta (IL-1 F2)	IL-2	IL-3	IL-4	IL-5	IL-6	IL-7	IL-8 (CXCL8)	IL-10
3	IL-12 p40/p70	IL-13	IL-15	IFN- gamma	MCP-1 (CCL2)	MCP-2 (CCL8)	MCP-3 (CCL7)	M-CSF	MDC (CCL22)	MIG (CXCL9)	MIP-1 beta (CCL4)
4	MIP-1 delta	RANTES (CCL5)	SCF	SDF-1 alpha	TARC (CCL17)	TGF beta 1	TNF alpha	TNF beta (TNFSF1B)	EGF	IGF-1	Angiogenin
5	OSM	TPO	VEGF-A	PDGF-BB	Leptin	BDNF	BLC (CXCL13)	Ck beta 8-1 (CCL23)	Eotaxin-1 (CCL11)	Eotaxin-2 (CCL24)	Eotaxin-3 (CCL26)
6	FGF-4	FGF-6	FGF-7 (KGF)	FGF-9	FLT-3 Ligand	Fractalkine (CX3CL1)	GCP-2 (CXCL6)	GDNF	HGF	IGFBP-1	IGFBP-2
7	IGFBP-3	IGFBP-4	IL-16	IP-10 (CXCL10)	LIF	LIGHT (TNFSF14)	MCP-4 (CCL13)	MIF	MIP-3 alpha	NAP-2 (CXCL7)	NT-3
8	NT-4	OPN (SPP1)	OPG (TNFRSF11)	PARC	PLGF	TGF beta 2	TGF beta 3	TIMP-1	TIMP-2	POS	POS

A. Taken from Raybiotech.com



B

Figure 8.3: Cytokine Arrays